

Integration of Organic Rankine Cycles for Waste Heat Recovery in Industrial Processes

THÈSE N° 6536 (2015)

PRÉSENTÉE LE 20 FÉVRIER 2015

À LA FACULTÉ DES SCIENCES ET TECHNIQUES DE L'INGÉNIEUR
LABORATOIRE D'ÉNERGÉTIQUE INDUSTRIELLE
PROGRAMME DOCTORAL EN ENERGIE

ÉCOLE POLYTECHNIQUE FÉDÉRALE DE LAUSANNE

POUR L'OBTENTION DU GRADE DE DOCTEUR ÈS SCIENCES

PAR

Matthias BENDIG

acceptée sur proposition du jury:

Dr J. Van Herle, président du jury
Prof. F. Maréchal, Prof. D. Favrat, directeurs de thèse
Prof. S. Harvey, rapporteur
Prof. G. Heyen, rapporteur
Prof. K. Hungerbühler, rapporteur



ÉCOLE POLYTECHNIQUE
FÉDÉRALE DE LAUSANNE

Suisse
2015

Der junge Alexander eroberte Indien.

Er allein?

Cäsar schlug die Gallier.

Hatte er nicht wenigstens einen Koch bei sich?

— Bertolt Brecht

Acknowledgements

In four years I could not have written this thesis had it not been for the help and preliminary work of a great too many people to name here individually. Precious advice and support, academic and beyond, offered by colleagues, friends and family were some of the basic ingredients required for the making of this work. Especially whilst writing, but also prior to this I was given endless patience by my wife and all those around me.

Special thanks must be given to my thesis director, Professor Maréchal, who with his near infinite creativity and ambition always showed new paths to take. Every discussion led to a plethora of new inputs and hints, many of which have proved fruitful. My thesis would not have been possible without him. Additionally, my co-director Professor Favrat, shared his rich experience from academia and engineering to improve the work I have done. Not only was he available for help with this thesis but also throughout the entire “LOVE” project, making the practical work on the ORC demonstrators more valuable.

At this place, I also want to thank the entire team of the “LOVE” project. Gaia, Hanna, Daniela, Massimiliano, Georges, Eric, Urs, Thomas and Thomas, Marc, Carlos, Alfredo, Antonio, Adrian, Regis, Elias, Dr. Clodic, Prof. Püttgen (in no particular order) and many others formed a great team that was essential in making this project a success. Especially memorable are our meetings to discuss the multiple challenges with the demonstrators which generally ending with a great meal.

Many thanks also to Nestec/Nestlé. Every discussion with Laurent, Rudolf and Adrian led to improvements that helped produce the results presented here. Not only did financial support of Nestec/Nestle make this thesis possible, but also their availability for studying a real process and implementing some energy saving measures.

Acknowledgements

The positive work environment and friendly atmosphere, the professional opinions and team spirit make it a joy to work at EPFL with you all. Formerly LENI, now IPESE and FUELMAT, are groups formed of generous and talented people which created the feeling of being part of a big family. Responsiveness and availability of Brigitte, Irene, Susanne, along with the software and hardware expertise of Nicolas have saved me more than once. Exceptional office mates are no guarantee so I feel extremely fortunate to have shared an office with Laurence, Priscilla and Thierry who made my stay more fun and more productive. Each day was an enrichment: discussions, shared meals and laughter with all of my colleagues will be missed.

Life during my PhD has been made immeasurably easier by my family and friends and they deserve a great deal of thanks. All through these years of studying and working I have been able to count on my parents, brothers, friends and of course my wife to be there for me.

Before I let you read the thesis I want to especially thank the jury of my defense and all the people who have helped me with proofreading. Thanks to the comments and corrections proposed this thesis was much improved.

Lausanne, 2015

Matthias

Abstract

Developing a methodology that allows identifying maximum electricity production with the help of Organic Rankine Cycles (ORC) from the waste heat of an industrial process, at the lowest specific cost, without jeopardising the increase of the industrial process's thermal efficiency. Such is the goal of this thesis. In order to reach this goal, a software tool which is able to identify the most suitable cycle for a heat source regarding electricity production and cost efficiency is developed and explained in detail. Three main areas of research can be identified, the definition of waste heat, the analysis of experimental data with the help of data reconciliation and the identification of a suitable working fluid and operation parameters of an ORC for any given heat source.

A method for identifying, characterising and quantifying the available waste heat, which can be converted into a useful form, for any industrial system, is presented. A distinction is made between avoidable and unavoidable waste heat. Combined pinch analysis and exergy analysis is used to characterise the waste heat potential of a given process. Based on the study of two industrial processes, it will become clear how the constraints of a waste heat analysis influence the outcome and the potential for the integration of ORCs. The studies illustrate how the increase in energy efficiency and degree of heat recovery and integration of a process can be contradictory to the production of electricity with ORCs. The concept of data reconciliation is needed for the measurements, collected from two ORC demonstrators. Apart from "classical" data reconciliation, a new method is presented, which consists in including parameters as virtual measurements and time dependency of measurements. This increases the redundancy of the system and thus the overall accuracy of the reconciled values. A methodology, capable of choosing the designpoint, a suitable working fluid and a cycle configuration, for the lowest specific investment cost while at the same time maximising the electricity output, for a given process environment is developed. The new methodology uses a multi objective optimisation (master optimisation) and Mixed Integer Linear Programming (MILP) problem (slave optimisation). A novel approach of combining multi objective non-linear master optimisations with single objective linear slave optimisations is introduced, increasing the reliability of the algorithm.

Keywords: Waste heat, Organic Rankine Cycle (ORC), Pinch analysis, process integration, exergy, thermo-economic, multi objective optimisation.

Zusammenfassung

Ziel dieser Dissertation ist die Entwicklung einer Methode, welche es ermöglicht die grösstmögliche Menge elektrischen Stroms für die niedrigst möglichen spezifischen Kosten unter Einsatz von Organic Rankine Cycles (ORC) zu bestimmen, ohne dadurch eine Effizienzsteigerung des Industrieprozesses selbst zu gefährden oder zu blockieren. Um dies zu erreichen wurde ein Software Tool entwickelt, welches den mit Blick auf Stromerzeugung und Kosteneffizienz am besten geeigneten Kreisprozess für eine gegebene Wärmequelle und -senke ermittelt. Drei Hauptthemengebiete können unterschieden werden, die Definition von Waste Heat (Abwärme), die Analyse von experimentellen Messdaten unterstützt durch Data Reconciliation und die Bestimmung von optimalen ORCs und ihrer Betriebsparameter für eine beliebige Wärmequelle.

Eine Methode zur Ermittlung, Charakterisierung und Quantifizierung von verfügbarer Abwärme von Industrieprozessen, welche in eine nutzbare Form umgewandelt werden kann, wird präsentiert. Es wird unterschieden zwischen vermeidbarer und unvermeidbarer Abwärme. Pinch und Exergy Analyse werden kombiniert um das Abärmepotential zu charakterisieren. Aufbauend auf der Untersuchung zweier Industrieprozesse wird gezeigt, welchen Einfluss die Vorgaben einer Abwärmestudie auf ihr Ergebnis haben und das Potential für den Einsatz von ORCs bestimmen. Die Analyse zeigt, wie das Potential zur Stromerzeugung mit zunehmender Prozessintensivierung und Prozesseffizienz abnimmt. Data Reconciliation wird eingeführt und zur Untersuchung der Messergebnisse zweier ORC-Demonstrationseinheiten angewandt. Zusätzlich zur "klassischen" Data Reconciliation führen wir eine innovative Erweiterung ein, welche Parameter als virtuelle Messungen verwendet und die Zeitabhängigkeit zwischen zwei Messperioden ausnutzt. Hierdurch lässt sich die Redundanz des Systems erhöhen und so die Präzision der durch Data Reconciliation bestimmten Werte. Das Software Tool und die zugrunde liegende Methode wird vorgestellt. Diese neuartige Methode verbindet eine Paretooptimierung (auf dem Master-Level) mit einem Mixed Integer Linear Programming (MILP) Optimierungsproblem (auf dem Slave-Level) und führt einen neuen Ansatz zur Steigerung der Zuverlässigkeit bei der Ermittlung der Paretooptima ein.

Stichwörter: Abwärme, Organic Rankine Cycle (ORC), Pinch Analyse, Prozessintensivierung, Exergy, Thermo-Ökonomie, Paretooptimierung.

Contents

Acknowledgements	i
Abstract (English/Deutsch)	iii
List of Figures	xi
List of Tables	xvii
List of Abbreviations and Symbols	xix
Introduction	1
1 Defining Waste Heat	19
1.1 State of the Art	19
1.2 Objectives	22
1.3 Finding the Waste Heat Potential	23
1.3.1 Identifying the Work Potential	24
1.3.2 Application of Pinch Analysis in the Context of Waste Heat	28
1.3.3 Heat Released by a Process	29
1.3.4 Global Exergy Balance	30
1.3.5 Heat Transfer Exergy Losses	30
1.3.6 Energy Conversion System Integration	32
1.4 Changing the Global Energy Balance	33
1.5 Other Sources of Exergy from an Industrial Process	33
1.6 Definition of Waste Heat as Reserve and Resource	34
1.7 Discussion	35
1.8 Conclusion	35
2 Waste Heat Recovery: Studies and Examples	37
2.1 Objectives	37
2.2 Structure	37
2.3 Soluble Coffee	39
2.3.1 Soluble Instant Coffee – Process-Description	39
2.3.2 End of Pipe Heat Recovery	41
2.3.3 Integration	41
	vii

Contents

2.3.4	Redesign	44
2.4	Cement	47
2.4.1	Cement – Process-Description	47
2.4.2	End of Pipe Heat Recovery	49
2.4.3	Integration	60
2.4.4	Redesign	66
2.5	Conclusion	70
3	Waste Heat Valorisation System Characterisation	73
3.1	Objectives	73
3.2	State of the Art of Data Reconciliation	74
3.3	Enhanced Data Reconciliation	75
3.4	Approach	76
3.5	A Posteriori Accuracy	77
3.6	Implementation	78
3.6.1	Illustrative Example	78
3.7	Steady State	79
3.7.1	CASE 1 – Initial Values Preparation Process	79
3.7.2	Non-linearities	82
3.7.3	CASE 2 – Measurements Subject to Noise	82
3.7.4	CASE 3 – Over Specified Systems	85
3.7.5	CASE 4 – Under Specified Systems	87
3.8	Non-Steady State – CASE 5	88
3.9	Application to LOVE-Demonstrators	93
3.9.1	Model Description	93
3.9.2	Turbine Isentropic Efficiency	95
3.9.3	Heat Transfer Coefficient	97
3.9.4	System Exergy Efficiency	101
3.10	Conclusion	103
4	Suitable Cycle Identification	105
4.1	Objectives	105
4.2	State of the Art	105
4.3	Method Description – Multi-Objective-Optimisation	111
4.3.1	Objective Function	113
4.3.2	Parameters and Constraints	114
4.3.3	Genetic Algorithm	115
4.3.4	Thermodynamic Models I: Thermodynamic Cycles	116
4.3.5	Thermodynamic Models II	120
4.3.6	Economic Models	123
4.3.7	Integration – MILP-Solver	131
4.3.8	Post-Calculation – Indicators	133
4.4	Solution Reliability Increase	135

4.5	Multiple Cycles and Multi Stage Cycles	137
4.6	Application and Discussion	138
4.6.1	Impacts of Size, Heat Sink Temperature and Minimum Temperature Difference using the Example of the Kollenbach Heat Source	139
4.6.2	Discussion of the Pareto Curves, Solution Reliability Increase and the Specific Investment Cost Using the Example of the Cement Heat Source used with the Commercial ORC	146
4.6.3	Integration of ORCs into the Soluble Instant Coffee Process	156
4.7	Conclusion	156
5	Conclusion	159
5.1	Results	159
5.2	Perspectives	163
A	Working Fluids	167
B	Streams of Cement Model	175
C	Economic Estimation of Electricity Generation Cost	179
	Bibliography	194
	Curriculum Vitae	195

List of Figures

1	World total final energy consumption by fuel 1971 to 2012 in Mtoe (International Energy Agency, 2014e).	2
2	Trend in CO_2 emissions from fossil fuel combustion (International Energy Agency, 2014b).	2
3	Carnot factor: efficiency limit with a heat sink at 15 °C.	4
4	Global savings from adoption of best practice commercial technologies (BAT) in manufacturing industries, upper estimate (primary energy equivalents).	5
5	Estimation of the world waste heat potential after implementing BAT energy efficiency measures, compared to the total final energy consumption of the world industry (107 EJ).	6
6	Construction of a hot composite curve, individual streams from process analysis (left) and summed up to composite curve (right) (Kemp, 2011)	6
7	Composite curves with and without corrected temperatures and grand composite curves with temperature and Carnot factor.	8
8	Carnot factor: technology situation with regard to the theoretical limit with a heat sink at 15 °C.	9
9	Use of district heating for waste heat recovery, (left) without and (right) with efficiency measures on the process.	10
10	Schema of a Rankine cycle.	11
11	Examples of dry (cyclohexane), wet (water) and isentropic (R123) working fluids (Jorge Facão, 2009).	12
12	Temperature-entropy (T-s) diagram of different Rankine cycles.	13
13	Integration of waste heat recovery with ORC, district heating and heat pump.	14
1.1	General representation of an industrial process with entering and leaving material and energy flows (modified after Maréchal and Kalitventzeff (1998)).	20
1.2	Example process, showing heat sinks and sources.	23
1.3	Work potential of the example process' (end of pipe) cooling requirements, in current configuration.	25
1.4	Schema of theoretical heat and work flows with an ideal transformation system.	26
1.5	Corrected hot and cold composite curves of example process, with explanations.	29
1.6	Corrected hot and cold Carnot composite curves of example process, showing heat transfer exergy and residual heat exergy.	31
1.7	Corrected carnot grand composite curve of example process with explications.	32

List of Figures

1.8	Exergy that can be accessed only by changing the energy balance: (a) above the pinch point, (b) in between pinch points, (c) in a large exergy pocket.	34
2.1	Schema of the instant coffee process.	40
2.2	Heat temperature profile of end of pipe residual heat in the instant coffee process, normalised.	42
2.3	Heat exergy of end of pipe residual heat in the instant coffee process, normalised.	42
2.4	Grand composite curve of the instant coffee process, without sub atmospheric parts, normalised.	43
2.5	Carnot grand composite curve of the instant coffee process, without sub atmospheric parts, normalised.	43
2.6	Grand composite curve of the redesigned instant coffee process, without sub atmospheric parts and without torrefaction, normalised.	45
2.7	Grand composite curve of the redesigned instant coffee process, without sub atmospheric parts and without torrefaction, normalised.	46
2.8	Simplified schematic of the cement process.	48
2.9	End of pipe heat sources of the cement process.	51
2.10	End of pipe heat sources of the cement process, exergy.	52
2.11	Schema of the Höver demonstrator	54
2.12	Höver demonstrator heat exchange.	57
2.13	Detailed PCU heat exchange, design.	57
2.14	Detailed PCU heat exchange, real.	58
2.15	Schema of the Kollenbach demonstrator.	59
2.16	Composite curve of a representative cement process.	64
2.17	Grand composite curve of a representative cement process.	64
2.18	Integrated composite curve of a representative cement process showing evacuated heat.	65
2.19	Integrated composite curve of a representative cement process showing heat losses.	65
2.20	Grand composite curve of extreme case 1.	68
2.21	Grand composite curve of extreme case 2.	69
2.22	Composite curve (a) and integrated composite curve (b) of extreme case 1. . . .	71
2.23	Composite curve (a) and integrated composite curve (b) of extreme case 2. . . .	71
3.1	Schematic of Data Reconciliation and Enhanced Data Reconciliation.	76
3.2	Schematic of Water-to-Air-Heat-Exchanger.	79
3.3	A posteriori inaccuracies of re-injected values, 5 % and 100 % initial values CASE 1.1.	81
3.4	Detail of a posteriori inaccuracies of re-injected values, 5 % and 100 % initial values CASE 1.1.	81
3.5	A posteriori inaccuracies of re-injected variables, CASE 2.1.	83
3.6	Relative differences between true and reconciled values of re-injected variables CASE 2.1.	84

3.7	Relative differences between true and reconciled values of re-injected variables CASE 2.2.	85
3.8	Relative differences between true and reconciled values in analogy to CASE 2.2 but with conventional reconciliation.	85
3.9	A posteriori inaccuracies in analogy to CASE 2.2 but with conventional reconciliation.	86
3.10	Distribution of average Drel values of measured variables for raw, conventionally and enhanced reconciled data.	87
3.11	Relative differences between true and reconciled values of re-injected variables CASE 4.1.	88
3.12	Relative Humidity reconciled and true values, CASE 5.1.	89
3.13	Relative differences between true and reconciled values of re-injected variables and Air Outlet Temperature CASE 5.1.	89
3.14	Penalty CASE 5.1 and Penalty of conventional Reconciliation.	90
3.15	Penalty of CASE 5.1 with different initial inaccuracies (1.5 % to 100 %).	90
3.16	Relative differences between true and reconciled values of re-injected variable “heat load” CASE 5.2.	91
3.17	Panorama photo of the LOVE demonstrator in Höver.	94
3.18	Temperature measurement before and after application of moving average.	95
3.19	Cryostar turbine specifications.	96
3.20	Model of the turbine used for reconciliation.	97
3.21	Isentropic efficiency of LOVE-turbine reconciled.	98
3.22	Friction and cooling losses of LOVE-turbogenerator reconciled.	99
3.23	Relation between volume flow rate $\frac{m^3}{s}$ and heat transfer coefficient $\frac{W}{m^2 \cdot K}$	100
3.24	Relation between volume flow rate $\frac{m^3}{s}$ and heat transfer coefficient $\frac{W}{m^2 \cdot K}$ measured on the 23rd September 2013.	100
3.25	Heat transfer coefficient of the direct boiler with the ambient.	101
3.26	Sankey diagram of the Höver demonstrator showing exergy losses.	102
3.27	Sankey diagram of the Kollenbach demonstrator showing exergy losses.	102
4.1	Algorithm of cycle identification embedded in integration with Multi Objective Optimisation.	112
4.2	T-s-diagram of a “simple” ORC with R1234yf, turbine inlet temperature at 120 °C and turbine inlet pressure at 30 bar.	117
4.3	T-s-diagram of a supercritical ORC with R1234yf, turbine inlet temperature at 120 °C and turbine inlet pressure at 40 bar.	118
4.4	T-s-diagram of an ORC the mixture R407, turbine inlet temperature at 90 °C and turbine inlet pressure at 30 bar.	119
4.5	T-s-diagram of an ORC the supercritical mixture R407, turbine inlet temperature at 110 °C and turbine inlet pressure at 49 bar.	120
4.6	Linearisation of cost function – Turbine.	128
4.7	Linearisation of cost function – Pump.	129

List of Figures

4.8	Linearisation of cost function – Heat Exchanger.	129
4.9	Algorithm detail of cycle identification showing before (left) and after (right) the reliability increase.	136
4.10	Integrated grand composite curve of R245fa ORC with Kollenbach heat source.	139
4.11	Impact of heat source load on net electricity generation and specific investment cost.	140
4.12	Impact of heat source load on net electricity generation and exergy efficiency.	141
4.13	Impact of heat sink inlet temperature on net electricity generation.	141
4.14	Impact of heat sink inlet temperature on exergy efficiency.	142
4.15	Impact of ΔT_{\min} on net electricity generation.	142
4.16	Impact of ΔT_{\min} on specific investment cost.	143
4.17	Impact of ΔT_{\min} on the share of the different equipments on the investment cost.	144
4.18	Pareto front of the integration of ORCs into a waste heat source from the Kollenbach cement process with both MILP objective functions.	144
4.19	Integrated grand composite curve and cost distribution of Acetone ORC with Kollenbach heat source.	145
4.20	Integrated grand composite curve and cost distribution of R422D ORC with Kollenbach heat source.	145
4.21	Pareto front of the integration of ORCs into a waste heat source from the cement process, allowing maximum one cycle with both MILP objective functions.	146
4.22	Pareto front of the integration of ORCs into a waste heat source from the cement process, allowing maximum two cycles with both MILP objective functions.	147
4.23	Impact of ΔT_{\min} on specific investment cost.	148
4.24	Impact of ΔT_{\min} on net electricity generation.	148
4.25	Histogram of the chosen MILP solution for an optimisation where one cycles is allowed and specific investment cost minimisation is the MILP objective function.	149
4.26	Histogram of the chosen MILP solution for an optimisation where two cycles are allowed and power maximisation is the MILP objective function.	150
4.27	Histogram of the chosen MILP solution for an optimisation where two cycles are allowed and cost minimisation is the MILP objective function.	151
4.28	Histogram of the chosen MILP solution out of the 15-best for an optimisation where two cycles are allowed and cost minimisation is the MILP objective function.	152
4.29	Pareto front of the integration of ORCs into a waste heat source from the cement process, allowing maximum two cycles with cost minimisation as MILP objective function for 10-best and 15-best.	152
4.30	Integrated grand composite curve and cost distribution of Propylcyclohexane ORC with cement heat source.	154
4.31	Integrated grand composite curve and cost distribution of Dodecane ORC with cement heat source.	154
4.32	Integrated grand composite curve and cost distribution of two ORCs with Dodecane and Toluene with cement heat source.	155

4.33 Pareto front of the integration of ORCs into the soluble instant coffee process, for the three analysis (end of pipe, integration and partial redesign).	156
--	-----

List of Tables

2.1	Hot Gases from Cement Plant.	52
2.2	Gases for LOVE-Demonstrators.	54
2.3	LOVE-Demonstrators, nominal parameters.	55
2.4	Nominal and real behaviour of PCU.	55
2.5	Commercially available ORC and district heating.	62
2.6	Cement process and ORC potential.	69
3.1	Available measurements in the example process.	79
3.2	Evolution of the Drel values Case 2.	84
3.3	Analysis of redundant case.	86
3.4	D_{rel} values of case 4.1.	88
3.5	D_{rel} values of case 5.1.	90
3.6	Impact of inaccuracy values in transient processes.	92
4.1	Summary of different working fluids studies, Part I, (Quoilin et al., 2011).	107
4.2	Summary of different working fluids studies, Part II, (Quoilin et al., 2011).	108
4.3	Assumptions made to calculate the ORC.	120
4.4	Equipment Cost Data.	125
4.5	Equipment Pressure Factors.	126
4.6	Material Factors.	126
4.7	Constants for Bare Module Factors.	126
4.8	Linearised Equipment Cost Data.	128
A.1	Pure Fluids from REFPROP Data Base Part I.	168
A.2	Pure Fluids from REFPROP Data Base Part II.	169
A.3	Pure Fluids from REFPROP Data Base Part III.	170
A.4	Pure Fluids from REFPROP Data Base Part IV.	171
A.5	Pure Fluids from REFPROP Data Base Part V.	172
A.6	Mixtures from REFPROP Data Base Part I.	173
A.7	Mixtures from REFPROP Data Base Part II.	174
C.1	Cost per kWh of electricity C_{gen} in USD /kWh, for $t_{pb} = 5$ years, as a function of t_{op} and $C_{TM,spec}$	180

List of Tables

C.2 Cost per kWh of electricity C_{gen} in USD /kWh, for $t_{\text{pb}} = 10$ years, as a function of t_{op} and $C_{\text{TM,spec}}$ 180

C.3 Cost per kWh of electricity C_{gen} in USD /kWh, for $t_{\text{pb}} = 15$ years, as a function of t_{op} and $C_{\text{TM,spec}}$ 181

List of Abbreviations and Symbols

Abbreviations

BAT	Best Practise Commercial Technologies
BAT	Best Available Technologies
CAMD	Computer Aided Molecular Design
CCS	Carbon Capture and Storage
CS	Carbon Steel
Cu	Copper
EOS	Equation of State
FG	Flue Gas
FiTu	Finned Tube Heat Exchanger
GDP	Gross Domestic Product
GHG	Green House Gas
GWP	Global Warming Potential
HEN	Heat Exchanger Network
IEA	International Energy Agency
LMTD	Logarithmic Mean Temperature Difference
LOVE	Low Temperature Heat Valorisation Towards Electricity Generation
LTHC	Low Temperature Heat Valorisation Cycle
MER	Minimum Energy Requirement
MILP	Multi Integer Linear Programming
MOGA	Multi Objective Genetic Algorithm
MOO	Multi Objective Optimisation
MVR	Mechanical Vapour Recompression
NPV	Net Present Value
ODP	Ozon Depletin Potential
OMTS	Octamethyltrisiloxane
ORC	Organic Rankine Cycle
OTEC	Ocean Thermal Energy Conversion
PCU	Packed Column Unit
PUO	Process Unit Operation
SS	Stainless Steel
TE	Thermoelectric

List of Abbreviations and Symbols

TFC	Total Final Energy Consumption
WHR	Waste Heat Recovery

Symbols - Latin

A	div.	Sizing Parameter
A	m^2	Surface Area
A	-	Derivative Matrix
B	-	Derivative Matrix
B	-	Parameter
C	div.	Constants, Vectorial
C	USD	Cost
$C_{1,2,3}$	-	Parameters
C_{MILP}	USD	Linearised Total Value
$C_{p,l}^0$	USD	Linearised Purchasing Cost
c_p	$\frac{J}{kg \cdot K}$	specific heat capacity
C_p^0	USD	Purchasing Cost
d	m	Hydraulic Diameter
D_{rel}	%	Sum of the Relative Differences Between Reconciled and True Values
\dot{E}	W	Exergy Rate
\dot{E}	W	Electrical Power
\dot{E}	W	Shaft Power
\dot{E}_q	W	Heat Exergy Rate
\dot{E}_y	W	Transformation Exergy Rate
F	-	Factor
f	-/ kg	Multiplication Factor
f	-	Constraint Functions (Mass and Energy Balances)
F_{BM}	-	Bare Module Cost
F_p	-	Pressure Correction
\dot{H}	W	Enthalpy Flow Rate
h	$\frac{J}{kg}$	Mass Specific Enthalpy
h	-	Constraint Functions (Mass, Energy Balances, Others)
i	%	Depreciation/Interest Rate
I	-	Integer Variable
I_t	-	Cepci Index
J	J	Coenergy
k	$\frac{J}{kg}$	Mass Specific Coenthalpy
k	$\frac{W}{m \cdot K}$	Thermal Conductivity
K	-	Parameters
K_{Ph}	-	Correction Factor For Phase Limit
$\dot{L}_{turbogen}$	W	Friction and Cooling Losses
L	-	Parameter

L	-	Lagrangian
LMTD	K	Logarithmic Mean Temperature Difference
\dot{m}	$\frac{\text{kg}}{\text{s}}$	Mass Flow Rate
M	-	Sensitivity Matrix
n	-	Counter
NPV	USD	Net Present Value
Nu	-	Nusselt Number
Obj	-	Objective Function
p	bar	Pressure
p_c	bar	Critical Pressure
Pr	-	Prandtl Number
\dot{Q}	W	Heat Rate
\dot{q}	$\frac{\text{W}}{\text{kg}}$	Mass Specific Heat Rate
R_t	USD	Return in Period t
Re	-	Reynolds Number
\dot{R}_k	W	Heat Rate from Section k
s	$\frac{\text{J}}{\text{kg} \cdot \text{K}}$	Mass Specific Entropy
s	-	Constraint Functions (Parameter Dependent Functions)
T	K	Temperature
t	s	Time
T_B	K	Normal Boiling Temperature
T_C	K	Critical Temperature
U	J	Internal Energy
u	$\frac{\text{J}}{\text{kg}}$	Mass Specific Internal Energy
U	$\frac{\text{kW}}{\text{m}^2 \cdot \text{K}}$	Heat Transfer Coefficient
V	m^3	Volume
W	-	Weight Matrix
\dot{x}	-	Vapour Fraction in Flow
\hat{Y}	div.	Measurement Values, Vectorial
\hat{y}	div.	Measurement Value
y	div.	Reconciled Value
Y	div.	Reconciled Values, Vectorial

Symbols - Greek

α	$\frac{\text{kW}}{\text{m}^2 \cdot \text{K}}$	Local/Film Heat Transfer Coefficient
Δ	-	Difference
ΔT_{\min}	K	Minimum Temperature Difference
Δh^0	$\frac{\text{J}}{\text{kg}}$	Isobaric and Mass Specific Lower Heating Value
Δk	$\frac{\text{J}}{\text{kg}}$	Isobaric and Mass Specific Exergy Value
Δk^0	$\frac{\text{J}}{\text{kg}}$	Isobaric and Mass Specific Exergy Value
η_{is}	-	Isentropic Efficiency

List of Abbreviations and Symbols

η_{ex}	-	Exergy Efficiency
Θ	-	Carnot Factor
ρ'	$\frac{\text{kg}}{\text{m}^3}$	Liquid Fluid Density
ρ''	$\frac{\text{kg}}{\text{m}^3}$	Gaseous Fluid Density
σ	-	Standard Deviation/Inaccuracy
τ_D^*	-	Dimensionless Shear Stress
φ	%	Relative Humidity

Superscripts

- + positive when entering the system
- positive when leaving the system
- * in corrected temperature

Subscripts and Indexes

a	ambient
B	boiling
BM	bare module
C	critical
clk	clinker
cond	condensation
cooling	cooling utility
cw	cooling water
cz	including kinetic and potential energy
dp	dew point
el	elctrical
evap	evaporation
F	film
g	gas
heating	heating utility
i	counter
in	entering
ki	counter
l	laminar
min	minimal/minimum
n	normal conditions
out	leaving
p	pressure/isobaric
pump	pump
π	parameter
sink	heat sink
source	heat source

spec	specific
src	source
sub	subcooling
t	time/timestep
t	turbulent
TM	total module
turb	turbine

Introduction

Energy is one of the main drivers of modern society, therefore it is associated with growth and well-being. As a consequence, the overall global energy consumption is increasing (figure 1), this leads to an increase in CO_2 and other greenhouse gas (GHG) emissions (figure 2), which amplify climate change.

In an effort to limit climate change to a low level, many countries make an effort to decouple the effects of growth of their gross domestic product (GDP) and their GHG emissions (International Energy Agency, 2014d; United Nations Framework Convention on Climate Change, 1997). Because 69 % of global anthropogenic greenhouse gas emissions have their origin in energy use, the use of GHG neutral or low carbon technologies, such as renewable energies or carbon capture and storage (CCS), play key roles in the abatement of GHG emissions. Another key role is played by the implementation of efficiency measures. The International Energy Agency (IEA) calls efficiency the “*first fuel*” (International Energy Agency, 2013) and state:

“Energy efficiency improvements since the 1970s in 11 IEA member countries saved 56 exajoules (EJ) or 1337 Mtoe [Mega Tons of Oil Equivalent] in 2011. Avoided energy use was larger than the supply of oil (1202 Mtoe), electricity (552 Mtoe) or natural gas (509 Mtoe) in 2011; these savings equate to 59 % of TFC [Total Final Consumption] in the 11 IEA member countries that year. In monetary terms, 56 EJ has a value of USD 743 billion (given an average global price of energy at USD 13.96 per gigajoule [GJ]).” (International Energy Agency, 2014d, p. 16).

The industrial sector has an important share in energy and fuel consumption: 29 % of the worldwide total final energy consumption (TFC) in 2011 was attributed to industry (International Energy Agency, 2014e). The worldwide total final energy consumption (TFC) which is used in form of heat represents 47 % (with industry accounting for 44 % of these) (International Energy Agency, 2011). Thus, it seems logical that a large part of the aforementioned increases in energy efficiency should be made in the industrial sector.

Another way of increasing the use of the fuel input into an industrial process (or increasing the generated value per unit of energy) is to convert waste heat into additional products, such as electricity. In a report (Energetics and US DOE, 2004) it was estimated that 20 % to 50 % of

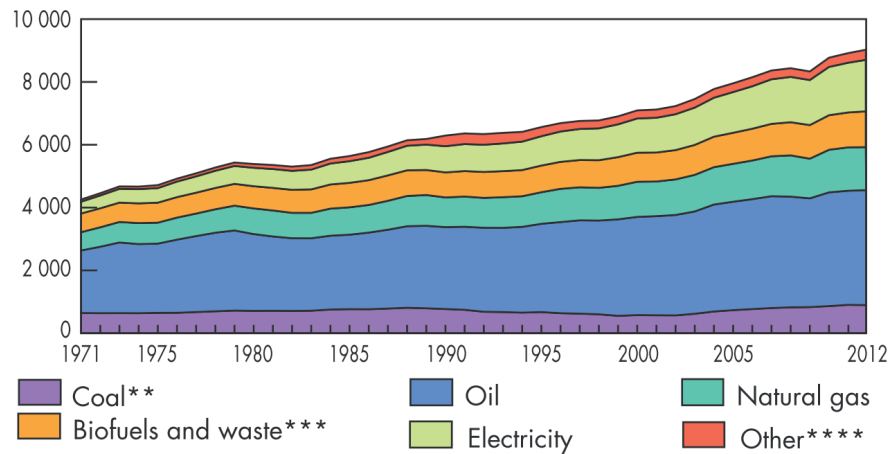


Figure 1: World total final energy consumption by fuel 1971 to 2012 in Mtoe (International Energy Agency, 2014e).

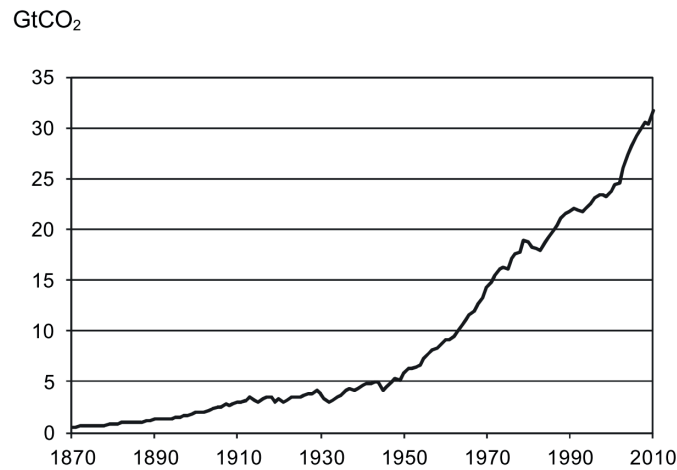


Figure 2: Trend in CO₂ emissions from fossil fuel combustion (International Energy Agency, 2014b).

all energy input of industrial processes leave the process in form of waste heat. The potential for waste heat conversion is therefore very large.

In this context the two laws of thermodynamics have to be considered. The first law relates the energy efficiency to the waste heat production: increasing process efficiency reduces waste heat production and even reduces specific energy consumption. The second law of thermodynamics defines the quality of the heat. It states that the amount of useful energy in form of work or electricity that can be produced by waste heat conversion depends on its temperature level and on the ambient temperature.

Electricity and heat represent 42 % of the world CO₂ emissions (International Energy Agency, 2014b). The electricity production from waste heat can therefore have an important impact on CO₂ emissions if it substitutes power production from the existing power plants. A further (micro economic) motivation for waste heat use for electricity generation could be the reduc-

tion of electricity imports and thus cost and dependency on local utilities and electricity grid (International Energy Agency, 2014a).

However, if the industrial sector is supposed to make an important contribution to the reduction of greenhouse gases, the installation of waste heat recovery for external services and the increase of process efficiency by heat recovery within the process could be contradictory: The reduction of the fuel consumption by increase of the process efficiency has an impact which is simple to estimate, for each kWh of heat which is not needed, one kWh of fuel is saved. Whereas, a system to produce electricity from heat which is placed downstream of the process will have an efficiency, significantly smaller than one. This is due to thermodynamic and technical limitations and especially significant for heat at low temperatures. From a climate protection point of view, it seems indicated to give priority to the reduction of the fuel input by increasing a process' internal efficiency.

This leads to several questions which we try to answer in this thesis:

- Considering the energy efficiency measures, how do we define the waste heat of a process?
- How can we quantify the waste heat potential?
- How can we access the waste heat potential and produce a maximum of electricity?

After giving the broad context and motivation for this thesis, we will give some basic definitions and explanations.

The Carnot Factor

The Carnot factor Θ defines the theoretically derived upper limit of thermodynamic efficiency. For thermodynamic cycle between a heat source with the temperature T_{source} and a heat sink with the temperature T_{sink} it is given by

$$\Theta = 1 - \frac{T_{\text{sink}}}{T_{\text{source}}}. \quad (1)$$

With this limit, it is easy to understand that electricity production potential increases with the temperature of the heat source since the heat sink is in general the environment (Borel and Favrat, 2010). Figure 3 shows how the maximum efficiency develops as function of the temperature difference between a heat sink at 15 °C and a heat source. Also shown are 60 % of the theoretical maximum Θ which is representing an efficient Organic Rankine Cycle.

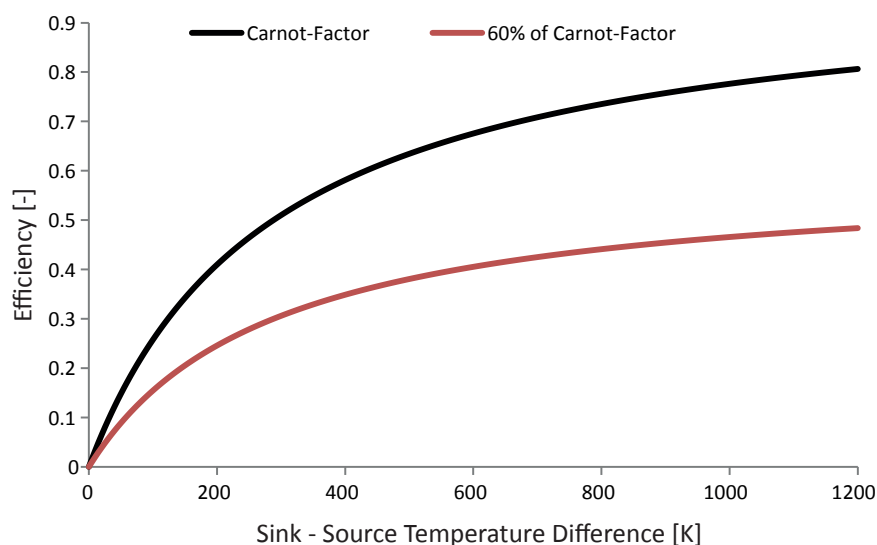


Figure 3: Carnot factor: efficiency limit with a heat sink at 15 °C.

Waste Heat and Energy Efficiency Potentials

The possible competition between the use of waste heat (e.g. for electricity production) and avoiding the creation of waste heat, renders the estimation of waste heat recovery (WHR) potential a difficult task. Some considerations will however give an order of magnitude. The estimation stated above considered that 20 % to 50 % of all energy input into industrial processes leaves in the form of waste heat (Energetics and US DOE, 2004). But how much of this is can be avoided?

In figure 4, the upper estimate of saving potentials by application of best practice commercial technologies in manufacturing industries is shown (International Energy Agency, 2007). The total savings from the adoption of Best Practice Commercial Technologies (BAT) in manufacturing Industries are estimated to be up to 38 EJ of primary energy equivalents per year. The transformation from global primary to final energy has a factor of roughly 0.68. If we assume, in a first approximation, that this factor is assigned proportionally to the consumers and forms of energy, it could be applied to get to the final energy equivalents of the possible savings (International Energy Agency, 2014e) (This is of course a very strong simplification). This means that up to 25 EJ of the total final energy consumption could be saved per year.

The world wide total final energy consumption of the industry was 107 EJ in 2011 (International Energy Agency, 2014e). If we consider the estimate of 50 % of energy leaving the industrial processes in the form of heat, it represents 54 EJ of waste heat. Even if all the BAT efficiency measures are applied, the quantity of available waste heat could be as high as 28 EJ per year or a constant average heat flow rate of 884 GW.

If the entire waste heat was at 100 °C and the available heat sink at the world average temperature of around 15 °C, the Carnot factor gives a limit of 25.8 % maximum efficiency, or 15.5 % at

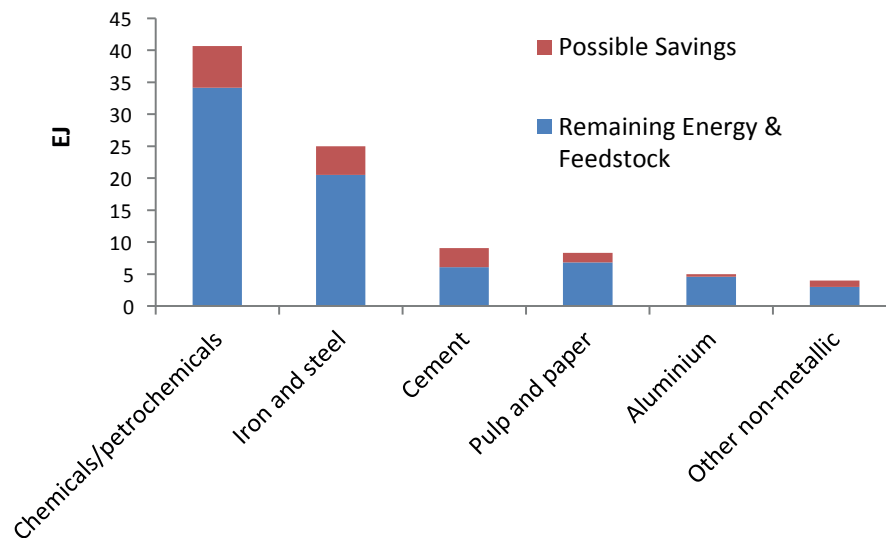


Figure 4: Global savings from adoption of best practice commercial technologies (BAT) in manufacturing industries, upper estimate (primary energy equivalents).

60 % of the Carnot factor. The average world electricity generation in 2011 was 2586 GW, if it was possible to convert 15.5 % of the total waste heat into electricity, about 5.3 % of the global electricity generation could be covered by waste heat without emitting additional CO_2 during the generation. Assuming a CO_2 emission of 506.75 g/kWh (world average for electricity and heat output 2007 (European Energy Agency, 2014)), results in saved electricity production in other plants which is equivalent to a reduction of 608.4 Million tons of CO_2 per year. Actually, the efficiency measures would also lead to considerable GHG emission reductions in the process and a reduction of the electricity consumption. If we consider that the 25 EJ of energy savings from BAT measures would emit the same amount of CO_2 per kWh, the resulting reduction would from BAT measures be as high as 3607 Million tons of CO_2 per year (figure 5). Therefore, motivation of this thesis is thus: *How can the waste heat potential be tapped while at the same time improving the energy efficiency of the industrial processes?*

Pinch Analysis

A tool that we use throughout the thesis is Pinch analysis. It is used for in chapter 1 for the definition of waste heat in the analysis and optimisation/integration of industrial processes in chapter 2, in the evaluation of accessibility/availability of waste heat and in the optimal integration of the waste heat recovery system in chapter 4. The method was developed by Linnhoff and Flower (1982) and is a way to identify *heat recovery* possibilities within a process in a manner such that the overall heat consumption of the process is minimal (Minimal Energy Requirement (MER)). A detailed description of the method can be found in Kemp (2011). We do, however, shortly describe the basic aspects here. In Pinch analysis, processing operations are analysed in order to identify if and at which temperature they need heating or cooling to perform their function. The analysis of the process results in a list of heating and cooling

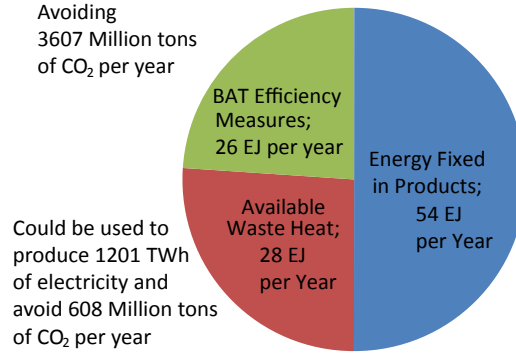


Figure 5: Estimation of the world waste heat potential after implementing BAT energy efficiency measures, compared to the total final energy consumption of the world industry (107 EJ).

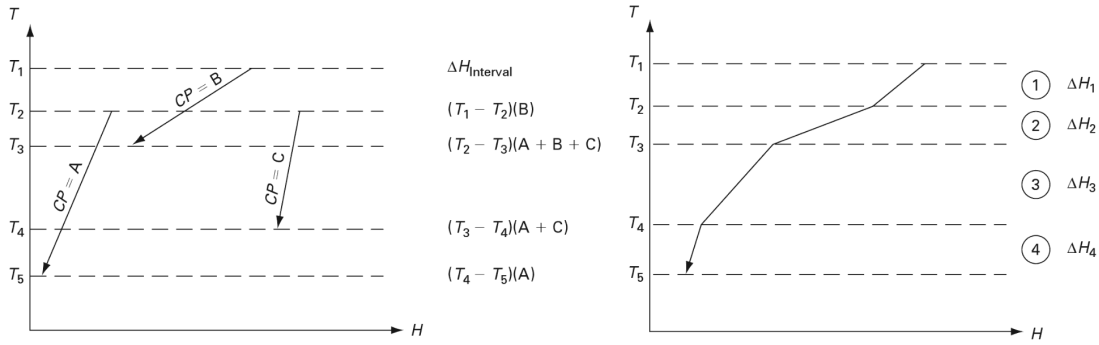


Figure 6: Construction of a hot composite curve, individual streams from process analysis (left) and summed up to composite curve (right) (Kemp, 2011).

requirements, stating the temperatures and the quantities (enthalpies) of the needed heat streams. Heat which has to be evacuated from a unit is referred to as *hot stream* or *cooling requirement*, it can be used as a heat source. If a process unit needs heating, it is referred to as *cold stream* or *heating requirement* since it needs to be heated up and can be used as a heat sink. Subsequently, all *hot* and all *cold streams* are summed up to form the *hot* and *cold composite curves*, respectively. These curves show how much heat is required or has to be evacuated at which temperature. The construction of a hot composite curve is demonstrated in figure 6.

Once the composite curves, including all hot and cold streams, are prepared, they are used to identify the amount of heat than can be recovered within the process. In order to do so, a minimum temperature difference ΔT_{\min} between hot and cold streams for a typical heat exchange is defined. ΔT_{\min} depends on the heated and cooled materials and their thermodynamic states as well as the available heat exchanger surface. Oftentimes, the corresponding $\Delta T_{\min}/2$ is directly added or subtracted to or from the respective stream temperature, leading to a composite curve with *corrected temperatures* which show the available heat or needed

cooling requirements of the process. If corrected temperatures are used, it will be either written explicitly or marked with an asterisk (*). In figure 7 (a) and (b), it is shown how the MER is identified by horizontally sliding the *cold composite curve* under the *hot composite curve*, each with corrected temperatures, until they touch. The point in which they touch is called *pinch point*, or often abbreviated as *pinch*. By recovering heat from the *hot streams* to heat up the *cold streams*, not only the need of a hot utility is reduced but also the deployment of a cooling utility shrinks by the same amount. This is called the *more-in more-out principle*. As ΔT_{\min} can be reduced by using a larger heat exchange area, the choice of ΔT_{\min} is hence a trade-off between the *investment in heat exchanger surface* and *energy saving*. The use of computer models plays a crucial role in this context. With well defined energy cost(s) and investments, they allow to identify an economic minimum if energy cost and investment in a *Heat Exchanger Network (HEN)* are well defined.

Another way to represent the process is the *grand composite curve*. It shows the horizontal distance, ΔQ , between the *hot* and *cold composite curves* as a function of the temperature (figure 7 (c)). Both diagrams, *composite curves* and *grand composite curve*, can be modified by replacing the temperature with the corresponding Carnot factor $\Theta = 1 - \frac{T_a}{T}$ with the *ambient temperature* T_a . Thus, the heat exergy is represented by the surface in the diagram (figure 7 (d)). In order to optimise the *exergy efficiency* of a process, the area between hot and cold curves has to be minimized.

The Pinch analysis divides the process into two subsystems, *above* and *below* the *pinch point*. Above the pinch point, it is characterized by an overall need for heating (heat sink). Below, there is an overall necessity for cooling (heat source). As a consequence, no stream above the pinch point should be cooled by a cold utility but rather by internal heat exchange, and no stream below the pinch point should be heated by means of a hot utility. Additionally, no internal heat exchange should cross the pinch point (no stream below the pinch should be heated with a stream from above), in order to meet the MER.

Pinch analysis is also used to place heat pumps (Townsend and Linnhoff, 1983), and helps as well with the introduction of heat exchanger networks (Linnhoff and Hindmarsh, 1983) which is under constant development as shown in Smith et al. (2010) and Wang et al. (2012a). Many more application examples can be found in Klemes (2013). Maréchal and Kalitventzeff (1997) have introduced the use of rectangles integrated in the Grand composite curve, to identify the possible situation of ORCs and the pressure levels within the ORCs.

Waste Heat Recovery Technologies

In the following we discuss different technologies for the recovery of waste heat and their efficiencies. At first, the direct use of recovered waste heat is discussed, then technologies for converting heat to electricity are presented. A simplified situation of the technologies regarding their efficiency compared to the Carnot factor is shown in figure 8. This section shows why organic Rankine cycles have been chosen as the conversion technology in this

Introduction

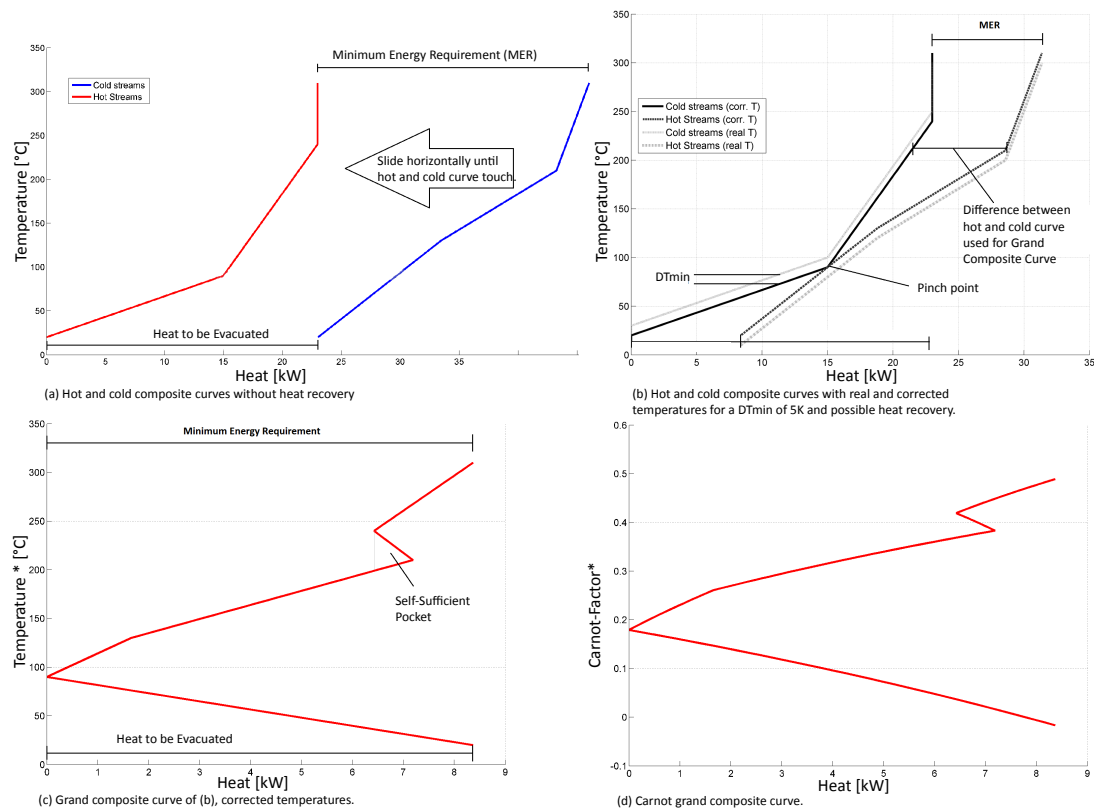


Figure 7: Composite curves (a) without (top left) and (b) without corrected temperatures (top right) and grand composite curves (c) with temperature (bottom left) and (d) Carnot factor (bottom right).

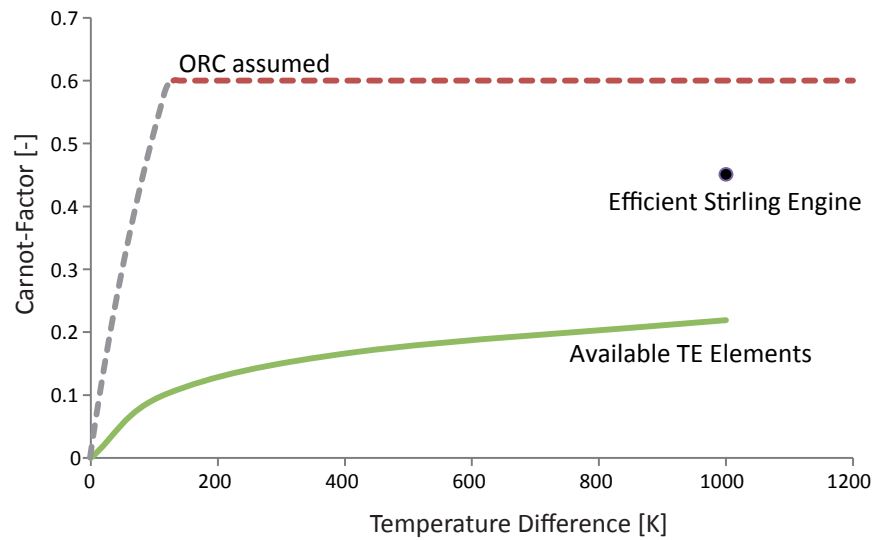


Figure 8: Carnot factor: technology situation with regard to the theoretical limit with a heat sink at 15 °C.

thesis. In chapter 4 it will be seen that efficient ORCs reach exergy efficiencies above 60 %. However, for very low temperature differences (grey line) the temperature gradient in the heat exchangers decreases the possible exergy efficiency.

Space heating: Even though, this thesis focuses on the generation of electricity from waste heat, the use of heat (especially at low temperatures) can also be interesting for space heating for example in the form of district heating networks. The advantage of the use in space heating is that no transformation is necessary, only the transport of the heat to the consumer has to be organised. This is typically done with water or pressurised water. The temperature levels used in heat distribution systems are typically between 40 °C and 80 °C and the heat distribution efficiency can be very high (90 %). However, it has to be mentioned that the heat demand is varying with time and seasons. It is thus difficult to evaluate the waste heat valorisation only with the first law of thermodynamics (Perry et al., 2008). Examples for the use of waste heat for district heating can be found in Perry et al. (2008), Holmgren (2006) and Morandin et al. (2014).

The example of district heating shows clearly why the use of a first law of thermodynamics perspective on waste heat is not sufficient. In figure 9, the use of waste heat by a district heating network is shown. It can be seen that the increase of energy efficiency of the process (application of efficiency measures) does not reduce the minimum energy requirement or the heat delivered by the hot utility, since the heating requirement of the district heating stays unchanged. The heat demand of the district heating has to be satisfied and if less waste heat is available, this is done by an increased heat transfer from the hot utility to the district heating. However, the temperature at which the heat is needed changes visibly, while the process needs heat at high temperature, the district heating needs it at low temperature. The grey area represents the possible exergy savings, if the hot utility delivers the heat always exactly at the

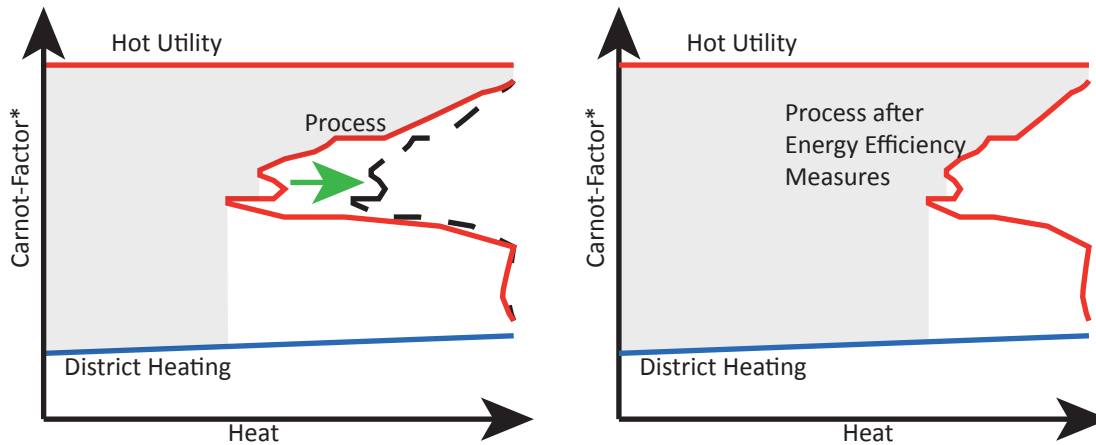


Figure 9: Use of district heating for waste heat recovery, (left) without and (right) with efficiency measures on the process.

required temperature, it is visibly larger, after applying the energy efficiency measures. Thus, decreasing the energy demand of the process has increased the potential to save exergy. This illustrates the need for exergy analysis.

Thermoelectric (TE) systems: TE systems for electricity generation use the Seebeck effect, that means that they consist of two semiconductors (p-type and n-type) which form a thermocouple. If heat is applied to one side, electrons are “pushed” from the n-type material and “holes” from the p-type material towards the cold side, thus creating a potential difference between the two semiconductors which can be used in a circuit in the form of current. Thermoelectric systems exist for a wide range of temperatures up to above 1000 °C and have the advantage of no moving parts, which makes them potentially maintenance free (Rowe, 1995). Unfortunately TE elements available today are not only costly, but also have relatively low efficiencies. At over 1000 °C the efficiency is still under 20 % and at 400 °C they do not reach 10 %. They are however advantageous at very small sizes, since mechanical systems have physical limits of size reduction (Vining, 2009).

Stirling Engines: The Stirling engine can be applied even with very low temperature differences between heat source and sink. It is a reciprocating engine in which a gas stays in the cylinders without direct contact to the heat sources. It has the reputation of being reliable with low maintenance (Kongtragool and Wongwises, 2003). The Stirling cycle can theoretically reach a high efficiency (it is actually equivalent to the Carnot efficiency), however the machines internal irreversibilities are often substantial and at over 1000 °C a Stirling engine realistically has an efficiency between 20 % and 35 % (Hsu et al., 2003).

Rankine Cycles: The Rankine Cycle (or Clausius Rankine Cycle) using water as a working fluid is generally used in large thermal power plants. A schema of the Rankine cycle, is shown in figure 10, where \dot{Q} is heat and \dot{E} is (shaft) work (Borel and Favrat, 2010). In a Rankine cycle

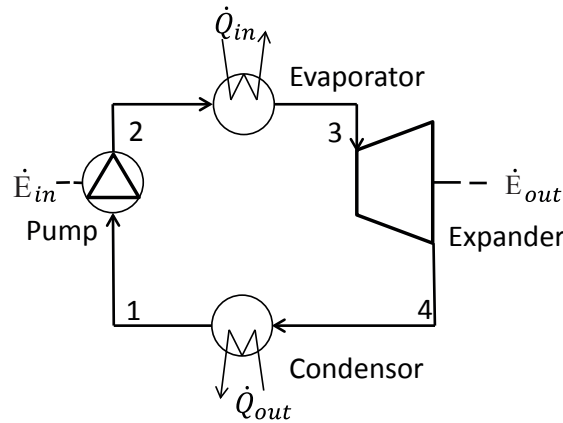


Figure 10: Schema of a Rankine cycle.

the working fluid (at condensation pressure) is pumped \dot{E}_{in} to a higher pressure (1-2), it is preheated, evaporated and possibly superheated (2-3) \dot{Q}_{in} , it enters the expander (in this work, generally a turbine) where the work \dot{E}_{out} is recovered (3-4), to close the cycle, the steam exiting the expander is (4-1) de-superheated, condensed and possibly sub-cooled \dot{Q}_{out} before it enters the pump again. The work that is used to drive a generator is recovered from the turbine.

Water is, however, not the only fluid that can be used as a working fluid within such a machine. Quoilin and Lemort (2009) state that water cycles have a higher efficiency at high temperatures, they need however pressures of 60 bar and higher to be efficient, which could be seen as a risk in certain industries and increases maintenance of a machine and the size of the used equipments. Other fluids can be used, which have lower boiling pressures and temperatures. Also the shape of the T-s-curve influences the possible use; three types of fluids can be distinguished when looking at the condensation curve:

- wet fluids with condensation curves $\frac{dT}{ds} < 0$
- isentropic with condensation curves $\frac{dT}{ds} = \infty$
- dry fluids with condensation curves $\frac{dT}{ds} > 0$

In figure 11, it can be seen how this influences the use of a Rankine cycle, if a wet fluid is not superheated at the intake of the turbine, the fluid will leave the turbine partially liquid, for a dry fluid it leaves superheated (Jorge Facão, 2009).

Furthermore, it is possible to use mixtures of working fluids, which have beneficial properties. A working fluid mixture shows a more or less strong temperature glide during the evaporation (instead of obtaining a “plateau” in the case of a pure working fluid) (Angelino and Colonna di Paliano, 1998). This can be used to better fit the cycle to heat sinks and sources (figure 12, the area around the critical point has been approximated).

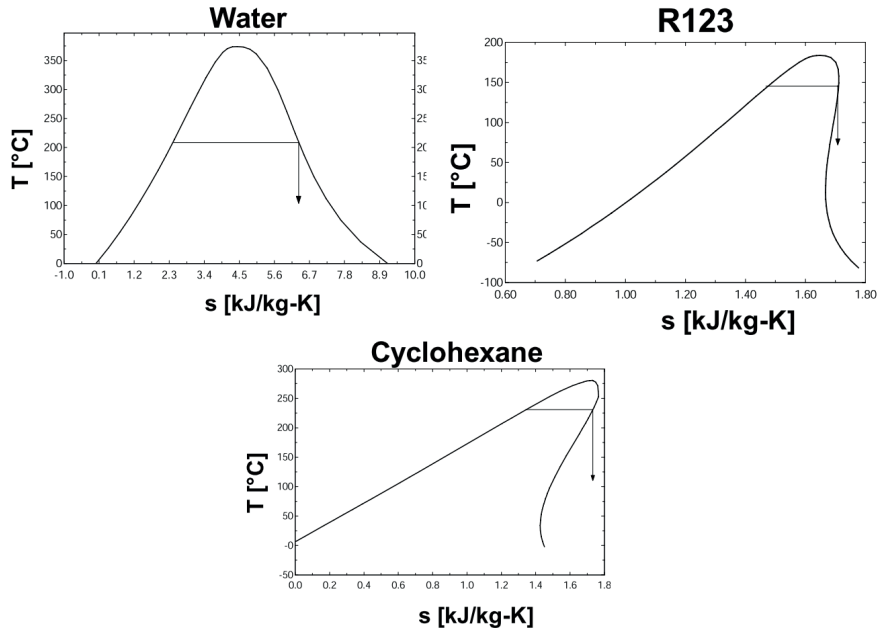


Figure 11: Examples of dry (cyclohexane), wet (water) and isentropic (R123) working fluids (Jorge Facão, 2009).

By changing the thermodynamic parameters of the cycle, the properties can be influenced. Heating the evaporated gas further, leads to a superheated turbine inlet, using a pump outlet/-turbine inlet pressure above the critical point will avoid the working fluid to go through the 2-phase-area, called supercritical cycle (Schuster et al., 2010). Figure 12 shows examples for the different cycles.

A Rankine cycle which uses an organic working fluid is consequently called *Organic Rankine Cycle (ORC)*. We use this term for cycles with or without superheating, for supercritical cycles (also called transcritical) and those with mixtures as working fluids.

ORCs can be applied in many different sectors such as the cogeneration in biomass combustion plant (Drescher and Brüggemann, 2007), in geothermal plants (Shengjun et al., 2011), with solar heat (Tchanche et al., 2009), as bottoming cycles in conventional power plants (Roy et al., 2010) and for internal combustion engines (Vaja and Gambarotta, 2010) which are forms of waste heat recovery or even in Ocean Thermal Energy Conversion (OTEC) (Uehara and Ikegami, 1990). Thus, the technology is quite mature and well documented as will be shown in chapter 4.

The broad range of possible working fluids that can be used in the Rankine cycle lead to an applicability in a large temperature range and thus ease the adaptation to different heat sources. Therefore, this technology is ideal for the use in waste heat recovery (Quoilin et al., 2011). The main focus is on organic fluids (ORCs) even though other fluids, like water and ammonia, will be considered in the identification of suitable cycles. The exhaustive list of all working fluids can be found in the tables A.1 to A.7 in appendix A. The integration of an ORC

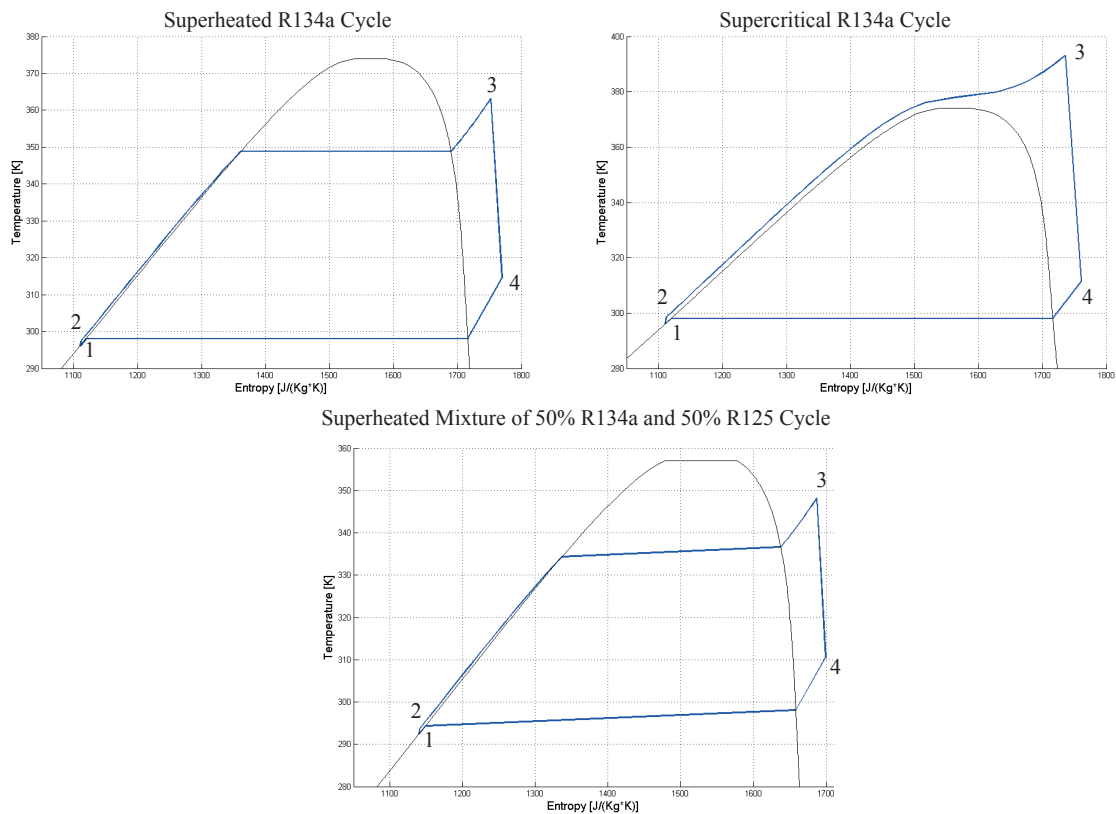


Figure 12: Temperature-entropy (T-s) diagram of different Rankine cycles.

into a process is shown in figure 13. The figure also shows how the ORC could be used, to drive a heat pump, thus decreasing the need for the hot utility.

The *Kalina cycle* has been much discussed, it shows higher theoretical efficiencies compared to ORCs in some applications by using a binary working fluid mixture of ammonia and water. This pronounced advantage has unfortunately not been observed yet in real installations and the reliability of the technology is questioned as well (DiPippo, 2004). The mentioned drawbacks might be due to the maturity of the ORC compared to the rather rarely installed Kalina cycle, we thus do not study this technology explicitly. However, the methodology we introduce applies to mixtures in the same way as to pure fluids.

The “LOVE” project

This thesis was written in the context of a European Framework 7 project entitled “LOW-temperature heat Valorisation towards Electricity production” (LOVE). The project was conducted by a consortium of eight partners, two with an academic background and six from industry. Goal of the LOVE project was to demonstrate how the energy efficiency of a process industry could be improved by converting low temperature waste heat (below 120 °C) into

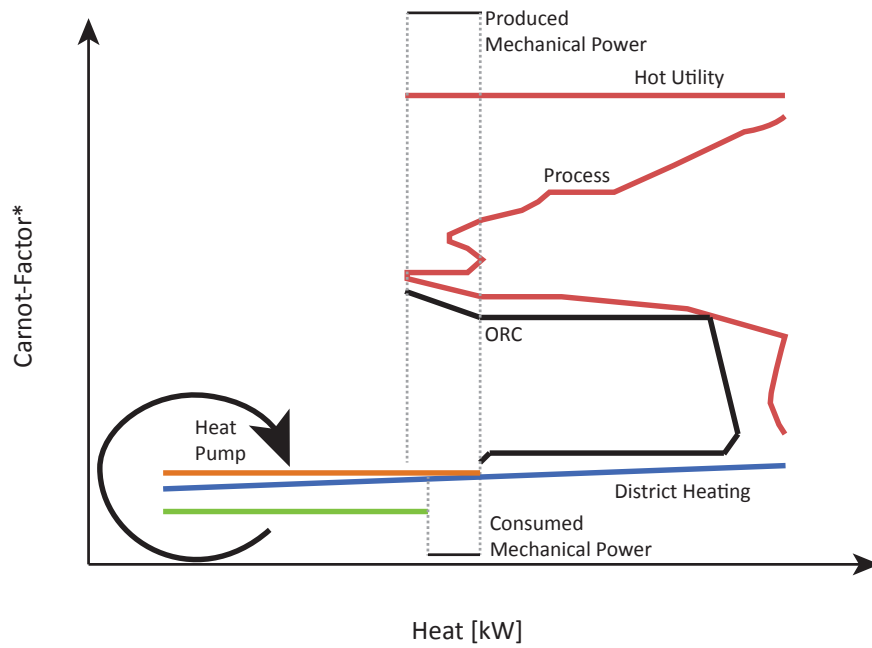


Figure 13: Integration of waste heat recovery with ORC, district heating and heat pump.

electricity. During the project two ORC demonstrators were built, installed and tested, in order to validate the technical feasibility of the waste heat conversion.

Outline of the thesis

Developing a methodology that allows identifying maximum electricity production with the help of Organic Rankine Cycles from the waste heat of an industrial process, at the lowest specific cost, without jeopardising the increase of the process's thermal efficiency.

In the above paragraph we summarised the topic of and motivation for this thesis. In order to reach these goals, a software tool which is able to identify the most suitable cycle for a heat source in regards to electricity produced and cost efficiency is developed and explained in detail. Before we can develop the tool we must identify the waste heat sources of industrial processes (which requires defining waste heat as such), in order to quantify the ORC potential. Additionally, we can benefit from the experience gained in the LOVE project in general and with the demonstrators in particular. The measurement data from the LOVE demonstrators is used to calibrate certain aspects of the tool. To this end, the data has to be prepared and analysed.

Hereafter, an overview of the thesis structure is given, stating the questions we try to answer and the conclusions we want to give in each chapter. At the beginning of each chapter we recall these points and then give an introduction to the topic under study. We can identify three main areas of research, the definition of waste heat, the analysis of experimental data with the help of data reconciliation and the identification of a suitable working fluid and operation parameters of an ORC. For every area, we include the state of the art in the respective chapters. Each chapter brings an additional element to the topic, resulting in the end into a novel global methodology. We close this thesis by recalling the main findings. The chapters of the thesis are:

Defining Waste Heat**Chapter 1**

Defining, identifying and quantifying the waste heat potential of an industrial process.

In this chapter, we see that multiple definitions of waste heat exist in literature, however most of them are implicit. It is pointed out that some authors consider waste heat simply as any cooling or hot matter stream leaving the process. Some definitions from literature have the notion of prioritising heat recovery within the process over implementing ORCs or other technologies. However, to the best of our knowledge, there is no methodology available defining qualitative as well as quantitative potentials. Thus, a method for identifying, characterising and quantifying the available waste heat of an industrial system that can be converted into a useful form is presented. A distinction is made between avoidable and

Introduction

unavoidable waste heat. The avoidable waste heat is the amount of waste heat that can be avoided if one implements heat recovery or heat revalorisation measures. This distinction is especially important when it comes to deciding on an investment for the integration of a waste heat valorisation process. Combined pinch analysis and exergy analysis is used to characterise the waste heat potential of a given process.

Waste Heat Recovery: Studies and Examples

Chapter 2

Studying waste heat potentials of the cement and the soluble instant coffee production processes, showing how different depth of studies and perspectives influence the result of the possible electricity production. Identifying the experiences from the LOVE demonstrators which can help building a more realistic ORC identification tool.

Based on two industrial processes, we study the identification of the waste heat recovery potential in a given system. Using the definition of the heat transfer requirement of the process unit operations, we analyse the heat recovery by heat exchange and the heat revalorisation techniques that can be used in the process and therefore define the waste heat production potential of the process. We show applications and studies which were conducted throughout the thesis. It will become clear how the constraints of each study influence the outcome of a waste heat recovery analysis. The studies illustrate how the increase in energy efficiency and degree of heat recovery and integration of a process can be contradictory to the production of electricity with ORCs. Additionally, we demonstrate in one example how the integration of a commercially available ORC can be improved using integration techniques and Pinch analysis. Eventually, the LOVE demonstrators are introduced and key learnings identified.

Waste Heat Valorisation System Characterisation

Chapter 3

Reconciling measurement data of the LOVE demonstrators with little redundancy, with the aim of characterising the performances of the tested Rankine cycles and identifying process unit parameters.

We introduce the concept of data reconciliation. It is needed for the measurements, collected from the LOVE demonstrators. Unfortunately, the measurements showed large incoherencies, which result from the difficult industrial environment prevailing in the cement industry. Turbulent gas flows, inhomogeneous temperature profiles and condensation on tube walls and thermocouples contributed to these incoherencies. Apart from “classical” data reconciliation,

we present a new method, by including the use of parameters as virtual measurements and the time dependency of measurements. This increases the redundancy of the system and thus the overall reliability. We analyse the methodology using an unbiased virtual set of stationary measurements of a simple heat exchanger. We then apply the methodology of reconciliation to the data measured during the LOVE project and gain thus valuable information which is used to calibrate the software tool used for the identification of suitable ORCs for a given heat source.

Suitable Cycle Identification

Chapter 4

Introducing a methodology allowing for any waste heat source, the identification of optimal Organic Rankine Cycles, regarding specific investment cost and the amount of electricity produced.

Recent publications show that the identification of suitable working fluids is in general done by considering a more or less small number of fluids and a predefined cycle configuration (single-stage, two stage, super or transcritical etc.). In chapter 4 we develop a methodology, capable of choosing the designpoint, a suitable working fluid and a cycle configuration, for the lowest specific investment cost while at the same time maximising the electricity output, for a given process environment. Qualitative and quantitative heuristic criteria such as Global Warming Potential (GWP) and Ozone Depletion Potential (ODP) are used to orientate the decision. The new methodology uses a genetic algorithm for the multi objective optimisation (master optimisation) and Mixed Integer Linear Programming (MILP) problem (slave optimisation) for sizing of the cycles. The crucial point of this methodology is the choice of the cycle configuration and working fluid within the MILP slave problem, thus reducing the quantity of decision variables used in the master problem (multi objective optimisation). The methodology is validated using examples from chapter 2.

Conclusion

Chapter 5

In the conclusions we present the strengths and weaknesses of the developed methodology and give some perspectives for future development.

1 Defining Waste Heat

After showing the context of this thesis, we will now look at the first procedure that is needed for the integration of organic Rankine cycles into industrial processes: The definition of waste heat and identification of the waste heat potential. This chapter is based on the paper Bendig et al. (2012), presented at the PRES conference 2012 and the paper Bendig et al. (2013).

The definition of waste heat is revealed to be complex. A suitable definition as resource and reserve, interesting for statisticians and stakeholders will be given. The recommendation to consider waste heat only after realising possible saving opportunities is introduced. This last recommendation is not only the key guideline throughout this thesis, it is also addressed to policy makers and industrials.

1.1 State of the Art

Cost savings, the conservation of fossil resources, the limited availability of renewable resources, restrictive legislation and considerations about the image of a company are the driving forces behind the development of more efficient processes. The importance of energy efficiency is obvious since it has not only been a major topic in energy research (Klemeš and Varbanov, 2012) but also been emphasised by economic and political actors. For example the International Energy Agency (IEA) foresees in the IEA 450 Scenario that more than 50 % of the CO_2 -abatement will result from energy efficiency (International Energy Agency, 2009b). One way to increase the value added per unit of energy spend is the use of waste heat to produce additional services like electricity or space heating. Figure 1.1 shows the representation of an industrial process in a general way, as a system converting raw materials into products and byproducts by the use of energy as a driving force. Increasing the efficiency would be equivalent to redirecting more of the vertical outlet streams into horizontal outlet streams.

“Waste heat” is a commonly used term in literature. Even though or because everybody has an idea of its meaning, formal definitions are scarce and most of the time insufficient. Synonymously used terms are “excess heat”, “residual heat”, “low grade heat” (Ammar et al.,

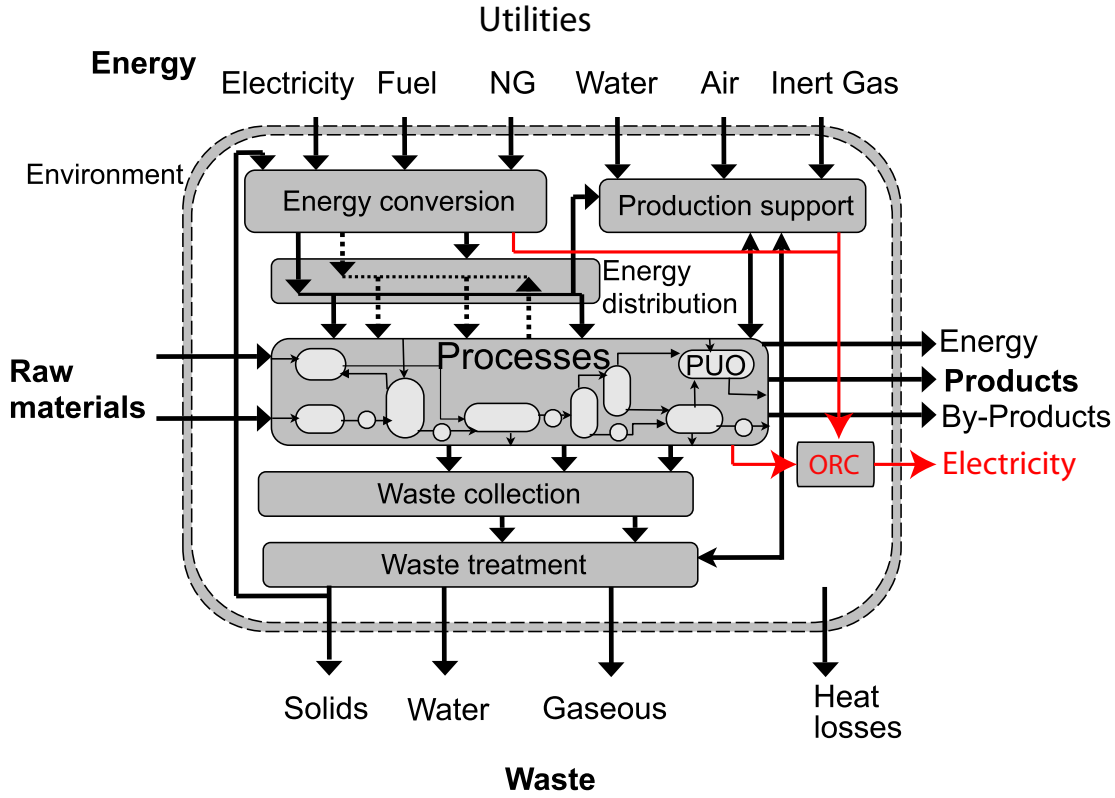


Figure 1.1: General representation of an industrial process with entering and leaving material and energy flows (modified after Maréchal and Kalitventzeff (1998)).

2012), “secondary heat” (Hnat and Coles, 1985) and in some cases “conversion losses” or more general “inefficiencies” (International Energy Agency, 2009b).

The majority of the literature (Goldstick and Thumann, 1986) and legislators (International Energy Agency, 2014c) define waste heat simply as heat dissipated to the environment, often regardless of its temperature and possible use and re-use. This simple analysis of a process in order to identify waste heat is strictly governed by the first law of thermodynamics and is based on the energy balance (the higher the input, the higher the output). Ammar et al. (2012) go a step further in their analysis, introducing a notion of usefulness within the process. They define low grade waste heat as the heat that is not usable for heat recovery within the process (temperature wise). This low grade waste heat is thus at a temperature T_{source} which is below the temperature $T_{\text{source,min}}$ marking the lowest economically viable heat recovery within the process. At the same time they set a lower limit to the low grade waste heat which is $T_{\text{sink}} + \Delta T_{\text{min}}$ (equation 1.1), where T_{sink} is the temperature of the heat sink (for example the environment) and ΔT_{min} is the minimum temperature difference needed in the heat exchangers to make a transfer into the heat sink feasible.

$$T_{\text{source,min}} > T_{\text{source}} > T_{\text{sink}} + \Delta T_{\text{min}} \quad (1.1)$$

This definition conveys the idea of heat recycling and thus process efficiency optimisation with a clear hierarchy:

1. Heat recycling within the process (reduction of resource consumption by re-use of available heat).
2. Heat recovery by a secondary process (delivering other useful services and thus by expanding the system boundaries).

Even though this definition is considering the heat recovery possibilities in the process, it does not take into account the quantity of heat available at different temperature levels. In the situation, where more heat is available at high temperatures than the process can recover, the opportunities for recovery in a secondary process of this (high temperature heat) would be missed. In other words, not all the heat at a temperature equal to or above $T_{\text{source,min}}$ can necessarily be used within the process since temperature is not the only criteria for heat recovery, there must also be a heat sink equivalent to the heat load. In cases where the available heat at high temperatures can be entirely used within the process the definition can however be correct regarding heat loads.

The above mentioned approaches ignore asking the question of the energy input into the system which would be a consistent way of applying the first law of thermodynamics.

Available Tools

The concept of *Pinch analysis* is introduced in the Introduction of this thesis and explained in detail in Linnhoff and Flower (1982) and Kemp (2011). It is a method to identify economically viable internal heat recovery within a process. It also allows to identify where to place heat pumps (Townsend and Linnhoff, 1983) and calculating their optimal integration (Becker et al., 2012). Pinch analysis helps as well with the introduction of heat exchanger networks (Linnhoff and Hindmarsh, 1983). Pinch analysis fills thus a gap that the above definitions of waste heat leave. Further, it identifies the minimum energy requirement of a process, which has to be delivered by heat sources; it also defines a minimum energy requirement for cooling/evacuation of heat, which could be understood as waste heat. These minimum energy requirements make it possible to distinguish between avoidable (not optimised) and unavoidable (occurs even if optimised) heat input and output.

Another method that has to be considered is exergy analysis (Szargut, 1979). It allows identifying exergy losses within a system and gives thus a tool for identifying the unit operations which lead to big losses. Many authors have worked on this concept to evaluate system performances (Marmolejo-Correa and Gundersen, 2012), to identify ways to reduce the losses in a system (Benali et al., 2012) and to use it as an objective function for energy optimisation problems (Gerber and Maréchal, 2012). Linnhoff and Dhole (1992) have combined exergy analysis with the introduction of Carnot composite curves. Applied to balanced composite curves, this can

be used to visualise heat exergy losses in the heat exchange system of a process (Maréchal and Favrat, 2005). Sorin and Rheault (2007) use exergy analysis for process intensification and Aspelund et al. (2007) extend Pinch analysis by the use of exergy analysis. Cziesla et al. (2006) uses the concept of avoidable and unavoidable exergy destruction. Studies exist, using the exergy concept for the integration of waste heat (Stijepovic and Linke, 2011). Also, a great number of studies using exergy analysis for integration of low temperature Organic Rankine Cycles (ORC) (Quoilin et al., 2011), generally however these studies implicitly define waste heat or consider it as "given" without any clear definition.

1.2 Objectives

Defining, identifying and quantifying the waste heat potential of an industrial process.

It can be seen from the literature that there are several partially overlapping definitions of waste heat that are deduced from the first law of thermodynamics (waste heat as heat "discharged to the environment"), or which take into account possible internal heat recovery within the process simply by comparing temperatures. However, there is need for a definition, which takes into account two considerations:

1. Distinguish between avoidable and unavoidable waste heat in order to avoid making investments in valorisation technologies (like ORC) with relatively low efficiencies, instead of making the process itself more efficient and thus reduce the fuel input.
2. Estimate the use that can be recovered from the waste heat.

This definition has to be done in a way that future improvements of a process are not inhibited by investments in waste heat recovery systems that might become obsolete by increasing the process' efficiency. Thus a methodology is needed to identify the potential of usable waste heat, pointing out economic commitments attached. The tools of Pinch analysis and process integration, especially the concept of maximum heat recovery which takes into account temperature levels as well as the heat balance, are at disposition in order to identify and quantify heat available in a process. In order to quantify the possible use of the energy and to extent the concept beyond the first law and Pinch analysis, the tools of exergy analysis are readily available.

Throughout this chapter, an example process will be used, in order to visualise different theoretical considerations, at the end of the chapter the findings are discussed and the definition for waste heat is proposed.

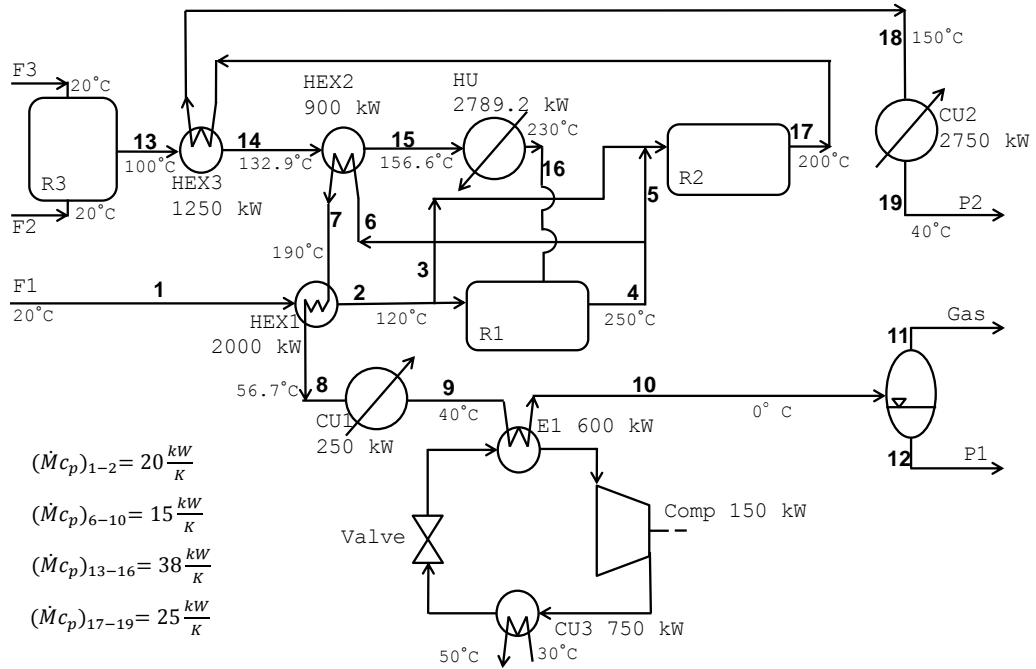


Figure 1.2: Example process, showing heat sinks and sources.

1.3 Finding the Waste Heat Potential

A simple process (figure 1.2), consists of three entering raw material feeds; Feed 1 (F1) is heated by internal heat exchange (HEX1) and then split into two parts. One part is entering reactor 1 (R1) (exothermal) while the other part is mixed with a part of the product from reactor 1 (R1) and conveyed to reactor 2 (R2) (endothermal). From reactor 2 (R2) comes product 2 (P2) which is cooled down, first by internal heat recovery (HEX3) then by a cold utility (CU2). The other part of the product from reactor 1 (R1) is a mixture of product 1 (P1) and gas (Gas), it is cooled down before leaving the system, the cooling is done by use of internal heat exchange (HEX2 and HEX1), a cold utility (CU1) (e.g. cooling water) and a refrigeration cycle (E1, Comp, CU3, Valve). Feed 2 (F2) and feed 3 (F3) are brought to reaction in reactor 3 (R3) (exothermal) and the product is heated up by internal heat recovery (HEX2) and a hot utility (HU) before entering reactor 1 (R1). We can identify three sources of heat, the heat released at the condenser (CU3) of the refrigeration cycle and the heat released between states 8 and 9 as well as between 18 and 19.

These sources add up to a total available heat of 3750 kW. The possible waste heat valorisation in a secondary process (such as the Organic Rankine Cycle) not only depends on the quantity of heat available, but also on the temperature at which it can be recovered. A measure for the

usefulness of heat is the extractable work or heat exergy \dot{E}_q^- (equation 1.2). The notations used here are those of Borel and Favrat (2010). The superscript + or - indicate that a value is positive when entering the system (+) or positive when leaving the system (-). \dot{E}_q^- is calculated for a heat exchange following the temperature-enthalpy profile from the inlet (in) temperature to the needed target (target) temperature of the heat requirement \dot{Q}^- for a given process unit.

$$\dot{E}_q^- = \int_{\text{in}}^{\text{target}} \left(1 - \frac{T_a}{T(\dot{Q})}\right) \delta \dot{Q}^- = \int_{\text{in}}^{\text{target}} \Theta(\dot{Q}) \delta \dot{Q}^- \quad (1.2)$$

with the Carnot factor Θ :

$$\Theta = 1 - \frac{T_a}{T} \quad (1.3)$$

where the index a indicates ambient condition.

If we look at the heat that is evacuated from the process in an end of pipe manner, the maximum extractable work from all heat sources (figure 1.2) could thus be measured with the heat exergy \dot{E}_q^- (equation 1.2). It can be graphically represented by the surface between a Carnot composite curve and the ambience temperature level ($\Theta = 0$). This is done by plotting the Carnot factor as a function of enthalpy (equation 1.3) as shown in figure 1.3. For the example process, the exergy potential represents 543.3 kW.

An investment into a secondary process to convert the work potential could be made. For example a Rankine cycles could be integrated with the hot streams and a cold source to produce mechanical power. Assuming upper energy conversion efficiencies, as can be seen in chapter 4, one can estimate the production of mechanical power \dot{E}_q^- as being around 60 % of the potential, here 326 kW_{el}. However, it is also possible to change the energy balance by doing additional heat recovery within the process, as can be seen from the flowsheet. Internal heat recovery will reduce the heat requirement of the process and will reduce the heat load of the cooling system by energy balance. This is called the "more in, more out" - principle (Townsend and Linnhoff, 1983). Both, the amount of remaining waste heat and its temperature levels will be affected. This means that internal heat recovery and the use of waste heat valorisation techniques are competing. This leads to two questions: How can the entire work potential be quantified and visualised (Section 1.3.1) and how can an analysis be made to systematically identify the minimum amount of waste heat (Section 1.3.2)?

1.3.1 Identifying the Work Potential

The process is divided into process unit operations (PUO), which are directly participating in the physical operations of the transformation of raw materials into (pre/by-) products on one hand and utilities which are delivering the necessary means (heat as a driving force and cooling) to the process operation units on the other hand. The PUOs can be distinguished

1.3. Finding the Waste Heat Potential

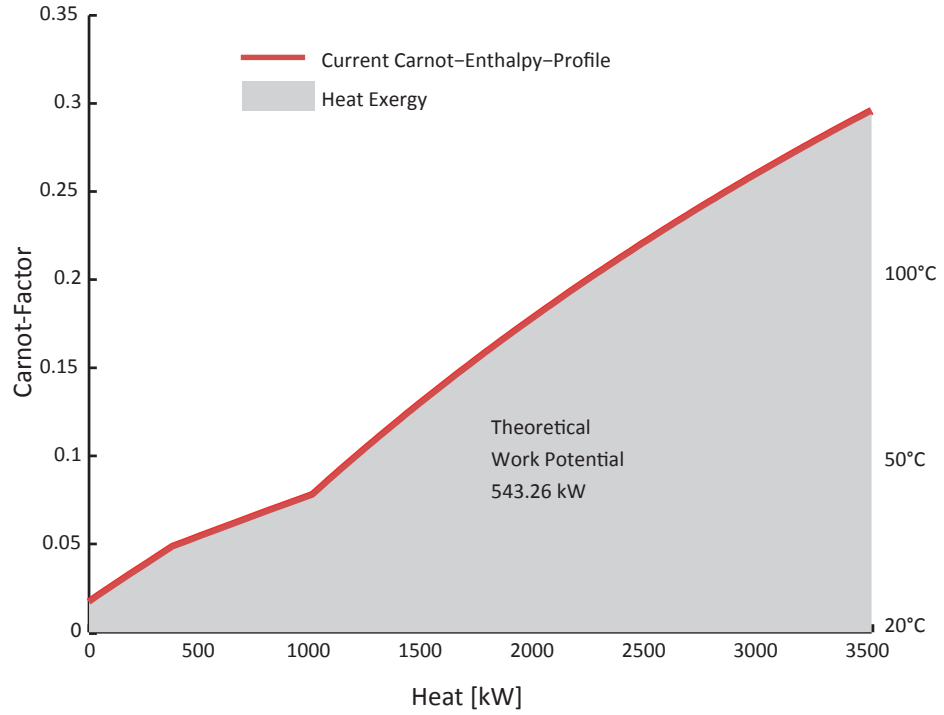


Figure 1.3: Work potential of the example process' (end of pipe) cooling requirements, in current configuration.

by their corresponding heat requirements: heat demanding units and units needing cooling. By analysing the PUOs on the flowsheet, one can define the heat transfer requirements that are needed to convert the raw materials (F1 to F3) into products (P1 and P2) and byproducts (Gas). One can distinguish between cooling requirements (6 to 10 and 17 to 19) and heating requirements (1 to 2 and 13 to 16). All cooling requirements above the ambient temperature ($\dot{Q}_{\text{heat sources}}^-$) can be assumed to be converted into work using the Carnot factor (equation 1.3). One can imagine this as a sequence of ideal Carnot cycles producing work ($\dot{E}_{\text{cooling}}^-$). In the same way, one can imagine the entire heating requirements above the ambient temperature ($\dot{Q}_{\text{heat sinks}}^+$) to be supplied by ideal heat pumping in Carnot cycles corresponding therefore to a work demand $\dot{E}_{\text{heating}}^+$ (equation 1.3). A special role is attributed to the streams below the ambient temperature since there the sign of the work potential is inversed. In order to evacuate heat ($\dot{Q}_{\text{heat sources},r}^-$) work has to be spent ($\dot{E}_{\text{cooling},r}^-$) and while heating a stream ($\dot{Q}_{\text{heat sinks},r}^+$) work ($\dot{E}_{\text{heating},r}^+$) is recoverable. This is schematically depicted in figure 1.4. The energy balance with the ambience of this system can be stated as the heat that has to be delivered or evacuated after adding all work and heat terms. The heat balance is shown in equation 1.4 and the work balance in equation 1.5.

$$\dot{Q}_{\text{ambience}}^+ = (\dot{Q}_{\text{in},r}^+ + \dot{E}_{\text{heating},r}^-) + (\dot{Q}_{\text{in}}^+ - \dot{E}_{\text{heating}}^+) - (\dot{Q}_{\text{out}}^- + \dot{E}_{\text{cooling},r}^+) - (\dot{Q}_{\text{out},r}^- - \dot{E}_{\text{cooling}}^-) \quad (1.4)$$

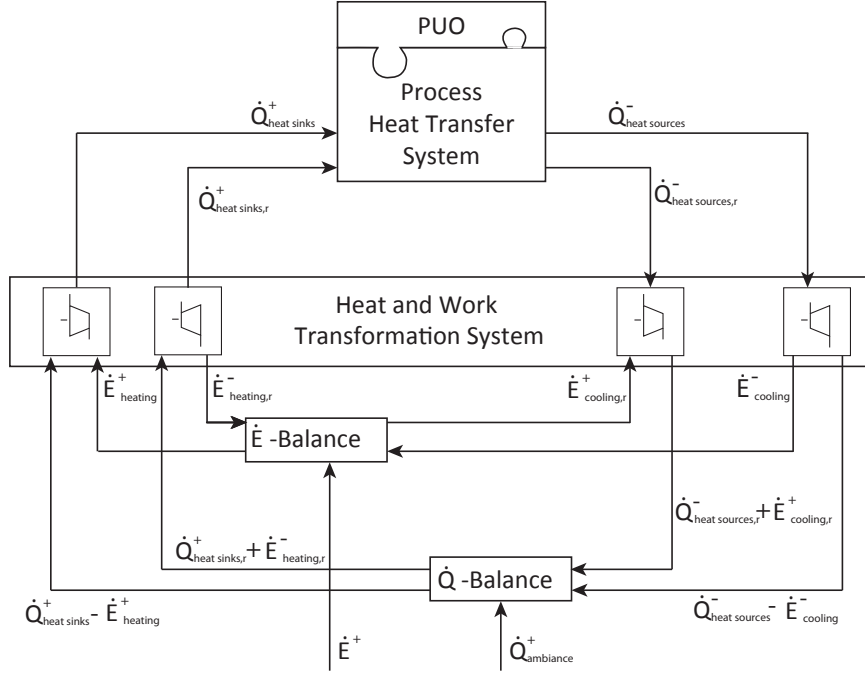


Figure 1.4: Schematic of theoretical heat and work flows with an ideal transformation system.

$$\dot{E}^+ = \dot{E}_{\text{heating}}^+ + \dot{E}_{\text{cooling},r}^+ - \dot{E}_{\text{heating},r}^- - \dot{E}_{\text{cooling}}^- \quad (1.5)$$

The exergy balance of the system streams indicates if the process is potentially a net producer or consumer of work (equation 1.6). It represents the work that can be gained by cooling the streams above the ambient temperature and heating the streams below with ideal Carnot cycles minus the work that has to be invested in ideal Carnot heat pumps to heat the streams above the ambient.

$$\dot{E}_{q,\text{balance}}^+ = \sum_{i=1}^{N_i} \int_{\text{in},i}^{\text{target},i} \Theta(\dot{Q}) \delta \dot{Q}_{\text{sink},i}^+ - \sum_{j=1}^{N_j} \int_{\text{in},j}^{\text{target},j} \Theta(\dot{Q}) \delta \dot{Q}_{\text{source},j}^- \quad (1.6)$$

Where N_i and N_j are the number of considered streams.

A process is exergy demanding due to the temperature differences within the heat exchangers, unless there is heat production in process units or entering or leaving feeds are not at ambient temperature. In the example process the exergy balance is 28.2 kW, which means that the process is overall exergy demanding. But, a positive balance does not necessarily mean that there is no exergy recovery possible, since other sources of exergy might be available. Borel

1.3. Finding the Waste Heat Potential

and Favrat (2010) define maximum work or exergy \dot{E}_{total}^- as the sum of all heat exergies \dot{E}_q^- all amounts of work and electricity \dot{E}^- and all transformation exergies \dot{E}_y^- (equation 1.7).

$$\dot{E}_{\text{total}}^- = \sum [\dot{E}^-] + \sum [\dot{E}_q^-] + \sum [\dot{E}_y^-] \quad (1.7)$$

The transformation exergy \dot{E}_y^- (equation 1.8) concerns all the exergy involved in changes to the material streams (pressure changes, chemical reactions etc.).

$$\dot{E}_y^- = \sum [k_{cz,j} \dot{m}_j^-] - \frac{dJ_{cz}}{dt} \quad (1.8)$$

Where the total specific coenthalpy (equation 1.9) is defined as:

$$k_{cz} = h_{cz} - T_a s. \quad (1.9)$$

The total specific enthalpy (equation 1.10), including enthalpy and entropy of formation is:

$$h_{cz} = u + \frac{\bar{C}^2}{2} + g\bar{Z} + \nu P. \quad (1.10)$$

Where \bar{Z} is the relative altitude and \bar{C} the absolute velocity. The total coenergy (equation 1.11) is defined as:

$$J_{cz} = U_{cz} + p_a V - T_a S. \quad (1.11)$$

Where U_{cz} is total internal energy, p_a the atmospheric pressure, V is volume and S entropy. Since it is a term of accumulation it is nul for stationary systems. Furthermore, we will not consider any exergy potential from the altitude or kinetic exergy.

It is thus possible to complete the above balance (equation 1.6) by adding the streams that correspond to the hot utility. The hot utility adds exergy to the system in the form of fuel (e.g. natural gas) and may consume electricity. A methane boiler with an efficiency of 95 % with reference to the heat of the hot utility demand is used in the example process.

Adding fuel and electricity input to the exergy balance, the total extractable work is calculated (equation 1.12):

$$\begin{aligned} \dot{E}_{q,\text{balance incl. hot utility}}^+ = & \sum_{i=1}^{Ni} \int_{\text{in},i}^{\text{target},i} \Theta(\dot{Q}) \delta \dot{Q}_{\text{sink},i}^+ - \sum_{j=1}^{Nj} \int_{\text{in},j}^{\text{target},j} \Theta(\dot{Q}) \delta \dot{Q}_{\text{source},j}^- \\ & - \Delta k_{\text{fuel}} \dot{M}_{\text{fuel}}^+ - \dot{E}_{\text{electricity}}^+ \end{aligned} \quad (1.12)$$

It is important to mention that the heat load of the cooling system is not identified as a work potential. Since it is released to the environment and has therefore lost all its exergy. A value of -3729.5 kW of ideally extractable work is obtained in the example process. The analysis made here is based on given process unit operations that are neither optimised regarding their

internal exergy losses, nor for internal heat recovery within the process. This analysis does therefore not give an indication on how avoidable waste heat can be avoided and where and how the work potential can be recovered. To resolve this we use the tools provided by Pinch analysis.

1.3.2 Application of Pinch Analysis in the Context of Waste Heat

Pinch analysis (Kemp, 2011) is a way to calculate the maximum heat recovery by counter current heat exchange within a process. This is conducted, such that the overall heat consumption of the process is minimal (Minimum Energy Requirement (MER)) using the heat transfer requirements of the process units (section 1.3.1). In Pinch analysis all hot and all cold streams are summed up to form the hot and cold composite curve, respectively.

We introduce the minimum temperature differences ΔT_{\min} between hot and cold streams for the heat exchanges. ΔT_{\min} depends on the heated and cooled fluids and on the thermodynamic states as well as the needed heat exchanger surface. Oftentimes, and thus also in this thesis, the corresponding $\Delta T_{\min}/2$ is directly added or subtracted to or from the respective stream temperature. Ideally, a specific $\Delta T_{k,\min}/2$ is attributed to each stream segment k , it is a function of the expected film heat transfer coefficient and the heat load in this segment (Marechal and Kalitventzeff, 2006; Bolliger et al., 2007). This leads to a corrected composite curve with the corrected temperatures (equation 1.13), marked by an asterisk as superscript (*) (Maréchal, 2010).

$$T_k^* = T_k \pm \Delta T_{k,\min}/2 \quad (1.13)$$

The correct choice of ΔT_{\min} is crucial since it represents a trade-off between the investment in heat exchanger surface and energy savings. It guarantees that an identified heat recovery will be economically viable. In the example process ΔT_{\min} is 5 K for an assumed set of economic conditions. The hot and cold composite curves in corrected temperatures are displayed in a temperature-enthalpy diagram, then the cold composite curve is slid horizontally along the enthalpy axis under the hot composite curve until the two curves touch. The point where they touch is called pinch point (see figure 1.5). It can be seen that the heat is cascaded from the hot utilities through the process.

In the example process the resulting minimum energy requirement is 789.2 kW which is 2000 kW or 71.7 % less than the current heat requirement and results in a reduction of the available (end of pipe) wasted heat by the same amount. In other words, by integrating heat recovery the amount of heat that can be used for secondary services has been reduced by 2000 kW in comparison to a strictly end of pipe perspective.

Before looking at waste heat conversion, further ways to increase the energy efficiency of the process can be explored. Other techniques of process integration show that introducing heat pumps, vapour recompression, pressurised condensers etc, can increase the heat recovery

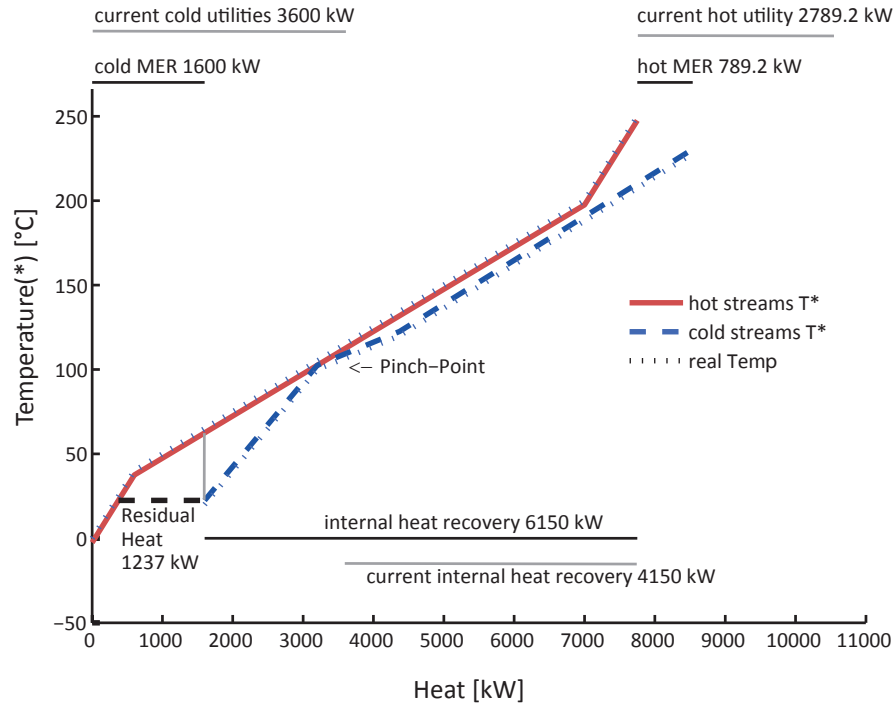


Figure 1.5: Corrected hot and cold composite curves of example process, with explanations.

and exergy efficiency by bringing streams from below to above the Pinch (Maréchal and Kalitventzeff, 1998). In the example process none of these options is viable. Examples for the application of the process integration methods are available e.g. for sites with heat pump integration (Becker et al., 2012) and for the agro-food industry (Muller et al., 2007). Such modifications can be understood as a (partial) redesign of the process.

1.3.3 Heat Released by a Process

The overall heat-release by a process can be characterised with the help of energy balances. The introduction of the heat cascade makes it possible to distinguish between *avoidable* and *residual* (unavoidable) heat above the ambient temperature. It is possible to add the heat to be evacuated by refrigeration, below the ambient temperature. The part below the ambient temperature will not be treated in detail in this publication.

Residual Heat

The use of the heat cascade allows identifying the maximum recoverable heat in an economically viable heat exchanger network and in consequence to deduce the amount of heat to be evacuated below the pinch point and above the ambient temperature. This requires the use of a cold utility above the ambient temperature (figure 1.5). The heat, with a positive Carnot factor which has to be evacuated will be called the residual heat. The temperature enthalpy

profile of the residual heat can be deduced from the grand composite curves in corrected temperatures as shown in figure 1.5. The residual heat can be used for any purpose without affecting the energy bill of the process. This is the unavoidable amount of waste heat that a process produces, in optimum heat recovery conditions. The residual heat is -1237 kW above ambient temperature with an exergetic value of 166.4 kW, in the example process.

Avoidable Waste Heat

All additional heat from the process, that is used for waste heat valorisation leads to an inefficient operation due to the “more in, more out”-principle. Which means that the additional heat is in fact the result of a surplus of heat input that has been spent in the process via the hot utilities. In the example the avoidable part corresponds to 66% of the original 2000 kW.

1.3.4 Global Exergy Balance

Combining Pinch analysis with the analysis of work potential as seen above in sections 1.3.1 and 1.3.2, makes it possible to identify the minimum global exergy that has to be evacuated from the process. This is done by adding the needed heat exergy of the Minimum Energy Requirement to the exergy balance (equation 1.6 modified with corrected temperatures).

$$\dot{E}_{q, \text{minimum global}}^+ = \sum_{i=1}^{N_i} \int_{\text{in}, i}^{\text{target}, i} \Theta^*(\dot{Q}) \delta \dot{Q}_{\text{heat sink}, i}^+ - \sum_{j=1}^{N_j} \int_{\text{in}, j}^{\text{target}, j} \Theta^*(\dot{Q}) \delta \dot{Q}_{\text{heat source}, j}^+ + \int_{\text{in}}^{\text{target}} \Theta^*(\dot{Q}) \delta \dot{Q}_{\text{MER-hot utility}}^+ \quad (1.14)$$

Graphically (figure 1.6) this can be represented by two surfaces equivalent to available exergy and two equivalent to exergy inputs. Applying this to the example process, the global exergy balance (equation 1.14) is -205.3 kW.

1.3.5 Heat Transfer Exergy Losses

The difference between the work potential from the residual heat and the total unavoidable work potential is the exergy destroyed in the heat exchange above the pinch point. This heat transfer exergy cannot be used without changing the energy balances of the system. The amount is graphically represented by the area between the hot and cold composite curves above the pinch point in the Carnot composite curve diagram (Maréchal and Favrat, 2005) (figure 1.6). It does not include the 3 kW exergy loss induced by the unavoidable ΔT_{\min} within

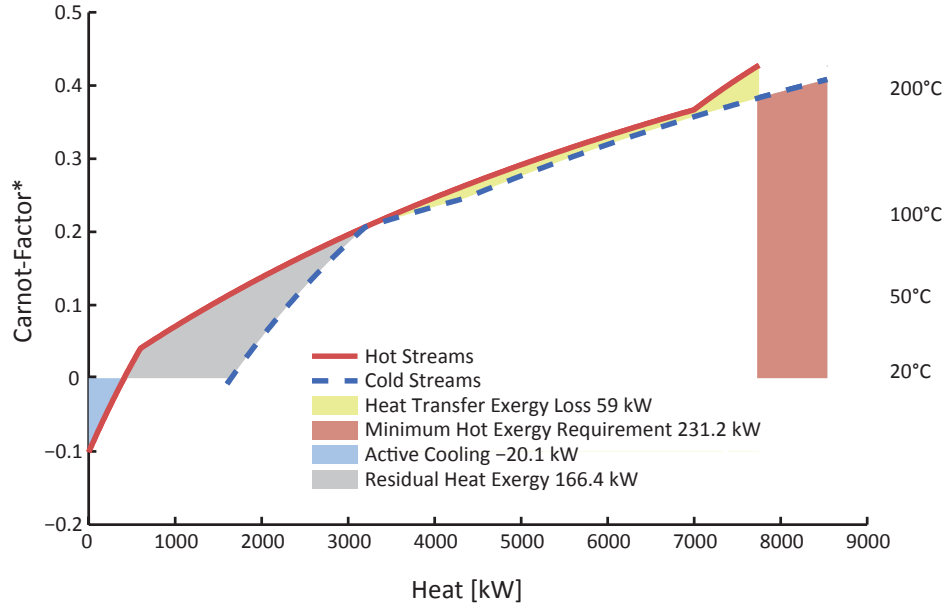


Figure 1.6: Corrected hot and cold Carnot composite curves of example process, showing interjacent and residual heat exergy.

the heat exchangers, since that is economically inaccessible. Mathematically the heat transfer exergy loss $\dot{L}_{\text{heat transfer}}$ can be expressed in equation 1.15.

$$\begin{aligned} \dot{L}_{\text{heat transfer}} = & \sum_{i=1}^{N_i} \int_{\text{in},i}^{\text{target},i} \Theta^*(\dot{Q}) \delta \dot{Q}_{\text{heat sink},i}^+ - \sum_{j=1}^{N_j} \int_{\text{in},j}^{\text{target},j} \Theta^*(\dot{Q}) \delta \dot{Q}_{\text{heat source},j}^- \\ & - \dot{E}_{\text{residual heat}}^+ - \dot{E}_{\text{cooling},r}^- \int_{\text{in}}^{\text{target}} \Theta^*(\dot{Q}) \delta \dot{Q}_{\text{MER-hot utility}}^+ \end{aligned} \quad (1.15)$$

In a simple heat exchanger network this exergy is unavoidably destroyed (Borel and Favrat, 2010) it represents -59 kW in the example process. Minimising the transfer losses, improves the overall efficiency of a system. The heat exergy loss is part of the waste exergy potential, even though it is no heat and can only be accessed by changing the energy balance of the system. Figure 1.6 illustrates the potential of the heat transfer exergy losses.

The accessibility of the exergy below the pinch point depends highly on the shape of the composite curve and the desired application. Exergy below the ambient temperature can be used as a heat sink e.g. for an ORC or for delivering cooling services for external users (e.g. air conditioning). Figure 1.7 shows the grand carnot composite curve corresponding to the composite curves in figure 1.6. The grand composite curve is useful for the integration of utilities. Grand composite curve means that the horizontal difference between the hot and cold composite curves ($\Delta \dot{Q}$) is plotted as a function of T^* . By replacing T^* with the corresponding Carnot factor Θ^* the grand carnot composite curve is drawn.

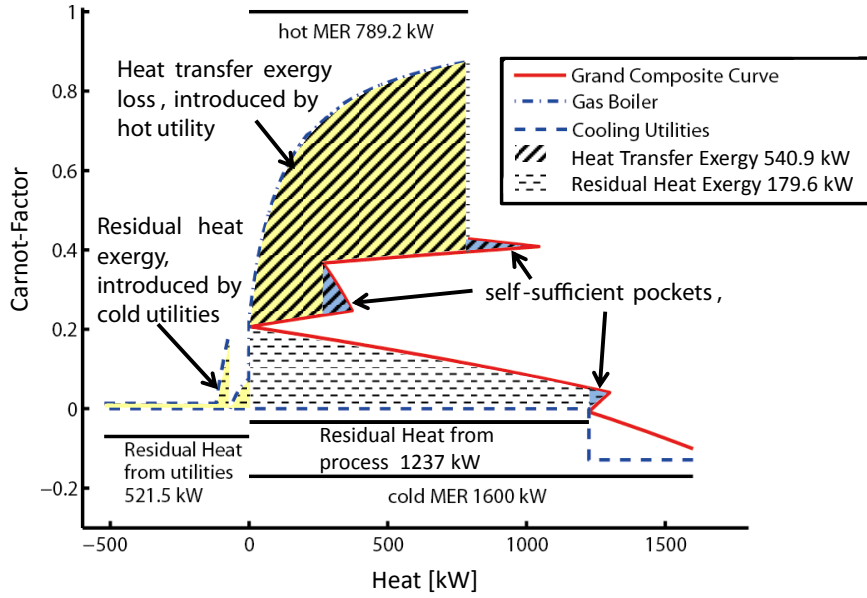


Figure 1.7: Corrected Carnot grand composite curve of example process with explanations.

1.3.6 Energy Conversion System Integration

A difficulty is the accessibility of the exergy potential, especially above the pinch point. A general rule can be stated: The heat transfer exergy loss above the lowest pinch point is not accessible without changing the energy balances. This is due to the fact that an additional amount of energy is taken out of the system above the Pinch if we use this exergy. Increasing the energy input above the pinch point is either achieved by importing energy from a resource or using heat available below the Pinch via a heat pump or pumping it from the environment. The integration of optimised utilities into the analysis is leading to a change in the potential of residual heat and heat transfer exergy losses. Therefore, the integration with utilities and heat recovery options has to be done simultaneously in order to find adapted solutions. Figure 1.7 illustrates this for the example process: a gas boiler is assumed as a hot utility and a refrigeration cycle (the same as shown in figure 1.1 using ammonia and with a compressor isentropic efficiency of 75 %) as well as cooling water are assumed as cold utilities.

If the boiler is assumed to burn methane and has an energetic efficiency of 95 % we can estimate the exergy input:

$$\begin{aligned} \dot{L}_{\text{combustion}} &= \Delta k_{\text{CH}_4}^0 \frac{MER}{0.95 \cdot \Delta h_{i, \text{CH}_4}^0} - \int_{\text{in}}^{\text{target}} \Theta(\dot{Q}) \delta \dot{Q}_{\text{combustion gases}}^- \\ &= 934.34 \text{ kW} - 583.04 \text{ kW} = 351.3 \text{ kW} \end{aligned} \quad (1.16)$$

Where $\underline{\Delta}h_{i,\text{CH}_4}^0$ is the isobaric and mass specific lower heating value and $\underline{\Delta}k_{\text{CH}_4}^0$ is the isobaric and mass specific exergy value of methane (Borel and Favrat, 2010).

The transformation exergy lost in the hot utilities (due to chemical reactions) is -351.3 kW and the internal heat exergy losses within the process and between process and utilities is -540.9 kW . It can be seen that the use of a heat pump around the pinch point would give access to a large potential of additional exergy above the pinch point or allows reducing the combustible input. Further improvements could be the use cogeneration to additionally produce electricity from the exergy above the pinch point.

1.4 Changing the Global Energy Balance

As mentioned above, it can be difficult to exploit an exergy potential which is trapped in place where not enough or no energy can be extracted. This can happen in three cases, when the exergy is above the pinch point (a), when it is in between two pinch points (b), when it is in a large exergy pocket, but the residual heat is not sufficient to exploit the potential (almost activation of second pinch point) (c). In these cases the energy balance must be modified by adding more energy. This can be done for example by including a cogeneration unit, increasing the existing hot utility or by adding an additional heat pump. If and how it is done depends on the economic viability of the options. Figure 1.8 illustrates the three cases (a) to (c) and shows an example of the integration of a heat pump in order to access the exergy in an exergy (or self-sufficient) pocket. If an ORC is integrated into the self-sufficient pocket (from case (c)), the heat from the condenser and cooler is not sufficient to satisfy the heat requirements of the process. In order to use the full exergy potential in the ORC, it is necessary to satisfy the heating requirements, for example with a heat pump. The heat pump uses heat from the process (at lower temperature) and from the environment.

1.5 Other Sources of Exergy from an Industrial Process

During this analysis the regard has turned from the concentration on sensible heat towards the recovery of work potential or exergy from a process. Since in this thesis we will look at waste heat, we will focus on the heat exergy below the pinch point. But for completeness, there are other exergy sources that can be considered for efficiency improvement or electricity generation. These are for example pressure drops within the process operation units which may be avoidable but also all physical streams that leave the process not in equilibrium with the ambience and still have an above ambient pressure, or a chemical exergy potential. Especially streams which are chemically valuable can often be used as secondary fuels. The International Energy Agency (2007) estimates the potential of primary energy savings due to the use of these waste streams to be between 1.5 EJ and 2.3 EJ per year. Also, the choice of the system boundaries of the process has a major influence on the integration: the larger the

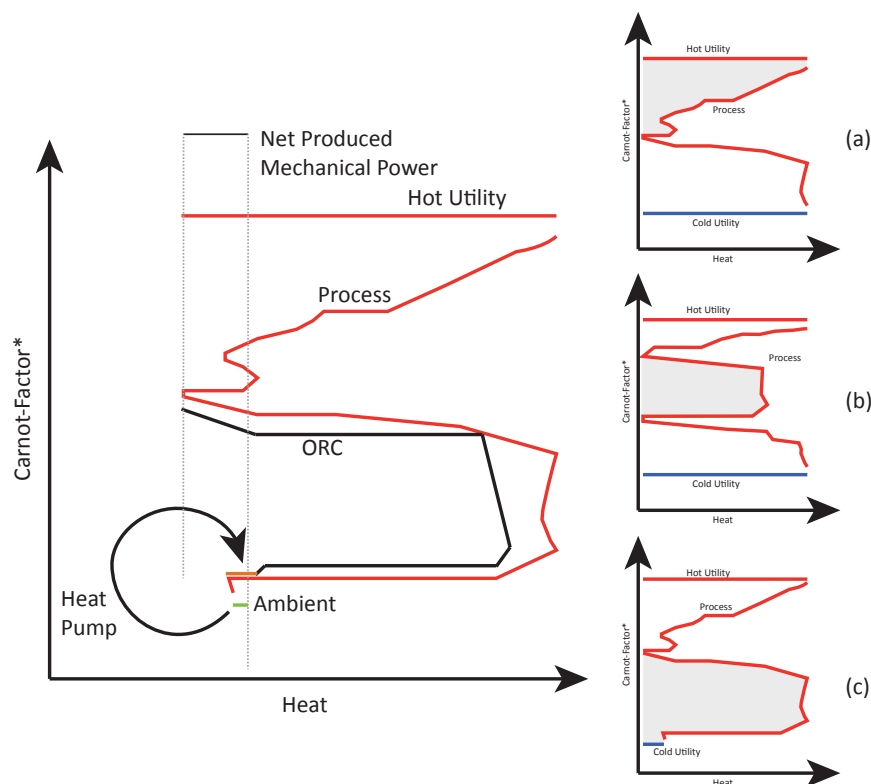


Figure 1.8: Exergy that can be accessed only by changing the energy balance: (a) above the pinch point, (b) in between pinch points, (c) in a large exergy pocket.

system boundaries are chosen, the higher the potential for integration measures and thus the smaller is the amount of actual unavoidable waste heat (Brown et al., 2005).

1.6 Definition of Waste Heat as Reserve and Resource

With these considerations we are able to give a definition on waste heat in analogy to other energy vectors, such as coal or gas:

Reserve: Waste heat as a reserve is the net exergy that unavoidably leaves a process or is lost within it, after its integration, minus the exergy that cannot be recovered for technical or economic reasons.

Resource: Waste heat as a resource is exergy that unavoidably leaves a process or is lost within it independent of the technological choices made within the process.

The waste heat reserve is thus defined in respect to the constraints of the used technology and economic aspects while the waste heat resource is a theoretical potential. With changing

energy prices, the results of the process integration change; the values are also influenced by evolving technologies. That means that both values may change. This is another analogy since natural reserves and resources are subject to changes due to changing prices, additional exploration and evolution of exploitation techniques.

1.7 Discussion

In this chapter we developed a methodology for the definition of waste heat, which combines different approaches and principles.

From the simple definition "Waste heat is heat released to the environment" we deduce the principle: "Maximise the use of heat leaving the process ($\dot{Q}_{\text{process,out}}^-$)".

From Pinch analysis and process integration we convert the principle of "minimising the heat input ($\dot{Q}_{\text{process,in}}^+$)" to "minimising the energy input and maximising the internal heat recovery which results into the minimisation of the heat release to the environment".

With Exergy analysis we are able to characterise the exergy values attached to physical streams and in consequence the exergy lost and destroyed (\dot{E}_{loss}) within the energy conversion systems and the heat recovery in the process.

Combining these concepts, we propose to maximise the use of the exergy value of energy leaving the system ($\dot{E}_{\text{process,out}}^-$) while minimising the total exergy losses (\dot{E}_{loss}) by a better integration or redesign of the energy conversion system within economic constraints.

The example process which is used for illustration shows a waste heat release of 3750 kW with an exergetic value of 543.3 kW following the first simple definition of (end of pipe) waste heat. When defining waste heat following the proposed definition, including heat recovery and energy conversion (reducing the need for hot and cold utilities by 2000 kW each), the available heat is 1758.5 kW and the exergy available is 1074.8 kW. Among this exergy 179.6 kW are available below the pinch point and above ambient temperature therefore they represent the exergetic value of the residual heat (1758.5 kW see figure 1.7). 351.3 kW is the amount of exergy lost in the combustion and would require changing the chemical path of the fuel (e.g. use of fuel cell) to be accessible. The remaining 540.9 kW of exergy lost above the pinch point can only be accessed by changing the energy conversion system and therefore the overall energy balances. 3 kW of exergy are unavoidably destroyed due to the ΔT_{min} assumption economically required for the heat recovery system.

1.8 Conclusion

During the analysis we saw that Waste Heat is not simply the amount of heat that a process releases to the environment in its current design. We advocate a use of the term Waste Heat in a thoughtful way, in respect to the real potential of extractable work. We point out

the difference between avoidable and unavoidable waste heat. The avoidable waste heat should not be used for a secondary application, in order not to block investments into energy efficiency. We define waste heat as the sum of the exergy that is available in a process after pinch analysis, economically viable heat recovery, process integration and energy conversion (utility) integration with the help of exergy analysis. This definition leads to different results for the waste heat potential of a process, depending on the economic environment. Also it requires a deep understanding of the process and process integration techniques. However, it prevents any investment in secondary processes before being sure that available heat is not better used within the process. For statisticians, the definition as reserve and resource maybe applicable (especially in combination with existing best available techniques (BAT) as proposed by the IEA (International Energy Agency, 2007)). For policy makers, a definition, requiring an in-depth analysis of heat recovery possibilities may be interesting, if a programme for supporting or subsidising ORC for waste heat recovery is made. This way it can be avoided to subsidise the inefficient use of resources (fuel) in a process (leading to a high amount of waste heat), but rather push for process efficiency measures first. For industry it is important to be aware that an investment into an ORC might block the improvement of the process itself and should be done after careful consideration of heat saving opportunities.

It is shown that a certain part of the exergy is not available due to ΔT_{\min} in the heat exchanges and that the use of the biggest parts of the exergy (from the hot utilities) is accessible by either adding heat from the environment via heat pumping or by use of additional fuel/combustibles.

This definition gives a tool for engineers to quantify rigorously the potential for waste heat recovery within their process and being able to distinguish between avoidable and unavoidable waste heat. With this definition it is possible to situate a conducted analysis of a process: Were only the end of pipe sources of heat considered? Was the possible internal heat recovery included in the analysis (integration)? Were possibilities for modifications to the process or the utilities considered (redesign)? For use in this thesis, we will concentrate on the potential that is below the pinch point and does not need the modification of the overall energy balances (addition of fuel or electricity for heat pumping).

2 Waste Heat Recovery: Studies and Examples

After discussing the theoretical aspects of the definition of *waste heat* we take a closer look at how this can be applied to problems and examples from industry and experimental installations which were studied throughout the thesis.

This chapter illustrates how the recommendation to apply heat integration before considering the use of ORCs impacts the available waste heat potential.

2.1 Objectives

Studying waste heat potentials of the cement and the soluble instant coffee production processes, showing how different depth of studies and perspectives influence the result of the possible electricity production. Identifying the experiences from the LOVE demonstrators which can help building a more realistic ORC identification tool.

The depth of a waste heat analysis and its constraints have a big influence on the recoverable waste heat potential that is identified. We study how the increase of energy efficiency of the process itself will influence the possible electricity generation. We show this by identifying the work potential of the residual heat (below the pinch point). In one example we study if and how Pinch analysis can help to identify a suitable commercial ORC and how it should be installed. Further, we analyse the LOVE demonstrators and the experiences we can gain from them in order to improve the methodology for identification of a suitable ORC for a given process.

2.2 Structure

The analyses show that industrial and practical requirements and constraints lead to a bouquet of types of studies all with a different perspective. For an easier understanding we will

distinguish between three approaches in order of increasing depth and complexity when it comes to the identification and use of Waste Heat:

- *End of Pipe Heat Recovery*

Using the “end of pipe heat” that is rejected by a process in its current state can help identify the *theoretical work potential* of the cooling requirements without modifying the process itself. This can lead to the use of avoidable waste heat. It is, however, the approach that is most commonly used for the identification of waste heat potentials due to its lower degree of complexity and ease of implementation as can be seen in chapter 1. Three examples will be used for illustration. Two examples are taken from the *cement industry* and one is a study that was conducted in the context of this thesis in a plant producing *soluble instant coffee*. All three have the same type of analysis in common, the end of pipe sources of residual heat are analysed and their potential for the delivery of additional services is quantified. The instant coffee process has been analysed further and integration of the process as well as partial redesign will be discussed. The cement process has been analysed from different angles and theoretical integration and partial redesign will also be discussed, based on a model.

- *Integration into Existing Plants*

The integration of waste heat recovery technologies in an existing plant allows to access exergy pockets below the pinch point. It makes a pinch analysis necessary and reveals potential for internal heat recovery. With this analysis is made sure that the possibilities for heat recovery within the process are realised before the heat is used for secondary purposes. Therefore, only unavoidable waste heat is used. However the process must be studied in detail and all heating and cooling requirements identified.

- *Redesign*

This is a scenario tool in order to see where a development could go. Process modifications are studied and the utility system can be adapted to access exergy above the pinch point or between pinch points. In the studies presented here, we see that the industrial processes show lower potential for waste heat use. However, the energy input is decreased, if it is integrated or partially redesigned. The redesign of a process with the goal of minimising the heat input is not an evident procedure. It is to be understood as a tool to evaluate where the limits of integration including the modification of process unit operations might be. It is not to be understood as a clear indication on how to build the process, unless all economic, security and reliability issues are included in the analysis. With this approach, the instant coffee process is presented including the measures that resulted from the study conducted in collaboration with Nestlé. The cement process, based on a representative process model, with loosened technological constraints is studied to reveal a possible limit of waste heat recovery.

For each of these approaches one or more examples will be shown, coming either from theoretical considerations or from the experiences made with and in industry throughout the thesis.

2.3 Soluble Coffee

A study on a Nestlé process for the production of soluble instant coffee (Nescafé) was conducted in preparation of this work. One goal of the study was to identify possible energy savings, another goal was to reveal the waste heat potential that could be used for electricity production. The study was conducted in close collaboration with two engineers from Nestlé, every step and measure was discussed, modified and re-checked in a feedback loop until a satisfactory result was found. This feedback loop was crucial for the implementation, since it made sure that realistic and applicable results were produced, and more importantly that the measures had supporters from within the plant and process staff. Due to confidentiality concerns, not every detail of the study will be disclosed in this thesis. The process that is presented here, is situated at a site with several other processes and a central utility system delivering the heating and cooling services. This means that a total site integration (Pouransari et al., 2014) or a total site analysis (Maréchal and Kalitventzeff, 1998) would be the best way to identify savings and possible interactions between the processes (Brown et al., 2005). An example of a chemical cluster can be found in Hackl et al. (2010, 2011) and a resulting possibility for using the heat in a district heating network in Morandin et al. (2014). In this case, however, the analysis only focussed on the process under discussion, this is due to the fact that other processes on site were planned to be exchanged, modernised or stopped without a fix schedule, thus leaving their future energy profile unknown. This leads to a situation where a modification of the utility system regarding temperatures and energy vectors is not sensible in the immediate future.

As a result of the analysis several energy saving measures with a better practice approach, could be realised within a short time horizon. Other measures requiring installations and modifications to the process were realised after the necessary planning and engineering period. More projects are in the pipeline. Another interesting point, regarding these savings, is the possibility to use the same measures in other Nescafé plants of the same type. This reduces the necessary engineering and risk (since the measures have been tested) and multiplies the impact of the conducted study. In this chapter we will show some of the larger end of pipe sources of heat that were found before the study was conducted.

2.3.1 Soluble Instant Coffee – Process-Description

The production of soluble instant coffee starts with the roasting of the coffee beans, a step in which the raw beans are heated, to dry them and then heated further to temperatures from 170 to 230 °C (Illy and Viani, 2005) undergoing the reactions needed in order to make the wanted coffee (Yeretzian et al., 2002). Afterwards the beans are rapidly cooled down, to stop

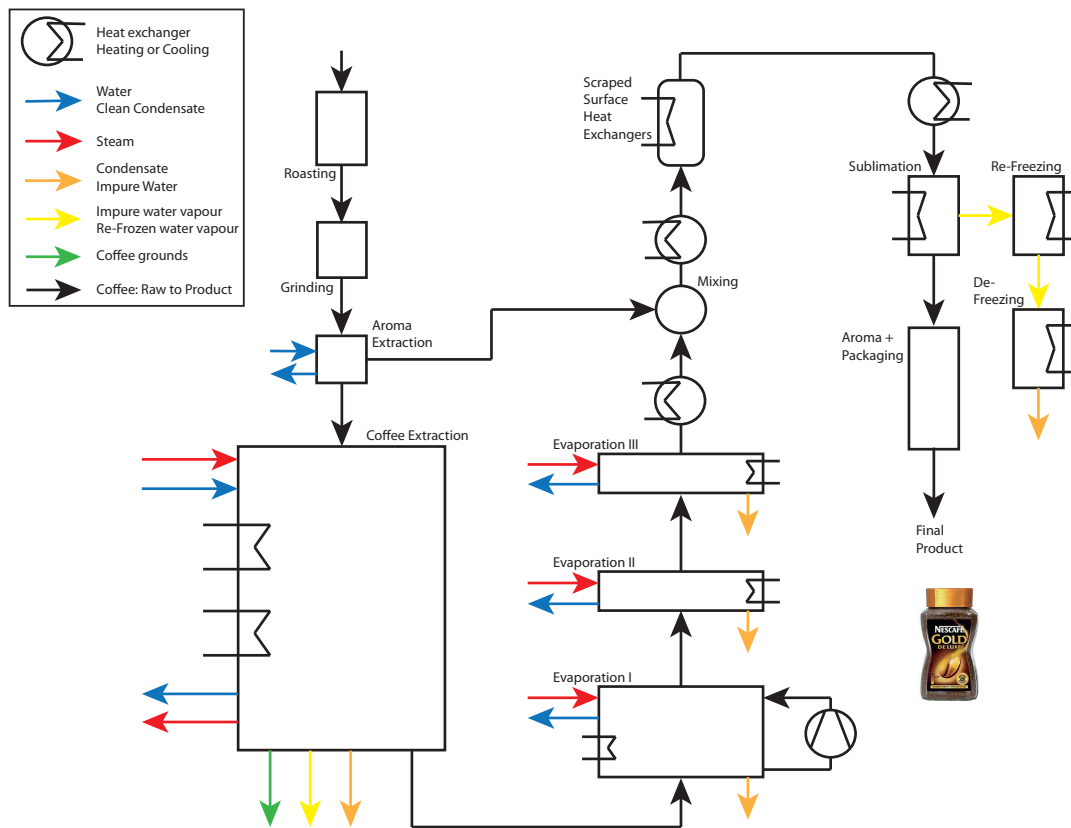


Figure 2.1: Schema of the instant coffee process.

the reactions. From there the beans are transported to the mill and ground to powder. In the following stage the most volatile aromas are separated, these will be reapplied to the finished instant coffee. After this the ground roast coffee is mixed with recirculated water from the coffee extraction process. The coffee extraction process consists of numerous steps, making heating and cooling as well as the addition of liquid water and steam necessary. Several mass flows leave the process: clean and impure water and steam, condensate, coffee grounds and as a product coffee solved in water. An efficient extraction is not only important for the taste of the final product, it is also crucial for the cost effectiveness of the plant, since the extraction defines the raw bean input to product ratio.

The resulting coffee has a higher solid content than coffee for direct consumption. In order to reduce the water content further, the coffee then undergoes three steps of evaporation, from which the first evaporates the largest amount of water. The first step reduces the mass flow rate to approximately 25 % and is (partially) equipped with mechanical vapour recompression (MVR). The other two steps are (partially) using steam ejectors and reduce the steam to about 10 % of the initial mass flow rate.

The resulting coffee concentrate is cooled down, mixed with a part of the prior extracted aromas and cooled further close to the freezing temperature. At this temperature it enters

the scraped surface heat exchangers which produce a partially liquid partially frozen slurry. Then the freeze drying itself is conducted, first the slurry is frozen completely, afterwards the water is sublimated (using heat) in a vacuum, leaving behind the dry instant coffee which is afterwards processed for packaging. The “cold” steam from the sublimation is refrozen on a cooling surface which is then de-iced allowing the condensate/melted liquid to be evacuated. The process is shown schematically in figure 2.1

A detailed thermal model was prepared with the measurements and estimations from the process. It considers over 130 heating and cooling requirements from the different process unit operations. It was checked with measurements from the process. Since the site contains several other processes, a clear attribution of the fuel consumption is not possible due to missing measurements. However, the application of saving measures had the expected results. The model can thus be seen as validated. This model was used in order to identify the potential for energy savings as well as the units and places, which have to be modified in order to realise them. We have normalised the heat represented in this chapter for confidentiality reasons. The normalisation is done with regard to the end of pipe residual heat.

2.3.2 End of Pipe Heat Recovery

The end of pipe heat sources, which were identified by the process staff, are mainly from two origins. The first is the roasting process which produces hot gases with up to 350 °C. It originates in the combustion of natural gas, used for heating and drying the beans. The gases are then vented to the environment. The other heat source is the so called *bubble tank*. During the coffee extraction, a stream of water vapour is generated which can carry impurities, thus it can not be re-cycled into the steam network. This steam can vary in temperature and pressure and is poured into an open water tank, which at the same time regulates the pressure, reduces the temperature and cleans the stream. The tank produces, however, considerable amounts of wet air. Since the biggest part of the steam is condensed within the tank and the tank is at atmospheric pressure we consider it as a heat source at exactly 100 °C.

In addition to these two large heat sources, several smaller ones at lower temperatures could be used as well. The temperature enthalpy profile of the end of pipe heat is shown in figure 2.2. We can estimate that from the 100 percent of this available heat about 15.8 % could be recovered in the form of electricity, shown in figure 2.3, if we apply the rule of thumb that 60 % of the *heat exergy* can be transformed to electricity. The temperatures of up to 350 °C are also interesting for recovery. It is however obvious that 80 % of the heat is available at or below 100 °C.

2.3.3 Integration

With the measurements from the process we have build a thermal representation of the entire instant coffee making. All heating and cooling requirements have been mapped regarding their temperature and enthalpy. We have corrected each temperature by adding a $\Delta T_{k,min}/2$

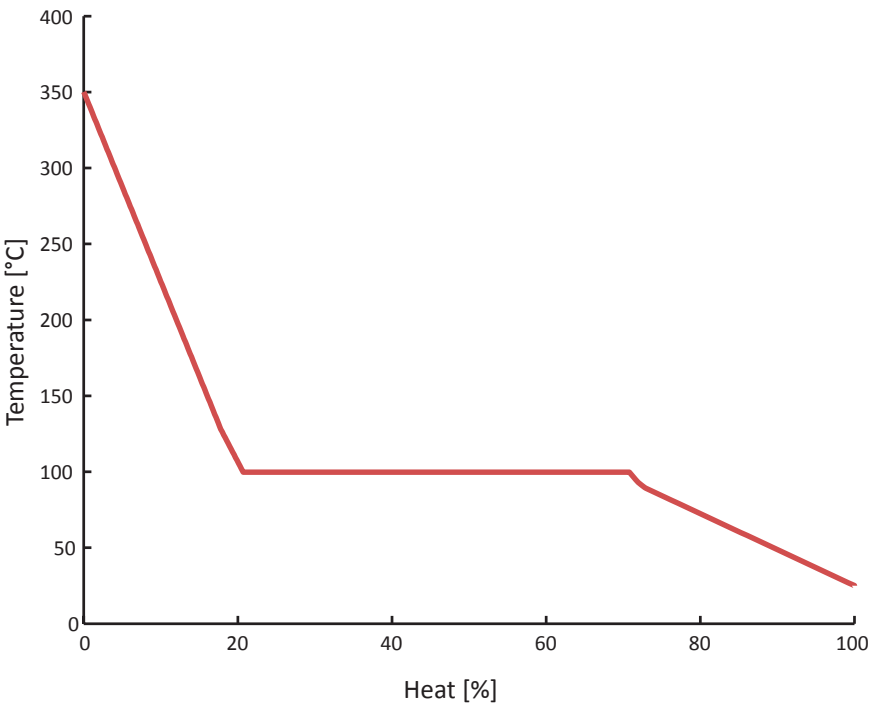


Figure 2.2: Heat temperature profile of end of pipe residual heat in the instant coffee process, normalised.

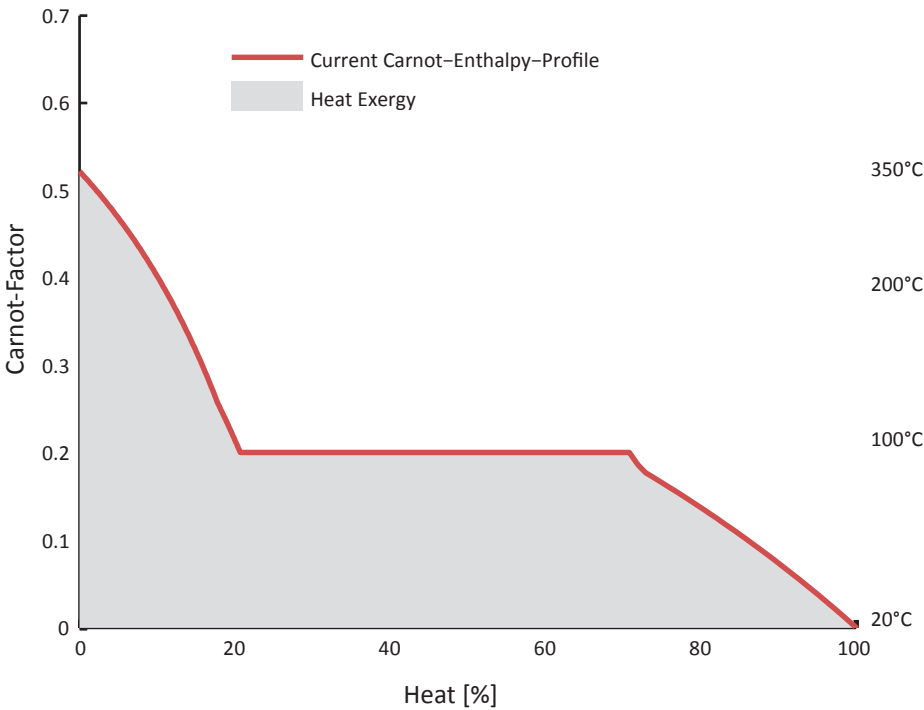


Figure 2.3: Heat exergy of end of pipe residual heat in the instant coffee process, normalised.

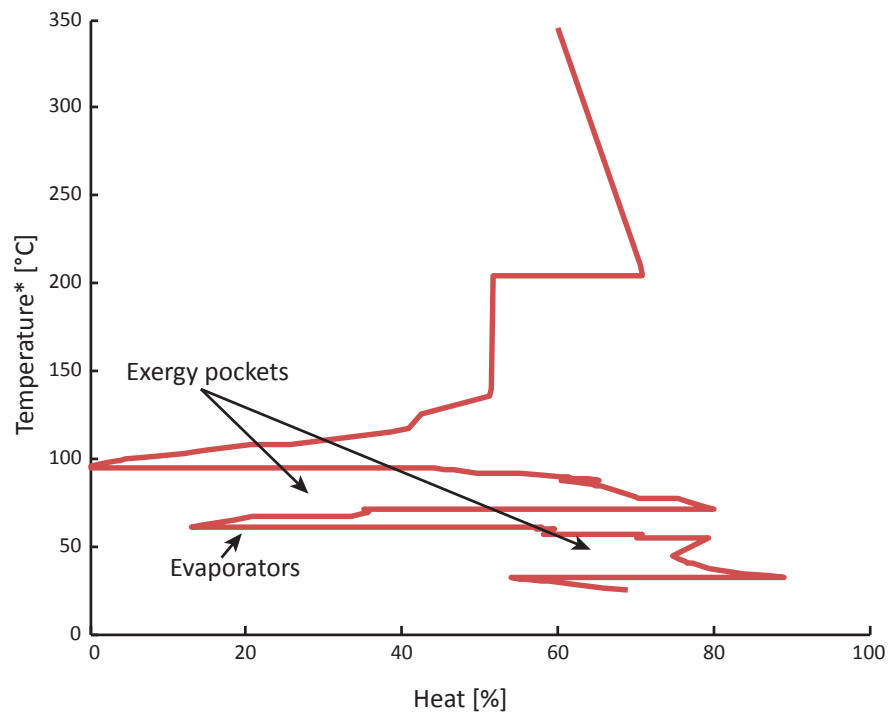


Figure 2.4: Grand composite curve of the instant coffee process, without sub atmospheric parts, normalised.

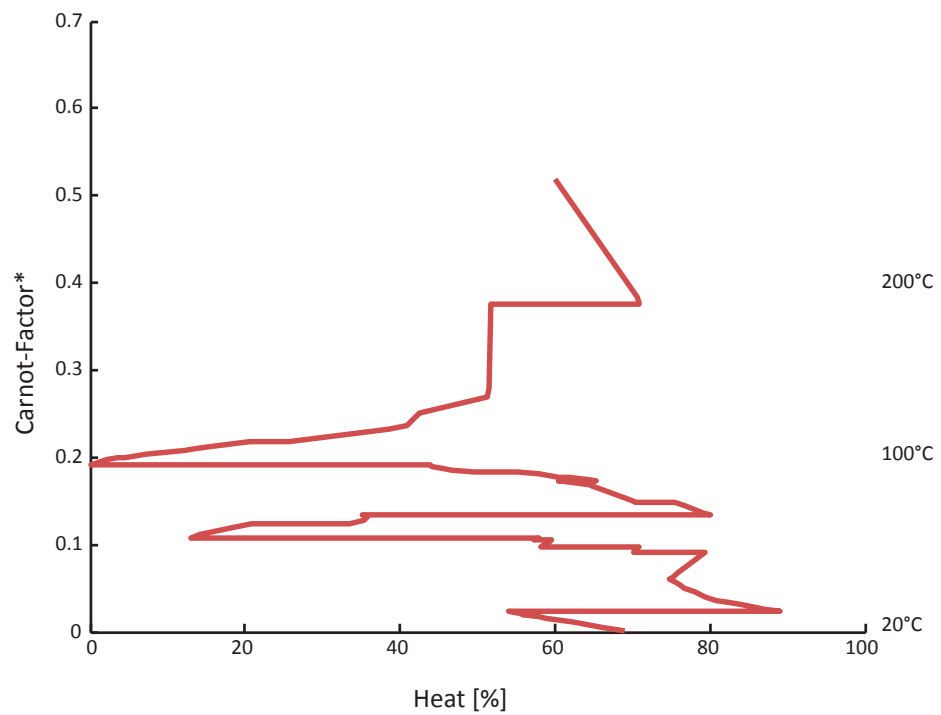


Figure 2.5: Carnot grand composite curve of the instant coffee process, without sub atmospheric parts, normalised.

(as described in equation 1.13), representing a realistic heat exchange for each stream (k). Only 69 % of the heat that was available, in the end of pipe study, is available after integration. The evaporation units, which work below atmospheric pressure, can be seen. They do not create a pinch point in this situation, because the mechanical vapour re-compression (MVR) system is over designed, with regard to a situation with complete internal heat recovery (shown in the grand composite curve, figure 2.4). If the heat for evaporation was delivered from within the process, the MVR could be smaller. The cooling requirements below ambient temperatures have been removed from the graphs, since they do not influence the potential for waste heat recovery directly. (The refrigeration cycles have a condensation level close to ambient temperature.) Without the MVR, the evaporation and condensation plateaus of the evaporators would define the pinch point. In the represented situation however the pinch point is slightly below 100 °C and we can see that the hot gases from the roasting process are not available for the use of an ORC. The heat should rather be reused within the process, reducing the heat input from the steam network and thus the overall fuel consumption. An exergy pocket is situated between the bubble tank and the evaporators, but since the temperature difference is below 30 K and at temperatures below 100 °C the exergy content is relatively small. Overall for 100 kW of residual heat evacuated, 11.7 kW of heat exergy are available (figure 2.5). Given the low temperature of the available heat that could be used for secondary services and the difficult accessibility in the exergy pockets, the production of electricity would have a very low efficiency. Direct use of the heat in a low temperature district heating network would be a better possibility.

2.3.4 Redesign

For the instant coffee production, an analysis of all process parts was conducted with the goal to identify energy saving potentials, which can be realised by modifications to the process, but without impacting the product. An additional constraint was introduced regarding the hot gases from roasting. These will not be available as a heat source, anymore. The reason being that another project at Nestlé had started during our cooperation in which a boiler was developed, using the hot gases from the roaster to produce steam that can be injected into the steam network. This project was done to reduce the fuel input into the sites boilers and could be understood as a way of process intensification.

A major modification is introduced, regarding the way the steam is treated, which was formerly condensed in the bubble tank. Instead of condensing in one open tank, two additional pressurised vessels are introduced. The steam is condensed at the temperatures corresponding to the pressure in the tanks. Steam and condensate are separated in a flash unit, before entering the next step (second pressurised vessel or open bubble tank respectively). These pressurised vessels (and some other modifications) allow a reduction of the overall heat input by over 20 % points as compared to the integrated situation discussed in section 2.3.4 (which is itself an improvement on the situation of the process before the study). However, the absence of the heat from the roasting introduces additional hot utility. Therefore, the overall amount

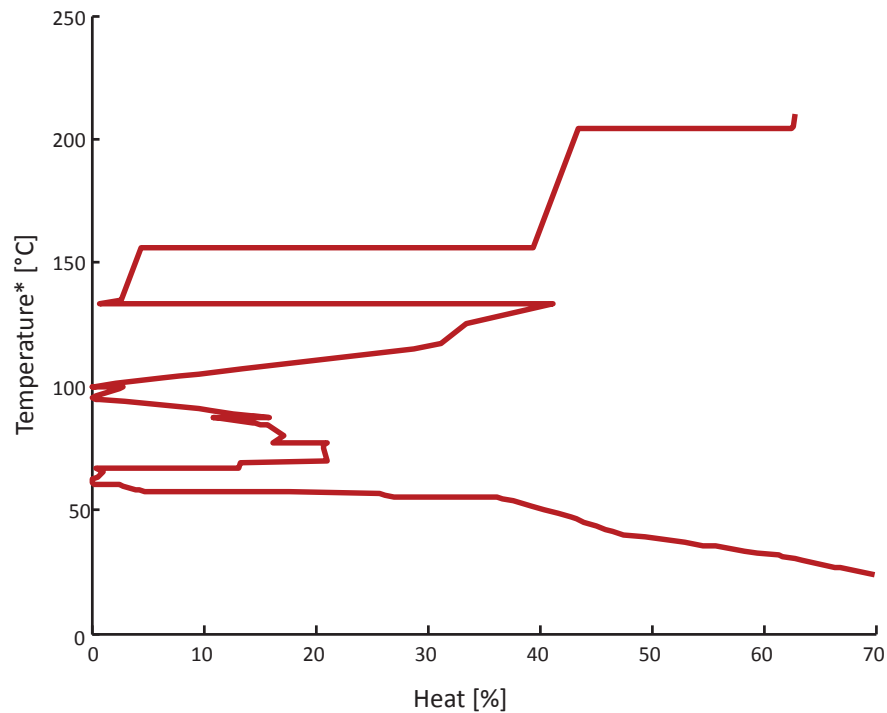


Figure 2.6: Grand composite curve of the redesigned instant coffee process, without sub atmospheric parts and without torrefaction, normalised.

of residual heat is about 70 % of the amount found in the end of pipe situation. Another major modification is the introduction of additional mechanical vapour recompression in the evaporation units. It is done to the exact extent as to activate a new pinch point. It should be noted, that not all measures proposed in the study have been applied yet and the ones that were realised have been partially modified. This was done, in order to respect constraints that were not included in this analysis (space availability, the time window for modifications, annual maintenance period etc.).

The resulting grand composite curve of this analysis including major process modifications is shown in figure 2.6. The fact that several pinch points are activated shows the degree of integration that is reached. As shown in chapter 1 the use of exergy in pockets between two pinch points as well as exergy above the highest pinch point is only possible by the addition of energy from utilities meaning by the input of additional fuel. As we have seen in the case of the integrated process, the potential for electricity production is limited by the low available temperatures and direct use of the heat for example in a district heating network should be considered. The Carnot grand composite curve (figure 2.7) shows the heat exergy potential which is less than 5.7 kW per 100 kW of heat that has to be extracted. The entire heat that was available above the lowest pinch point is reused within the process, at an efficiency of (nearly) one hundred percent. In other words, using the end of pipe heat as waste heat would have come at the cost of achieved energy savings, which were achieved by integration and partial redesign. The next step in integrating the process could be the integration of three heat pumps

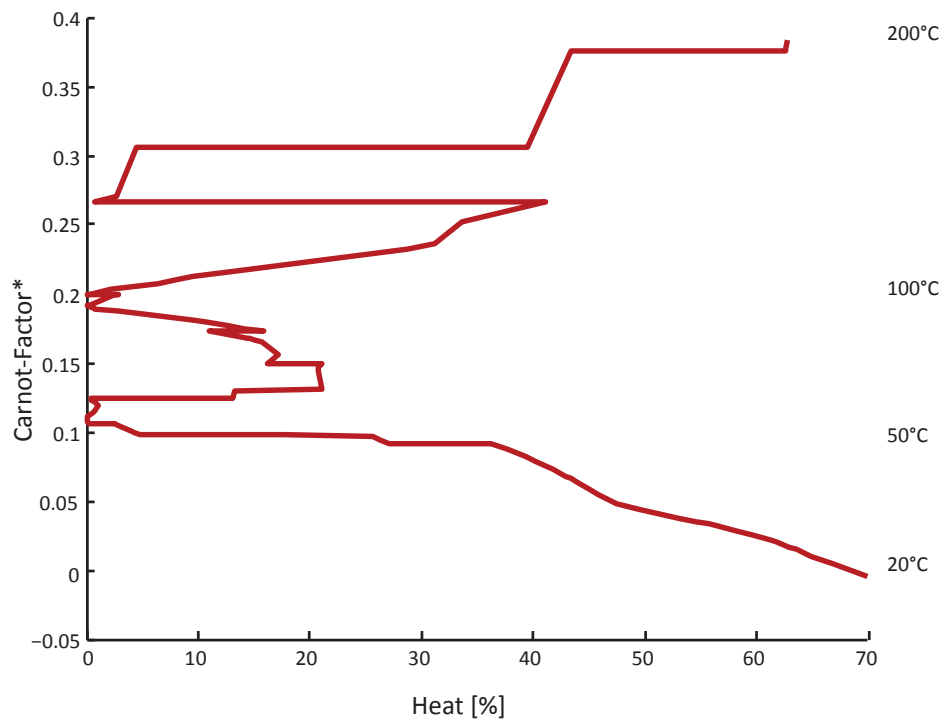


Figure 2.7: Grand composite curve of the redesigned instant coffee process, without sub atmospheric parts and without torrefaction, normalised.

around the three pinch points. If all three are activated, the minimum energy requirement could be decreased further. However, this option was not economically viable.

2.4 Cement

The Cement process is one of the processes regularly cited (Engin and Ari, 2005; Worrell et al., 2001) when it comes to waste heat, this is due to the high temperatures that can be found in the process mass streams and the order of magnitude of the mass flow rates and thus the order of magnitude of the enthalpy flow rates. Hot gases leave the process at several points, sometimes at high temperatures, and several installations with waste heat recovery and valorisation via Rankine Cycles exist in the world (Karellas et al., 2013).

2.4.1 Cement – Process-Description

The Cement-Industry has undergone great changes in the last century (Hewlett, 2004). During this time major technology shifts have increased the quality and the capacity of the process, while simultaneously greatly reducing its energy consumption. The industrial production of cement started with the introduction of the bee hive kiln which was strictly run in a batch process (Hewlett, 2004). Passing by the wet, semi-dry and finally resulting in the dry process, cement production was made continuous. Today only a few wet and semi-dry plants are still running. Here only the dry process will be considered as it is by far predominant in Europe.

The dry process started out with a relatively simple rotating kiln, and evolved due to the introduction of cyclone preheaters and precalciners over the last 50 years (Hewlett, 2004; Bendig et al., 2014a). One reason to install waste heat recovery in cement plants is the availability: apart from a few weeks of maintenance, a cement plant is running 24 hours /day and 7 days /week and also the distribution of plants in the world is wide, since cement is relatively expensive to transport for a price per tonne which is low.

The Cement making process is depicted in figure 2.8 and the general description is based on the sources Worrell et al. (2001); Hewlett (2004); International Energy Agency (2009a); Peray (1986, 1979); Sprung (2000) and CENTRE and Bureau (2013). Cement plants are typically erected near deposits of calcareous materials (limestone, marl, chalk) containing high concentrations of calcium carbonate ($CaCO_3$). The material is extracted in a quarry, crushed, transported to the cement plant and ground. Oftentimes during crushing and grinding it is mixed with additional materials containing iron (-oxide) (Fe_2O_3), alumina (Al_2O_3) and silica (SiO_2) to precisely adjust the chemical composition and form the so called *raw meal*. Sources of these additional materials may also be the combustibles (like tyres which contain iron).

In general the raw mill is build in a way that hot gasses coming from the preheating tower are used to dry and start heating the raw meal. The hot gases from the mill are filtered and send to a stack. The solids enter the preheating tower from the top. The tower consists of a series of cyclones in which the raw meal is in direct contact with hot gases from the kiln. The heat exchange is in pseudo counter flow, since the raw meal is transported from the top to the bottom cyclone while the gases enter at the bottom and leave the preheating tower at the top, depending on the plant, they are piped to the raw mill and/or directly to the filters and stack.

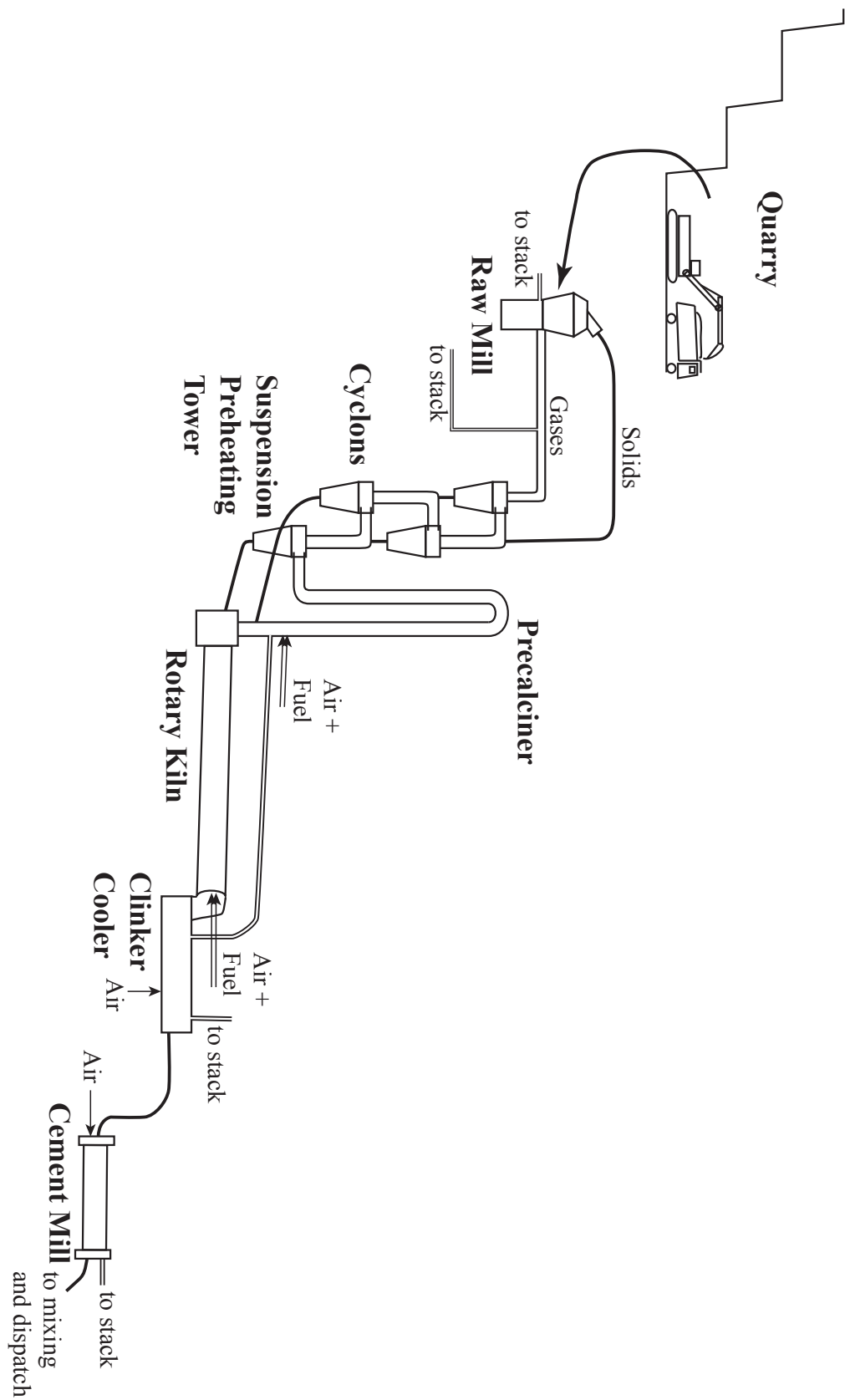


Figure 2.8: Simplified schematic of the cement process.

In Europe there are typically four or five stages of cyclones while some big plants in Asia and Oceania can have more stages of cyclones, depending on the humidity of the raw materials.

The more modern (or often modernised) cement plants are equipped with a precalciner. This process unit is placed in between the last two cyclone stages and is equipped with a burner/combustion chamber. As the name states, up to 90 % of the calcination (reaction $\text{CaCO}_3 \rightarrow \text{CaO} + \text{CO}_2$) takes place in the precalciner.

After leaving the preheating tower's last cyclone stage, the hot meal enters a rotary kiln in which the remaining calcination and the actual clinker burning is taking place. The rotary kiln is fired from the opposite side of the raw meal inlet, but there might be additional fuel input together with the meal, for larger combustibles (e.g. tyres). The solids have to reach a temperature of 1450 °C in the kiln, in order for the clinkerization reactions (and melting processes) to take place. The flame and gas temperatures are considerably higher. The entire rotating kiln is inclined towards the clinker outlet and the material is transported towards the outlet and mixed due to the turning movement.

At the outlet of the kiln the clinker falls onto the clinker cooler (in modern processes it is a grate cooler) and is cooled down, quickly at first and then slower. This is achieved by blowing air from below through the grates. A part of that heated air directly enters the kiln (where it is needed as a source of oxygen for the combustion), a part is conducted to the precalciner, if one is installed, and the rest (called *mid air* and/or *end air*) is sent, first to a filter then to a stack and vented into the environment.

The cooled down clinker is stored and depending on the dispatch, blended with gypsum (sometimes also slags, fly ashes, pozzolanas or other materials), ground and blended. The grinding takes place in the cement mill, which is typically a ball mill. To control the temperature and humidity, water can be sprayed during the grinding. Hot air is produced during this process due to the mechanical friction and impacts as well as remaining heat in the clinker. This hot air is filtered and vented to the environment.

2.4.2 End of Pipe Heat Recovery

There are four major streams of hot gas, which are leaving the system after being filtered. They could be recovered at the outlet of the raw mill, the preheating tower, the cement mill and the clinker cooler. Depending on the specific plant, they can vary in temperature and mass flow rate.

Representative Process

We have build a model to study possibilities for heat recovery and will describe it in the following. If needed a more detailed description can be found in Mian (2012) as well as Mian

et al. (2013) and Bendig et al. (2014a). All concerned heating and cooling requirements are also listed in appendix B. The thermal energy consumption of the representative process is $3.1 \text{ GJ} / t_{\text{clk}}$ which corresponds well to the consumption found in literature (Worrell et al., 2001), the model can thus be seen as validated.

The model was designed to show a representative modern cement process as it can be found in Europe. It was developed in collaboration with experts of HOLCIM AG and CEMEX SAB. The following units are part of the model:

- *Raw Mill*

In the raw mill, the raw material coming from the quarries and silos enters at an assumed humidity of 3 % (mass) at an ambient temperature of 25 °C. The raw meal leaves the mill with humidity of 0.1 % (mass) and at a temperature of 50 °C. The gases coming from the suspension preheating tower with 30.8 % (molar) of CO_2 and a humidity of 6.1 % (molar) at a temperature of 390 °C heat and dry the raw meal.

- *Suspension Preheater/Cyclones*

At the top of the 4 cyclones the raw meal enters at 50 °C and “falls” through the cyclones in contact with the gas in counter flow. The meal passes the precalciner before entering the last cyclone at 850 °C. The gases coming from the precalciner enter in the second cyclone from the bottom at 880 °C and with a CO_2 concentration of 31.5 % (molar) and leave at the top cyclone at 390 °C, with a CO_2 concentration of 31.6 % (molar).

- *Precalciner*

In the precalciner the raw meal enters at 626 °C and is heated up until the calcination reaction takes place, calcining 92 % of the meal. To simplify, we assume that the calcination happens at a constant temperature of 850 °C. The meal leaves the precalciner at 850 °C and enters the bottom cyclone of the preheating tower. The gases that enter the precalciner coming from the kiln have a temperature of 850 °C. Additionally air coming from the clinker cooler at about 1050 °C and slightly heated ambient air at 60 °C are added. Additional fuel is used for combustion.

- *Kiln*

In the kiln, the precalcinated hot meal coming from the preheating tower and precalciner enters at 850 °C and a calcination rate of 92 %. Within the kiln (which has a diameter of about 6 m) the meal is mixed and heated while the kiln is turning. (With the meal, secondary fuels can be injected, often spent or unsafe tires.) At the other end of the kiln the primary burner injects fuel and ambient combustion air at about 40 °C. Air from the clinker cooler enters through the clinker outlet at about 1000 °C. Within the kiln, the gases and solids move in counter flow. The gases reach a temperature of 2000 °C in the burning zone and the solids are heated up to about 1450 °C, thus the clinkerisation reactions take place.

- *Clinker Cooler*

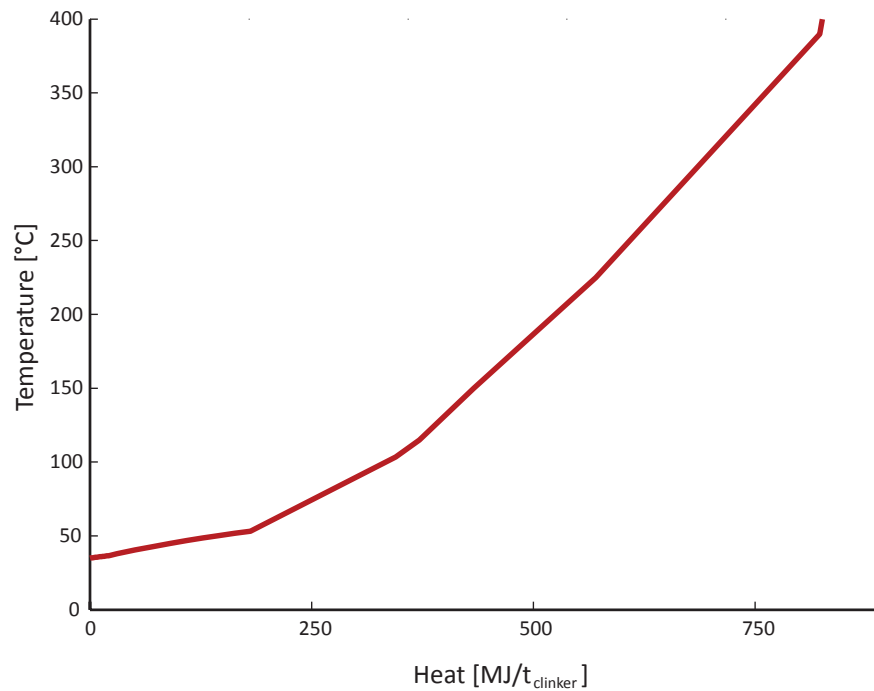


Figure 2.9: End of pipe heat sources of the cement process.

The clinker falling out of the kiln at about 1450 °C enters the grate clinker cooler. Cooling air is blown from below through the grates, cooling the clinker quickly, the air is then extracted in zones. The hottest part of it goes directly into the kiln and a second fraction is piped to the precalciner, the rest leaves the cooler at temperatures of 225 °C and 400 °C. The clinker leaves the clinker cooler at 100 °C.

- *Cement/Clinker Mill* In the cement mill, the clinker is ground into a powder. Depending on the mode of operation the clinker enters cold or with remaining heat from the kiln. There is a high production of heat stemming from friction due to the grinding process in this ball mill. Water may be injected for temperature and quality control. A stream of humid air leaves the mill with a temperature of 115 °C.

- *Auxiliaries*

The auxiliaries are other units that include hot or cold streams of minor importance.

All mechanisms that include large quantities of heat are either within these units or within their input and output streams.

With the help of this model we can calculate the end of pipe heat sources. The gas compositions, the temperatures, mass flow rates and the enthalpy that could be gained by cooling the streams down to 35 °C are listed in table 2.1. The index *clk* stands for *clinker*.

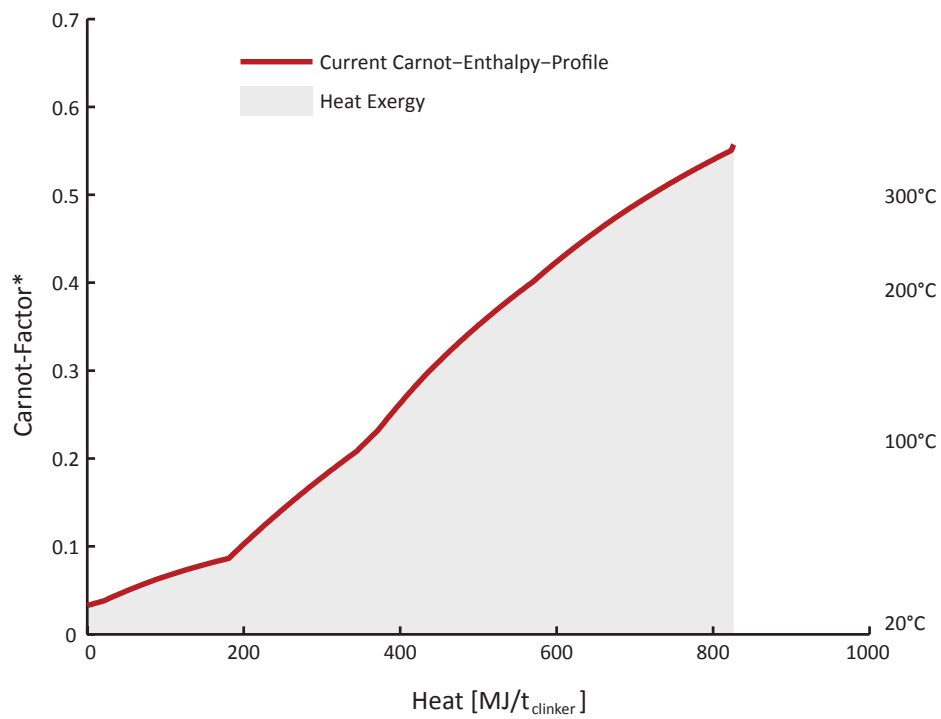


Figure 2.10: End of pipe heat sources of the cement process, exergy.

Table 2.1: Hot Gases from Cement Plant.

Gas Origin	N_2 % _{v,dry}	O_2 % _{v,dry}	CO_2 % _{v,dry}	H_2O % _{v,wet}	SO_2 % _{v,dry}	T °C	\dot{m} kg _{wet} / t _{clk}	ΔH MJ / t _{clk}
Raw Mill	67	2	30	14	<1	103	878	176
Preheating Tower	66	<1	32	6	<1	390	1125	435
Clinker Cooler								
- mid air	79	21	-	1	-	400	290	112
- end air	79	21	-	1	-	225	290	57
Cement Mill	79	21	-	1	-	115	559	46

All these heat sources sum up to an available enthalpy of $826 \text{ MJ} / t_{\text{clk}}$ or for a cement plant with a daily production of $3500 t_{\text{clk}} / \text{d}$ the enthalpy flow equals 33.26 MW . The temperature-enthalpy profile of all these gases combined, figure 2.9, shows that more than half of the heat is at a temperature below 200°C . The *heat exergy* is $230 \text{ MJ} / t_{\text{clk}}$ if an ambient temperature T_a of 25°C is assumed. This ambient temperature is rather high for Europe and is mainly reached in summer, thus it can be seen as a conservative assumption when it comes to evaluating the exergy potential. The potential is visualised as the surface under the Carnot-Enthalpy-Curve in figure 2.10.

If we could convert approximately 60 % of the *heat exergy* into electricity by the use of one or more *Clausius Rankine Cycles* with adapted working fluids, temperatures and pressures. This means an estimated $138 \text{ MJ}_{\text{el}} / t_{\text{clk}}$ could be produced which is equivalent to $5.6 \text{ MW}_{\text{el}}$ for a plant with a daily production of $3500 t_{\text{clk}} / \text{d}$.

Cement – LOVE-Demonstrators

The European Framework Seven *Low-Temperature Heat Valorisation Towards Electricity Production* (LOVE)-project included the installation of two ORC-demonstrators in two cement plants. One of the particularities of the project was the upper temperature limit of 120°C imposed by the call for proposals. The LOVE-consortium chose two heat sources for the installation of the demonstrators: the hot (combustion) gas coming from the raw mill and the hot air coming from the cement mill. The two demonstrators were not installed permanently, thus the turbine, the generator, the cooling tower and other units were moved from one site to the other. The experience with these demonstrators is described in Herzog et al. (2014) and was presented at the ECOS-Conference 2014.

Demonstrator – Höver

The Cement Plant in Höver, Germany (near Hannover) fits the above description of the cement process with the particularity that it is not equipped with a precalciner. The gas-stream that was used for the LOVE-demonstrator was taken from the filtered flue gases coming from the raw mill. The flue gas stream (index FG) was characterised in two measurement campaigns and the findings used for the design of the demonstrators are shown in table 2.2. According to these values the demonstrator was designed. The indices are *dp* for *dew point*, *n* for *normal conditions* and *g* for *gas*. It can be seen that these values differ from those in table 2.1. This is due to the different factory set-up (no precalciner) and air infiltration. The nominal values of the operating parameters are given in table 2.3. The indices are *in* for *inlet*, *evap* for *evaporation*, *cw* for *cooling water*, *cond* for *condensation* and *src* for *source*. By looking at the volume flow rates, it can be seen that about one quarter of the total stream is taken for the demonstrator, this is due to the LOVE-project proposal which included the construction of demonstrators up to $100 \text{ kW}_{\text{el}}$.

Table 2.2: Gases for LOVE-Demonstrators.

Gas Origin	N_2 % _{v,dry}	O_2 % _{v,dry}	CO_2 % _{v,dry}	SO_2 ppm	T °C	T _{dp} °C	$\dot{V}_{g,wet}$ $\frac{m^3}{h}$	$\dot{V}_{n,g,dry}$ m^3/h
Höver Raw Mill	~72	~8	~20	~50	112.0	61.7	~400 000	~225 000
Kollenbach Cement Mill	~79	~21	-	-	110.0	60.0	~56 080	~32 000

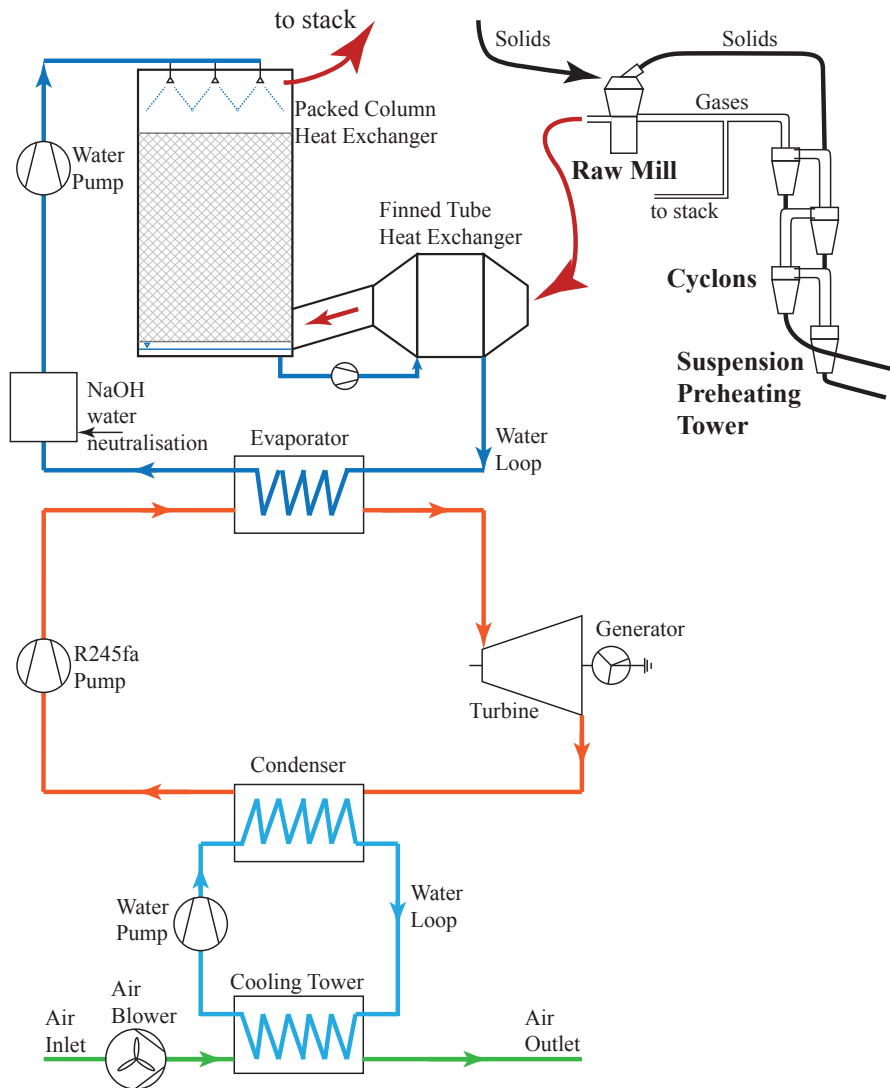


Figure 2.11: Schema of the demonstrator as it was used in the Höver cement plant, using an intermediate water loop and direct water-gas contact.

Table 2.3: LOVE-Demonstrators, nominal parameters.

	$T_{g,in}$ °C	T_{dp} °C	T_{evap} °C	$T_{cw,in}$ °C	T_{cond} °C	\dot{M}_{R245fa} $\frac{kg}{s}$	\dot{M}_{Cw} $\frac{kg}{s}$	\dot{Q}_{src} kW	\dot{E} kW _{el}	ϵ_{orc} %	$\dot{V}_{g,wet}$ $\frac{m^3}{h}$	$\dot{V}_{g,wet}$ $\frac{m_n^3}{h}$	SO_2 ppm	Dust $\frac{mg}{m_n^3}$
Demonstrator Höfer Plant	112.0	61.7	62.7	25	30.7	7.22	10	1550	100	~6.4	101000	56300	~50	< 10
Kollenbach Cement Mill	110.0	60.0	62.7	25	30.7	3.90	5.3	820	53	~6.4	56080	32000	-	< 10

Table 2.4: Nominal and real behaviour of PCU.

	$T_{g,in}$ °C	$T_{g,PCU,in}$ °C	$T_{g,out}$ °C	$T_{w,in}$ °C	$T_{w,FiTu,in}$ °C	$T_{w,out}$ °C	T_{dp} °C	$\dot{m}_{g,wet}$ $\frac{kg}{s}$	$\dot{M}_{g,dry}$ $\frac{kg}{s}$	\dot{m}_w $\frac{kg}{s}$	\dot{m}_{co} $\frac{kg}{s}$	\dot{m}_{ev} $\frac{kg}{s}$	\dot{Q}_{FiTu} kW	\dot{Q}_{PCU} kW	\dot{Q}_{evap} kW
Nominal	112.0	61.7	61.16	55.0	61.7	97.0	61.7	25.47	22.0	9.6	0.107	0.0	1434.02	284.25	0.0
Real	112.0	61.7	56.03	55.0	56.17	97.0	55.7	23.34	21.0	7.53	0.014	0.059	1277.09	38.55	7.67

A schematic of the Höver demonstrator is depicted in figure 2.11. The heat extraction from the gas streams is done by a separate water loop, one part with a Finned Tube heat exchanger (FiTu) and the other part with a Packed Column Unit (PCU) in which the water and the hot flue gases are in direct contact and part of the latent heat can be extracted. Due to the direct contact $NaOH$ neutralisation of the loop water was necessary in order to keep the water from becoming too acid while absorbing SO_2 originating from the combustion. While most of the installation was done in stainless steel, the fins of the FiTu were alumina and the tubes copper for cost reasons, the packaging of the PCU was a polymer. In the three months testing period, the demonstrator did run 55h in total. This relatively short time period of use is due to several factors:

- *Operation:* An operator had to be controlling the operation, there was no time to develop an automation system. Making it impossible to operate for the entire day and leading to additional time used for start-ups.
- *Corrosion:* One consequence of the the long downtimes of the demonstrator is the destruction of equipment parts due to corrosion. The neutralisation system was designed to keep control of the pH in the water loop while the system was running, it showed ineffective during downtime. The FiTu and PCU were separated from the flue gas stream during downtime by a flap. This flap let through a small fraction of the flue gases, due to the high total volume flow, this fraction was enough to accumulate a large quantity of acidic condensate at the bottom of the PCU, which was cool during downtime. When starting up, this acidic water was pumped through the FiTu, which had copper tubes connected to the otherwise stainless steel tubes by a small carbon steel tube. First the carbon steel, then the copper tubes were breaching, attempts to repair the leaks only helped for a few hours until the next leak would break open. An additional decisive factor leading to this very fast corrosion was vibration caused by the blower that was used to transport the cooled down flue gases to the stack, mechanically connected to the FiTu via an I-beam.
- *Turbine trips:* The turbine had very strict security settings, including a narrow temperature window for the working fluid at the inlet. The Turbine turned at a speed of 10200 rpm, that means that all the working fluid in the turbine had to be evaporated and then the turbine brought up to speed before opening the inlet or outlet valves. But the opening of the valves led to flashing effects (due to pressure drop) and fluctuating temperatures. The R245fa-inlet temperature fluctuated mostly at start-up or change of regime leading the turbine to trip.
- *Imprecise measurements:* The installation had very few redundant measurements, this together with the challenging environment made the measured values only partially reliable. Especially the gas flow rates and temperatures near the dew point were difficult to measure and rather imprecise. This led to difficulties in the control of the demonstrator, thus intensifying the above problems.

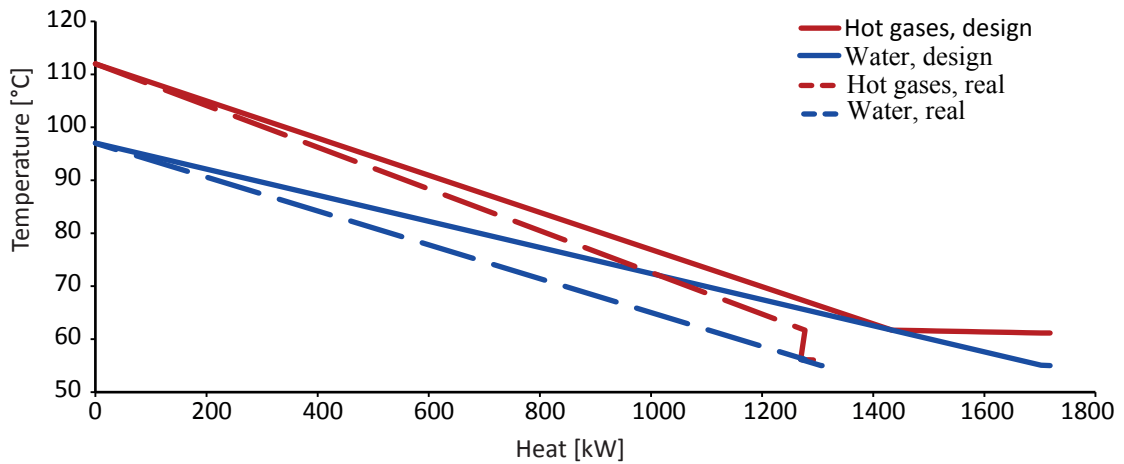


Figure 2.12: Höver demonstrator heat exchange.

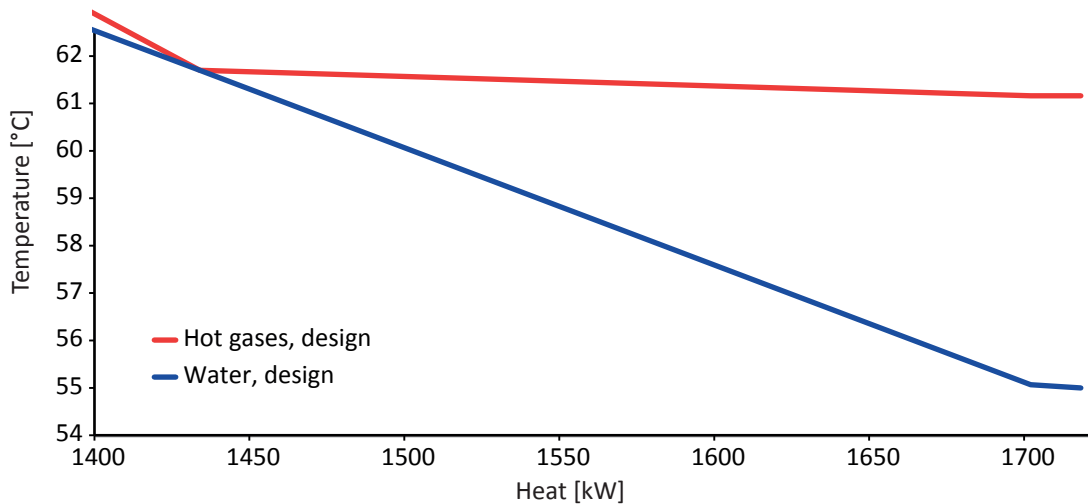


Figure 2.13: Detailed PCU heat exchange, design.

The real life performance of the installation was rather different from the nominal values. One reason was the change of the flue gas composition. Changes in the fuels and the raw materials (due to a not entirely homogeneous quarry) changed the humidity as compared to the one seen in the pre-measurement campaigns. This led to dew points mostly between 50 °C and 60 °C which is significantly lower than the nominal dew point of about 61.7 °C. The effect was an unplanned behaviour of the PCU, leading to evaporation of water from the water loop. In figure 2.12 the heat exchange is presented, the crucial point being that the injection of water into the PCU is done to condense part of the humidity in the flue gases. Two factors are important for that: The gas has to enter the PCU at the dew point (or at least as close as possible) and the water that is sprayed in has to be cold enough to recover a considerable amount of heat from the gas (and at the same time condense part of the humidity). The gas cooling delivers the largest part of the heat to the water. The water and the gas get in direct

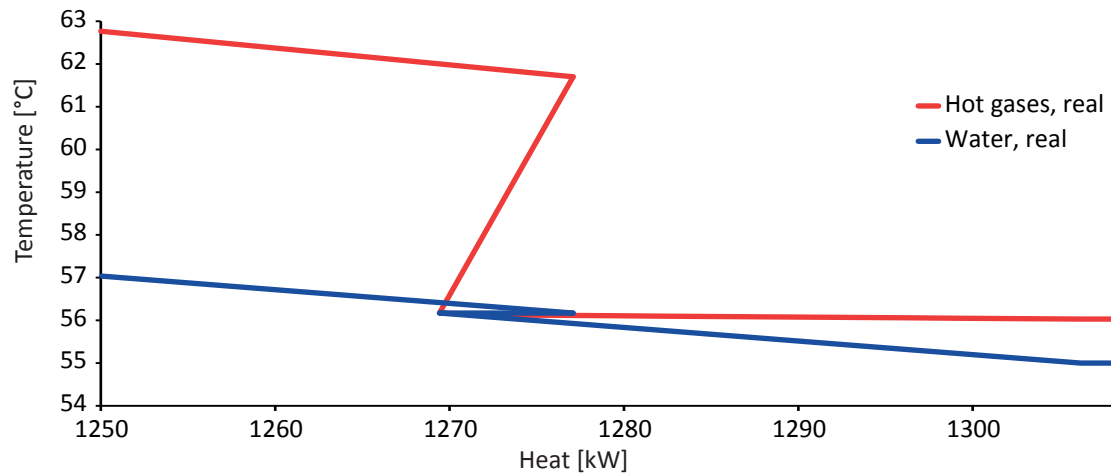


Figure 2.14: Detailed PCU heat exchange, real.

contact exactly at the dew point at which they also have an identical temperature, this is at the bottom of the PCU, directly before the water is collected and send to the FiTu. Then, the gas cools down in direct contact with the water, the condensing water from the gas stream is represented as being transferred at the gas outlet of the PCU for better visibility, even though it happens all along the cooling/condensation. In figure 2.13 the heat exchange detail of the PCU is depicted as it was supposed to happen, in figure 2.14 the detail of the PCU heat exchange how it took place in real life operation is shown. The observed dew point is at 55.7 °C, the gas enters the PCU at roughly the same temperature as the supposed dew point 61.7 °C. This leads to an evaporation of water as the gas gets in contact with it and a temperature drop of the gas to 56.2 °C. All key values are presented in table 2.4.

The value \dot{Q}_{evap} identifies the enthalpy loss which is due to the evaporation of water in the PCU. The net water balance of the PCU is $+0.107 \frac{\text{kg}}{\text{s}}$ for the design situation and $-0.045 \frac{\text{kg}}{\text{s}}$ for the real situation. In order to keep the water loop operationable a water make-up has to be supplied. The make-up water is at water grid temperature and induces thus an additional temperature drop. The performance of the demonstrator was far from the nominal one. The produced power reached a maximum at approximately 80 kW_{el} throughout the test period (at a test with an increased flue gas intake) and the overall system efficiency (recovered heat-to-electricity) was mainly between 3 % and 3.5 %.

The difficulties in measuring and controlling the system in order to reach better performances led to the development of a data reconciliation methodology explained in chapter 3.

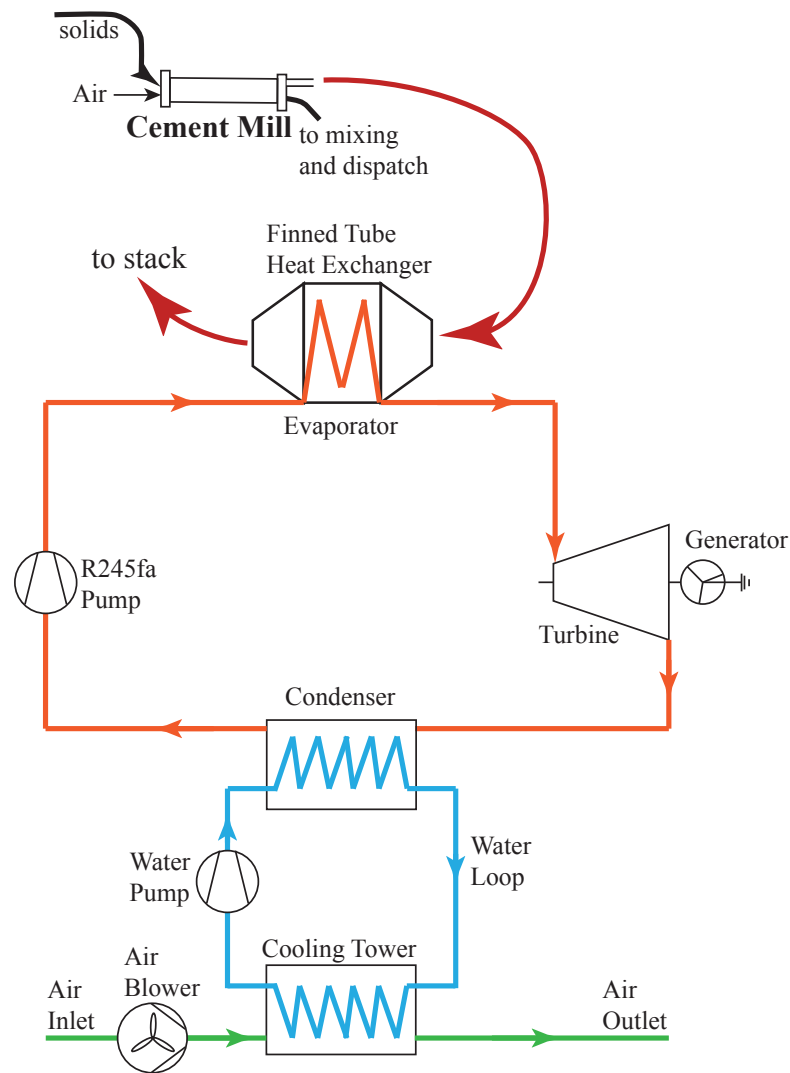


Figure 2.15: Schema of the demonstrator as it was used in the Kollenbach cement plant, using finned tube heat exchanger as direct boiler.

Demonstrator – Kollenbach/Beckum

The demonstrator at the Kollenbach cement plant used a different heat source and had a different design than the one above. It used a direct boiler for the working fluid and no intermediate water loop. A schematic of the set-up can be seen in figure 2.15. In table 2.2 the results of the measurement campaign are shown and the resulting design parameters are stated in table 2.3. The heat source is gas that leaves the cement mill and was heated not by combustion but by mechanical movement in the mill and during the grinding process. Since it is not a flue gas from combustion, the composition is that of air with some additional humidity and some dust. In order to avoid cloaking of the direct boiler heat exchanger, it is installed after dedusting.

The Kollenbach demonstrator showed less problems than the Höver one. This was due to the learning curve in the operation and the less difficult set-up as well as less aggressive heat source. The total operation time was 516 h and many more test points could be reached, giving a better understanding of the behaviour of the installation. The maximum power that could be produced was 42 kW_{el} instead of the 50 kW_{el} we aimed at. The lower than expected power generation was mainly due to two factors: for one the process was modernised in the year after the measurement campaign and secondly the cement types that were produced did not exactly match those produced throughout the measurement campaign. This led to lower temperatures and lower volume flow rates.

Difficulties during operation arose from the measurement of the gas flow rate and temperature. The conducts were winding for space reasons, this made the flow turbulent. But the *Pitot tube* type measuring equipment could only estimate the flow rate based on the velocity at one spot. Additionally the temperature of the gas was inhomogeneous over the section of the tube, thus a precise measurement of either flow rate or energy content was not possible. We used data reconciliation to estimate those.

The system efficiency of the Kollenbach demonstrator was in the same range as in Höver, meaning between 3 % and 3.5 %, this might seem surprising, but can be explained by the equivalent evaporation temperature as seen in the Höver demonstrator.

The electrical power shown in this chapter is the power produced by the generator. That means that the power used to run the cooling system is not taken into account. The cooling tower, which was the same for both installations was rented and not adapted to the exact needs. The cooling power of the tower was not linearly controllable, it could only switch on or off three arrays of fans if the temperature of the cooling water raised to much. Also, the cooling water was pumped through simple firefighter tubes (fire hose), which led to a high pressure drop and thus pumping energy. In the case of the Kollenbach demonstrator the power consumption of the cooling system and other auxiliaries sometimes exceeded the generated power. The encountered problems with heat exchangers, which are not well designed regarding the desired exchange and the cooling system, which was very energy intensive, show the necessity for energy integration during the planing phase. Also measurements which can be trusted for correct planing and during operation are necessary.

2.4.3 Integration

Integration of a Commercial ORC

With one of our industrial partners, a study was done on a Cement Plant that uses parts of the current cooling requirements to supply a district heating network. Even though economically this might be a challenging project, it can also lead to better acceptance of the cement plant and its impact on the environment and landscape by the local population. In cooperation with people from the plant we analysed the opportunities for the replacement of the old, installation

of an additional heat exchanger for the district heating and the possible combination with a commercially available ORC.

Even though this analysis has not been done following a complete Pinch analysis of the process, it is a step towards a proper integration into the process: instead of simply using the outlet mass flows that are (anyway) vented to the environment, the heat is recovered in two spots of the process where one is in between two process units. Our goal was not to find the optimal solution but to give a comparison between the proposed commercial product and what we estimated with a better integration into the heat sources, for the negotiations. After looping back with the manufacturer of the commercially available installation, a suitable solution, with one of their “off the shelf” products was found, that allowed for simultaneous use of the district heating with changing heat demand and electricity production with the ORC.

The first source is hot air from the clinker cooler which can be cooled down from 300 °C to 120 °C, the second source is heat from cooling down the hot gases leaving the suspension preheating tower before they enter the raw mill from 400 °C to 210 °C. The space heating and warm water requirements of the district heating network are not constant over time. The minimum heat demand of the network is about 2 MW and the maximum about 8 MW. We analysed this in intervals of two MW in order to see the impact on heat recovery and electricity production. The network has a feed-in temperature of 130 °C and a back water temperature of 75 °C. In agreement with the manufacturer, a thermal-oil loop was introduced in order to recover heat from the sources and deliver it to the cycle and district heating. The working fluid used by the commercial machine is hexamethyldisiloxane (also called MM), which behaves very similarly to toluene.

In order to give the experts from the industrial partners a better negotiating position, we compared the first proposals of the manufacturers commercial machines with our solutions. With the feedback from our calculations, the final proposal for an ORC done by the commercial manufacturer showed a higher performance due to a better part load behaviour and better integration with the process. The total energy available from the heat sources is about 14.280 MW. The produced electrical power, as it was calculated by the manufacturer with their ORC is shown in table 2.5. It is remarkable that the net to gross power ratio is increasing with decreasing power. Another interesting point is the cycle efficiency (heat input to net power) is decreasing by only one percent point or about 4.8 %. The specific cost for such a system are about 1300 €/kW_{installed} including the cooling system and about 1150 €/kW_{installed} without the cooling system.

In order to compare the solution of the commercial unit and what a “made to measure” solution could deliver, we calculated a supercritical cycle using R134a and a single stage cycle using toluene, both without a thermal-oil loop (direct boiling), both with a design point for 12.280 MW heat input. Also we allowed to use the heat from further cooling of the gas from the clinker cooler. The toluene cycle would produce approximately 27 % and the supercritical cycle approximately 40 % more electricity. The constraints that were applied allowed only for

Chapter 2. Waste Heat Recovery: Studies and Examples

Table 2.5: Commercially available ORC and histrect heating (values from vendor).

District Heating:		2 MW	4 MW	6 MW	8 MW
Available Heat for ORC	MW	12.280	10.280	8.280	6.280
Produced Power, gross	MW	2.540	2.152	1.714	1.248
Produced Power, net	MW	2.422	2.060	1.648	1.201
Produced Power of Design	%	100	83.7	67.4	51.1
Power net to gross	%	95.4	95.7	96.1	96.2
Cycle efficiency, net	%	20.7	20.9	20.7	19.9

one stage cycles, these limited the number of degrees of freedom in a way, that we used a several stage sensitivity analysis in order to find these optimised cycles.

Even though there is a margin for amelioration regarding the commercial solution, the cooperation lead to a concept that produces on average 37 % more electricity than the manufacturers first proposal due to better integration and a more suitable cycle. This proves that the application of Pinch analysis techniques can be used to improve the quality of integration of an ORC into an industrial process and validates our methodology.

Representative Process

Here, we analyse the theoretical potential of the above described representative cement process. All concerned heating and cooling requirements are also listed in appendix B. We can see from figure 2.16 and figure 2.17 that the composite curves are pinched at the highest combustion temperature, and that there is a high temperature difference between the cold and hot curve from there on. This reveals the amount of exergy that is destroyed in the heat transfer (only being used for heat exchange speed). The thermal energy consumption of the representative process is $3.1 \text{ GJ} / t_{\text{clk}}$. We showed in Mian et al. (2013) that there is potential for integration of heat recovery technologies, additionally we could see above that more than $100 \text{ MJ}_{\text{el}} / t_{\text{clk}}$ of electricity could be produced in a modern cement process by integration of one or more organic Rankine cycles with one or more stages, without having to completely redesign the process. For a process which produces $3500 t_{\text{clk}} / \text{d}$ this is equivalent to an installed power of about 4 MW_{el} . Another possibility would be to use the wasted heat within the process, which makes rethinking of the process (-layout) necessary. However in a long-lasting industry with installations that sometimes produce for over half a century and a challenging business environment, development takes time. For this reason we present one option for further integration: preheating of combustion air. Several configurations are imaginable for this:

- *Hot gases directly from the cement mill*

Today, the hot air from the cement mill is dedusted before being sent to a stack. Instead of the stack it could be used as combustion air in the kiln and/or precalciner. However

the temperature is relatively low (90 °C to 120 °C) and depending on the market situation, the mill does not always run.

- *Hot gases from the cement mill, further heated by kiln gases*

The air from the cement mill could be heated further by the use of the hot gases from the kiln (and possibly precalciner), e.g. after they leave the suspension preheaters and before they enter the raw mill. Again the functioning of the cement mill might be an obstacle.

- *Hot gases from cement mill, further heated by clinker cooler gas*

The air from the cement mill could be heated further by the use of the hot gases from the clinker cooler. Again the functioning of the cement mill might be an obstacle.

- *Hot gases directly from the clinker cooler*

The hot air coming from the clinker cooler is already partially used as combustion air; the degree of usage could be increased.

- *Heat combustion gases with hot gases from the kiln*

A heat exchanger can be used to heat the combustion air with the gases from the kiln (and possibly precalciner) e.g. after the suspension preheaters and before the raw mill.

- *Heat combustion gases with hot gases from the clinker cooler*

The combustion air could be heated by the use of the hot gases from the clinker cooler.

- *Combinations of the above*

It is also possible to combine the above mentioned configurations; this might be especially interesting in plants with other operation modes and technologies.

In our model of a representative process, the quantity of primary combustion air and the quantity of ambient combustion air for the burner in the precalciner have a ratio of approximately 1:2. Both streams could be preheated. It has to be mentioned that preheating can lead to higher flame temperature, which increases the formation of NO_x; we thus recommend the use of efficient exhaust gas treatment. The heat that could be reused within the process by preheating the combustion gases directly reduces the necessary heat input, due to the energy balance. Depending on the mass flow rates and the humidity level, more than 30 MJ / t_{clk} of heat could be saved per 100 K of preheating both streams. It should be kept in mind that the very low cost of fuels at the moment makes an investment into preheating technologies economically challenging (Satterthwaite, 2013). Furthermore, we can see from the simulation results that about 780 MJ / t_{clk} are evacuated to the environment with material streams; figure 2.18 illustrates this by the means of an integrated composite curve, showing the Grand composite Curve of all evacuated heat recovery potential (red) and the Grand Composite Curve of the remaining streams (blue). The Grand Composite Curve is built by drawing the heat difference (horizontal) between hot and cold composite curve over the temperature. The heat losses, figure 2.19, are about 670 MJ / t_{clk} which leave the system over the walls of the process units.

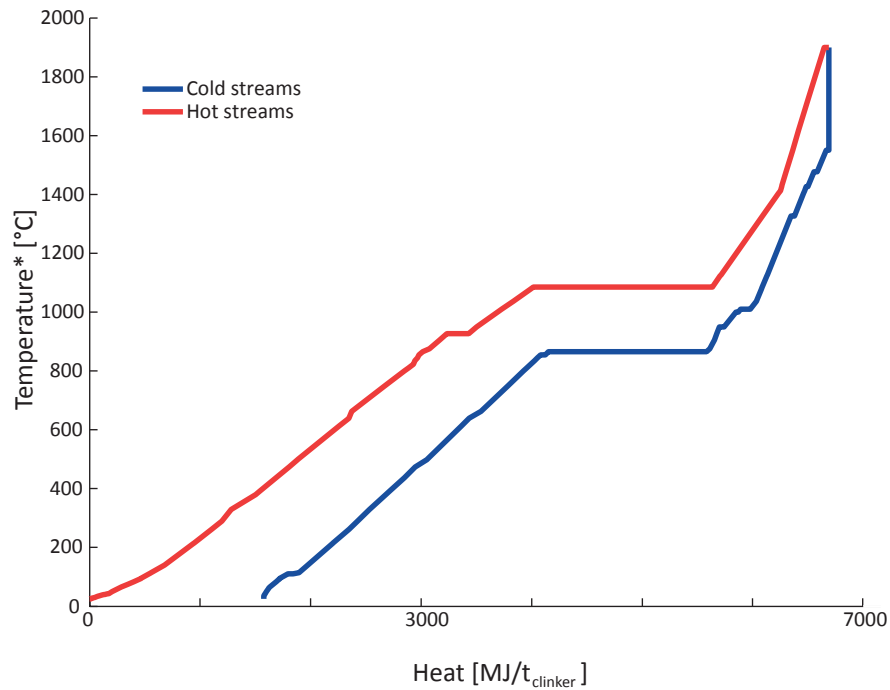


Figure 2.16: Composite curve of a representative cement process.

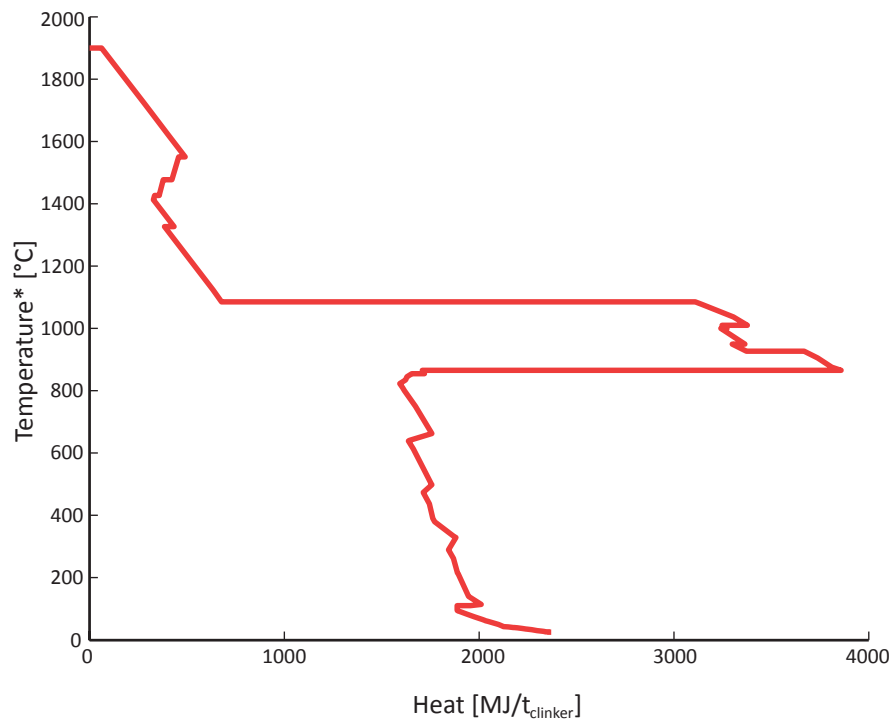


Figure 2.17: Grand composite curve of a representative cement process.

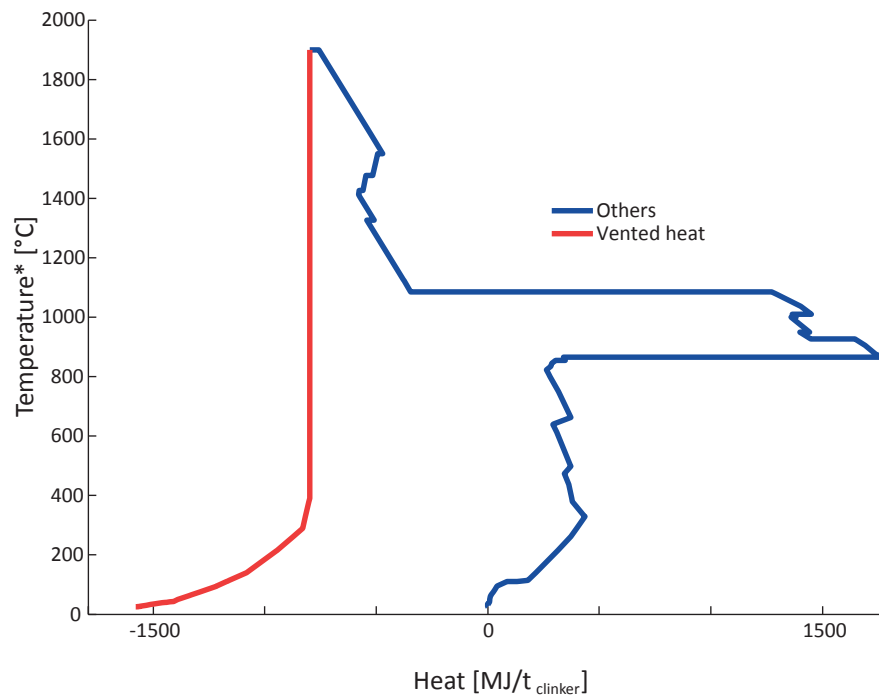


Figure 2.18: Integrated composite curve of a representative cement process showing evacuated heat.

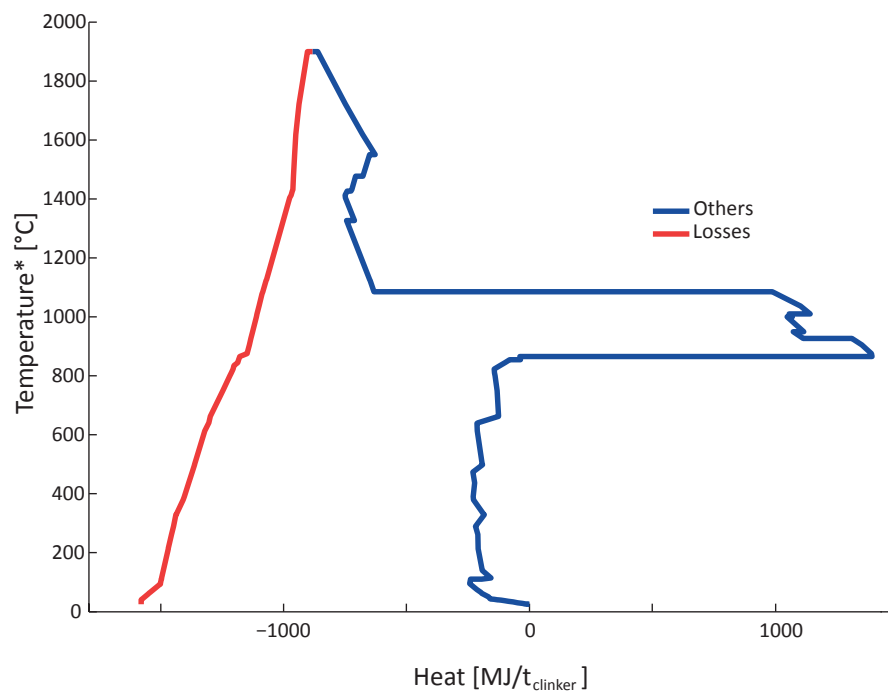


Figure 2.19: Integrated composite curve of a representative cement process showing heat losses.

2.4.4 Redesign

To pretend to be able to redesign the entire cement process as a sub-chapter in one doctoral thesis is of course presumptuous, we rather want to try to explore the limits of a possible integration of the process-streams. In order to achieve this, we only look at the process steps that directly take part in the transformation of the raw materials into clinker, while ignoring the technology constraints of the process as it is today. This way we want to show how a redesign of the system could theoretically lead to a modernised process with higher energy efficiency. It should be noted that no process corresponding to these limits exists yet and to achieve it, the used techniques would probably have to change drastically. In order to guarantee the economic feasibility of the integrated process we keep the minimum temperature differences of the representative production line we described above. These vary between 5 °C and 100 °C. In the integrated process the following steps are considered:

- Heating of raw materials
- Drying of raw materials
- Calcination and clinkerisation
- Cooling of the CO_2 produced by calcination
- Cooling of clinker
- Combustion of coal
- Cooling of combustion gases
- Preheating of air for combustion

All other steps are dependent on the technology used and might be avoidable in future times. For the modelling of this process several major assumptions were made mainly on drying, preheating and heat losses.

Drying

The most crucial assumption is that of the lowest possible drying temperature of the raw material. This temperature will define the lower pinch point of the system. As we saw above, in the representative process the drying takes place within the raw material mill, the hot gases from the suspension preheater tower (cyclones) are used for this. The advantage of the high temperature of these gases is the speed of drying (approx. 2 seconds). It seems therefore logical that a lower drying temperature even if energetically advantageous, makes a higher exchange surface and probably a longer exposure time necessary. Modelling a low temperature drying process, can be done in several ways. We assume a drying process that uses hot air in direct contact with the raw material; several configurations are possible. Two extreme cases can be defined:

1. The raw material and the drying air leave the drying process at the same temperature, the lowest temperature possible (in figure 2.22 this is the ambient temperature plus the minimum temperature difference for the heat exchange which equals 45 °C). The mass flow rate of the air is defined by the outlet at which the air is saturated with humidity (relative humidity at 100 %). The water within the raw materials enters the drying process at ambient temperature. In consequence the drying air has to be heated up to 187 °C. In this configuration the combustion gases should ideally be preheated up to about 540 °C for a global minimum in fuel consumption.
2. The other extreme is to fix the drying air inlet temperature, instead of the relative humidity of the outlet. This implies an increased mass flow rate but a reduced drying temperature. To demonstrate this we fixed the drying air inlet temperature to 85 °C (40 °C above the outlet). The result can be seen in figure 2.23. The exact trade-off between mass flow rate (fan power) and low temperature requirement depends on investment and energy costs. The supplementary air requires more heat for heating. The ideal preheating temperature would be around 490 °C.

As a result it can be said that without any additional measures, the first extreme seems advantageous. The second extreme could nevertheless be interesting for example if a steam cycle was integrated.

Preheating

The other crucial technology is the air preheating. Since for the combustion a large quantity of air is needed. If this air is preheated, the combustion temperature is raised. This principle should be used by preheating the combustion air to the highest temperature possible. Typical modern multi-fuel burners used in cement plants do not allow a very high preheating temperature (<80 °C), further development in this area could lead to improvements in the fuel consumption of cement processes, on the other hand, high preheating temperatures are technologically challenging. Preheating of the fuels could be an option, the problem being that the fuel temperature should not exceed the temperature at which the gasification of the volatile compounds starts. The volatile compounds, could be lost, which is environmentally critical and leads to a loss in heat capacity, additionally the risk of self-ignition is higher. Preheating large quantities of coal or petcock would also require considerable installations which is an additional obstacle. Thus we will not consider preheating fuels.

Losses

A number of losses can be identified in the cement process. They occur due to heat transfer from the inner streams through the process walls to the environment. As we saw above the total amount of losses in the representative process is about 780 MJ / t_{clinker} . The kiln is a major contributor to the losses. The difficulty of estimating the proportion of the losses, which could

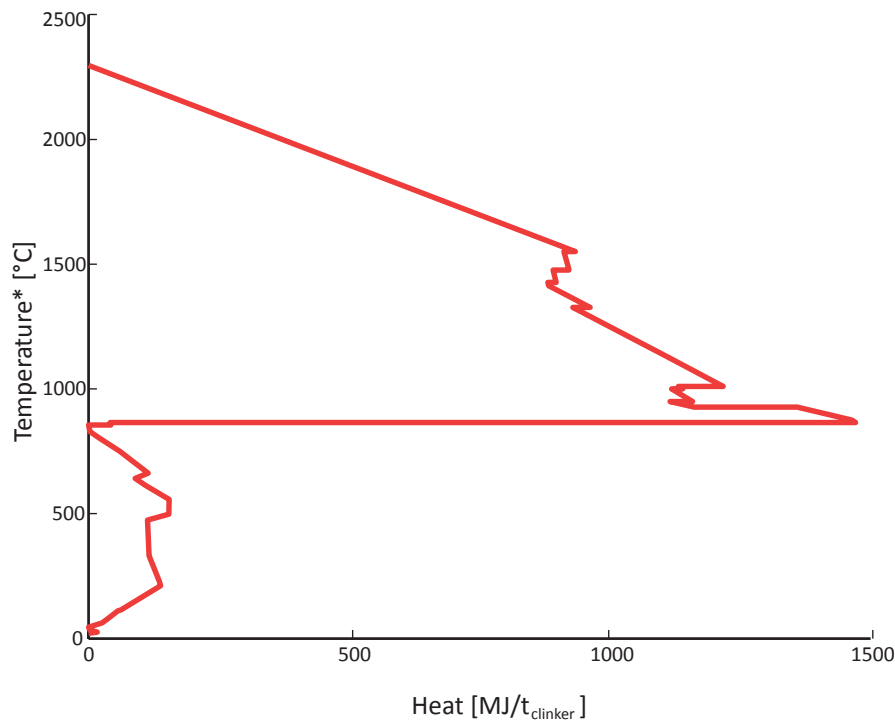


Figure 2.20: Grand composite curve of extreme case 1.

be avoided or reused as heat, results from the fact that the temperature gradient is used in the kiln to create a layer of clinker around the refractory bricks. These protect the refractory and the steel from impacts and higher temperatures. If the kiln was insulated, it could reduce the resistance and lifetime of both kiln and refractory. Since we are not considering the technology constraints, we assume nevertheless that no losses occur or that they can be recovered in the optimised process. Further assumptions are:

- 3 % Humidity in raw materials
- Stoichiometric combustion
- Neglecting crystallization energies

This integrated process would reduce the energy consumption to $2215 \text{ MJ/t}_{\text{clinker}}$ which is over 28 % less than the representative modern process shown above. Reaching this would require larger equipment due to the smaller temperature differences.

The composite curves of the integrated process in figure 2.20 to figure 2.23 show the limit of the heat recovery potential caused by the lower pinch point (drying). The temperatures below this pinch point are not interesting for recovery of heat for electricity production. We can however see that there is still a considerable amount of exergy destroyed between the combustion gases and the process streams. Unfortunately accessing this exergy is challenging. As a blue-sky concept it is imaginable to introduce an “ultra-high” temperature Brayton cycle

2.5 Conclusion

In this chapter, we have seen three depth of study and perspectives to identify waste heat. All three may be found in application, the end of pipe approach is seen commonly. It is easier to make a study on waste heat following this approach than any other, since it does not require a deep understanding of the process or investment into the process (for internal heat recovery). It does however not identify possible fuel savings or efficiency improvements and may be expensive in the long run, if a high investment is made using avoidable waste heat that would better be used within the process (with a high efficiency).

The experiences made with the LOVE demonstrators have shown that imprecise measurements lead to a faulty integration of the ORC with the heat sources and thus to low efficiencies and low electricity production. Another key learning is that unexpected behaviour might lead to material problems, it is thus most suitable to use stainless steel heat exchangers for waste heat recovery in order to avoid corrosion in aggressive environments. Important as well was the fact that a simple design, using a direct boiler with a short distance to the turbine, instead of an intermediate cycle and a condensation unit led to far better operation times and more stable operation. Finally the use of a cooling system which is sized according to the needs of the ORC is crucial, otherwise the cooling system decreases the electricity production strongly.

It is further shown how Pinch analysis can be used to identify the potential for integration of a secondary heat recovery technology into a process, it reveals at the same time possibilities for heat recovery within the process and allows an intensive use of the available heat within the heat cascade. The application of Pinch analysis to integrate a commercially available ORC with predefined heat sources has shown, that it is a valuable technique to improve the quantity of electricity produced.

The re-design of process can be seen as a scenario tool or a further step of process intensification, the process unit operations may be changed or the utility system modified in order to realise energy savings. The resulting amount of waste heat can be understood as a benchmark, revealing how much heat and exergy are available in a situation, in which the process has been thermally optimised. In our study conducted for and with Nestlé we have seen that it was economically interesting to realise process modifications and that the resulting temperature of available waste heat was at such a low temperature that the integration of an ORC is not the best choice.

In case of the representative cement process, it is remarkable that the waste heat recovery potential is close to zero and no waste heat recovery seems applicable, if the total energy balance of the process remains unchanged.

All three depth of study have merits, we do however advocate to not stop a study after an end-of-pipe analysis, in order to avoid making an investment which might reveal itself to be blocking a more efficient process and direct fuel savings. We will use the results of this chapter for the ORC-identification tool that is presented in chapter 4.

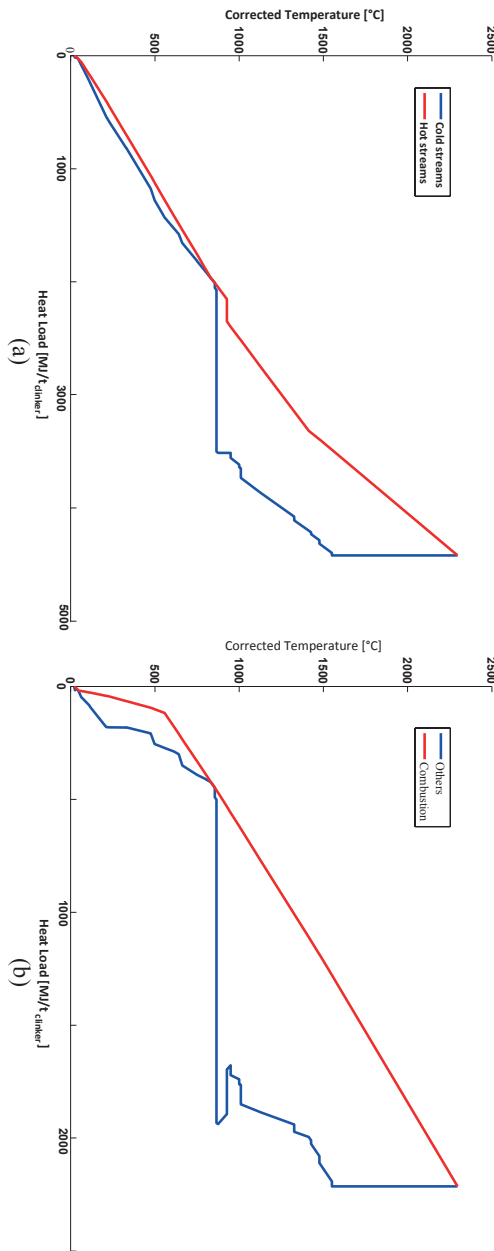


Figure 2.22: Composite curve (a) and integrated composite curve (b) of extreme case 1.

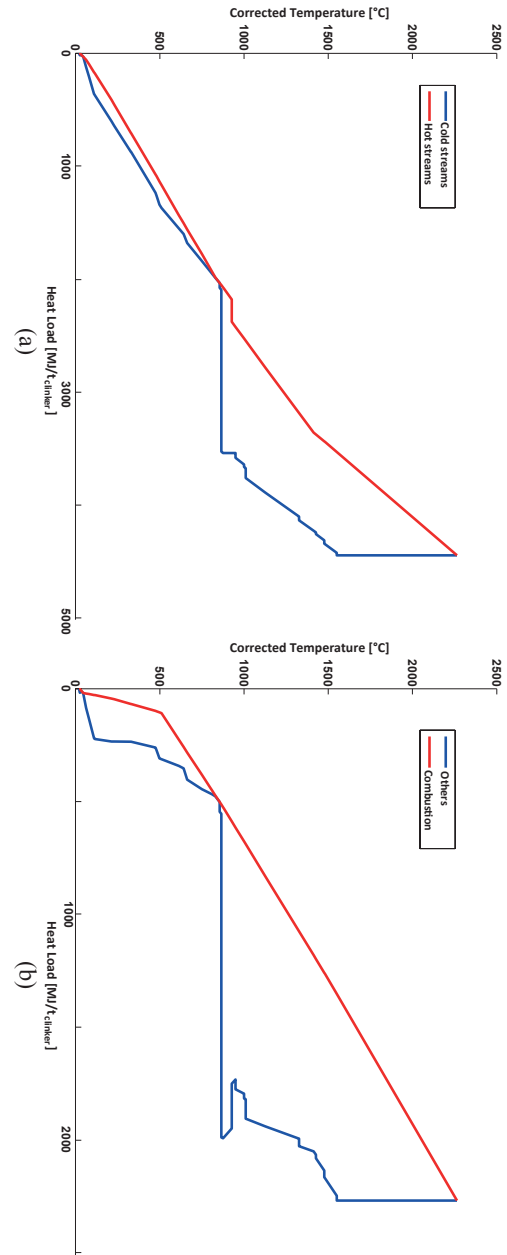


Figure 2.23: Composite curve (a) and integrated composite curve (b) of extreme case 2.

3 Waste Heat Valorisation System Characterisation

Through the LOVE project two demonstrators were installed in two different cement plants as described above in chapter 2. We are in the lucky situation where we have actual experience with the use of these two low temperature ORC demonstrators and access to the measurement data in addition to the waste heat analysis also presented in the previous chapter. Some of the results from the demonstrators will be used to verify the ORC identification tool and therefore we look closely at the measurements. The problem we encountered during the measuring period was the small number of redundant measurements and sometimes contradictory results from the measurements we had. Thus we decided to use data reconciliation (also called *least square method*) in order to have a coherent set of data regarding the physical constraints imposed by models, representing the demonstrators. Thus the confidence into the reconciled values could be increased. Additionally, a development for a new methodology, which we call *Enhanced Data Reconciliation*, was introduced and tested. In the following the differences between “classical” and enhanced data reconciliation will be explained, identifying limits and possibilities of both methods. The method has been published and presented in the peer reviewed conference ECOS 2014 (Bendig et al., 2014b).

As an outcome the possibilities and limits of enhanced data reconciliations are shown and the data of the “LOVE” project are analysed. Parameters which can be used for the calibration of the ORC tool are identified and quantified.

3.1 Objectives

Reconciling measurement data of the LOVE demonstrators with little redundancy, with the aim of characterising the performances of the tested Rankine cycles and identifying process unit parameters.

The overall objective is to reconcile the data from the LOVE demonstrators in a way that they deliver coherent information about the functioning of organic Rankine cycles at low temperatures in waste heat recovery. To achieve this we rely on data reconciliation, but we also

develop a new methodology that can improve the reconciliation for data sets with low degree of redundancy. We will extract the information, helping us calibrating the ORC identification tool.

3.2 State of the Art of Data Reconciliation

Data Reconciliation has been used extensively in industries and research areas where a high precision of production or experimental variables and parameters is necessary. This is the case for example in the chemical and pharmaceutical industry but as well in nuclear power plants or university experiments. A set of reconciled data is more coherent with the physical constraints that characterise the measured system, than the corresponding set of measurements. In other words, all mass and energy balances are closed and temperatures are coherent, if the constraining model is done carefully. A global overview of data analysis can be found in Romagnoli et al. (1999). The methodology of data reconciliation in chemical engineering is often attributed to Kuehn and Davidson (1976); whereas the first application to an industrial process is attributed to Reilly and Carpani (1963), as described in Crowe (1996). This methodology is based on least squares which Stigler (1990) says was first published by Legendre (Legendre, 1805). The working principle of data reconciliation is to minimise the weighted sum of all squared differences between measurements and corresponding reconciled values (Equation 3.1). Since the reconciled values are connected (via the equations of the model), this leads to the most probable state of the system corresponding to the set of measurements. Practically, this means that a software model of the mass and energy balances of the installation is programmed. All thermodynamic states within the (sub-)system(s) are estimated and compared to the measured values, then the sum of the weighted squared differences between estimations and errors is minimised by adapting the estimations accordingly. The most probable conditions that actually prevail in the set-up or operational unit are those where the sum square error is minimal:

$$\min_{y,x} \sum_i \frac{(y_{i,t} - \hat{y}_{i,t})^2}{\sigma_i^2} \quad (3.1)$$

subject to $f_t(y_t, x_t) = 0$ (constraints: energy and mass balances)

where:

y	Reconciled value of the measured variable
\hat{y}	Value of measurement
x	Unmeasured variable, parameter
σ	Standard deviation or inaccuracy of measurement i
i	Index of measurement (point)
t	Index of timestep

The methodology profits from a large number of measurements and redundancy as well as a large number of equations connecting the different measurements and parameters (Kretsovalis and Mah, 1987). Data reconciliation as described is suited for steady process and quasi steady situations. Reading on Data reconciliation in dynamic situations can be done for example in Minet et al. (2001) and in Ullrich et al. (2009). A special application of data reconciliation is parameter identification as described by Romagnoli et al. (1999). Parameter identification minimises the reconciliation problem for all previous time-steps in one equation:

$$\min_{y_t, x_t, \pi} \sum_t \sum_i \frac{(y_{i,t} - \hat{y}_{i,t})^2}{\sigma_i^2} \quad (3.2)$$

subject to $f_t(y_t, x_t) = 0$ (constraints: energy and mass balances) $\forall t$
 $s_t(y_t, x_t, \pi) = 0$ (other constraints depending on parameters) $\forall t$

3.3 Enhanced Data Reconciliation

In many cases however, only a small number of measurements is available and redundancies are scarce. For these cases we developed a methodology, which can transport information from one measuring period to another by creating “virtual” measurements. The idea consists in measuring in time intervals that are short enough in order to “re-inject” parameters or variables of a measurement period t into the reconciliation of the measurement data from the following time period $t+1$ in the form of measurements. We mark the re-injected variables y_π with the index π . The estimation of the standard deviation of $\hat{y}_{\pi,t}$ is considered to be equal to the variance of $y_{\pi,t-1}$ (Further explained in Section 3.5). The hypothesis that the true values of the re-injected variables are constant over time is made:

$$y_{\pi,true,t} = y_{\pi,true,t-1} \quad (3.3)$$

We thus have:

$$\min_{y_t, x_t, y_\pi, t} \left(\sum_i \frac{(y_{i,t} - \hat{y}_{i,t})^2}{\sigma_i^2} + \sum_i \frac{(y_{\pi,i,t} - \hat{y}_{\pi,i,t-1})^2}{\hat{\sigma}_{\pi,i,t-1}^2} \right) \quad (3.4)$$

With the definitions:

$$y_t = \{y_t, y_\pi\}$$

$$\hat{y}_t = \{\hat{y}_t, \hat{y}_{\pi,t-1}\}$$

$$f_t = \{f_t(y_t, x_t), s(y_t, x_t, y_\pi, t)\}$$

And a now time dependent $\sigma_t = \{\sigma_i, \hat{\sigma}_{\pi,i,t-1}\}$

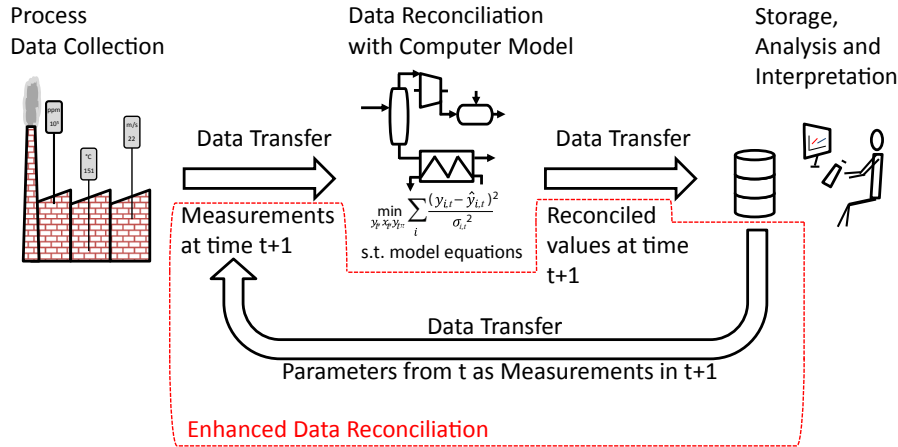


Figure 3.1: Schematic of Data Reconciliation and Enhanced Data Reconciliation.

We finally get:

$$\min_{y_t, x_t, y_{\pi,t}} \sum_i \frac{(y_{i,t} - \hat{y}_{i,t})^2}{\sigma_{i,t}^2} \quad (3.5)$$

subject to $h_t(y_t, x_t, y_{\pi,t}) = 0$ (constraints: energy and mass balances, others)

The functioning is depicted in figure 3.1. This increases the information/redundancy of the system and thus the overall precision. The methodology proposed here, does not need any further information from the steps before, other than the chosen variables themselves and the corresponding a posteriori accuracies of just one time step before. This way all information from previous measurements is indirectly included. Additionally the re-injected values are treated exactly like measurements and thus are optimised within the same step as the physical measurements, making the calculation quick and easy to implement into any existing software. These characteristics also make the methodology ideal for online use.

3.4 Approach

To demonstrate the methodology we will firstly introduce the calculation of the a posteriori accuracy. Afterwards the implementation and the example process will be described. Then we will have a look at several cases which demonstrate the possibilities and limits of the approach. The first case will help understand the influence of the initial values for re-injected variables and their inaccuracies. From the second case on we will introduce a set of steady measurements which is subject to noise. We will analyse the influence of non-linearities in the equations describing the system. In case 3 and 4 we will see how over- or under-specified systems behave when using enhanced reconciliation. Finally in Case 5, a non-steady process will be analysed. In all cases we assume the sets of measurements to be free of gross error and the results of conventional reconciliation will be given for comparison.

3.5 A Posteriori Accuracy

To use this methodology we rely on the a posteriori standard deviation of the reconciled values: showing Equation 3.1 in vectorial form we get Equation 3.6.

$$\min_{Y,X} (Y_t - \hat{Y}_t)^T W_t (Y_t - \hat{Y}_t) \quad (3.6)$$

subject to (linear or linearized) $A_t X_t + B_t Y_t + C_t$

Where

$$W_t = \text{diag}\left(\frac{1}{\sigma_{i,t}^2}\right) \quad \text{Weight Matrix}$$

and

$$\begin{aligned} A &= \text{Matrix of constraint derivatives with respect to } X \\ B &= \text{Matrix of constraint derivatives with respect to } Y \end{aligned}$$

Using the Lagrange formulation:

$$\min_{Y,X,\lambda} L = (Y_t - \hat{Y}_t)^T W_t (Y_t - \hat{Y}_t) + 2\lambda_t^T (A_t X_t + B_t Y_t + C_t) \quad (3.7)$$

Assuming stationary conditions (derivations of L to X, Y and λ are null) we get:

$$MV = D \quad (3.8)$$

Where

$$M_t = \begin{bmatrix} W_t & 0 & A_t^T \\ 0 & 0 & B_t^T \\ A_t & B_t & 0 \end{bmatrix}; \quad V = \begin{bmatrix} Y_t \\ X_t \\ \lambda_t \end{bmatrix}; \quad D = \begin{bmatrix} W_t \hat{Y}_t \\ 0 \\ -C_t \end{bmatrix}$$

So the reconciliation problem becomes:

$$V = M^{-1} D \quad (3.9)$$

The sensitivity Matrix $M^{-1}(m + n \times p$, where m is the number of measured and n the number of unmeasured variables, p is the number of constraints) gives the possibility to see the influences of the variables amongst each other (regarding both, the value of the variables and the corresponding standard deviations), but also to give an estimate on the confidence or variance of the reconciled value:

$$\text{var}(Y_{i,t}) = \sum_{j=1}^m \frac{(M^{-1})_{i,j,t}^2}{\text{var}(\hat{Y}_j)} \quad (3.10)$$

and

$$var(X_{i,t}) = \sum_{j=1}^m \frac{(M^{-1})_{n+i,j,t}^2}{var(\hat{Y}_j)} \quad (3.11)$$

The above is described in Heyen et al. (1996).

This is of great significance: if a variable can be determined not only by the corresponding measurement, but also via calculation using other measurements and/or parameters, then the confidence in the reconciled values is much higher and the a posteriori inaccuracy is going to be small (oftentimes one order of magnitude smaller than the estimated a priori inaccuracy). We can thus use the a posteriori inaccuracy in order to see, if the re-injected variables are calculated with high precision, also we can use them as a priori inaccuracies for the next calculation step:

A posteriori accuracy for re-injected variables (pseudo measurements):

$$\hat{\sigma}_{\pi,i,t} = var(Y_{\pi,i,t-1}) \quad (3.12)$$

3.6 Implementation

For the results published here we used the commercial software Belsim Vali (Belsim, 2011) in order to make the reconciliation.

A Matlab (MathWorks, 2012) program was used to handle the data flows, recover the data coming from the measuring system, prepare it for the reconciliation, launch the reconciliation, recover the reconciled files and store them adequately. In figure 3.1 you can see the work flow visualised.

3.6.1 Illustrative Example

For testing the methodology we have created a very simple example and a number of “virtual” measurements (we will talk about these below). The example process consists of a simple water-to-air-heat-exchanger as could be used as cooling device in an industrial process (figure 3.2). We assume that the water enters the heat exchanger at 50 °C and leaves at 25 °C, the mass flow rate is assumed to be 1 $\frac{\text{kg}}{\text{s}}$. Pressure at the entrance is 1 bar, the pressure drop 0.1 bar. On the air side we assume an entrance temperature of 15 °C and an outlet temperature of 35 °C, the pressure is 1.2 bar at the entrance and the pressure drop is 1.5 mbar. The air humidity at the entrance is 80 % consecutively the mass flow rate is 5.219 $\frac{\text{kg}}{\text{s}}$ and the humidity at the outlet 24.065 %. We will refer to these values as “true values”.

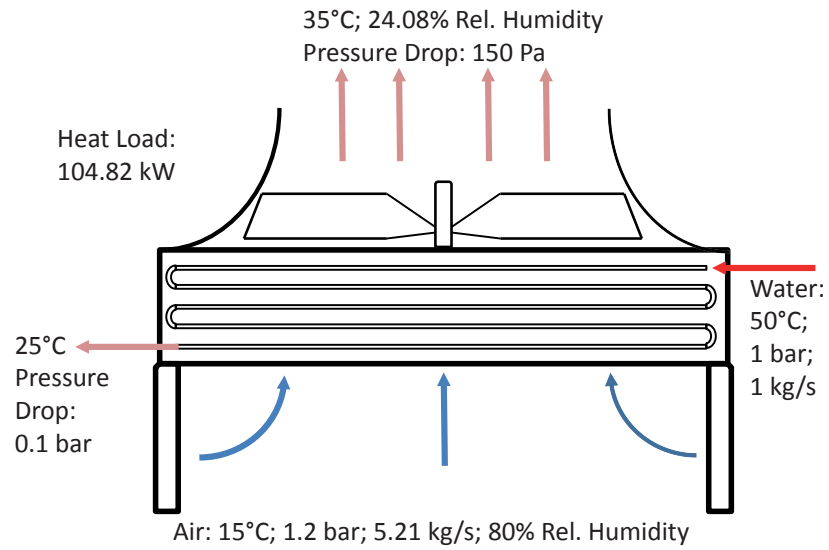


Figure 3.2: Schematic of Water-to-Air-Heat-Exchanger.

Table 3.1: Available measurements in the example process.

Water side			Air side		
Water inlet temperature	$T_{w,in}$	°C	Air inlet temperature	$T_{air,in}$	°C
Water inlet mass flow rate	$\dot{m}_{w,in}$	$\frac{kg}{s}$	Air inlet pressure	$p_{air,in}$	bar
Water inlet pressure	$p_{w,in}$	bar	Air inlet humidity	$\varphi_{air,in}$	%
Water outlet temperature	$T_{w,out}$	°C	Air outlet temperature	$T_{air,out}$	°C
Water outlet pressure	$p_{w,out}$	bar	Air outlet pressure	$p_{air,out}$	bar

3.7 Steady State

3.7.1 CASE 1 – Initial Values Preparation Process

In order to illustrate the ideal behaviour of enhanced reconciliation we created a set of measurements which all represent the true values. For this we assume to have the measurements in table 3.1 available:

We assume the pressure drops to be fix and introduce them as parameters in our model. This means that there is a redundancy concerning the pressures on water and air sides: two measurements plus one fixed parameter (pressure drop). All other variables are measured once or are calculable without redundancy. As a result, the variation of the measurements has a bigger influence on the reconciled values.

We introduce four variables (including two parameters) for re-injection and thus enhanced reconciliation:

- Air mass flow rate

Chapter 3. Waste Heat Valorisation System Characterisation

- Air outlet humidity
- Heat load
- Heat transfer coefficient

The heat load corresponding to the true values is 104.825 kW and the heat transfer coefficient (assuming a heat exchanger surface of 15 m², not counting fins) is of 0.5667 $\frac{\text{kW}}{\text{m}^2 \cdot \text{K}}$. For this example we chose a simple approach, more complex calculations of heat transfers are shown in chapter 4, section 4.3.5.

For all the measurements we use the exact value with a supposed inaccuracy σ of 1 %. We will call this set-up CASE 1. Using it we can analyse the influence of the initial values and inaccuracies:

At first, CASE 1.1, we use rough estimates of the four re-injected values as initial “virtual” measurements:

Air mass flow rate:	$m_{air,in}$	5.2 $\frac{\text{kg}}{\text{s}}$
Air outlet relative humidity:	$\varphi_{air,out}$	25 %
Heat load:	\dot{Q}	104 kW
Heat transfer coefficient:	U	0.5 $\frac{\text{kW}}{\text{m}^2 \cdot \text{K}}$

To test the behaviour of the enhanced reconciliation we inject these values with an inaccuracy value of:

- a: 5 %
- b: 100 %

In order to compare the results, two measures of quality are used:

- The a posteriori inaccuracy (equation 3.12).
- the sum of the relative differences between reconciled and true values (Equation 3.1).

$$D_{rel,t} = \sum_i \left(\frac{\sqrt{(y_{b,i,t} - y_{i,t})^2}}{y_{b,i,t}} \right) * 100 \text{ [%]} \quad (3.13)$$

Where $y_{b,i}$ is the true value of variable i .

The development of the inaccuracies of the four re-injected variables of CASE 1.1a (5 %) and 1.1b (100 %) are shown in figure 3.3 and a detail in figure 3.4. The values of the inaccuracies are shown as negative values; this is due to the Software Belsim Vali.

It can be seen that the first case leads to quicker reduction of inaccuracies, but the advantage becomes very small after a few hundred time steps. The sum of the inaccuracies of the 14

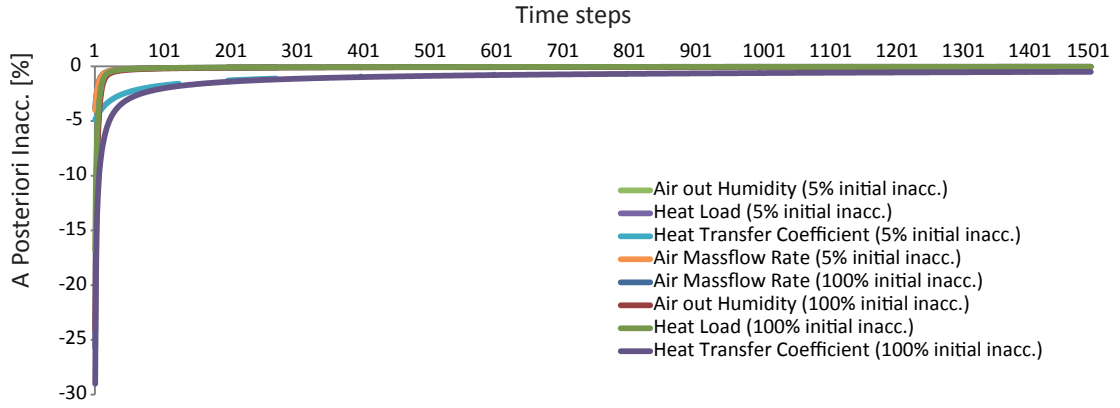


Figure 3.3: A posteriori inaccuracies of re-injected values, 5 % and 100 % initial values CASE 1.1.

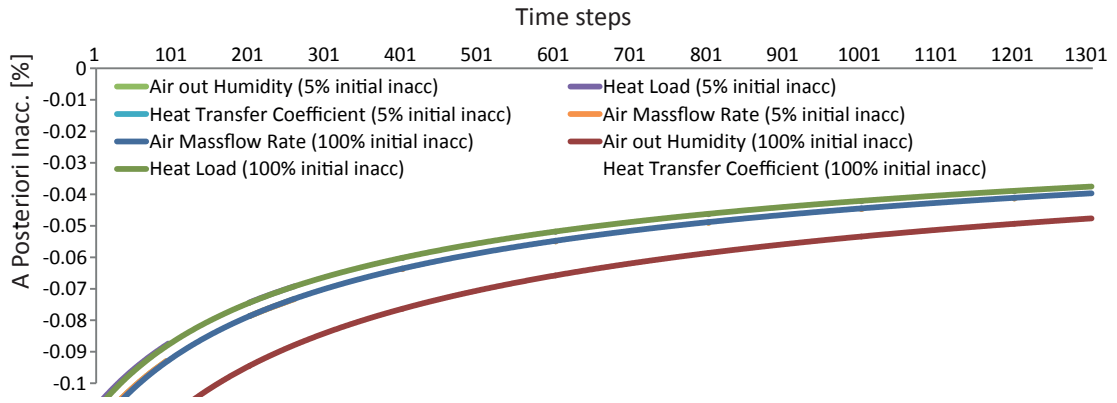


Figure 3.4: Detail of a posteriori inaccuracies of re-injected values, 5 % and 100 % initial values CASE 1.1.

above mentioned variables (measured and re-injected) of all the 1500 time steps shown in the graphs is 10470.3 % for case 1.1a and 10889.6 % for 1.1b, if we only look at the last one hundred time steps (from 1401 to 1500) we find 641.0 % (1.1a) and 641.1 % (1.1b). The inaccuracies of the heat transfer coefficient decrease considerably slower than those of the other variables. This is the effect of the smaller influence (redundancy) the other variables have on it. The more a variable is influenced by other variables, the quicker the inaccuracy will decrease.

From the lower inaccuracy (Equation 3.10 and 3.11) results a higher impact of the rough measurements. This has as an effect that the otherwise precise measurements are reconciled further apart from the true values in case 1.1a. Consequently, D_{rel} (equation 3.13) at time step 1500 is higher for Case 1.1a (12.1 %) than for 1.1b (0.9 %).

Replacing the rough estimations by a set of initial values that corresponds to the true values CASE 1.2 and test the two inaccuracies again (1.2a and 1.2b) shows that for a good estimation, the choice of lower inaccuracies is advantageous: the sum of all inaccuracies of all the 1500 time steps shown is 10505.4 % for case 1.2a and 10892.5 % for 1.2b, if we only look at the last one hundred time steps (from 1401 to 1500) we find 640.8 % (1.1a) and 641.2 % (1.1b). The figures for CASE 1.2 show the same trends and are overall very close to those of CASE 1.1. As

for D_{rel} of all 14 variables at time step 1500, we find values in the area of 10 % to 3 % in both cases, these differences result from rounding differences rather than the actual calculations, therefore we consider that the differences are too small to be significant.

3.7.2 Non-linearities

An inconvenience of reconciliation is the behaviour regarding non-linear relations. To illustrate this we take a simple example: the calculation of the logarithmic mean temperature difference (Equation 3.14).

$$LMTD = \frac{\Delta T_{hot\ side} - \Delta T_{cold\ side}}{\ln\left(\frac{\Delta T_{hot\ side}}{\Delta T_{cold\ side}}\right)} \quad (3.14)$$

Where $\Delta T_{hot\ side}$ is the temperature difference between the water inlet and the air outlet, $\Delta T_{cold\ side}$ is the temperature difference between the water outlet and the air inlet. This is done assuming a counter flow within the heat exchanger. Additionally the hypothesis of constant cp values is a prerequisite for the use of this formula (Borel and Favrat, 2010). If we use the true values with an added noise, even though the noise is symmetrical/the distribution is normal around the true values, a clear tendency (with one order of magnitude less than the amplitude of the variations) for the LMTD can be observed. The values are on average higher than the LMTD corresponding to the true values. In other words: equal amplitudes in different directions or on different variables do not have an equivalent influence on the calculated parameter. This illustrates that nonlinearities have to be treated carefully, especially because error propagation and the combination of several biases, induced by different nonlinear equations which are amongst each other also subject to relations (non-independent), can lead to high errors. This is also to be kept in mind if those parameters are used for the enhanced reconciliation directly, since the decrease of the “inaccuracy” leads then to an adjustment towards a biased value, especially for the earlier measurements. However this is not a problem uniquely concerning the new methodology of enhanced data reconciliation but concerns data reconciliation and parameter identification in general.

3.7.3 CASE 2 – Measurements Subject to Noise

Measurements even in an overall steady system are rarely as precise as assumed in the first calculations of CASE 1. In order to create sets of measurements that are more realistic, we used several methods to produce a well-defined noise around the true values. This is supposed to imitate noise induced by the measuring system and possibly local non-steady-conditions. This means that we assume the global conditions to be unchanged from the true conditions, even though the measurements vary around the true values. We used several (pseudo-)random generators for the variations, always going for a normal distribution with 95 % of all values between -1% and 1% around the true values (standard deviation of 0.5%) and a set of values that have a symmetric distribution of $\pm 1\%$ around the base, but that have been shuffled in a

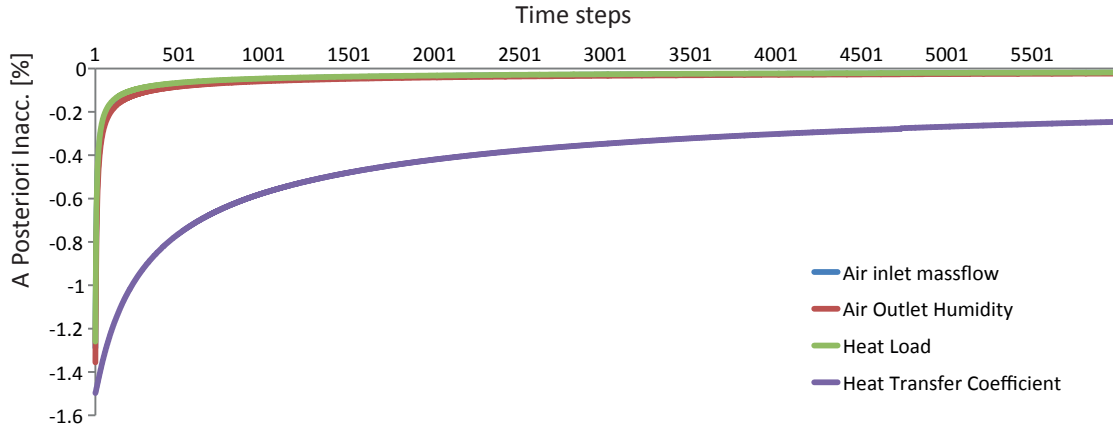


Figure 3.5: A posteriori inaccuracies of re-injected variables, CASE 2.1.

random order. The results for all these sets of measurements are equivalent, so we chose a normally distributed set of values generated with a latin hypercube sampling pseudo random generator provided by Mathworks/Matlab for the generation of the measurements used in this paper. Since we know the true values we start with an estimation of the four precise re-injected values (like in CASE 1.2), except for rounding errors. We analyse two sets of 6000 measurements. The first set (CASE 2.1) is a repetition of 1500 measurements four times; this gives us the possibility to evaluate the evolution within the enhanced reconciliation, and compare the influence of the changing re-injected values and their precisions on the same measured values. Figure 3.5 shows the evolution of the inaccuracies of the four re-injected values. Again, the negative sign of the percentages is due to the Software Belsim Vali.

It can be seen that the values decrease and reach a level below 0.1 % for all variables except the inaccuracy of the heat transfer coefficient, which is subject to less influence from other measurements and thus less redundancy. The relative differences of the reconciled re-injected values and the true values in percent are shown in figure 3.6. The periodic character, due to the four repetitions of the measurements is visible, especially regarding the heat transfer coefficient. It can also be seen that the relative differences are all below or around 0.1 % after approximately 2000 iterations.

To demonstrate the efficiency of the enhanced reconciliation, D_{rel} values of all 14 variables (ten measurements and four re-injected values) are analysed. We chose to base this analysis on the last 100 measurements of each iteration, meaning we analyse the measurements from 1401-1500, 2901-3000, 4401-4500 and 5901-6000. The results are presented in table 3.2.

Additionally to the increase in accuracy that we saw above, it can be seen that the D_{rel} values decrease over time and thus that the estimations get better. Compared to conventional reconciliation, the results are on average about 22 % better. To check if the tendencies seen with the repetition of the same 1500 values, is also valid for other sets of data we repeated the calculations. Below is one example with 6000 different values (CASE 2.2) (the first 1500 are

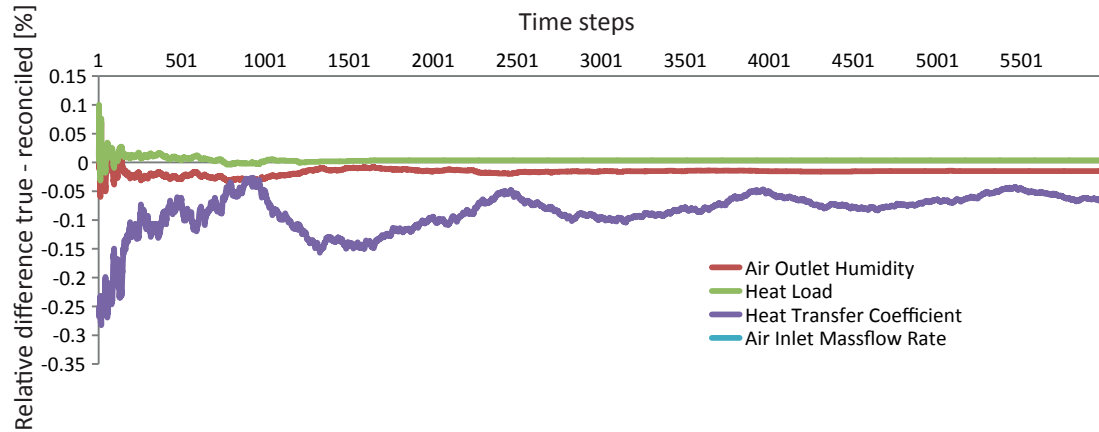


Figure 3.6: Relative differences between true and reconciled values of re-injected variables CASE 2.1.

Table 3.2: Evolution of the D_{rel} values Case 2.

D_{rel}	1401-1500	2901-3000	4401-4500	5901-6000	Conventional reconciliation
Average	4.355	4.320	4.302	4.290	5.238
Minimum	0.705	0.690	0.680	0.672	1.603
maximum	11.899	11.908	11.908	11.908	10.839

identical to CASE 2.1). The plot of the inaccuracies looks almost identical to that of CASE 2.1, shown above in figure 3.5. The relative differences to the true values is shown in figure 3.7. Again, the differences are very small, and after about 2400 time steps below 0.1 %.

Overall we can say that the evolution of the inaccuracies reveals a strong decrease over time. This stabilizes the reconciled values and influences the minimum of the sum of all penalties increasingly. Comparing the results from enhanced data reconciliation and classical data reconciliation we find the following results: the conventional reconciliation leads to much less stable reconciled values, as can be seen on the graphs below. The reconciled values follow the measured values to a large extent and the relative distance to the true values can be a lot higher for the four re-injected values as shown in figure 3.8. The relative differences can be over 3 %, whereas the average relative differences are in all four cases below 0.01, which means the distributions are more or less evenly around 0.

Also the inaccuracies do not decrease for the conventional reconciliation but they remain close to a certain value as can be seen in figure 3.9.

Even though the variables chosen for re-injection do not all stabilize exactly at the true value, the system shows in the sum less distance to the true values than the same system with conventional reconciliation. The relative distances and the inaccuracies are one to three orders of magnitude higher for conventional reconciliation.

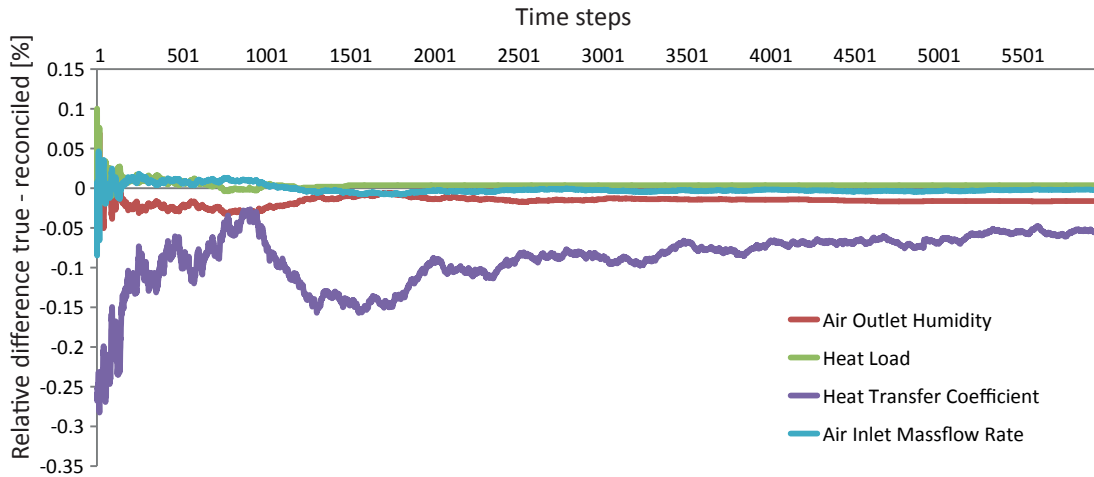


Figure 3.7: Relative differences between true and reconciled values of re-injected variables CASE 2.2.

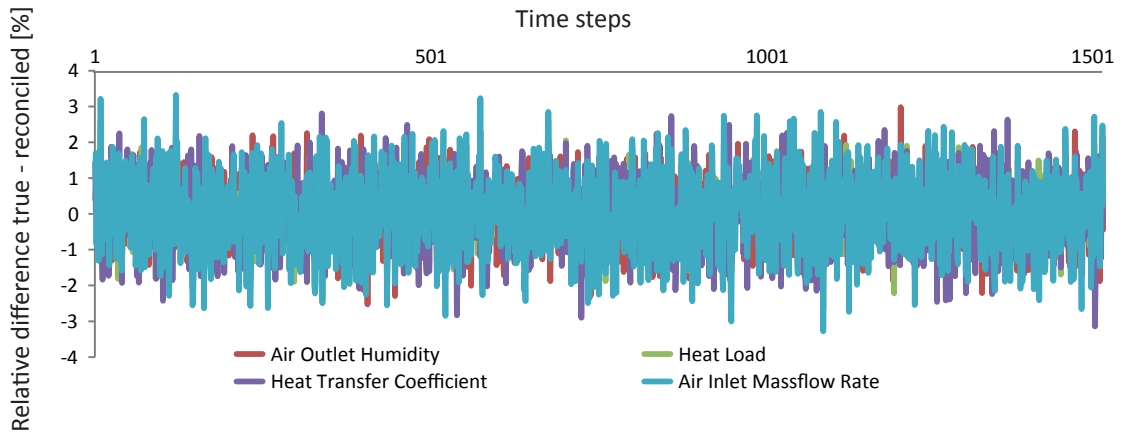


Figure 3.8: Relative differences between true and reconciled values in analogy to CASE 2.2 but with conventional reconciliation.

3.7.4 CASE 3 – Over Specified Systems

In steady state conditions the methodology seems especially useful to be used on processes with little to no redundancy on the measurements. In systems with redundancy the conventional reconciliation leads to more corrections of the measured variables since the measurements can be contradictory. To illustrate this we added two measurements to the process (CASE 3.1):

- Air inlet mass flow rate.
- Air outlet humidity.

The heat load and the heat transfer coefficient are, as before, used for re-injection as virtual measurements. Here, it makes sense to check the differences between raw, conventionally reconciled and enhanced reconciled data. Since the raw data should be used to calculate

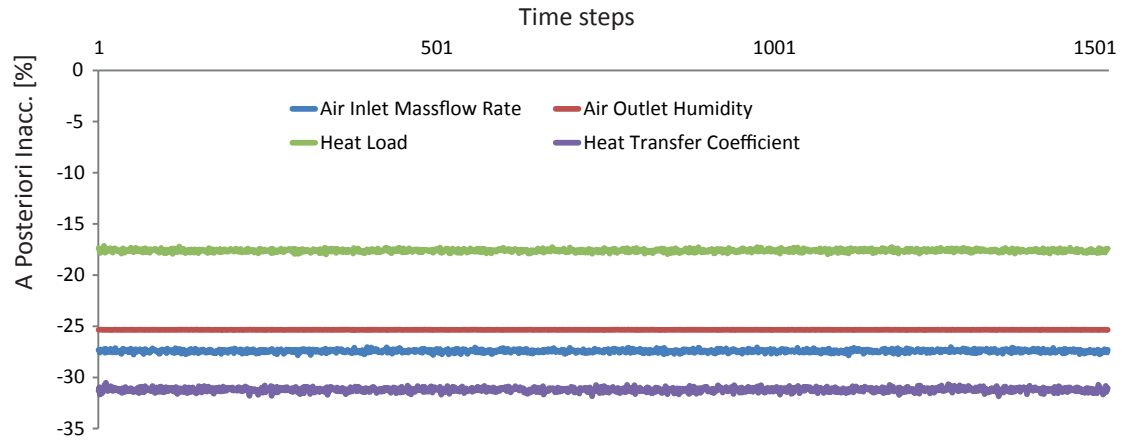


Figure 3.9: A posteriori inaccuracies in analogy to CASE 2.2 but with conventional reconciliation.

Table 3.3: Analysis of redundant case.

$D_{rel,mea}$ 1501-3000	Enhanced reconciliation	Conventional reconciliation	Raw measurements
Average	4.284	3.783	3.191
Standard Deviation	2.099	1.246	0.697
Average Inaccuracy, mea	0.67168	0.805	1
Average inaccuracy all	0.610	2.724	na

the heat load or the heat transfer coefficient (due to the fact that there are several ways to calculate them with the measurements which do not lead to the same result), we will look at the 12 measured variables only. We use the values from time step 1501 to 3000 since here the enhanced reconciliation already shows a certain degree of stability.

We can see from these numbers, shown in table 3.3, that the set of measurements has a relatively narrow distribution but a large inaccuracy and while the distribution is getting larger for conventional and enhanced reconciliation, the confidence in the values gets better. The average $D_{rel,\pi}$ of the re-injected variables is of 1.210 for the conventional reconciliation and 0.025 for the enhanced reconciliation. This shows the precision of the estimation of these parameters, and the difference of the average inaccuracies of all variables (including the re-injected ones) shows the advantage of the enhanced reconciliation in that regard.

In figure 3.10 the distribution is visualised by plotting a histogram of the average relative difference per measurement $D_{rel,mea}/12$, for the raw data, the conventionally reconciled and enhanced reconciled data. It can be seen that the peak (and also the average) is approximately at the same place but the distributions larger for the reconciled values. This is not surprising since the reconciled values have been calculated under several constraints, this leads to coherent data, with increased confidence in the values, but the errors are propagated and thus

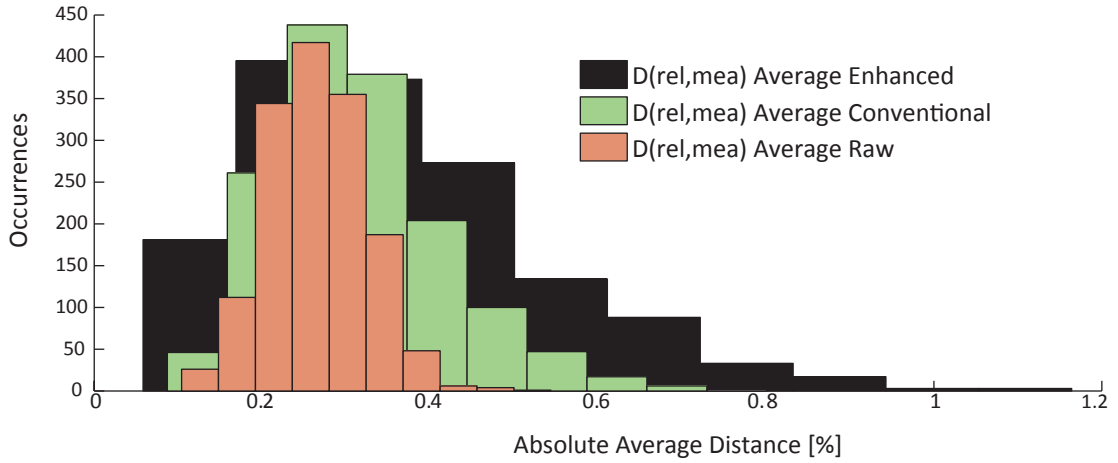


Figure 3.10: Distribution of average D_{rel} values of measured variables for raw, conventionally and enhanced reconciled data.

combine. The effect is even stronger for enhanced reconciliation since more constraints are added but the confidence in the values and especially in the parameters increases.

3.7.5 CASE 4 – Under Specified Systems

A special case is a situation with an amount of measurements that do not entirely allow to define the process (e.g. if a piece of the measuring equipment fails). In order to show the behaviour we will reduce the amount of available measurements by one compared to CASE 2, deleting the air outlet temperature (CASE 4.1). We introduce an estimation of 35.5 °C (instead of a true value of 35 °C) and an inaccuracy of 10 %. As measurements we use the same 1500 points as in CASE 2.1. From the results it can be seen that even though the amount of measurements would not allow to calculate the entire system we are able to reconcile values with a D_{rel} average of 1.457 for the last 100 time steps. At first it might be surprising that the average D_{rel} is lower than in CASE 3.1, but this can be explained by the fluctuation of the now missing measurement that is included in the cases before. Even though the first estimation is off, the reconciled values tend quickly towards the true value (figure 3.11).

In other words, the estimation of the other re-injected values gains more importance and since it was precise for this test, it leads to higher overall precision.

When we do conventional reconciliation and we suppose the same 35.5 °C and 10 % inaccuracy, the reconciled values are further off as can be seen in table 3.4.

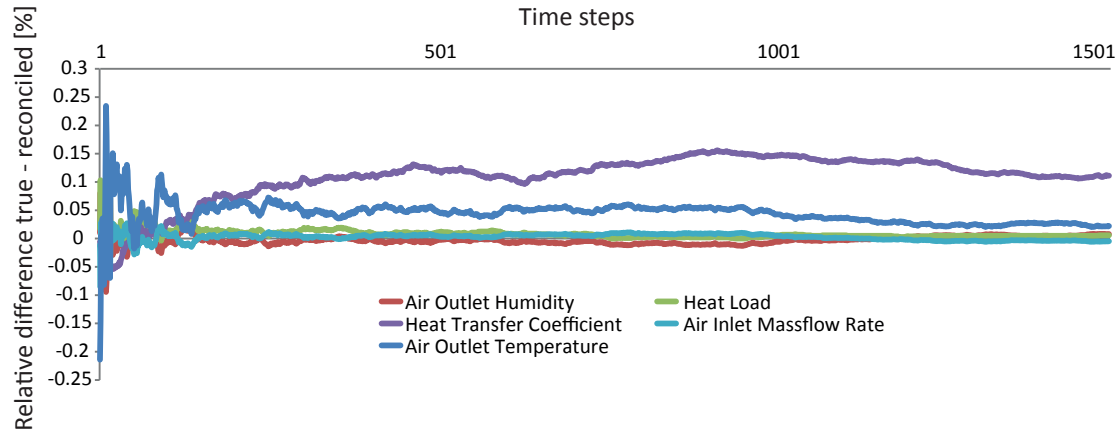


Figure 3.11: Relative differences between true and reconciled values of re-injected variables CASE 4.1.

Table 3.4: D_{rel} values of case 4.1.

D_{rel} 1501-3000	Enhanced reconciliation	Conventional reconciliation
Average	1.457	11.222
Minimum	0.424	9.049
Maximum	2.776	15.661
Average Penalty	0.378	0.259

3.8 Non-Steady State – CASE 5

The analysis is quite different for non-steady-state or transient processes. Under transient we understand situations which can be separated into quasi-steady state situations, in order to make reconciliation possible. The stabilising effect of the enhanced data reconciliation asks for careful modelling. In order to make the enhanced reconciliation work, it has to be made sure that the parameters for re-injection are actually constant. To demonstrate this we show a first case (CASE 5.1). The inaccuracies are not re-injected for this demonstration. We fixed the inaccuracies to 1.5 % and put as start values precise estimations as done above. The measurement values used are a variation of the true values. We applied an increase to the air inlet temperature from 15 to 20 °C, but keeping the heat load constant, the outlet temperature is increased from 35 to 38 °C. These two temperature changes affect the mass flow rate and the humidity at the air outlet as well as the heat transfer coefficient. The rest of the variables are assumed to be constant, we call this data set the non-steady true values. In CASE 5.1 we apply a gradient, which increases the temperature linearly and when arriving at the maximum temperature decreases it with the same slope; one “cycle” of increasing and decreasing is done in 1281 time steps. This is equivalent to a gradient of 0.052 % per time step regarding the air inlet temperature. The plot of the true and reconciled values of the air outlet humidity figure 3.12 and the relative distances figure 3.13 of the re-injected variables show the effect of the stabilization.

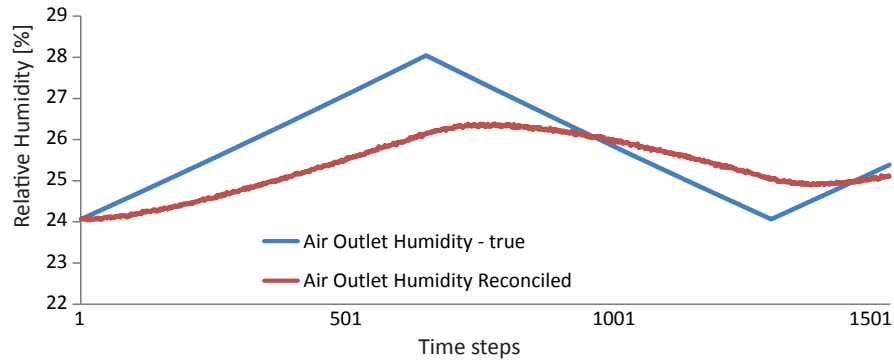


Figure 3.12: Relative Humidity reconciled and true values, CASE 5.1.

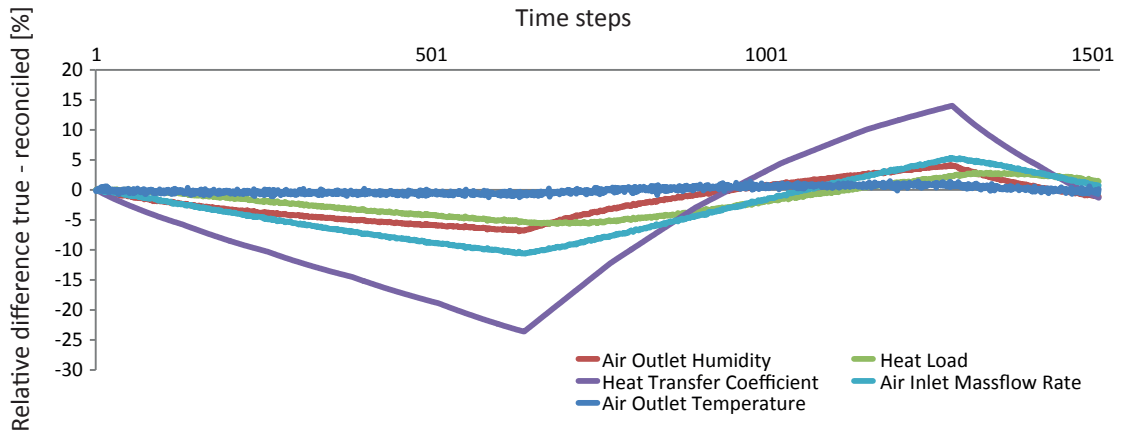


Figure 3.13: Relative differences between true and reconciled values of re-injected variables and Air Outlet Temperature CASE 5.1.

As we can see from figure 3.14 and table 3.5, the penalties are higher for the enhanced reconciliation; this could easily be used as an indicator for a process that should otherwise be stable. This can be especially interesting for tracking degradation or fouling of equipment.

We propose higher inaccuracies for non-steady states. Table 3.6 and figure 3.15 show the impact of the inaccuracies.

By looking at the physics of the model, the only constant parameter is identified to be the heat load. Thus a second non-stationary Case 5.2 is presented, which uses only the heat load as re-injected parameter. In figure 3.16 it can be seen, that the system is stabilized by this parameter. The D_{rel} value of this case is 4.446 %, the estimation of the parameter heat load is very precise.

In conclusion we can say that in the case of quasi-stationary transient situations the methodology can be used, but is very important to identify parameters that are actually constant.

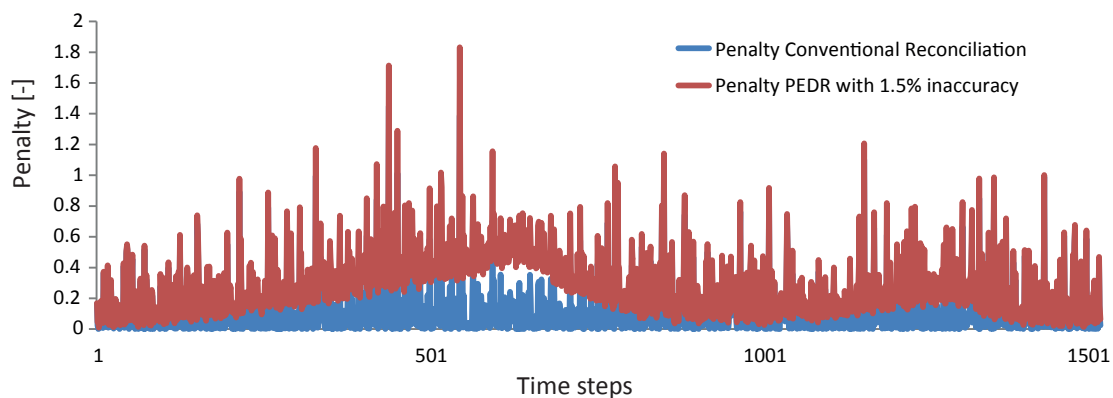


Figure 3.14: Penalty CASE 5.1 and Penalty of conventional Reconciliation.

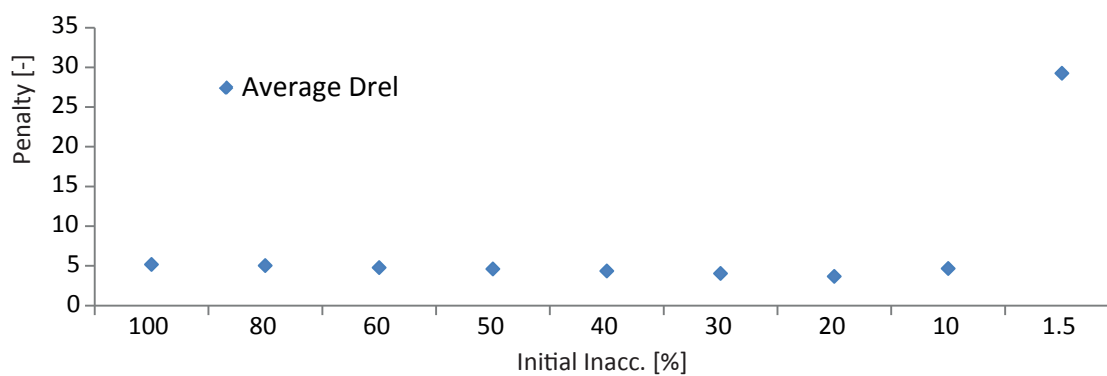


Figure 3.15: Penalty of CASE 5.1 with different initial inaccuracies (1.5 % to 100 %).

Table 3.5: D_{rel} values of case 5.1.

D_{rel} 1501-3000	Enhanced reconciliation	Conventional reconciliation
Average	29.238	5.514
Minimum	1.243	1.92
Maximum	61.565	13.072
Average Penalty	0.165	0.124

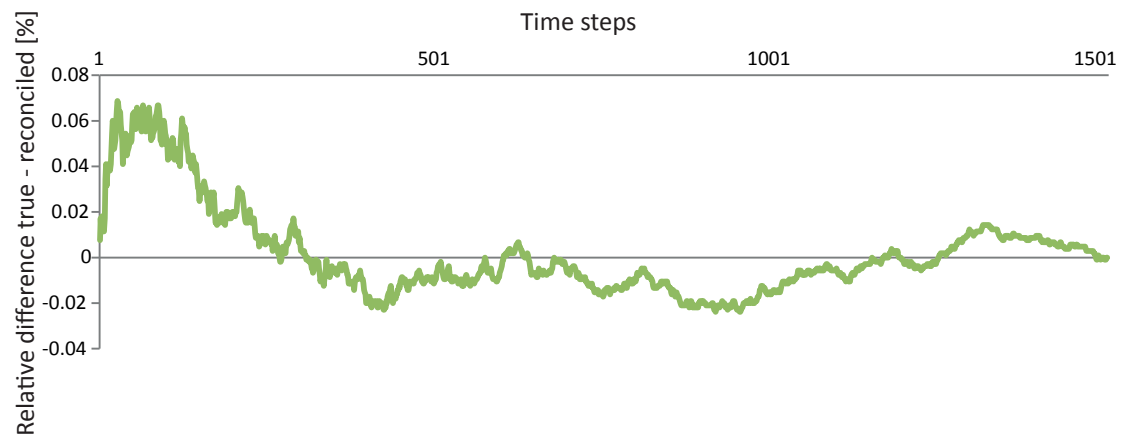


Figure 3.16: Relative differences between true and reconciled values of re-injected variable “heat load” CASE 5.2.

Table 3.6: Impact of inaccuracy values in transient processes.

	100 % inacc.	80 % inacc.	60 % inacc.	50 % inacc.	40 % inacc.	30 % inacc.	20 % inacc.	10 % inacc.	1.5 % inacc.	Conventional reconciliation
D_{rel} 1-1500										
Average	5.167	5.033	4.776	4.591	4.344	4.023	3.670	4.646	29.238	5.514
Minimum	1.788	1.728	1.555	1.327	1.145	1.126	1.362	1.480	1.243	1.920
Maximum	12.151	11.693	11.045	10.500	9.704	8.528	7.359	8.933	61.565	13.072
Average Penalty	0.124	0.126	0.125	0.125	0.126	0.126	0.128	0.129	0.165	0.124

3.9 Application to LOVE-Demonstrators

The data from the LOVE-Demonstrators (figure 2.15 and figure 2.11) have shown some strong incoherences, which led to heated discussions in the LOVE-Consortium. For example, the energy balance between the hot gases and the water loop showed a gap of sometimes more than 100 kW which is too much, to be explained by losses. The reasons for these incoherences were multiple: temperatures near the dew-point were disturbed by condensation on the thermocouples, the gas flows were turbulent and inhomogeneous due to winding piping, making it difficult to use them. We thus built flowsheeting models which represent the thermodynamics of the demonstrators and which could be used to reconcile the measured values.

We made tests with enhanced data reconciliation on the data from the demonstrators in order to increase the reliability of the reconciliation. Since the enhanced reconciliation uses information transfer between measuring periods, the state must be as steady as possible or the identified parameters independent of the changes. Unfortunately the experiments in Höver and Kollenbach were not steady enough to apply this novel method to the measurements in most cases. We used the enhanced data reconciliation on the identification of the heat transfer coefficient of the direct boiler with the environment. It was necessary to make a few assumptions for this, which are shown below.

3.9.1 Model Description

The model is programmed in Belsim Vali (Belsim, 2011) and controlled by a Matlab script (MathWorks, 2012), which saves the measurements in the right format, launches the Vali model, recovers the results and stores them in an accessible format. The application of the reconciliation is done in Vali for each set of data one by one.

The pretreatment of the raw data includes the application of a moving average. This is necessary because the distance between the different parts of equipment and the resulting transportation times of the fluids between them introduces a delay in occurring perturbations and changes of state. In other words, it is a way to enable the stationary model to receive a set of data which is coherent, without applying time shifts between measurements (measurement A at time t corresponds to measurement B at $t - 5$ etc.). It also has the advantage of reducing the influence of local fluctuations e.g. due to a turbulent flow pattern, which appears like “noise” in the raw data. The average is applied over a time period of 2 min and 35 s, which corresponds to the time the fluids need to circulate twice through the system for the installation in Höver. The decision to chose a period of time corresponding to the twice the circulation time through the system has been made, in order to average momentaneous perturbations with two unperturbed values. An example of how this affects the measured data is shown in figure 3.17. As can be seen in figure 3.18, the heat exchangers recovering the heat were in and on the roof of a building (on the left), while the containers containing the turbine, and



Figure 3.17: Panorama photo of the LOVE demonstrator in Höver.

other equipment were outside on the ground, leading to such a long circulation time. At the Kollenbach installation the direct boiler was installed next to the container containing the turbine, thus a shorter circulation time was achieved. Consequently the moving average was chosen shorter, 1 min and 30 s were sufficient.

The prepared data files in an Excel format were then read line by line (data set by data set) by the Matlab script and written into so called mea files. A mea file is a data format of Vali which allows the software to read it as a set of measurements corresponding to the tags of the model, with their corresponding inaccuracy. Vali reads the measurement data, does the reconciliation as described above in chapter 3 and writes an output file. The output file is then read by the matlab script and again the results are stored line by line (dataset by dataset) into a spreadsheet.

The flow sheeting model itself takes all thermodynamic constraints (heat and mass balances) into account. It is build in a way that parameters like the turbine isentropic efficiency can be identified. For some values a set of additional equations is added to the problem, either by the use of so called controllers, which link tags in simple linear equations or by the use of Flexcode which is a Fortran like programming language.

The types of measurements that where included are: temperatures, pressures, mass flow rates, chemical compositions, humidity, wattage of the generator. In case of the Höver demonstrator shown in figure 2.11 a total of 75 measurements were used for the data reconciliation. In case of the Kollenbach demonstrator shown in figure 2.15, 78 measurements were used. It is higher because in the first demonstrator quite a few measurements failed and were replaced only afterwards and with the experience from the first demonstrator additional measurement points were installed.

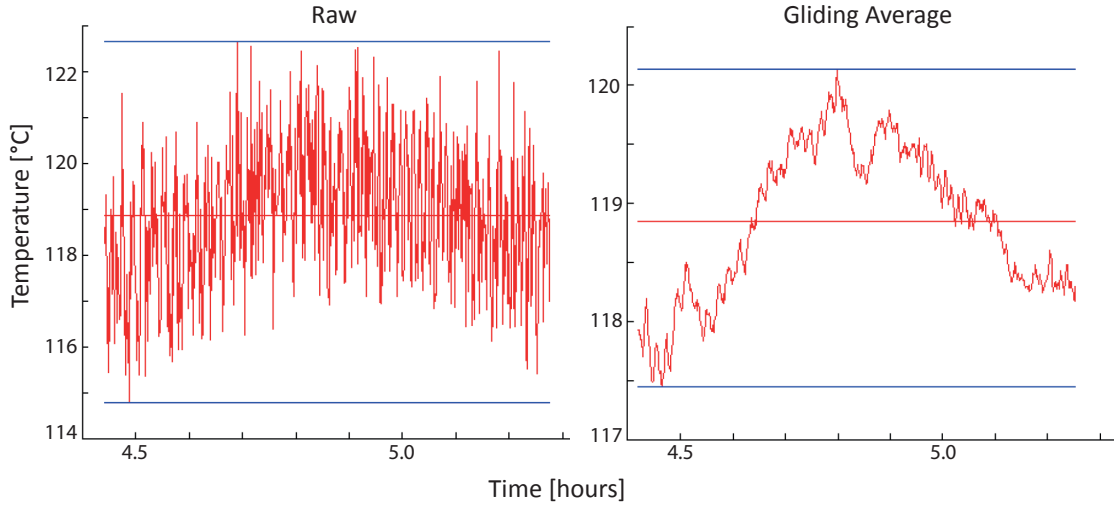


Figure 3.18: Temperature measurement before and after application of moving average.

Below we will show the analyses that have been used to calibrate the ORC identification tool.

3.9.2 Turbine Isentropic Efficiency

The turbine used in the project was especially designed and produced by Cryostar SA, a member of the LOVE-Consortium. It was designed to be used in both demonstrators with always the same inlet pressure. Some details of the turbine design-point can be seen in figure 3.19 which shows the information plate by Cryostar.

The isentropic efficiency of the turbine is interesting to be analysed in detail since it shows the behaviour of the turbine especially in part load conditions. Information about the part load behaviour can be used to identify the potential for improvement. It is defined as:

$$\eta_{is} = \frac{h_{in} - h_{out}}{h_{in} - h_{out,is}} \quad (3.15)$$

where the index *is* stands for isentropic, *in* and *out* denote the inlet and outlet of the fluid at the turbine respectively.

With the enthalpy difference

$$\dot{H}_{turbine} = \dot{H}_{in} - \dot{H}_{out} \quad (3.16)$$

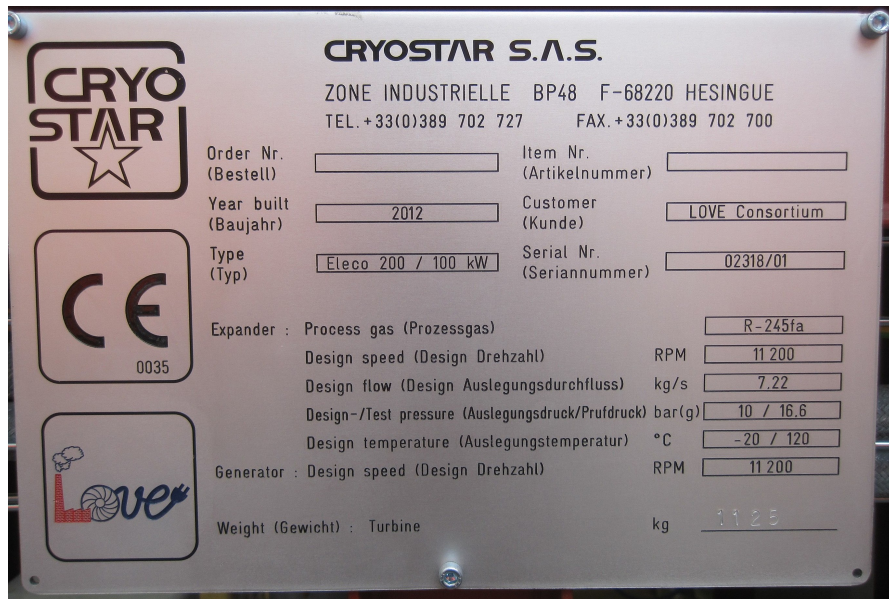


Figure 3.19: Cryostar turbine specifications.

the energy flow rate from the fluid is calculated. By subtracting the measurement of the electrical power, the combined friction and heat losses in the turbine (cooling) and generator are calculated:

$$\dot{L}_{\text{turbogen}} = \dot{H}_{\text{turbine}} - \dot{E}_{\text{mea}} \quad (3.17)$$

where L stands for losses, *turbogen* describes the set of turbine and generator, \dot{E}_{mea} is the measured electrical power. The heat losses are mainly cooling of the generator and the turbine, which is done by a very small flow of refrigerant. The refrigerant for cooling is extracted at the turbine inlet and re-injected at its outlet. The cooling loss is thus part of $\dot{L}_{\text{turbogen}}$.

In figure 3.20 the model of the turbine is shown. It can be seen that a “turbine” unit is used for the calculation of the isentropic efficiency, and a separate “blackbox” for the calculation of the friction and cooling losses.

Out of all the measuring periods only situations with the most steady behaviour were picked for further analysis. In figure 3.21 the range of stable measurements for the turbine isentropic efficiency is shown in relation to the produced power. Over 6000 measurements are included in this graph, which result from twelve measuring periods aiming at several different set-points. The range of each cluster shows the difficulty of stabilising the installation and is an indicator that the isentropic efficiency is not solely a function of the produced power. A clear trend however can be seen. The nominal power of 100 kW was not reached during the experiments, it is thus impossible to show the entire range of isentropic efficiencies. However, in discussions

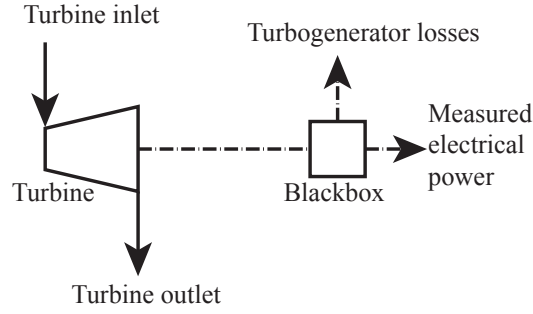


Figure 3.20: Model of the turbine used for reconciliation.

with Cryostar an efficiency of over 90 % was stated. An efficiency of 77 % at about 13 kW and thus about 13 % of the nominal power was observed, which shows the remarkable stability of the turbine behaviour throughout the entire domain of part-load use.

Figure 3.22 visualises the evolution of the friction and heat losses $\dot{L}_{\text{turbogen}}$ in the turbine and generator. The values which increase from about 8 kW to about 12 kW while more than quintupling the produced electricity, show that the need for internal cooling and the friction losses remain in the same order of magnitude. We could deduce that the cooling needs may vary with the volume and energy flow, it seems however reasonable to assume that the inner mechanical resistance and friction losses of the units stay almost constant, since the rotation speed is kept constant at 10 200 rpm (figure 3.19). These values can be used for improving the ORC identification tool, shown in the next chapter.

It can be seen that the isentropic efficiency is quite stable over the entire range of part load use, the same is true for the sum of friction and heat losses of the turbine and generator, this emphasizes the need for proper integration of the ORC into the process in order to produce a maximum amount of electricity in every situation. This also shows that the LOVE-Demonstrator can be used in a wide range of applications with fluctuating amounts of heat available, if they are above the needed inlet temperature of the turbine (which can only vary in a very narrow range).

3.9.3 Heat Transfer Coefficient

The other example that will be shown here is the heat transfer coefficient of the direct boiler. The heat transfer coefficient is the relation between the heat flow rate that is transferred over a surface per degree of temperature difference:

$$U = \frac{\dot{Q}_{\text{trans}}}{A_{\text{HEX}} \cdot \Delta T_{\text{LM}}} \quad (3.18)$$

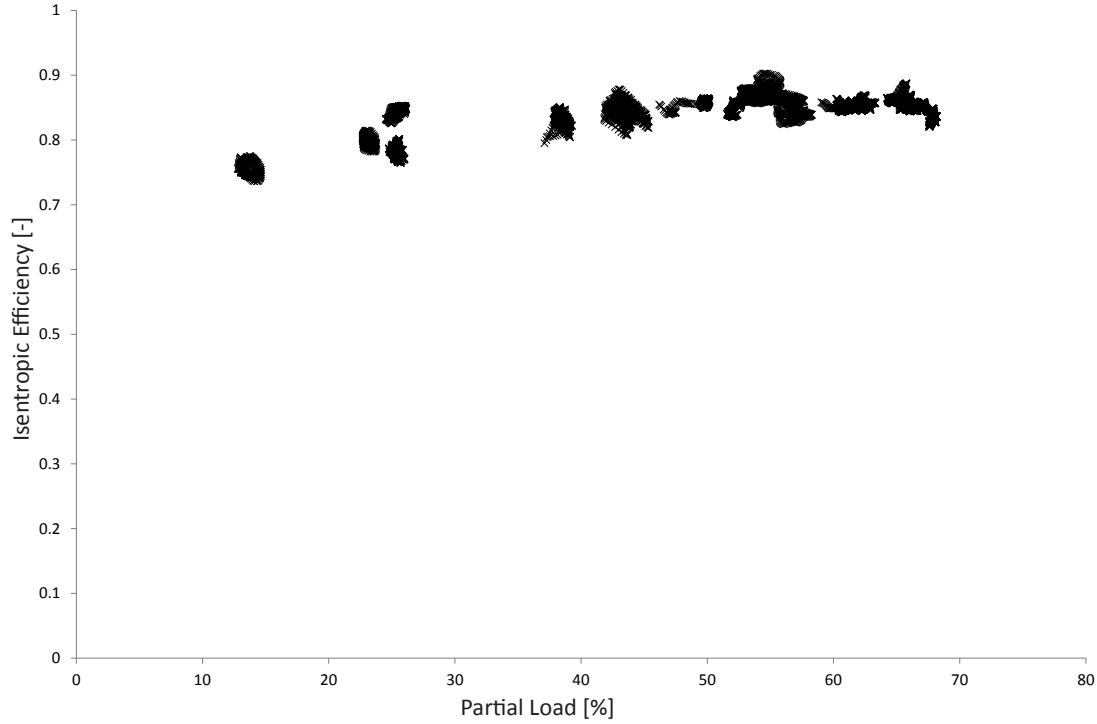


Figure 3.21: Isentropic efficiency of LOVE-turbine reconciled.

where \dot{Q}_{trans} is the transferred heat flow rate and A_{HEX} is the surface of the heat exchanger. The temperature difference ΔT_{LM} is calculated with the *LMTD* (equation 3.14). This is a simplification since we do not have any measurements of the real temperature within the heat exchanger available, the biggest error occurs since the working fluid phase change takes place at constant temperature. For the ORC-tool discussed in chapter 4 will use more precise heat transfer models, which is explained in section 4.3.5.

For this illustration we chose the heat transfer coefficient of the finned tube heat exchanger at the Kollenbach installation, since it is closest to the heat exchangers assumed for the ORC identification tool, chapter 4. In order to calculate the coefficient the Fortran-like Flex code is used, which is a tool of Belsim Vali.

Tags or variables are used for the thermal parameters, while the heat exchanger surface (3005 m^2) is hard coded. This corresponds to the total heat exchange surface composed of 137 m^2 of tube surface and 2868 m^2 of fin surface. This means a 'total surface' -to- 'tube surface' ratio of 21.93-to-1. We will use this for the economic models in chapter 4.

The heat transfer coefficients of the direct boiler shown in figure 3.23 are overall values, including preheating, evaporation and superheating of the working fluid. It is not trivial to estimate the heat exchange surfaces that are involved into each of the aforementioned steps, thus we will not divide the heat transfer to estimate individual values. The test points were all made with an evaporation temperature corresponding to an evaporation pressure

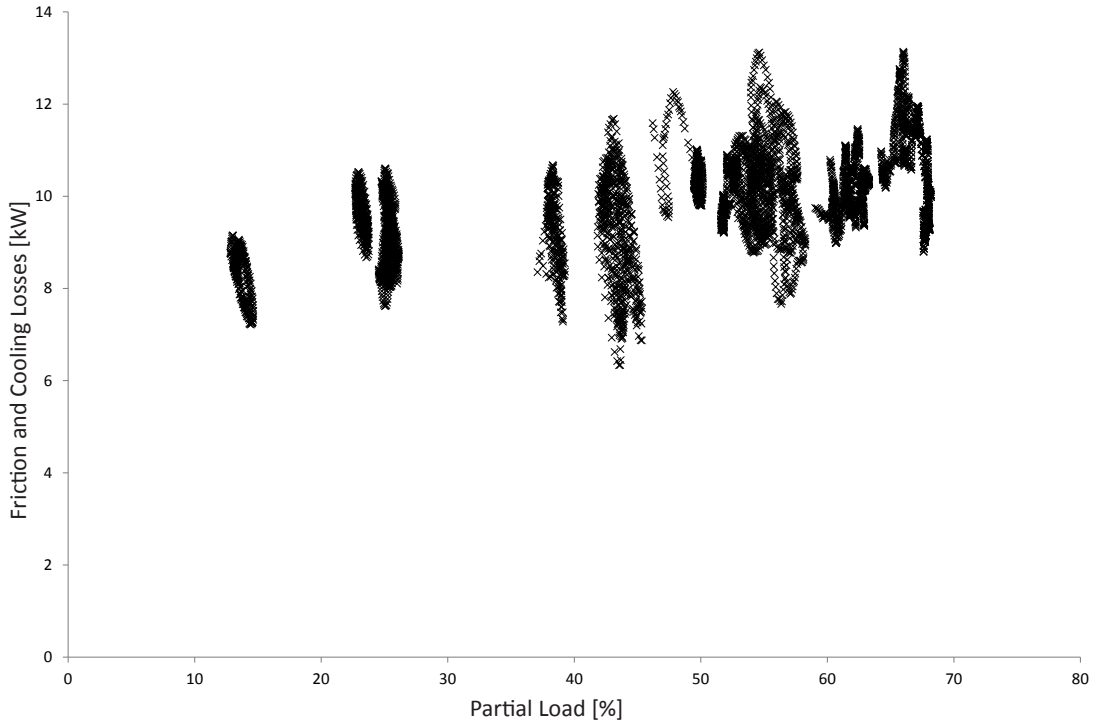


Figure 3.22: Friction and cooling losses of LOVE-turbogenerator reconciled.

of approximately 5 bar except for the ones that are encircled in red, which were made with an evaporation pressure of 4 bar. The values are in a range from about $85 \frac{\text{W}}{\text{m}^2 \cdot \text{K}}$ to about $135 \frac{\text{W}}{\text{m}^2 \cdot \text{K}}$. The dry fin efficiency was estimated to be 75 % (Maalouf et al., 2012a). The impact of the volume flow on the heat transfer coefficient is apparent, both for all measured data together and for each set point (cluster) individually. Figure 3.24 shows in detail the cluster of measurements (bottom left corner), taken on the 23. of September 2013, revealing the spreading of the measured points. The measurements are too scattered to use them for enhanced reconciliation in a meaningful way. Further more, no simple relation between volume flow rate, pressure and heat transfer coefficient is precise enough to describe the heat transfer coefficient sufficiently, even though they are obviously correlated.

A special case where we have applied enhanced reconciliation is the estimation of the heat transfer coefficient of the exterior of the direct boiler, which is not insulated. The difficulty here is that neither the mass flow rate of the hot gases nor their average temperature can be measured precisely due to a high degree of turbulence and an irregular temperature distribution. This means that there are too few measurements for a good estimation of the heat losses. Thus we can use an estimation of the cement specialists, who considered about $20 \frac{\text{W}}{\text{m}^2 \cdot \text{K}}$ for the heat transfer coefficient. This value was introduced as a “virtual measurement” and the reconciled values re-injected in the following time steps. Thus it is a combination of the cases 4 and 5 that we have seen before. The results can be seen in figure 3.25 and show that the reconciled values are all in the same magnitude. They have not yet converged to a

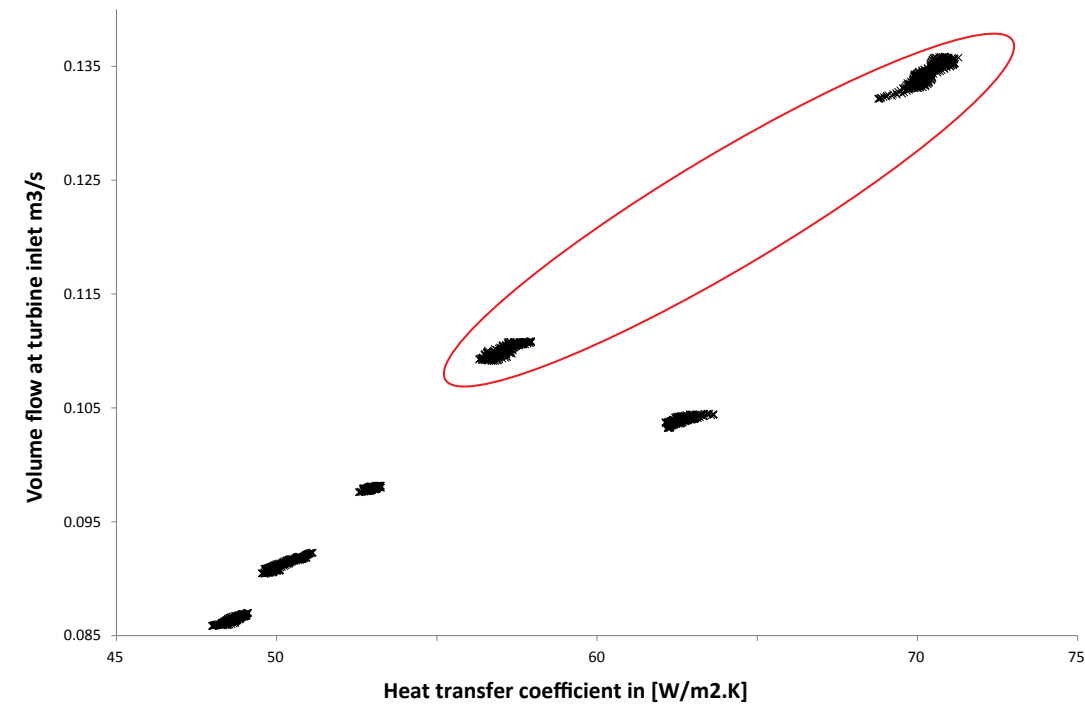


Figure 3.23: Relation between volume flow rate $\frac{\text{m}^3}{\text{s}}$ and heat transfer coefficient $\frac{\text{W}}{\text{m}^2 \cdot \text{K}}$.

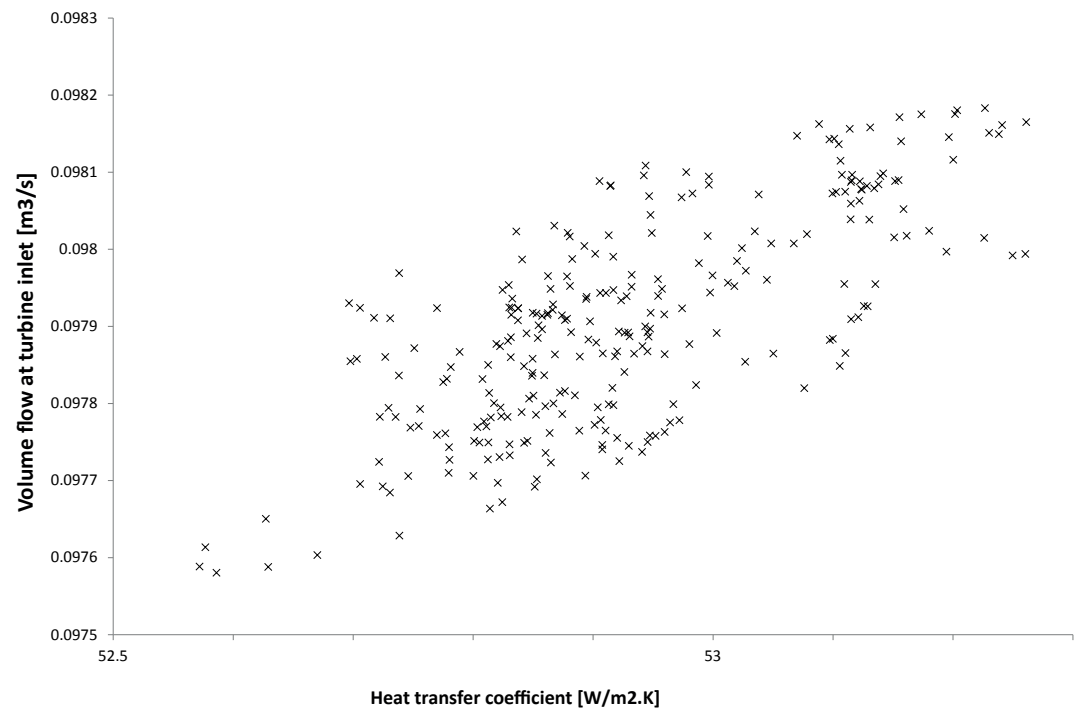


Figure 3.24: Relation between volume flow rate $\frac{\text{m}^3}{\text{s}}$ and heat transfer coefficient $\frac{\text{W}}{\text{m}^2 \cdot \text{K}}$ measured on the 23rd September 2013.

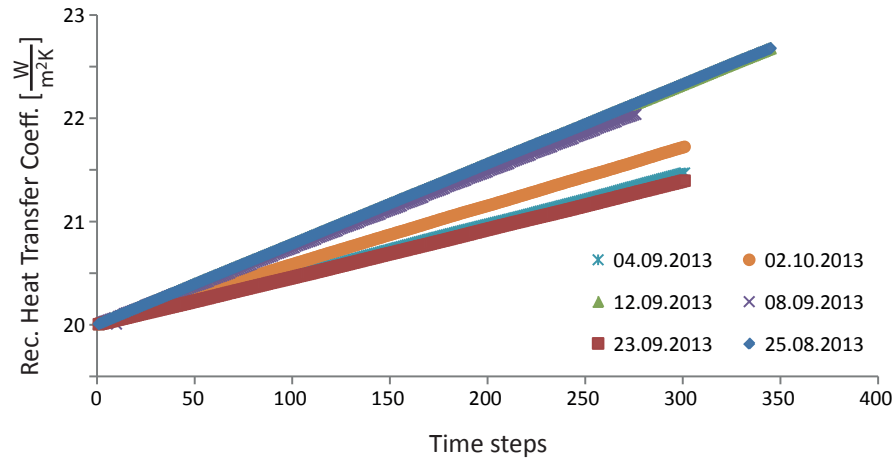


Figure 3.25: Heat transfer coefficient of the direct boiler with the ambient.

stable value since the measurement period was too short for that. Even though this does not lead to the true value of the heat losses with absolute certainty, the overall reconciled values of the demonstrator are coherent and there is no gap in the heat balances, as could be observed regularly in the not reconciled measurement data.

3.9.4 System Exergy Efficiency

With the reconciled data we were able to identify the exergy destruction in the demonstrators. Figure 3.26 shows these for the Höver demonstrator, it is interesting to see that the largest amount of the destruction is not at the level of the pump or turbine but at the level of the heat transfers. The destruction between the working fluid and the water circuit and from the water circuit to the working fluid account for 35.6 % points. Also, on the cold side the destruction is considerable accounting for 29.1 % from the condenser to the cooling water and from the cooling water to the environment.

For the Kollenbach site, where no water loop is used, figure 3.27 shows that the exergy destruction is lower. Again turbine and pump do not account for the largest amounts of exergy destruction, but the flue gas to evaporator destruction is considerable (32.8 %). Also, the destruction due to high cooling water temperature is quite high (11.7 %). This shows that the use of a direct boiler is beneficial. It also emphasises the importance of a good integration of heat sources and heat sinks, since those generate high exergy destruction.

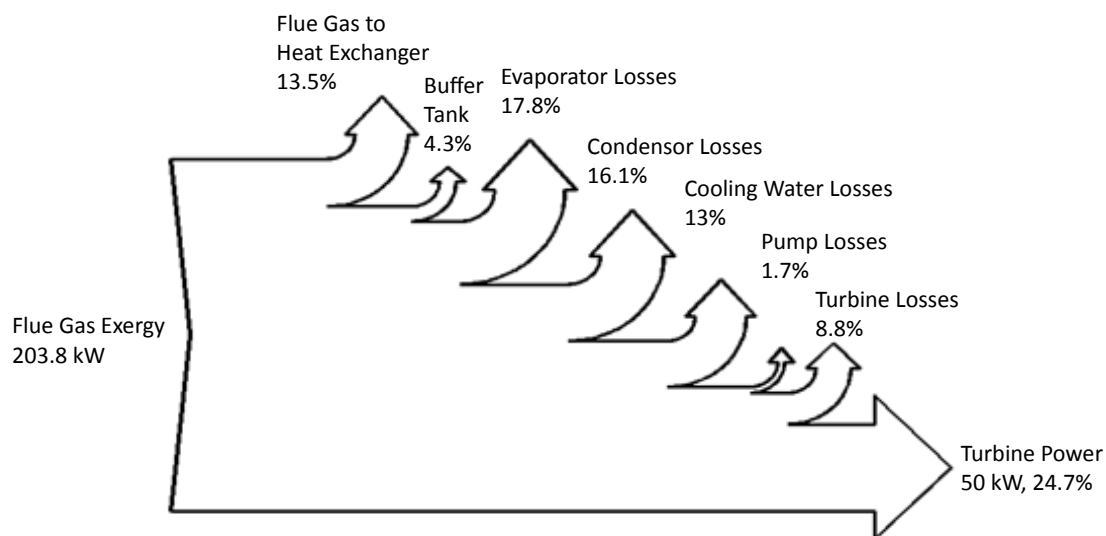


Figure 3.26: Sankey diagram of the Höver demonstrator showing exergy losses.

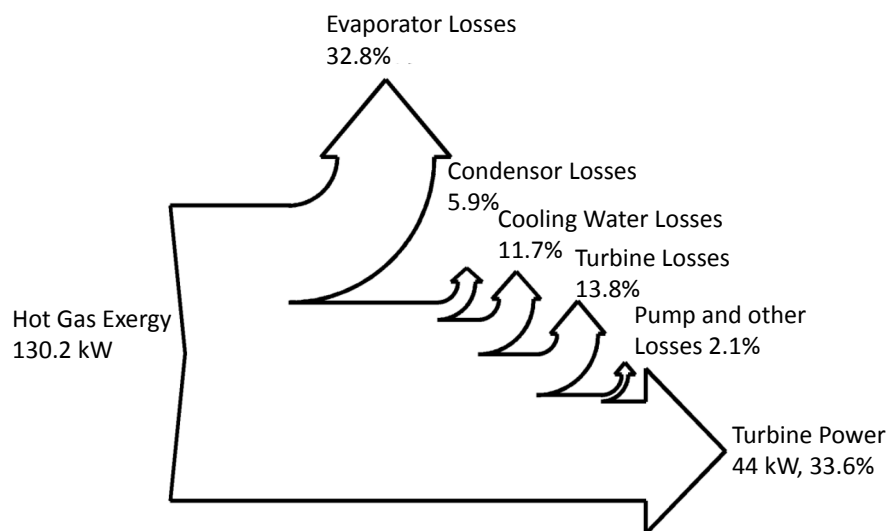


Figure 3.27: Sankey diagram of the Kollenbach demonstrator showing exergy losses.

3.10 Conclusion

In this chapter we introduced the method of classical data reconciliation. We then proposed a new methodology of (parameter) enhanced data reconciliation, taking advantage of time interdependencies between two measurements made within a short period of time. It consists in calculating variables (parameters) within a measured system and injecting these variables in the next time step of reconciliation as additional (virtual) measurements. Due to an example that was constructed we could show the influence of data reconciliation and enhanced data reconciliation on the accuracy between true and reconciled values. We showed that the methodology is effective for reducing the inaccuracy of the identified parameters. In the case of a setting where the measurements allow only for just calculating all variables, the difference between the reconciled and actual state of the process can be reduced. Thus the methodology is particularly interesting for processes which are measured without many redundancies. We also showed that the a priori inaccuracies for the initiation should be chosen large if the parameters were roughly estimated and can be smaller if they were well estimated. Since in general this is not known precisely, a large initial inaccuracy value should be chosen. For transient processes the methodology has limited use in two ways, either to identify unwanted non-steady behaviour, or like conventional reconciliation in order to better reconcile the measurements and increase the confidence in the reconciled values. The latter is possible only if the relation between the parameters and measurements is known and the parameters are not influenced by the transient behaviour.

Other than in traditional parameter identification, this methodology does not need any further information from the steps before $t - 1$. Also it only requires few information from time step $t - 1$: the chosen variables and the corresponding a posteriori accuracies. This way all information from previous measurements are indirectly included, making enhanced reconciliation ideal for online identification of parameters. Additionally the re-injected values are treated exactly like measurements and thus are optimised within the same step as the physical measurements, making the calculation quick and easy to implement into existing software. The limits are in transient processes, which fluctuate strongly and in which no relations with constant parameters can be identified. This makes enhanced data reconciliation ideal for the use in chemical processes which require a high precision, like in the production of pharmaceuticals.

Applying data reconciliation to the experimental data from the LOVE-project has improved the coherence of the data and thus made them interpretable. Calculating the relative difference between raw and true as well as reconciled and true values is of course not possible since the true values are unknown in experimental data. The data are used to check and validate assumptions made for the Organic Rankine Cycle tool, which is described in the next chapter. Even though we tried to apply enhanced data reconciliation to the experimental data, the results were not encouraging, leading to convergence problems, this is due to the fluctuations that were observed and to the fact that we did not have precise relations between measurements and parameters which are constant. The efforts to make the process steady did not have the success that was hoped for, when starting the LOVE project. One parameter however

for which we have applied the enhanced data reconciliation is the heat transfer coefficient of the external surface of the direct boiler, which we use to calculate heat losses.

We could gain valuable information for the ORC identification tool, developed in the following chapter, from the LOVE measurement data. The turbine isentropic efficiency is very stable even at extreme part loads. 77 % at a load of approximately 13 % of the nominal load, in a range from 27 % to 80 % of the nominal load, the turbine has an isentropic efficiency of about 85 %, we will use this value in the tool. Also, the friction and cooling losses of the turbine and generator could be estimated. They are in the range of $\dot{L}_{\text{turbogen}} = 10 \text{ kW}$ and do not increase or decrease much throughout the range of functioning. This is also what the manufacturer stated. We will thus apply this value in the tool. The overall heat transfer coefficient of the direct boiler was reconciled to be between $85 \frac{\text{W}}{\text{m}^2 \cdot \text{K}}$ and $140 \frac{\text{W}}{\text{m}^2 \cdot \text{K}}$. This will be used to validate our heat transfer models. We suppose that the heat losses to the environment of the direct boiler could be avoided by the application of insulation, we will thus not use it further for our methodology. Another important point is that the proper integration of the ORC with heat sources and heat sinks is crucial to reach a high overall efficiency, otherwise high levels of exergy destruction in the heat transfers are the consequence.

4 Suitable Cycle Identification

The use of low temperature (waste) heat for electricity production is limited on one hand by the low exergetic potential (Borel and Favrat, 2010) of the heat sources and by the investment cost on the other. High investment cost (Lazzaretto et al., 2011) in suitable technologies and low electricity prices for industry in many parts of Europe and the world accentuate this. This makes it necessary to carefully study all options necessary, including proper integration with the process. Identifying the right thermodynamic cycle to integrate with an industrial process depends on the actual waste heat potential found in the process, identified with the definition described in chapter 1 and methods in chapter 2. Once the potential has been quantified and qualified, a methodology can be applied to systematically identify adapted cycles for electricity production. We will extend the use of the term Organic Rankine Cycle (ORC) to cycles using mixtures as working fluids or which have a supercritical evaporation.

4.1 Objectives

Introducing a methodology allowing for any waste heat source, the identification of optimal Organic Rankine Cycles, regarding specific investment cost and the amount of electricity produced.

We propose a methodology that allows at the same time to identify and integrate (size) an ORC into an industrial process with the aim of transforming waste heat to the largest amount of electricity, while keeping the specific investment costs for the cycle as low as possible. All this should be done in a way, that as little working fluids are excluded from the analysis as possible, since no single fluid can be identified to be suitable for all heat sources.

4.2 State of the Art

The identification of a suitable cycle is difficult for numerous reasons, there is a large number of possible working fluids, the design of the cycle itself can have different forms (stages,

extraction etc.), pressure and temperature levels for a given fluid and cycle can be varied largely. Additionally the equipment to use can have different forms and materials. In the studies below and in tables 4.1 and 4.2 (from Quoilin et al. (2011)) we can see that there is no single fluid that arises from the studies, rather a distinct solution is needed for every heat source. In the table, (C., C. 2005) is Chammas and Clodic (2005), (D., B., 2007) is Drescher and Brüggemann (2007), (B.-G., N., 2007) is Borsukiewicz-Gozdur and Nowak (2007), (M. H. et al. 2007) is Madhawa Hettiarachchi et al. (2007), (D., B., 2009) is Desai and Bandyopadhyay (2009) and (M., M. 2010) is Mikielewicz and Mikielewicz (2010). WHR stands for waste heat recovery, ICE for internal combustion engine and CHP is combined heat and power.

Many studies have been carried out in an effort to identify suitable working fluids and/or parameters. Compared to water cycles which often have pressures above 60 bar, ORCs in most cases need lower pressures (Quoilin and Lemort, 2009), this decreases the complexity of the needed equipments, on the other hand they can show lower efficiencies for high temperature sources.

The studies use very different methodologies and are usually done for a single heat source: Sun and Li (2011) uses optimisation for the operating conditions of an ORC using R134a, by either maximising the net power generation or the system efficiency.

The use of ORC in solar plants is shown in Rayegan and Tao (2011) where the fluids are first preselected and then chosen by a sensitivity analysis. ORCs as bottoming cycles in power plants are discussed in Roy et al. (2010) in the form of a sensitivity analysis of the three fluids R12, R123 and R134a varying the turbine inlet pressure and temperature. 31 pure working fluids have been put to the test in a sensitivity analysis by Saleh et al. (2007) using the Backone equation of state (EOS) with the pressure limited to 20 bar. Liu et al. (2004) present a link between the cycle efficiency and critical temperature, but state that the link is weak and not sufficient for making a decision.

Hung (2001) does a sensitivity analysis on several fluids, looking at irreversibilities and pointing out that system efficiency and irreversibility reduction in the ORC often have opposite trends. Heberle and Brüggemann (2010) use exergy analysis for identification of a suitable working fluid, four fluids (R227ea, Isobutane, R245fa, Isopentane) are tested in a sensitivity type analysis. One of the studies with the largest number of analysed fluids analysed is Drescher and Brüggemann (2007). The study which was conducted for ORCs in biomass combustion mentions that the most commonly used is Octamethyltrisiloxane (OMTS). The analysis is done using the Peng-Robinson equation of state (EOS) and the entire database of the American Institute of Chemical Engineers, Design Institute for Physical Properties (DIPPR). Since the heat source is the combustion of biomass, the temperatures at the inlet are rather high. The conducted study analysed only thermodynamic parameters.

The use of fluid mixtures has been studied in Angelino and Colonna di Paliano (1998), arguing that wet natural heat sinks (like water streams, lakes, oceans etc.) have a rather isothermal character while dry sinks show rather a sloped temperature profile, which makes the use of

Table 4.1: Summary of different working fluids studies, Part I, (Quoilin et al., 2011).

Author(s)	Application	T_{cond} °C	T_{evap} °C	Considered Fluids	Recommended Fluids
Badr et al. (1990)	WHR	30–50	120	R11, R113, R114	R113
Maizza and Maizza (2001)	n/a	35–60	80–110	Unconventional Working Fluids	R123, R124
Liu et al. (2004)	WHR	30	150–200	R123, isopentane, HFE7100, Benzene Toluene, p-xylene	Benzene, Toluene, R123
(C., C. 2005)	ICE	55 (100 for water)	60–150 (150–260 for water)	Water, R123, Isopentane, R245ca, R245fa, Butane, Isobutene and R152a	Water, R245ca and isopentane
(D., B., 2007)	Biomass CHP	90 Heat sink	250 - 350 Heat source	Butylbenzene, Propylbenzene, Ethylbenzene, Toluene, OMTS	Butylbenzene
(M. H. et al. 2007)	Geothermal	30 Heat sink	70–90	Ammonia, n-Pentane, R123, PF5050	Ammonia
Lemort et al. (2007)	WHR	35	60–100	R245fa, R123, R134a, n-Pentane	R123, n-Pentane
Saleh et al. (2007)	Geothermal	30	100	Alkanes, fluorinated Alkanes, Ethers and fluorinated Ethers	R134, R245, R600, R245fa, R245ca, R601
(B.-G., N., 2007)	Geothermal	25	80–115	Propylene, R227ea, RC318, R236fa, Isobutane, R245fa	Propylene, R227ea, R245fa

Table 4.2: Summary of different working fluids studies, Part II, (Quoilin et al., 2011).

Author(s)	Application	T_{cond} °C	T_{evap} °C	Considered Fluids	Recommended Fluids
Mago et al. (2008)	WHR	25	100–210	R113, 123, R245ca, Isobutane	R113
Tchanche et al. (2009)	Solar	35	60–100	Refrigerants	R152a, R600, R290
Facão et al. (2008)	Solar	45	120 / 230	Water, n-Pentane HFE7100, Cyclohexane, Toluene, R245fa, n-Dodecane, Isobutane	n-Dodecane
Dai et al. (2009)	WHR	25	145 Heat source	Water, Ammonia, Butane, Isobutane R11, R123, R141b, R236ea, R245ca, R113	R236ea
(D., B., 2009)	WHR	40	120	Alkanes, Benzene, R113, R123, R141b, R236ea, R245ca, R245fa, R365mfc, Toluene	Toluene, Benzene
Gu et al. (2009)	WHR	50	80–220	R600a, R245fa, R123, R113	R113, R123
(M., M. 2010)	CHP	50	170	R365mfc, Heptane, Pentane, R12, R141b, Ethanol RC318, R227ea, R113, Isobutane, n-Butane, n-Hexane, Isopentane, neo-Pentane, R245fa, R236ea, C5F12, R236fa	Ethanol
Aljundi (2011)	n/a	30	50–140		n-Hexane

mixtures with a temperature glide on the hot and on the cold side interesting. StanMix was used for property estimation.

Schuster et al. (2010) analyse supercritical Organic Rankine Cycles, studying the sloped geometry, which adapts better to certain heat sources. They use a sensitivity analysis on several fluids. Chen et al. (2011) make a sensitivity analysis of 22 refrigerants which are mixed and used in supercritical cycles.

An application as a bottoming cycle is studied in Chen et al. (2006), amongst other fluids CO_2 in a supercritical cycle is compared to organic fluids and found thermodynamically better under certain conditions, back work ratio and cost are not considered.

In other papers similar analysis have been done by choosing a more (Maraver et al., 2012) or less (Heberle et al., 2012) large number of fluids and testing them with different parameters Schuster et al. (2009).

Other authors do not only look at the thermodynamic indicators but include others: For the use in Ocean Thermal Energy Conversion (OTEC) systems, very large (100 MW) ORCs are optimised with as an indicator the *heat exchanger surface-to-power output-ratio* by Uehara and Ikegami (1990). Shengjun et al. (2011) study ORCs with a 80 °C to 100 °C geothermal source in an iterative sensitivity analysis, calculating several indicators: thermal efficiency, exergy efficiency, recovery efficiency, heat exchanger area-to-power output, levelised energy cost. 16 fluids are analysed and the Turton (see below) method is used for cost estimation.

More sophisticated optimisation techniques are applied by some authors: in Wang et al. (2012b) a the *heat exchanger surface-to-power output-ratio* is used as an objective, the heat recovery efficiency is also analysed, both objectives are added to a single objective function (thus supposes that they are addable). The analysis includes thirteen fluids and is done with a simulated annealing algorithm. The use of optimisation algorithm is done by Dai et al. (2009) who use a genetic algorithm, with turbine inlet pressure and temperature as decision variable and the exergy efficiency as single objective. The optimisation is done for 10 fluids and the REFPROP database is used. A genetic algorithm is also used by Wang et al. (2013) the *heat exchanger surface-to-power output-ratio* as objective .

Madhawa Hettiarachchi et al. (2007) study four fluids for use in a geothermal heat source, stating that most geothermal sources are in a temperature range of 50 °C to 350 °C. Pressure drops in the heat exchangers are studied extensively (which we left aside in our methodology). The cycles are very large (10 MW) compared to the waste heat sources we saw during this thesis. They use an iterative steepest descent method for optimisation, decision variables are evaporation temperature, condensation temperature and the velocities of geothermal and cooling water, as an objective they use the ratio of *total heat exchanger surface* to *total net power*.

Papadopoulos et al. (2010) choose a different path to identify working fluids with the help of Computer Aided Molecular Design (CAMD) with group contribution methods, thus they are able to analyse working fluids which are not identified as of yet. Their study results also states that 90 % of the cost of the cycles are introduced by the heat exchanger cost.

The integration of ORC in Cement plants was studied by Karellas et al. (2013), using pressurised water in an intermediate circuit for heat transportation. A sensitivity analysis of four different organic fluids (R245fa, Neopentane, Pentane, Isopentane) is done and compared to a water cycle, concluding that a water steam cycle performs best thermodynamically. Another example for introduction of ORCs in Cement plants is presented by Legmann (2002).

All these methodologies are relatively heat source specific, or do not include investment cost except as a heat exchanger surface. Another problem is the pre-selection of fluids which can disqualify the method for some applications.

Two more complete and complex methodologies, partially similar to the one developed by us, have been presented: Quoilin et al. (2011) propose a sizing and cost optimisation tool with a few similarities to the methodology proposed below. They state that the use of regenerators is not advantageous in waste heat applications and exclude them, which we do not have to do since we are using heat integration. Similarly to us, they optimise power output (heat source to power) and not cycle efficiencies (cycle input to power). The optimisation is done in two steps, first the thermodynamic parameters, sizing and pressure drops are studied in an iterative sensitivity analysis and in a second step the economic parameters are optimised. Eight fluids are considered with the following decision variables for the optimisation of the specific investment cost: the evaporation pressure, condenser and evaporator pinch as well as the pressure drops in those two heat exchangers with a Simplex algorithm (which we also use for the MILP solver described below). The cost functions are very different from the ones we use and based on Belgian prices of the year 2010. The cycles that are shown have 3.5 kW and above with minimum costs of 2136 EUR /kW.

A methodology which was very recently published and which shows several similarities to the one presented here is proposed by Imran et al. (2014): a genetic algorithm is used for a multi objective optimisation, minimising the specific investment cost, maximising the efficiency. Five fluids are introduced in an iterative methodology, optimising some parameters. The Turton method is used for cost estimation as described below. The cycles which result produce between 30 kW and 120 kW and a specific cost of more than 3200 USD /kW.

The methodology proposed in this thesis, aims to analyse at the same time the economic indicators and thermodynamic indicators (in a multi objective optimisation) with a methodology that allows to choose between multiple fluids and cycle configurations. This is achieved combined with an integration into the industrial process. In the following we will describe the steps which are involved.

4.3 Method Description – Multi-Objective-Optimisation

The methodology for the identification of suitable cycles is based on a prior identification of the waste heat potential (as in chapter 1 and chapter 2) of an industrial process. The resulting composite curves will be used for the integration of the low temperature electricity production cycle (LTHC) (figure 4.1). The identification of suitable cycles is done with a Multi Objective Optimisation approach. In a multi objective optimisation, cycles are generated and integrated into the process by selecting a set of decision variables and then evaluated with respect to multiple objectives. The best solutions are kept in order to create a list of Pareto optimal solutions. A Pareto optimal set of solutions is reached, if the improvement of one objective can only be achieved by deterioration of at least one other objective (Leyland, 2002).

The multi objective optimisation thus identifies a set \vec{z} of solutions in the space which is defined by the decision variables, which satisfy the objective functions $F(\vec{z}, \vec{y})$:

$$\text{Minimise or Maximise}(F(\vec{z}, \vec{y})) \quad (4.1)$$

subject to:

$$\begin{aligned} \vec{h}(\vec{z}, \vec{y}) &= 0 \\ \vec{g}(\vec{z}, \vec{y}) &\leq 0 \\ \vec{L}(\vec{z}, \vec{y}) &= True \end{aligned} \quad (4.2)$$

The constraints (equations 4.2) represent the equalities ($\vec{h}(\vec{z}, \vec{y}) = 0$), inequalities ($\vec{g}(\vec{z}, \vec{y}) \leq 0$) and logical ($\vec{L}(\vec{z}, \vec{y}) = True$) equations that define the problem.

The optimisation we apply is organised in a master and slave part. The master part being the multi objective optimisation using a genetic algorithm and the slave optimisation, which does the integration (Pinch analysis) and has the form of a Mixed Integer Linear Programming (MILP) problem, with a single objective.

We use two optimisations for multiple reasons. The genetic algorithm allows to treat sub models like black boxes. This makes the combination with existing tools very easy, since they can be used as such and only the initial data have to be handed over and the results have to be recovered. No equations or derivatives have to be transferred. This is especially useful for thermodynamic models and for flowsheeting tools. It is unrealistic to recover the equations from these models or tools or to reprogram them. One reason why we do not solve the entire optimisation with the multi objective genetic algorithm is the resolution time. The resolution time of the genetic algorithm increases exponentially with the addition of every decision variable. This is due to the size of the search space which gains a new dimension per decision variable and the combinatory possibilities of different decision variable values. The other reason is the risk of not finding the global optimum. If many decision variables are used in the genetic algorithm, there is a higher risk that parts of the search space are not

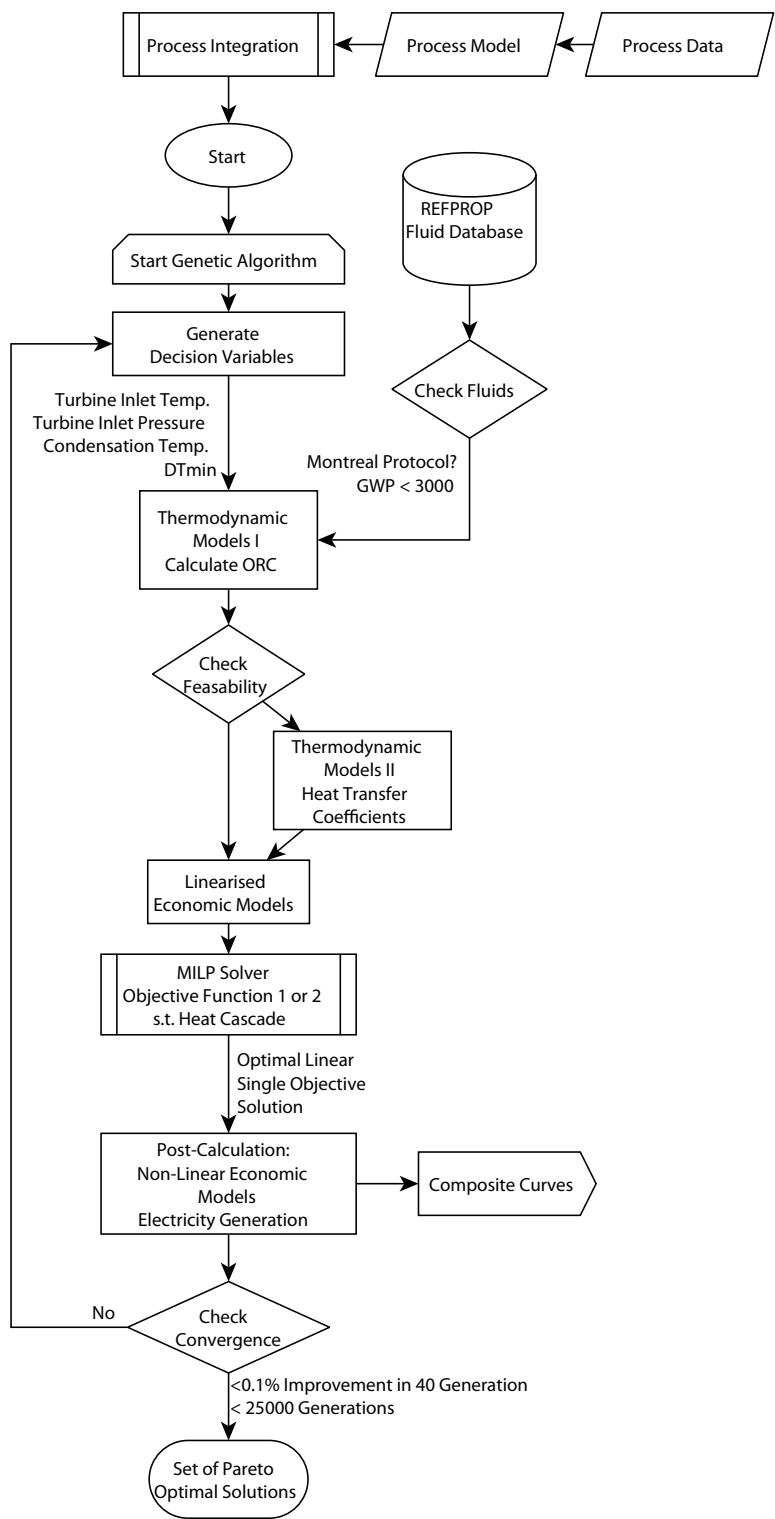


Figure 4.1: Algorithm of cycle identification embedded in integration with Multi Objective Optimisation.

analysed, thus the optimiser only converges to local optima instead of the global optimum. The exclusive use of a mixed integer linear programming solver is difficult as well. One reason is that many of the used equations are non-linear and performant and suitable mixed integer non-linear programming solvers are not available. A linearisation of all models would lead to a loss in precision, also it is unrealistic to redevelop all thermodynamic model equations with the precision that is available in external tools. Therefore, combining both types of solvers with the goal of using as little decision variables as possible in the genetic algorithm and to use the speed of the mixed integer linear programming solver for as many equations as possible is the compromise we chose.

4.3.1 Objective Function

In order to identify which cycles should be used within a particular industrial setting, one has to be clear about the objectives on which the choice is based. Possible objectives from different areas are: thermodynamic performance, economic indicators, environmental aspects, security of electricity supply etc. A trade-off between different objectives can be represented by a list of solutions, they are considered to have reached the optimum, if no objective can be increased without decreasing another. The final choice (or weight) between the objectives depends on the responsible persons for a possible investment.

Due to the design of our methodology (shown in figure 4.1) the master and slave optimisation do not have the same objective functions. The overall optimisation obtains the results of the master multi objective optimisation. The slave optimisation, however, has a single objective and a linear objective function. This means that the role of the slave optimisation is to orient the ORC choice towards the right solution. The solution is then re-evaluated in a post-calculation using the non-linear equations of the multi objective master optimisation.

In the master optimisation (the multi objective optimisation) we consider two types of objectives (and objective functions) which we believe are the most likely to be used for the decision:

Electricity Generation Maximisation:

$$\text{Obj 1} = \text{Max}(\dot{E}_{\text{el}}^-) \quad (4.3)$$

and

Specific Cost Minimisation:

$$\text{Obj 2} = \text{Min}(C_{\text{TM,spec}} = \frac{C_{\text{TM}}}{\dot{E}_{\text{el}}}) \quad (4.4)$$

Where C_{TM} is the total module cost and \dot{E}_{el} , how these are calculated is explained throughout this chapter. The maximisation of electricity production is equivalent to the increase of exergy efficiency, thus they can be interchanged. The objectives are calculated by the use of a post-calculation, after the integration, since at that point all necessary information are available. The post calculation will be described below in section 4.3.8. Also we will see that in the MILP slave optimisation (section 4.3.7), we have to chose one objective, which is due to the limitations of the solver and the available information is not exactly the same of the two mentioned above, this will be described in the section about the MILP.

4.3.2 Parameters and Constraints

There are several parameters that have to be set or chosen for the calculation of a cycle. Some parameters are set up front in order to meet requirements and others will be used as decision variables for the identification of the Pareto optimal solutions. There are qualitative and quantitative parameters that can be constrained before starting the optimisation. Examples of qualitative parameters are characteristics of the fluids like toxicity or flammability. Quantitative parameter are for example thermodynamic parameters like a maximum pressure or temperature limits.

It is important to set the constraints on those parameters carefully before starting the optimisation, because the resolution time depends exponentially on the space explored. Here we will constrain the example problems and chose a maximum Global Warming Potential (GWP) of the working fluids considered. Furthermore we will exclude all fluids that are already restricted in use under the Montreal Protocol (United Nations Environmental Programm, 2014).

As an important design parameter, the number of stages and cycles can be constrained to a certain number or to be larger or smaller than a certain number. To start with we will look at single cycles, in a later extension dual cycles will be explained.

In order to minimize the decision variables, the subcooling temperature difference is fixed as well as the mass flow rate of the cycle. The final mass flow rate and thus the size of the cycle will of course be adapted in the process integration step; this means that depending on the starting point (initial size), the solver of the integration step has to find a multiplication factor. In our experience, choosing a base size within one or two orders of magnitude of the final solution facilitates the quick convergence of the solver. The choice of fluids is limited to the REFPROP data base (Lemmon et al., 2010) which we use for all thermodynamic calculations in order to get coherent results. Other fixed parameters are turbine and pump isentropic efficiencies.

The decision variables used for the optimisation are:

- Turbine inlet temperature
- Turbine inlet/Evaporation Pressure

- Minimum Temperature Difference (ΔT_{\min}) in heat transfers
- Condensation Start Temperature

These parameters allow fitting different cycle configurations with different heat sources profiles and heat sinks. Also they allow a maximum flexibility in the choice of the cycle, since they can be applied to “classical” Organic Rankine cycles (with or without super heating) as well as for mixtures or supercritical cycles. We will use a limit of 50 bar for our analysis, since it was the maximum pressure that came up in the LOVE project in the discussions with the industrial partners. This limit reflects the security concerns that arise from high pressures and the risk of a leakage and the resulting dangers regarding the integrity of staff members and installations. The Turbine inlet temperature is limited by the maximum temperature of the heat source, the minimum temperature differences are left relatively wide between 0.5 °C and 30 °C. The condensation temperature is limited by the heat sink.

4.3.3 Genetic Algorithm

To generate the list of Pareto optimal solutions a genetic algorithm is used; it acts as an optimiser for the Multi Objective Optimisation. This algorithm is designed to copy the behaviour of an accelerated evolution. At first a number of random sets of decision variables, representing the genes, is created and the resulting cycles (individuals of initial population) are calculated. Afterwards the genes/decision variables can be combined from two individuals and/or mutated. The algorithm keeps the individuals that behave well regarding the objectives alive and thus creates families and converges towards the Pareto curve (set of Pareto optimal solutions). The advantage of this optimisation algorithm is that the physical models can be developed entirely separated, meaning also in separate software. Furthermore, no equations have to be passed on to the optimiser, only the results. This makes it extremely versatile and makes it especially suitable for non-continuous problems. In the first version of the tool that we developed, the OSMOSE platform (Bolliger, 2010) was used, this platform is combined with the Multi Objective Optimiser (called *MOO*) developed by Leyland (2002), which also has been used by Gerber (2012), Gassner (2010) and others. This platform was developed in the Matlab (MathWorks, 2012) language and had as an objective to be versatilely and applicable to many different problems. Unfortunately the creation of the mathematical model, which is then solved by the MILP solver explained below, did not satisfy all requirements for the tool in its current state. Especially the solution time was quite long. The entire tool was redeveloped using the programming language Python (Van Rossum, 2007), reducing and streamlining the functioning to only the required functions. We recoded the tool for use with this new version of OSMOSE, reducing the time for preparation of the mathematical model. The new tool also uses a different genetic algorithm which comes in the Dakota (Adams et al., 2006) package of mathematical solvers called Multi Objective Genetic Algorithm (MOGA) and explained in detail in Eddy and Lewis (2001). The set of decision variables that is generated by the genetic algorithm is first rounded (temperatures in K to the third digit after the dot and the pressure in kPa to the first) and then passed to the thermodynamic calculations.

4.3.4 Thermodynamic Models I: Thermodynamic Cycles

The thermodynamic models will be explained in two groups, the first group of thermodynamic models are used to calculate the states of the working fluids and the mechanical and thermal streams into and out of the cycles. The REFPROP (Lemmon et al., 2010) database and equations are used for the calculation of the cycles via a script that allows direct access to the REFPROP dynamic link library (dll).

The list of working fluids is given in appendix A, tables A.1 to A.5, where T_C is the critical temperature, p_C the critical pressure and T_B the normal boiling temperature. The data for these tables were taken from: Lemmon et al. (2010); Calm (2008); Calm and Hourahan (2007); United Nations Environmental Programm (2014); U.S. Environmental Protection Agency (2014c); European Parliament and Council of the European Union (2014); Forster et al. (2013); U.S. Environmental Protection Agency (2014b); United Nations Framework Convention on Climate Change (2014); Facão and Oliveira (2009); U.S. Environmental Protection Agency (2010); Tejon Carbajal (2009); U.S. Environmental Protection Agency (2014a) and Bundesamt für Umwelt (2014). The fluids which are already under control due to the Montreal Protocol (United Nations Environmental Programm, 2014) are listed in bold. Also in bold and with an asterisk (*) are substances which are excluded due to their special character (highly toxic, radioactive or for thermodynamic reasons (critical temperature below $-100\text{ }^{\circ}\text{C}$)). In table A.6 and A.7 all the mixtures are shown, again the bold ones are those already under control of the Montreal Protocol and thus excluded from the possible choices. R508a and b, R510a and R416a were also excluded due to convergence problems of REFPROP, for example near the critical point. It must also be noted that following decisions made after the Kyoto Protocol (United Nations Framework Convention on Climate Change, 1997) and in an effort to reduce the climate gas emissions throughout the EU and Switzerland, many other fluids will be unavailable or their acquisition or use will be possible only under certain conditions. These vary in the different legal frameworks (Bundesamt für Umwelt, 2014; European Parliament and Council of the European Union, 2014) and over time. We will try to address that by limiting the choice to working fluids with a GWP smaller than 3000.

The sequence of calculations for one set of decision variables is:

1. Check the feasibility:

- Is the set condensation temperature lower than the critical point?
- Is the set turbine inlet pressure above the condensation pressure resulting from the set condensation temperature?
- Is the set turbine inlet temperature above the evaporation temperature resulting from the set evaporation pressure?
- Is the turbine outlet “above” the two-phase-area?
- Are all thermodynamic parameters within the limits of the equations of state (EOS) defined in REFPROP?

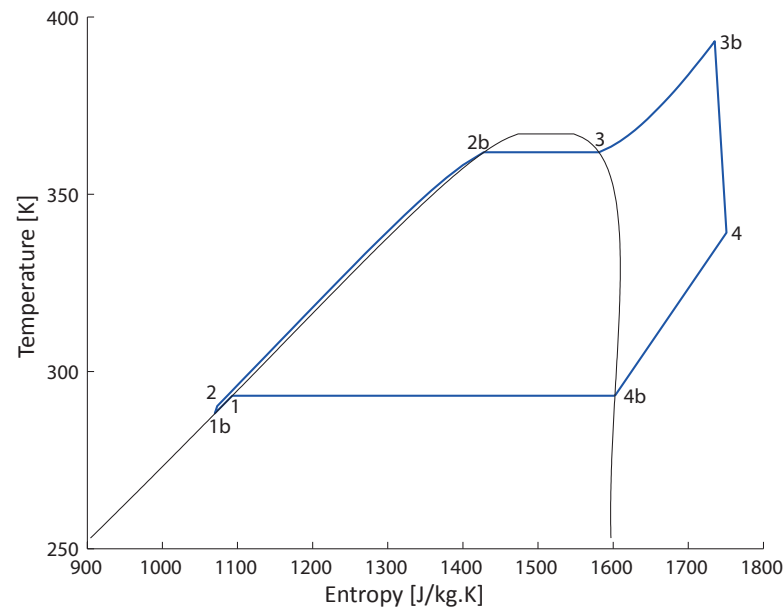


Figure 4.2: T-s-diagram of a “simple” ORC with R1234yf, turbine inlet temperature at 120 °C and turbine inlet pressure at 30 bar.

2. Check fluid by fluid what type of cycle applies (the area around the critical point has been approximated in the figures):

- Calculate simple ORC characteristics (Figure 4.2)
- Calculate mixture cycle characteristics (Figure 4.4)
- Calculate supercritical cycle characteristics (mixture (Figure 4.5) or single fluid (Figure 4.3))

In figure 4.2 we can see that the cycles consist of several steps:

1 to 1b:	Subcooling
1b to 2:	Pump/Pressure Increase
2 to 2b:	Preheating
2b to 3:	Evaporation
3 to 3b:	Superheating
3b to 4:	Expansion/Turbine
4 to 4b:	De-Superheating
4b to 1:	Condensation

In the supercritical cycles the heating is done directly from 2 to 4b and there are no distinguishable points 2b or 3, in order to model this, these parts have been discretised into 20 linear steps. In these steps the c_p is assumed to constant. The information we need for our model

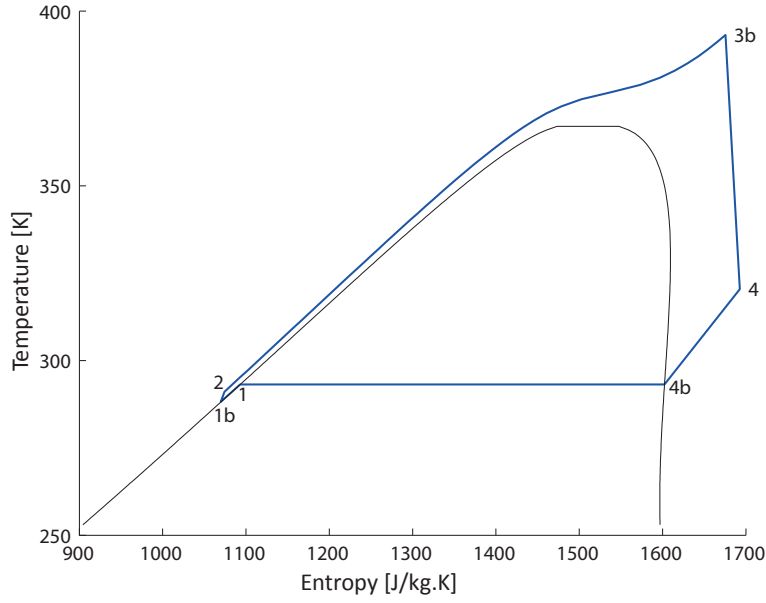


Figure 4.3: T-s diagram of a supercritical ORC with R1234yf, turbine inlet temperature at 120 °C and turbine inlet pressure at 40 bar.

are the temperatures and the heat flow rate between one point and the next it is calculated by e.g.:

$$\dot{Q}_{1-1b} = \dot{m}(h_{1b} - h_1) \quad (4.5)$$

Where \dot{m} is the mass flow rate and h_1 is the mass specific enthalpy at the first point and h_{1b} the mass specific enthalpy at the second point.

The isentropic efficiencies are considered as in chapter 3:

$$\eta_{is,turb} = \frac{h_{3b} - h_4}{h_{3b} - h_{4,is}} \quad (4.6)$$

where the index *is* stands for isentropic.

The shaft work of the turbine is given by:

$$\dot{E}_{turb} = \dot{m}(h_4 - h_{3b}) \quad (4.7)$$

It has a negative value.

And the shaft work of the pump (positive value) is:

$$\dot{E}_{pump} = \dot{m}(h_2 - h_{1b}) \quad (4.8)$$

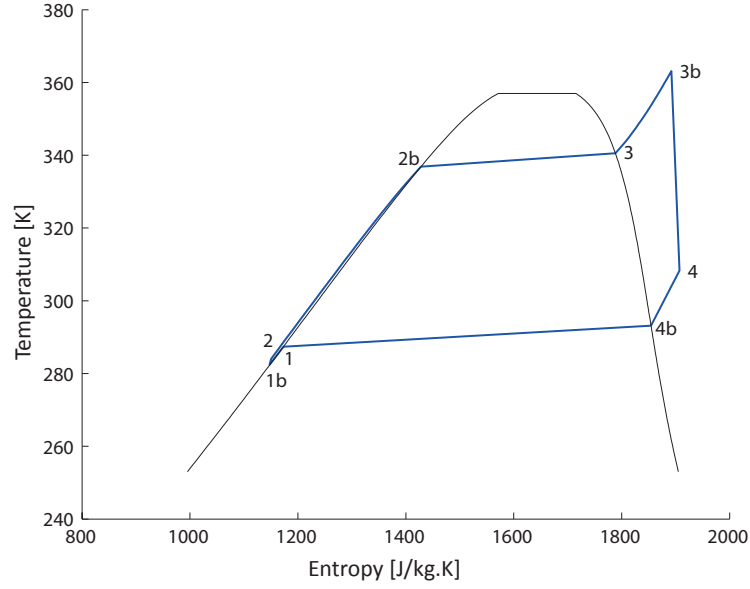


Figure 4.4: T-s-diagram of an ORC the mixture R407, turbine inlet temperature at 90 °C and turbine inlet pressure at 30 bar.

With

$$\eta_{is,pump} = \frac{h_{2s} - h_{1b}}{h_2 - h_{1b}} \quad (4.9)$$

The net shaft power is thus:

$$\dot{E}_{net} = \dot{E}_{turb} + \dot{E}_{pump} \quad (4.10)$$

The overall heat input is thus \dot{Q}_{2-3b} and the overall cooling requirement \dot{Q}_{4-1b} . We thus have an energy balance of:

$$\dot{Q}_{2-3b} + \dot{E}_{pump} + \dot{Q}_{4-1b} + \dot{E}_{turb} = 0 \quad (4.11)$$

All feasible cycles are then calculated entirely considering a mass flow rate of $\dot{m} = 1 \frac{\text{kg}}{\text{s}}$, this value is to be understood as an initial size, it will be multiplied by a factor which is determined in the MILP-Solver, determining the optimal size. In order to solve the models, the assumptions listed in table 4.3 are made.

The isentropic efficiencies have been chosen in accordance with the values observed during the LOVE project with the two demonstrators. With the above models, all heating and cooling requirements have been characterised and the turbine and pump work calculated. This is done for all working fluids, then all cycles are put to the test in the MILP-Solver (described below), which will give as a result the best cycle choice with the appropriate sizing.

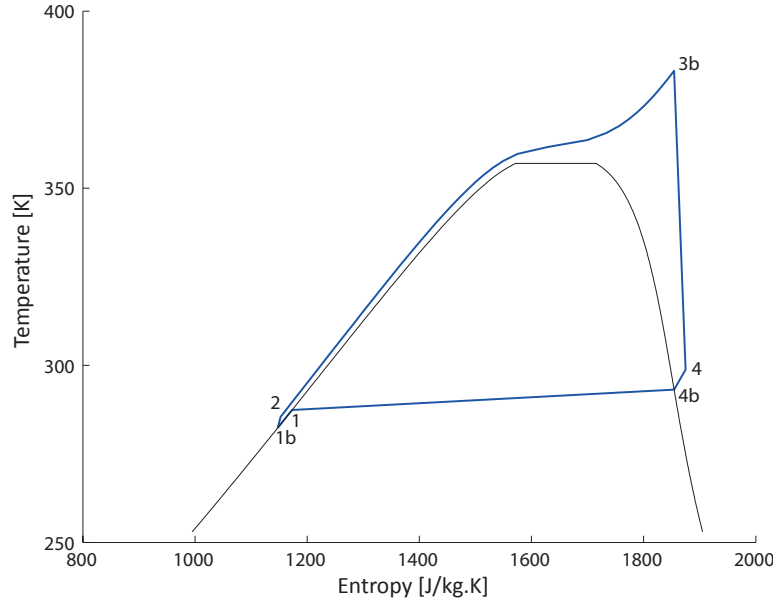


Figure 4.5: T-s-diagram of an ORC the supercritical mixture R407, turbine inlet temperature at 110 °C and turbine inlet pressure at 49 bar.

Table 4.3: Assumptions made to calculate the ORC.

Description		Value	Unit
Pump isentropic efficiency	$\eta_{is,pump}$	0.70	-
Turbine isentropic efficiency	$\eta_{is,turb}$	0.85	-
Subcooling after condensation	ΔT_{sub}	2	K
Number of discretisation steps for supercritical fluid temperature enthalpy profile		20	-

4.3.5 Thermodynamic Models II

The second set of thermodynamic models is used to calculate heat transfer coefficients followed by the resulting heat exchanger surfaces. The size of surfaces are needed for economic evaluation since the quantity of heat exchanged and the pinch temperature in a heat exchanger represent a trade-off with the investment cost. By calculating the heat transfer coefficients, it is possible to distinguish the different fluids further. The interest of this methodology is to identify relative behaviour of working fluids; we thus consider a model heat exchanger for all the fluids in order to calculate the heat transfer coefficients. This way the impact of the working fluid is made obvious. This is not supposed to give us the final design of the used heat exchanger, but rather to allow a ranking between the fluids possible.

The heat exchange surface calculation is done before the integration of the cycle into the process. For this reason it is impossible to obtain the final surface, which would require the

4.3. Method Description – Multi-Objective-Optimisation

final temperatures between heat sources and sinks. The temperature difference between sinks and sources is therefore assumed to be equal to ΔT_{\min} at every point (equation 4.12).

$$\Delta T_{\min} \text{ for } LMTD \quad (4.12)$$

Of course the final temperature differences are in most points higher than that and will thus lead to a smaller overall surface in the final cost estimation described below in the post-calculation. However, this estimation is conservative and less integrated solutions (with big temperature differences between cycle and process streams) are penalised in regard to well integrated (small temperature differences, close to ΔT_{\min}) solutions. This penalisation occurs because of a stronger overestimation of the heat exchanger surface.

The heat transfer coefficient cannot be calculated the same way in every situation. We follow the recommendations of the German Association of Engineers (Verein Deutscher Ingenieure (VDI)).

The Dittus-Boelter-Equation (Incropera et al., 2006) is used for all situations where no evaporation or condensation are involved, these are: Pre-heating; Super-heating; De-super-heating; Sub-cooling; Entire heating for Super-/Trans-Critical-Cycles. The equation is:

$$Nu = 0.23Re^{0.8} Pr^n \quad (4.13)$$

Where

$n = 0.4$	for heating
$n = 0.3$	for cooling
Re	Reynolds number
Pr	Prandtl number
Nu	Nusselt number

With the Nusselt number being:

$$Nu = \frac{\alpha d}{k} \quad (4.14)$$

Where α is the local heat transfer coefficient, d the hydraulic diameter and k the thermal conductivity of the fluid.

The VDI-Method Hbb (Verein Deutscher Ingenieure (VDI) and GVC, 2006) (supposed vertical tubes) is used for evaporation:

$$\frac{\alpha(z)_k}{\alpha_{LO}} = \left\{ (1 - \dot{x})^{0.01} \left[(1 - \dot{x})^{1.5} + 1.9\dot{x}^{0.6} \left(\frac{\rho'}{\rho''} \right)^{0.35} \right]^{-2.2} + \dot{x}^{0.6} \left[\frac{\alpha_{GO}}{\alpha_{LO}} \left(1 + 8(1 - \dot{x})^{0.7} \left(\frac{\rho'}{\rho''} \right)^{0.67} \right) \right]^{-2} \right\}^{-0.5}$$

(4.15)

Where

\dot{x}	fraction of vapour flow
ρ'	liquid fluid density
ρ''	gaseous fluid density

With the indices

LO	entire massflow liquid
GO	entire massflow gaseous

And z is the coordinate across the tube. The two local heat transfer coefficients α_{LO} and α_{GO} are calculated with the above equation 4.13. The local heat transfer coefficient in the vapour-liquid phase is then calculated in ten discrete points, varying \dot{x} from 0 to 1.

The VDI-Method Ja (Verein Deutscher Ingenieure (VDI) and GVC, 2006) (supposed vertical tubes) is used for condensation:

$$Nu_{F,x}^* = \sqrt{(K_{Ph,l} Nu_{F,x,l})^2 + (K_{Ph,t} Nu_{F,x,t})^2} \quad (4.16)$$

With the indices

t	turbulent
l	laminar
F	film

Where

K_{Ph}	the correction factor for phase limit.
----------	--

Which is calculated in the laminar case:

$$K_{Ph,l} = 1 + (\text{Pr}_F^{0.56} - 1) \tanh \tau_D^* \quad (4.17)$$

and for the turbulent flow:

$$K_{Ph,t} = 1 + (\text{Pr}_F^{0.08} - 1) \tanh \tau_D^* \quad (4.18)$$

Where τ_D^* is the dimensionless shear stress.

Again, the transfer coefficients are calculated in ten steps varying the value of \dot{x} from 1 to 0. The α values of the different steps are then averaged over the entire evaporation and condensation respectively. For the fluids which do not have the necessary equations in REFPROP (unfortunately this is the case of the Siloxanes) to calculate the local heat transfers, the coeffi-

4.3. Method Description – Multi-Objective-Optimisation

coefficients are assumed to be $2000 \frac{\text{W}}{\text{m}^2 \cdot \text{K}}$ for subcooling, $3500 \frac{\text{W}}{\text{m}^2 \cdot \text{K}}$ for preheating, superheating, de-superheating and condensation and $5000 \frac{\text{W}}{\text{m}^2 \cdot \text{K}}$ for evaporation.

The overall heat transfer coefficients are calculated with the relation:

$$U = \left(\frac{1}{\alpha_{\text{out}}} + \frac{1}{\alpha_{\text{steel}}} + \frac{1}{\alpha_{\text{ORC}}} \right)^{-1} \quad (4.19)$$

The heat transfer coefficient of the heat exchanger wall is assumed for a wall thickness of 0.002 m leading to $\alpha_{\text{steel}} = 8500 \frac{\text{W}}{\text{m}^2 \cdot \text{K}}$, this represents the conductivity. The hot side of the heat transfer is assumed to be hot air between 200 °C and 50 °C at ambient pressure, which leads to an average heat transfer coefficient for the hot side of $\alpha_{\text{out}} = 70 \frac{\text{W}}{\text{m}^2 \cdot \text{K}}$. The cooling is assumed to be done with liquid water at a temperature of 20 °C, we thus find a heat transfer coefficient of $\alpha_{\text{out}} = 1086 \frac{\text{W}}{\text{m}^2 \cdot \text{K}}$. The overall heat transfer coefficients of the heating is thus $U_{\text{heating}} = 68.08 \frac{\text{W}}{\text{m}^2 \cdot \text{K}}$, at the evaporation $U_{\text{heating}} = 68.48 \frac{\text{W}}{\text{m}^2 \cdot \text{K}}$, at the cooling and condensation $U_{\text{heating}} = 755.19 \frac{\text{W}}{\text{m}^2 \cdot \text{K}}$ and subcooling $U_{\text{heating}} = 650.00 \frac{\text{W}}{\text{m}^2 \cdot \text{K}}$. If we compare these values to those found in the LOVE direct boiler (figure 3.23) which are in the range of $85 \frac{\text{W}}{\text{m}^2 \cdot \text{K}}$ to $140 \frac{\text{W}}{\text{m}^2 \cdot \text{K}}$ for heating and evaporating the working fluid, the assumptions we made for the tool are very conservative and will lead to rather larger heat exchange surfaces, thus higher cost. This means that the tool also applies for a less optimised heat exchanger than the one used in the LOVE project which was studied in depth before installation (Maalouf et al., 2012b).

4.3.6 Economic Models

The MILP optimisation, solving the integration of the ORC into the process, can be set in a way that the integration is done, optimising different characteristics. If cost optimisation is selected for the integration, the solver will minimise the cost. If the mechanical power output is optimised, the solver will chose and integrate the cycles in a way that a maximum power output is achieved. For the mechanical power, the differences between the cycles is resulting from thermodynamics. For the cost optimisation however, cost functions have to be introduced in order to define the cost. The cost differences between fluids are made quantifiable by calculating grass root costs using the cost functions defined by Turton (2012) which are themselves a combination of methods proposed by Ulrich (1984) and data as well as correction factors by Peters and Timmerhaus (1991); Guthrie (1969b, 1974, 1969a); Ulrich (1984); Navarrete and Cole (2001), and Perry and Green (1997). The function for calculation of the purchasing cost (C_p^0) in US-Dollar of any type of equipment for ambient temperature and pressure conditions made of carbon steel (CS) is given by:

$$\log(C_p^0) = K_1 + K_2 \cdot \log(A) + K_3 \cdot (\log(A))^2 \quad (4.20)$$

Chapter 4. Suitable Cycle Identification

Where K_1 , K_2 and K_3 are equipment dependent parameters. A is the sizing parameter (“equipment cost attribute”), which gives a characteristic size information depending on the type of equipment.

If the gauge pressure is not equal to the ambient pressure, a correction factor F_p may have to be applied:

$$\log(F_p) = C_1 + C_2 \cdot \log(p_g) + C_3 \cdot (\log(p_g))^2 \quad (4.21)$$

Where C_1 , C_2 and C_3 are the equipment depending parameters and p_g is the gauge pressure in bar. We use the following relation to transform absolute pressure to gauge pressure:

$$p_{\text{gauge}}[\text{bar}] = p_{\text{absolute}}[\text{bar}] - 1\text{bar} \quad (4.22)$$

If the equipment is not made of carbon steel, a material factor F_M (table 4.6) has to be applied to account for the price differences of the materials and the different effort to process them.

The correction factors are included in the bare module factor F_{BM} :

$$F_{\text{BM}} = B_1 + B_2 F_M F_P \quad (4.23)$$

Where B_1 and B_2 are supposed to account for: Materials required for installation, labor for installation, freight, insurance, taxes, construction overhead, contractor engineering expenses, contingency, contractor fees, site development, auxiliary buildings, off-sites and utilities (electricity, water consumption during set-up).

The change of prices and inflation over time are taken into account, I_t and $I_{t,\text{ref}}$ are the corresponding indexes. $I_{t,\text{ref}}$ is the index of the year, in which the cost parameters were established and I_t is the most recent available, or the index of the year of interest. These CEPCI indexes (Chemical Engineering’s Plant Cost Index) are published by the journal of Chemical Engineering (Vatavuk, 2002). Since the data we use here were all accounted in 2001 prices the reference index is 397, as a reference we use the CEPCI of April 2013 (Chemical Engineering, 2013) which is 595.9:

$$\frac{I_t}{I_{t,\text{ref}}} = \frac{595.9}{397.0} \quad (4.24)$$

4.3. Method Description – Multi-Objective-Optimisation

Table 4.4: Equipment Cost Data.

Type of Equipment	K_1	K_2	K_3	Sizing parameter
Multiple Pipe Heat Exchanger	2.7652	0.7282	0.0783	Area, m ²
Radial Turbine	2.2476	1.4965	-0.1618	Fluid power, kW
Centrifugal Pump	3.3892	0.0536	0.1538	Shaft power, kW

Finally the total module costs, which represent the cost for a development of the ORC on an existing industrial site are calculated by adding an additional factor, which is quantified by Turton to be 1.18:

$$C_{TM} = 1.18 C_{BM} = 1.18 \sum_{i=1}^n C_{BM,i} \quad (4.25)$$

Where i is an equipment and n the sum of all equipments.

The total module cost as the sum of the cost for each piece of equipment of the installation is then:

$$C_{TM} = 1.18 \frac{I_t}{I_{t,ref}} \sum_{i=1}^n F_{BM,i} C_{p,i}^0 = 1.18 \frac{I_t}{I_{t,ref}} \sum_{i=1}^n (B_{1,i} + B_{2,i} F_{M,i} F_{p,i}) C_{p,i}^0 \quad (4.26)$$

For the tool, three types of equipment are considered: multiple pipe heat exchangers, radial turbine and centrifugal pump. The corresponding K values are shown in table 4.4, the pressure correction values are given in table 4.4. In this work we limit the decision variable of the turbine inlet pressure to 50 bar, the pressure corrections are valid up to a pressure of 100 bar. Above this value, other factors have to be used, which can be found in Turton (2012). The material factors are shown in table 4.6, only carbon steel (CS), copper (Cu) and stainless steel (SS) are considered. The turbine material factors replace the turbine bare module factors. The constants for the other bare module factors are summarized in table 4.7. As assumptions for the ORC tool, the materials used are: carbon steel for the pump and the turbine and stainless steel for the heat exchanger, tubes and shell, the pressures are calculated from the thermodynamic data.

We assume that the heat exchangers used are of the same type as the direct boiler that was used in the LOVE project, a finned tube heat exchanger. As we have seen in section 3.9 the heat exchanger surface in the heat exchanger was (3005 m² including the tubes and fins. This corresponds to 137 m² of tube surface and 2868 m² of fin surface. We also thus know that the ‘total surface’-to-‘tube surface’ ratio is 21.93-to-1. Since we are using multiple pipe heat exchangers for the cost estimation we can not use the entire surface for the cost calculation,

Chapter 4. Suitable Cycle Identification

Table 4.5: Equipment Pressure Factors.

Type of Equipment	C_1	C_2	C_3	Validity
Multiple Pipe Heat Exchanger	0	0	0	$p_g < 40$ bar
	0.6072	-0.9120	0.3327	$40 \text{ bar} < p_g < 100$ bar
Radial Turbine	0	0	0	-
Centrifugal Pump	0	0	0	$p_g < 10$ bar
	-0.3935	0.3957	-0.00226	$10 \text{ bar} < p_g < 100$ bar

Table 4.6: Material Factors.

Multiple Pipe Heat Exchanger

CS-shell/ CS-tube	CS-shell/ Cu-tube	Cu-shell/ Cu-tube	CS-shell/ SS-tube	SS-shell/ SS-tube
1	1.3	1.7	1.8	2.7

Centrifugal Pump

Cast Iron	Carbon Steel	Stainless Steel
1.5	2.3	4.4

Turbine

Carbon Steel	Stainless Steel
3.5	6.1

Table 4.7: Constants for Bare Module Factors.

Type of Equipment	B_1	B_2
Multiple Pipe Heat Exchanger	1.74	1.55
Centrifugal Pump	1.89	1.35

otherwise we will have a surface which is far too large. We will thus use only the tube surface for the sizing parameter A in the cost estimation. For the LOVE direct boiler, the purchasing cost were 39 300 EUR for an exchanger that was made with copper tubes and aluminium fin-sheets. If we apply the cost function (equation 4.20) with a surface of 137 m^2 we get a purchasing price of 47 713.85 USD with a conversion factor of 0.8 EUR /USD a price of 38 171.08 EUR is obtained for a carbon steel version. Since the evaporation pressure of the LOVE demonstrator is about 5 bar the pressure correction is unity, the material correction would probably be 1.3, even though the exact materials are not available. It should be noted here that before purchasing the LOVE direct boiler, inquiries for other materials had been made and a stainless steel version would have been twice as expensive, which also corresponds to the correction factor for a complete stainless steel unit which is little more than twice as large (2.7). It is obvious how close the estimated and the paid costs are, we thus consider this method validated and divide all surfaces estimated with the thermodynamic models II by the ‘total surface’-to-‘tube surface’ ratio of 21.93-to-1. However, since the tool is supposed to work with all kinds of waste heat streams, even very corrosive ones, we consider the heat exchangers to be made of stainless steel per default, thus we apply the material factor of 2.7. Furthermore, we consider that there are 3 heat exchangers per cycle, namely a preheater, evaporator and superheater, second an economiser and finally a de-superheater, condenser and subcooler. The total heat exchange area is divided by three. This assumes that the three heat exchangers have the same size. Physically this is of course a simplification and it is done on one hand to simplify calculations and on the other hand, the heat exchanger cost are over estimated and thus more conservative.

As for the cost of the turbine and the pump we use the cost equations as they are, they underestimate the purchasing cost of the units when compared to the LOVE demonstrator, but it has to be kept in mind that those were used for two very different installations and chosen accordingly. The LOVE turbine was developed solely for the LOVE project, including all the engineering and made to measure manufacturing. The cost for the LOVE turbine, including the generator, were 288 000 EUR, the turbine generator combination was developed for $100 \text{ kW}_{\text{el}}$ which is approximately equivalent to a “fluid power” of 110 kW since we have seen above that friction and cooling account for about 10 kW. If we calculate the purchase cost of such a turbine with equation 4.20 we reach a cost of 33 991.3 EUR. Including the correction factor of 3.5 for carbon steel bare module cost of 118 969 EUR is reached, this corresponds to costs of 1189.69 EUR / kW_{el} , considering the same losses as before. The high cost difference between the “LOVE” turbine and a turbine estimated with the Turton method can be explained by the experimental character of the tested turbine. In the “LOVE” project, the same turbine was used in both demonstrators and was designed especially for this, which increased the development cost drastically. The impact of size on the cost estimated with the Turton method can be seen, if compared to a larger scale turbine of $1000 \text{ kW}_{\text{el}}$. The specific cost are less than half for the $1000 \text{ kW}_{\text{el}}$ when compared to the $100 \text{ kW}_{\text{el}}$ one.

Chapter 4. Suitable Cycle Identification

Table 4.8: Linearised Equipment Cost Data.

Type of Equipment	L_1	L_2	Range	R^2
Radial Turbine	13110	273.92	100 to 250 kW	0.9977
Centrifugal Pump	2495.6	137.8	1 to 22 kW	0.9943
Multiple Pipe Heat Exchanger	114.01	338.83	10 to 100 m ²	0.9998

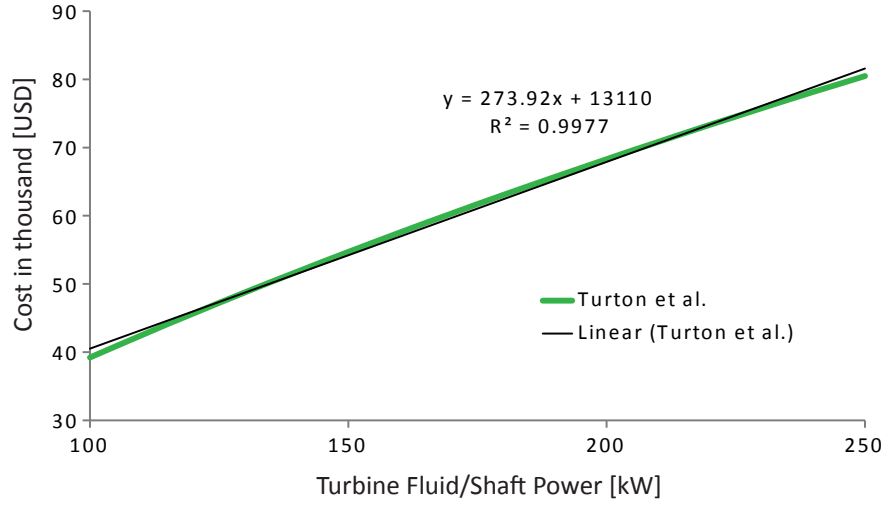


Figure 4.6: Linearisation of cost function – Turbine.

Economic Models for the MILP

The MILP solver, as the name states, can only use linear and integer equations. Thus cost equation of Turton (equation 4.20) has to be linearised for each piece of equipment to a form:

$$C_{p,l}^0 = L_1 + L_2 \cdot A \quad (4.27)$$

With respect to the linearisation A should satisfy:

$$A_{\min} \leq A \leq A_{\max} \quad (4.28)$$

Where A is the sizing parameter, and L_1 and L_2 describe the size dependent and independent impact on the cost. The results of a linearisation are shown in table 4.8, where range describes the sizing parameters between which the linearisation was done. If the size exceeds the range of the linearisation, the estimation will be less precise. However, the costs are recalculated in the post-calculation using the non-linearised equations.

4.3. Method Description – Multi-Objective-Optimisation

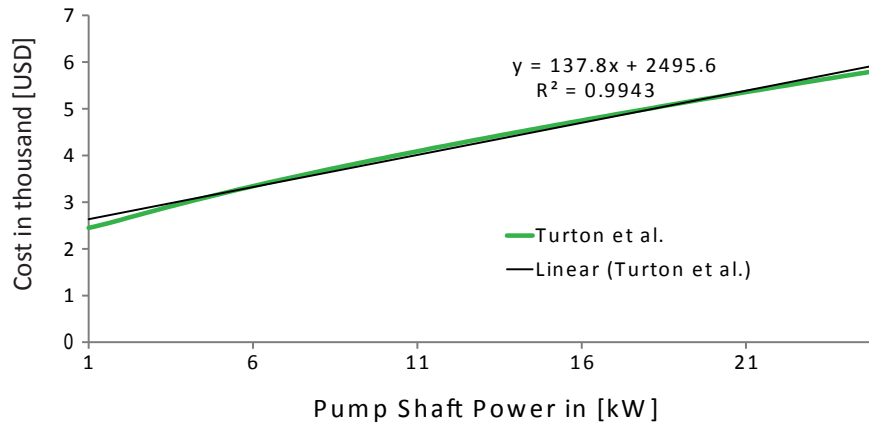


Figure 4.7: Linearisation of cost function – Pump.

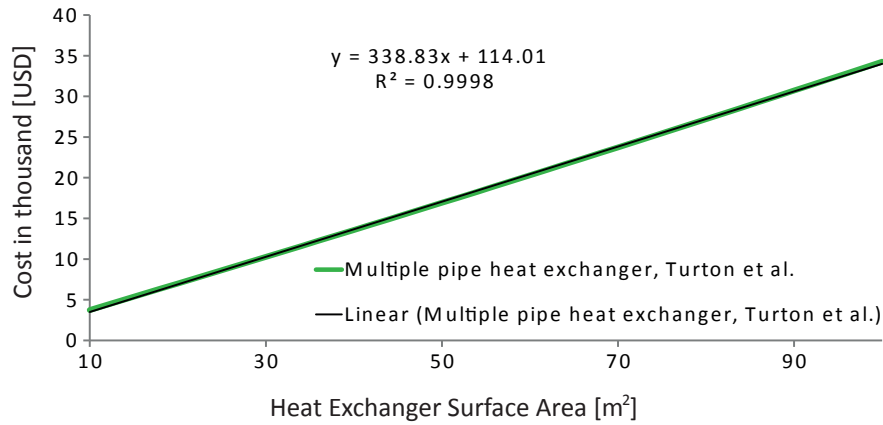


Figure 4.8: Linearisation of cost function – Heat Exchanger.

The correlation of the linearisation with the original cost functions is good since the range has been chosen relatively narrow. Exceeding the linearised area will lead to an overestimation of pump (31 % if exceeded 5 times) and expander cost (66 % if exceeded 5 times), and an underestimation of the heat exchanger cost (15 % if the heat exchange area is exceeded 5 times). Overall cost will be overestimated for larger installations. If the range of the system should be different, the cost calculations should be adapted. The linearisation of the three considered units is shown in the following figures 4.6 to 4.8).

We have seen that the objective function of the master optimisation minimises the specific investment cost equation 4.4. We can not calculate this in the slave optimisation since it is not linear for differently sized ORCs. As cost variables, the MILP solver accepts two types of cost, operation cost and investment cost. We will use this in order to do a work-around the

Chapter 4. Suitable Cycle Identification

impossibility of minimising the specific investment cost directly: we will calculate a simplified version of the *net present value* (Turton, 2012) and use it for the objective function.

$$NPV = \sum_{i=1}^n \frac{R_t}{(1+i)^t} \quad (4.29)$$

Where t is the a time period, R_t the return in period t and i the depreciation rate of the value.

We calculate the NPV for the yearly cost and revenues which consist of the operating cost R_{op} and the electricity sales R_{el} . Like in the publication by Lazzaretto et al. (2011) two per cent of the investment cost is assumed to occur as operation cost during the lifetime of the system. Lifetime t_l is assumed to be 15 years and yearly operating time $t_{op} = 8000$ h.

Since the markets for electricity and other energy sources have shown to be volatile and unpredictable during the last years, the prices (electricity and operation cost) are simply assumed to develop with the value of money, so the depreciation rate is assumed to be 0. We thus get:

$$NPV = \sum_{i=1}^n R_t \quad (4.30)$$

Heat recovery is mostly interesting for larger industrial sites, so the entire electricity is assumed to replace electricity import/purchase thus the price is based on the purchasing price taken from Eurostat 2012 (European Union, 2014) second semester for industry with 2,000 to 20.000 MWh Band and is $C_{el} = 0.1574$ EUR /kWh. The net shaft power \dot{E}_{net} includes turbine and pump shaft power.

Four values are calculated Cost1 and 2 describing the operating costs and electricity sales, Cinv1 and 2 describe the total module costs, the first values Cost1 and Cinv1 are calculated using the size independent part L_1 of equation 4.27:

$$Cost1 = 0.02 \cdot 1.18 \frac{I_t}{I_{t,ref}} \sum_{i=1}^n F_{BM,i} L_{1,p,i} \quad (4.31)$$

$$Cost2 = -t_{op} \cdot t_l \cdot C_{el} \cdot 1.32 \text{ USD /EUR} \cdot \dot{E}_{net} + 0.02 \cdot 1.18 \frac{I_t}{I_{t,ref}} \sum_{i=1}^n F_{BM,i} L_{2,p,i} \quad (4.32)$$

$$\text{Cinv1} = 1.18 \frac{I_t}{I_{t,\text{ref}}} \sum_{i=1}^n F_{\text{BM},i} L_{1,p,i} \quad (4.33)$$

$$\text{Cinv2} = 1.18 \frac{I_t}{I_{t,\text{ref}}} \sum_{i=1}^n F_{\text{BM},i} L_{2,p,i} \quad (4.34)$$

We can thus calculate the total lifetime value of the installation:

$$C_{\text{MILP}} = \text{Cost1} + \text{Cinv1} + f_i \cdot (\text{Cost2} + \text{Cinv2}) \quad (4.35)$$

Where f_i is the sizing parameter (or multiplication factor) of the ORC, that the MILP will use.

The costs calculated this way are not to be understood as final cost estimations of the installation. It is however a way to optimise the investment cost per produced electricity. In the post computation described below the cost are re-evaluated, especially as the temperature differences in the heat exchangers do not correspond to the final temperature differences, thus overestimating the cost of the equipment as explained above in the Thermodynamic Models II.

As pointed out at the beginning of this chapter, the objective functions of the MILP solver are not the same as the ones for the overall optimisation. They are used, to orient the solutions in the right direction. The post computation calculates the objective functions that are used for the set of Pareto optimal solutions. That means, the assumptions made above (electricity price, lifetime, yearly operation time etc.) do not impact the result directly. They are merely used to identify the right solutions, not to give real values. The solutions found by the MILP solver using the linear MILP objective functions are valid because both MILP objectives lead to Pareto solutions which occupy partially the same solution space.

4.3.7 Integration – MILP-Solver

The integration is done using the tools of Pinch analysis (Bolliger, 2010) and is executed by a Mixed Integer Linear Programming (MILP) solver. An MILP problem is a problem that contains at the same time linear equations (including equalities, maximisations and minimisations) as well as integer problems (these can be on-off problems, e.g. shall a unit be used or not, or negative and positive whole number problems for example for the number of stages in a cycle). Here a commercial solver is used to resolve a mathematical problem containing linear equations and integer values. We use a solver by IBM called ILOG CPLEX (IBM, 2009) and a

Chapter 4. Suitable Cycle Identification

mathematical language called AMPL (Fourer et al., 1990). The linear equations are the heat cascade and the sizing of the cycles as well as the objective functions and the cost functions.

The problem is constituted of several different elements (Maréchal and Kalitventzeff, 1998): the process streams (heating and cooling requirements, with index pro), the streams of the ORC, and the cooling utility. The process streams are not sizeable, while every unit (one ORC or cooling utility) can be scaled with a sizing factor f_i (for unit i) between $f_{i,\min}$ and $f_{i,\max}$ which are chosen by the optimiser. The units which can be sized, ORCs and cooling utility, are attributed an integer variable I_i which can turn the unit on or off. The entire problem is separated in temperature intervals (transferring the heat from the cooling requirements to the heating requirements from high temperatures to low temperatures) with the index k , corresponding to the occurring temperatures. Also heat transfer from a temperature interval at higher temperature to one at lower temperature is allowed, this amount of heat is designated by \dot{R}_k . Since we defined the heat in the thermodynamic models I for a mass flow rate of $\dot{m} = 1 \frac{\text{kg}}{\text{s}}$ we can suppose that for the sizeable units we get $\dot{Q}_{i,k} = \dot{q}_{i,k}$ in temperature interval k and the sizing factor f_i carries the mass units, for the process unit the heat is \dot{Q}_{pro} .

With this information the solved MILP problems become:

Electricity Generation Maximisation (linked to the heat cascade by equation 4.11):

$$\text{Obj 1} = \text{Max} \left(\sum_{i=1}^{n_i} f_i \cdot \dot{E}_{\text{net},i}^- \right) \quad (4.36)$$

or Total (lifetime) Cost Minimisation:

$$\text{Obj 2} = \text{Min} \left(\sum_{i=1}^{n_i} f_i \cdot C_{\text{MILP},i} \right) \quad (4.37)$$

Subject to:

$$\text{Heat Cascade} = \sum_{i=1}^{n_i} f_i \cdot \dot{q}_{i,k} + \sum_{p=1}^{n_{\text{pro}}} \dot{Q}_{p,\text{pro}} + \dot{R}_{k+1} - \dot{R}_k = 0 \quad \forall k = 1, \dots, n_k \quad (4.38)$$

$$I_i f_{i,\min} \leq f_i \leq I_i f_{i,\max} \quad (4.39)$$

$$R_k = 0 \quad \forall k = 1, n_k \quad (4.40)$$

$$I_i \in \{1, 0\} \quad (4.41)$$

Since a cycle has an integer variable I_i and a multiplication factor f_i , it is thus possible to add constraints which define the number of chosen cycles to the problem of the type:

$$\sum_{i=0}^n I_i = x \quad (4.42)$$

where n is the total number of cycles. On the right hand side of the equation x can be chosen freely between 1 and n (more precisely 0 and n although 0 would be nonsensical and lead to the trivial solution of not investing into an ORC) and the equation can also be set with the inequalities *less than or equal to* (“ \leq ”) or *greater than or equal to* (“ \geq ”). The integer problems give the possibility to use or not to use a proposed cycle. If more than one cycle is allowed, it is logical to increase the number of decision variables, the number of generated combinations of *turbine inlet temperature*, *turbine inlet pressure* and *condensation inlet temperature* should be multiplied by x (multiply by the number of units), thus several cycles with independent characteristics (pressure levels, temperatures etc) can be combined. This case is discussed in more detail in section 4.5. It should be noted that the resolution time of the solver strongly depends on the number of integer variables.

The MILP-Solver then solves the problem for all cycles corresponding to the set of decision variables at once, choosing amongst all “ I_i, f_i ” combinations that respect the constraints and satisfy the objective. This way, the optimisation chooses between all fluids from the REFPROP database that comply with the choices made in the beginning (Respecting the legislation, ODP, GWP limits etc) and which are feasible. The result is then treated in the post calculation.

4.3.8 Post-Calculation – Indicators

In the post-calculation, the results from the MILP-solver are treated and prepared before being passed on to the master optimisation/genetic algorithm. Both objectives are re-calculated based on the results of the MILP-solution, which always optimises only one objective.

Since we know at this point the hot and cold composite curve of the problem with the integrated ORC, it is possible to calculate the logarithmic mean temperature (LMTD) (equation 3.14) for every heating and cooling requirement of the cycle (or cycles) and with that the heat exchange surface is computed. The procedure for determining the temperature difference is explained in the case of a heating requirement:

1. For the entrance and the exit temperature of the heating requirement, the corresponding spot on the composite curve is identified.
2. The facing temperature, meaning the temperature that is horizontally on the other hot composite curve is identified. This is done by changing the format of the composite

curves from heat-temperature to temperature-heat coordinates (this has to be done carefully since they are not bijective).

3. The resulting temperature differences of both, inlet and outlet of the segment are used to calculate the LMTD.
4. If the temperature differences are equal, the temperature difference is used instead of the LMTD.
5. The surface A is calculated:

$$A = \frac{\dot{Q}}{U \cdot LMTD} \quad (4.43)$$

Where A is the surface, h the heat transfer coefficient obtained by the thermodynamic models II, and \dot{Q} is the transferred heat, which is calculated by multiplying the heat of that interval as it was determined with the thermodynamic models I with the multiplication factor, obtained in the integration with the MILP.

6. The surfaces of all sections are then summed up.

This methodology supposes strictly horizontal heat exchange (with regards to the composite curves) and parallel heat exchangers in the case of more heat transfers in the same temperature range. Thus we do not have to take care of any jumps or gradient changes of the composite curves within the temperature range of the heat exchange.

With the total heat exchange surfaces it is possible to re-evaluate the cost for the heat exchange, this is done very much as described above in the economic models. Since the calculation is not limited to linear equations any more, the original (non-linearised) equations of the economic models are used, this is especially important if the characteristic parameter exceeds the range used for linearisation. Again, 3 heat exchangers are assumed for every ORC, which are used for preheating, evaporating, superheating, de-superheating, condensation and subcooling, possibly including a regenerator, if the integration makes that useful. Also, the surface of each of the heat exchangers is not calculated one by one, but it is a third of the total surface, thus overestimating the cost, giving a more conservative total cost. This makes the calculation simpler, especially because the existence and size of an economiser (ORC to ORC heat exchange) does not have to be tested. For pump (shaft) and turbine (fluid) power, the calculated values from the thermodynamic models I are multiplied with the multiplication factors determined by the integration are used.

As objectives of the multi objective optimisation the tool uses as defaults:

- Net Electricity Generation:

$$\dot{E}_{el} = \dot{E}_{turb} + \dot{E}_{pump} + \dot{L}_{turbogen} \quad (4.44)$$

Where \dot{E} is the shaft work of the component. The losses $\dot{L}_{\text{turbogen}}$ are assumed to be 10 kW, in accordance with what was measured during the LOVE project (figure 3.22). However, this assumptions showed to be non-realistic and should be corrected as discussed in 4.6.1 and chapter 5.

- Specific Total Module Cost

$$C_{\text{TM,spec}} = \frac{C_{\text{TM}}}{\dot{E}_{\text{el}}} \quad (4.45)$$

In USD /kW_{installed}.

Another implemented possibility would be to use the (heat) exergy efficiency instead of the net generated electricity: This is done by dividing \dot{E}_{el} by the sum of the heat exergies of all process heating and cooling requirements:

$$\eta_{\text{ex}} = \frac{\dot{E}_{\text{el}}}{\dot{E}_q} \quad (4.46)$$

Also it is possible to calculate implemented performance indicators of the cycle(s) like cycle efficiency and back work ratio, however

The multi objective genetic algorithm optimiser is programmed to minimise the objectives, it is thus necessary to change the sign (here for the net generated electricity) accordingly, before sending the value.

It would be possible to calculate the production cost per kWh_{el} or the net present value (as we have done above for the MILP-optimiser), it is however dependent on the yearly operation time (now and future), the operation cost, the present and future electricity price and the depreciation or even inflation of money, therefore we prefer to look at the specific investment (total module cost).

4.4 Solution Reliability Increase

The chosen objective for the MILP-solver, can either be thermodynamic (maximizing the power output, equation 4.36) or economic (minimising the total “linear” cost, equation 4.37). After (re-)calculating the objectives in the post calculation, the resulting set of integer variables and multiplication factors (I_i, f_i) , together with the values of the objective functions, is passed back to the multi objective optimiser. The result depends on the chosen MILP objective. This can be seen as a reliability problem in the sense that it reveals the MILP to be the “bottleneck” of the entire procedure: the problem solved by the MILP is not the same as the problem solved by the master optimisation. Whenever an integration with a single objective is used in a multi objective optimisation this occurs. In other words, the chosen objective in the MILP problem decides towards which objective the Pareto front is developed.

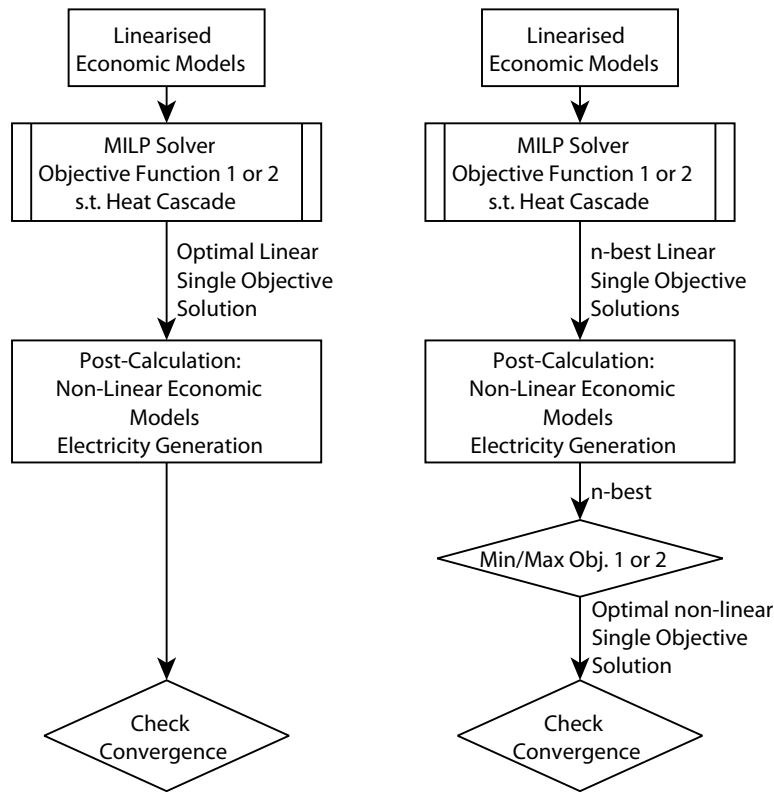


Figure 4.9: Algorithm detail of cycle identification showing before (left) and after (right) the reliability increase.

One way to counter this would be to use a solver that can optimise both objectives, thus not resulting in one solution but a function of solutions which are all Pareto optimal. For that it would be necessary to introduce the entire problem as mathematical functions into the slave optimisation, which is not realistic, especially for the thermodynamic data. Furthermore, many equations that are used upstream of the MILP are not linear, they either would have to be linearised (which is again not possible for the thermodynamic data) or a solver that can handle non-linear equations would have to be used.

We answer this issue by running the multi objective master optimisation one time per each of the two MILP objective functions. This increases the solution time, but is effective and does not make a complete redesign of the tool necessary.

The second problem, which shows the MILP as a bottleneck, is that the MILP can only handle linear equations. Therefore, the difference between the best solution and an n -best solution, generated by the MILP solver, could be within the imprecision of the linearisation. Thus, when evaluating the two options in the post calculation, the n -best MILP solution could actually be better than the best MILP solution. This can reveal problematic in the case where the economic objective is chosen for the integration (MILP problem).

The other source of possible “misjudgement” by the MILP solver occurs due to the temperature differences in the heat transfers, which cannot be determined before integration. This can be a problem if two solutions have a similar electric power generation, with one having smaller temperature differences than the other. The MILP will solve this problem with the ΔT_{\min} instead of the real LMTD, thus overestimating the cost of the solution with higher temperature differences. This might change the order of the solutions.

To react to the last two points we modified the way that AMPL recovers the output from the CPLEX MILP solver in a way that not the one best, but the n best solutions for I_i, f_i are calculated. We then apply the post calculation to all generated sets of I_i, f_i . With the list of n objective pairs we apply a simple minimisation. If objective function 1 is chosen in the MILP optimisation, we calculate:

$$\text{Min (Obj } 1_k) \tag{4.47}$$

And then return the pair of $\text{Obj } 1_k$ and $\text{Obj } 2_k$ for which objective 1 was minimal. All the results of the n -best solutions are stored and can be added to the set of solutions building the Pareto curve, if wanted. This novelty is represented in figure 4.9 which shows the concerned part of figure 4.1. We discuss the relevance and choice of n in the application section below.

4.5 Multiple Cycles and Multi Stage Cycles

The specific cost of a piece of equipment decreases with the size, with a small gradient for the heat exchanger and bigger gradients for the pump and turbine, therefore it is economically interesting to use bigger sized ORCs (economies of scale). However, if the shape of the heat sources enthalpy-temperature profile has a small gradient or jumps, it might be interesting to fit a heat recovery technology which allows to adapt better to the form of the composite curve. The need for flexible integration of the cycles with the process is already partially answered by the use of mixtures and supercritical cycles, which do not have an evaporation plateau, but rather a sloped evaporation (mixtures) or no clear evaporation at all (supercritical).

In cases with more complex shapes of the hot composite curves, including jumps, gradient changes or exergy pockets, more flexibility is advantageous. One solution to meet these requirements is the use of multiple ORCs. This is relatively easy to achieve by modifying the constraint function 4.42 in the way:

$$\sum_{i=0}^n I_i \geq 1 \tag{4.48}$$

This will make the MILP solver chose more cycles, if the objective function is met in a better way. However, since all cycle choices are calculated with the same set of decision variables,

they all have the same turbine inlet temperature and pressure as well as condensation inlet temperature. Therefore, this simple solution is not suitable for all types of heat sources, for example in presence of an exergy pocket.

The solution to this problem is the generation of an additional set of decision variables by the genetic algorithm, consisting of the turbine inlet temperature, the turbine inlet pressure and the condensation temperature. With these additional variables, the thermodynamic models and economic models are calculated for a second time, thus increasing the number of cycles put to the test in the MILP solver. The constraints function could then be set as:

$$\sum_{i=0}^n I_i \leq x \quad (4.49)$$

Where x is the number of independent sets of decision variables.

The use of multi stage cycles is also addressed with this approach. However, it supposes that a multi stage system cost as much as two single stage cycles, which is probably simplified.

The proposed methodology of using the n -best solutions from the MILP solver has a new importance, regarding the net electricity generated: if multiple cycles are allowed, the friction losses that have to be subtracted from the electricity generation have to be multiplied by the number of cycles, this is done in the post calculation, after the MILP solver:

$$\dot{E}_{el} = \sum_{i=0}^n \dot{E}_{turbine,i} + \sum_{i=0}^n \dot{E}_{pump,i} + \sum_{i=0}^n (I_i \cdot \dot{L}_{turbogen,i}) \quad (4.50)$$

However, the assumption of using a constant value for the cooling and friction losses has showed to be non-realistic and should be corrected as discussed in 4.6.1 and chapter 5. It can change the order of solutions, if two solutions with a similar sum of net shaft power are observed, but which have a different amount of cycles.

4.6 Application and Discussion

The working principles of the ORC selection tool have been explained. Hereafter we will analyse its behaviour with examples from chapter 2.

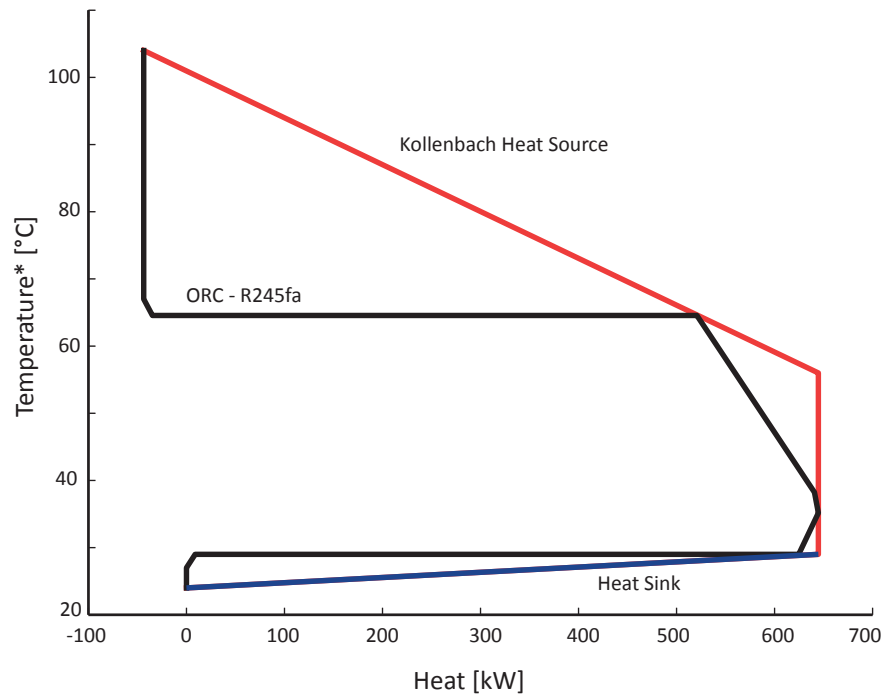


Figure 4.10: Integrated composite curve of R245fa ORC with Kollenbach heat source.

4.6.1 Impacts of Size, Heat Sink Temperature and Minimum Temperature Difference using the Example of the Kollenbach Heat Source

To begin with, we conduct a general analysis. This is done with the example of the heat source profile that has been observed on the Kollenbach heat source (on September 22, 2013). A cycle with R245fa will be integrated into the heat source, modifying some parameters in order to analyse specific behaviour. The heat source and heat sink that are used have the following characteristics:

Gas Inlet Temperature	108 °C
Gas Outlet Temperature	60 °C
Available Heat	688.3 kW
Cooling Water Inlet Temperature	20 °C
Cooling Water Outlet Temperature	25 °C

The ORC is integrated with the following parameters:

Turbine Inlet Temperature	63 °C
Condensation Temperature	33 °C
Turbine Inlet Pressure	4.7 bar
ΔT_{\min}	8 K

In figure 4.10 the ORC can be seen in the integrated composite curve of heat source and heat sink. The large exergy destruction above the cycle is obvious, the exergy efficiency of the cycle

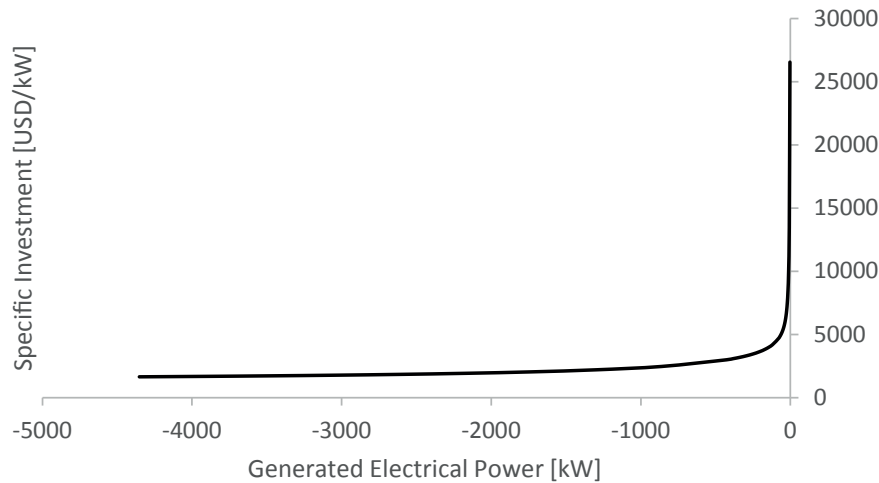


Figure 4.11: Impact of heat source load on net electricity generation and specific investment cost.

is 22 % (calculated with the lower temperature of the heat sink) and the generated electricity is 33.62 kW.

Impact of Size

Firstly, the impact of different sizes on the specific investment cost is analysed. This is achieved by multiplying the available heat of the source from 30 % of the observed size to 1000 %. Below 30 % the installation consumed more shaft power than it could produce. The resulting net electricity generation and specific investment cost are shown in figure 4.11, it is obvious that the cost decreases with increasing size. This is due to two effects, the first is the form of the cost functions, which show the same tendency, the second is the use of a fixed value for $\dot{L}_{\text{turbogen}}$ which probably does not represent the real impact, particularly for very small or very large turbines. We will talk about this in the conclusion (chapter 5). It becomes even more evident, if the exergy efficiency is considered instead of the specific investment cost as in figure 4.12.

Impact of the Heat Sink

The impact of the cold utility is particularly important for waste heat recovery at low temperatures because of the small overall temperature difference between heat source and sink (as we have seen in the introduction). We vary the heat sink inlet temperature (and outlet temperature in the same measure) from 5 °C to 25 °C at intervals of 5 K and adapt the ORC accordingly to show the impact. Figure 4.13 shows how the net electricity generation increases with a decrease in the cooling water inlet temperature. Figure 4.14 shows how it impacts the exergy efficiency. The available exergy changes by almost 25 % from 5 °C to 25 °C. This not only stresses, the importance of the right choice of cold utility for the application of waste heat valorisation with ORCs, but also underlines the importance of the condensation temperature as a decision variable.

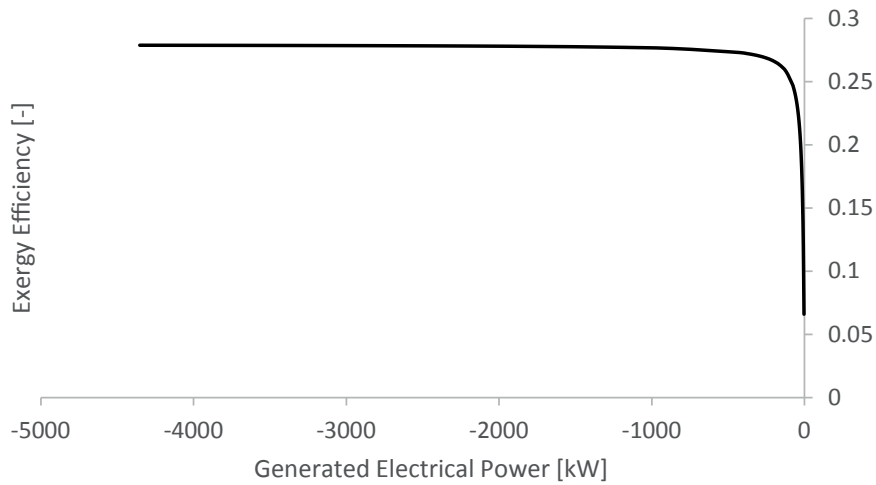


Figure 4.12: Impact of heat source load on net electricity generation and exergy efficiency.

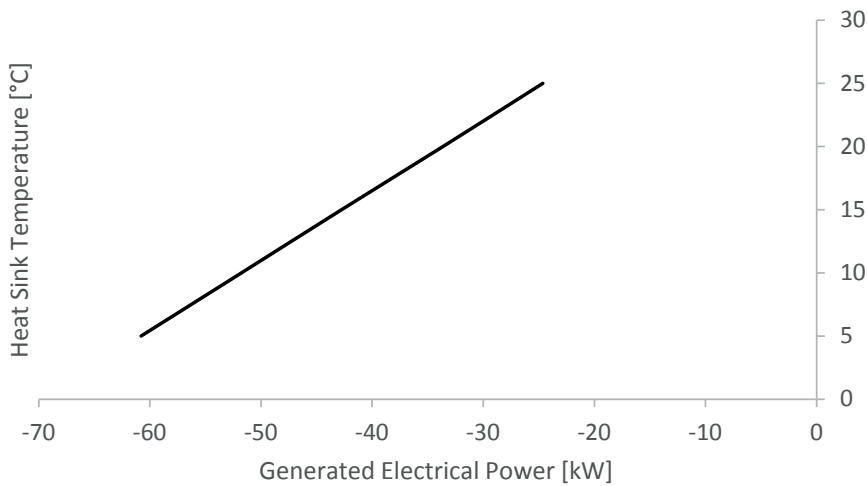


Figure 4.13: Impact of heat sink inlet temperature on net electricity generation.

Impact of the Minimum Temperature Difference

The influence of the minimum temperature difference between heating and cooling requirements (ΔT_{\min}) also has an important impact on the amount of electricity that can be exported from the installation. By varying ΔT_{\min} and increasing the evaporation pressure as well as decreasing the condensation pressure accordingly, the impact is demonstrated. Figure 4.15 and figure 4.16 show, respectively, how the net electricity generation is influenced and the resulting specific cost. The optimal specific investment cost is reached at approximately 4 °C for this installation. It reflects the trade-off between maximising the power output and keeping the investment cost for the heat exchange surface area small. At higher ΔT_{\min} the cost rises quickly, this is mainly due to the narrow available temperatures between heat sink and heat source, which decrease the produced power. The analysis shows how important the minimum temperature difference is as a decision variable.

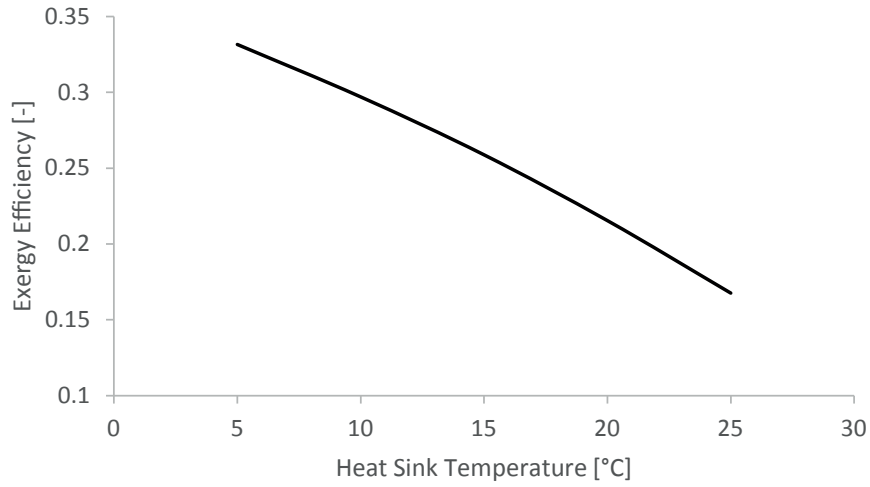


Figure 4.14: Impact of heat sink inlet temperature on exergy efficiency.

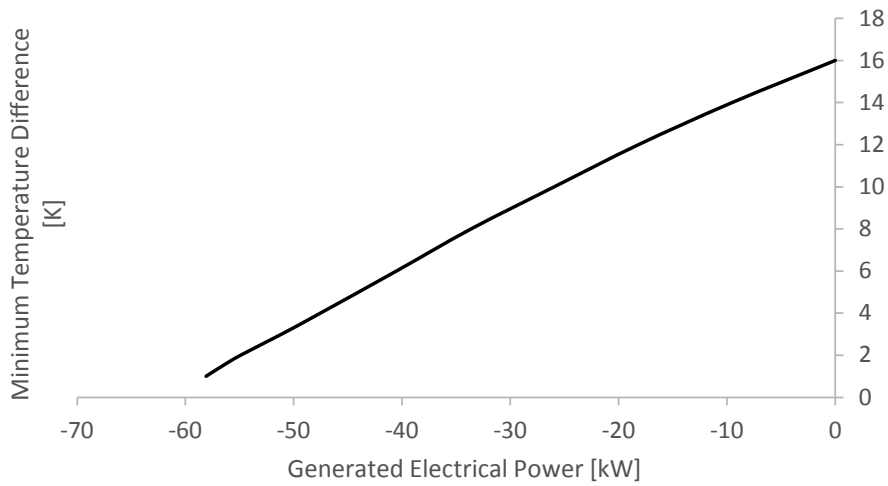


Figure 4.15: Impact of ΔT_{\min} on net electricity generation.

The chosen ΔT_{\min} does not only influence the overall cost, it also influences the shares of the turbine, the pump and the heat exchangers. Figure 4.17 shows these shares as a function of ΔT_{\min} .

Compared to the estimation found in Quoilin et al. (2011), who found a specific investment cost of 2700 EUR /kW for a cycle using R245fa with an output of 4.8 kW, the cost found here is considerably higher for the same size. However, they considered a heat source at 180 °C, which increases the available exergy substantially. Still, the cost of our methodology can be seen as too high for small installations, especially below 10 kW. This is due to the used cost functions and the constant value of $\dot{L}_{\text{turbogen}}$.

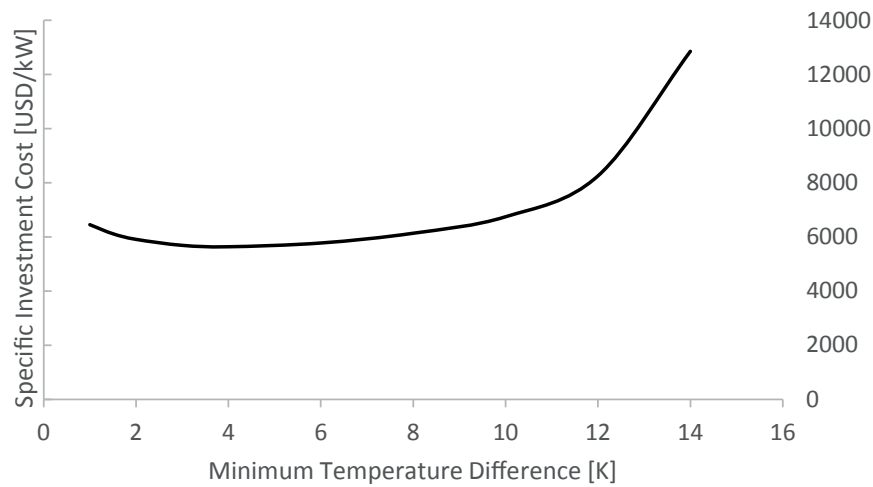


Figure 4.16: Impact of ΔT_{\min} on specific investment cost.

Other Solutions for Integration of a Single ORC with the Kollenbach Heat Source

Figure 4.18 shows the Pareto front for optimised integration of an ORC in the Kollenbach heat source. It can be seen that the electricity generation can reach 70 kW which corresponds to an exergy efficiency of 45 % with a specific investment cost of 14000 USD /kW. The cycle is shown in figure 4.19, the working fluid is surprisingly Acetone. The minimum temperature difference for this cycle is 1.5 K. The specific investment costs are distributed as follows: heat exchangers 25 %, turbine 65 % and pump 9 %. At this point it is important to mention, that the low pressure in the cycle (around 1.3 bar) leads to relatively high volumes. It is unclear, how well this is represented in the cost functions that are dependent only on one sizing parameter per type of equipment.

The specific investment cost could be as low as 4700 USD /kW for an ORC which produces 53 kW and has an exergy efficiency of 34 %. This is achieved with a cycle using the mixture R422D as a working fluid. The minimum temperature difference for this cycle is 1.5 K, as well. The specific investment costs are distributed as follows: heat exchangers 71 %, turbine 23 % and pump 6 %. The cycle is shown in figure 4.20.

Both examples show the use of ORC internal heat exchange. The statement that an economiser was not needed in waste heat recovery, made by Quoilin et al. (2011) can not be confirmed.

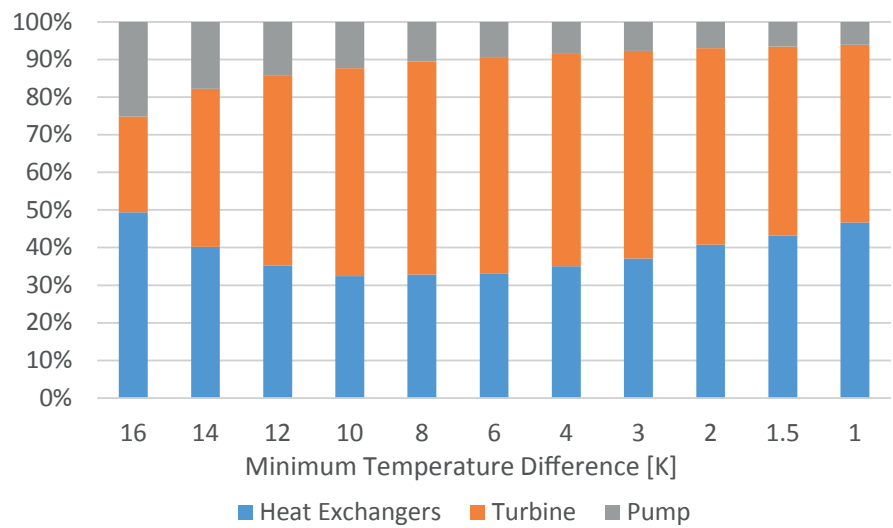


Figure 4.17: Impact of ΔT_{\min} on the share of the different equipments on the investment cost.

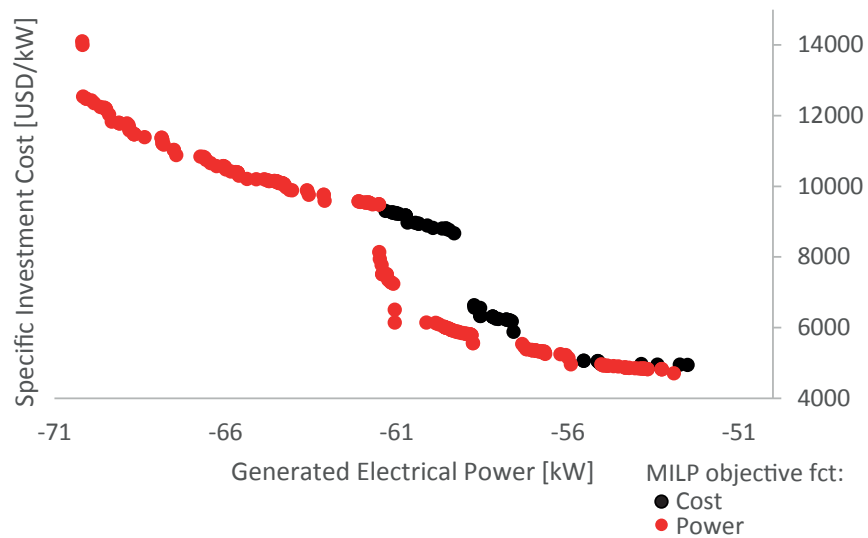


Figure 4.18: Pareto front of the integration of ORCs into a waste heat source from the Kollenbach cement process with both MILP objective functions.

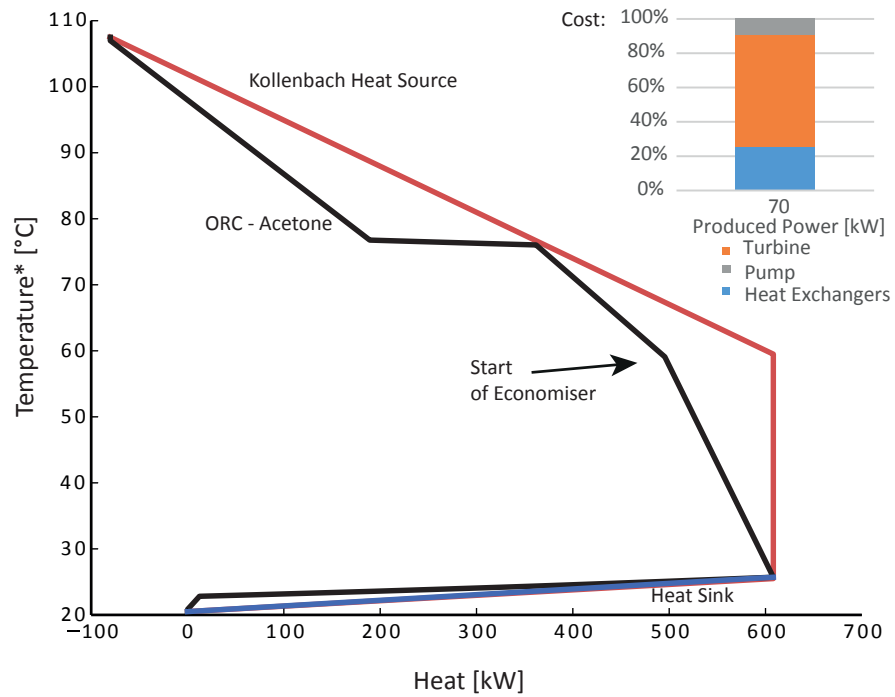


Figure 4.19: Integrated grand composite curve and cost distribution of Acetone ORC with Kollenbach heat source.

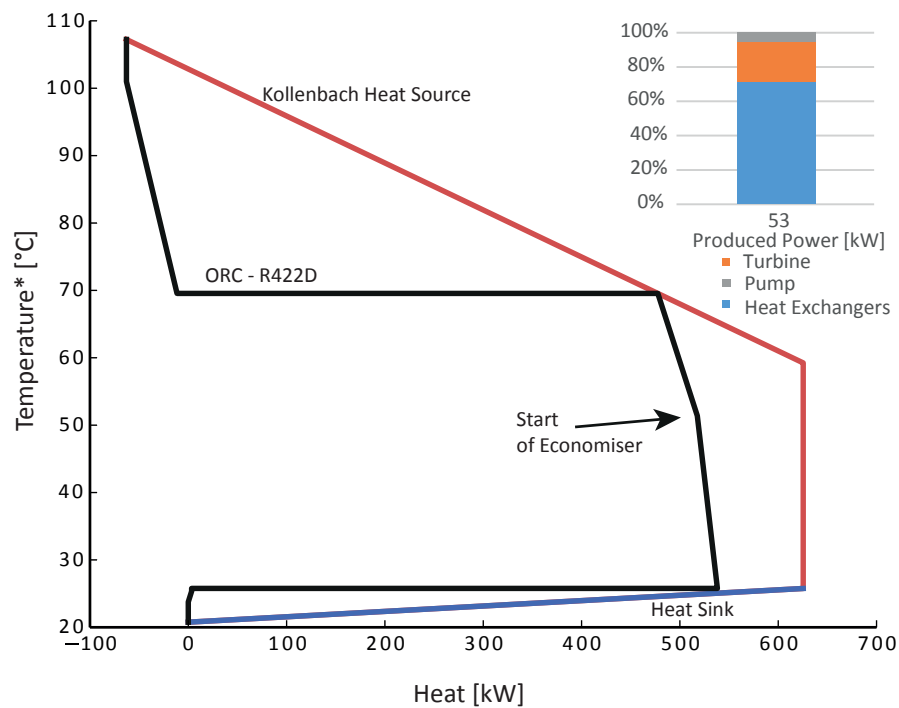


Figure 4.20: Integrated grand composite curve and cost distribution of R422D ORC with Kollenbach heat source.

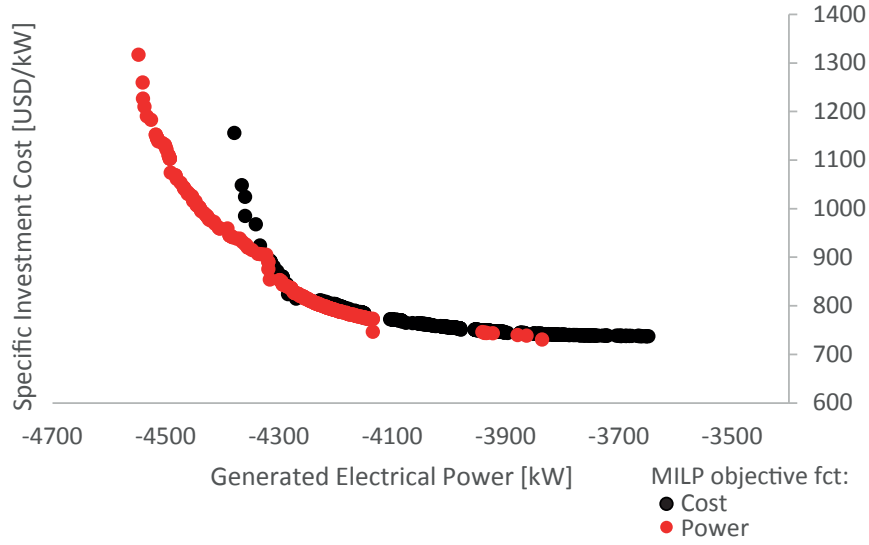


Figure 4.21: Pareto front of the integration of ORCs into a waste heat source from the cement process, allowing maximum one cycle with both MILP objective functions.

4.6.2 Discussion of the Pareto Curves, Solution Reliability Increase and the Specific Investment Cost Using the Example of the Cement Heat Source used with the Commercial ORC

The heat source that was discussed in chapter 2 in the context of the use with a commercially available ORC is used to demonstrate the Pareto curves. The source has two streams of hot gases which can be cooled down from 300 °C to 120 °C and from 400 °C to 210 °C, respectively. The available heat is 14 280 kW; 2000 kW will be used in district heating and the remaining can be used by the ORC (table 2.5). The heat sink that is assumed, is the one that was proposed by the manufacturer. It consists of cooling water entering at 25 °C and leaving at 40 °C.

The resulting Pareto front is shown in figure 4.21. The optimisation has been done with both MILP objectives (cost minimisation and power maximisation). It can be seen that the generated solutions are overlapping. However, the front of Pareto optimal solutions is made up of points generated by each of the optimisations. This validates the choice of using both of the objective functions in the MILP.

The Pareto front shown in figure 4.22 has been generated with the same heat source. However, the MILP problem was modified to allow two ORCs by setting the constraint of integer variables (cycles) to

$$\sum_{i=0}^n I_i \leq 2. \quad (4.51)$$

Again, both MILP objectives have led to solutions at a Pareto optimum and their choice is validated. The example for this large heat source shows that the integration of two ORCs has increased the maximum net generated electricity by almost 16 %, when compared to the

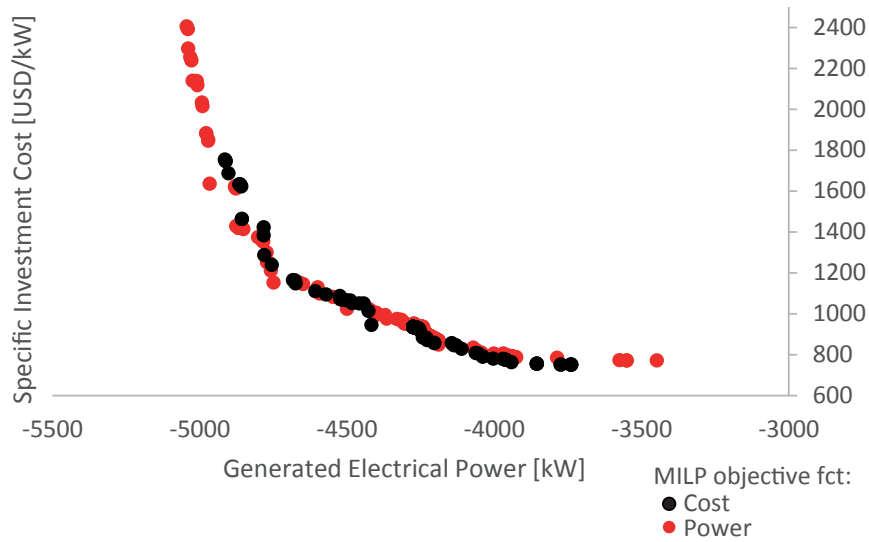


Figure 4.22: Pareto front of the integration of ORCs into a waste heat source from the cement process, allowing maximum two cycles with both MILP objective functions.

single ORC optimisation. However, the specific investment cost increases by 108 % with this additional power generation.

One experience we made is the necessity to set a specific investment cost for the trivial solution (no ORC), otherwise the solver pushed the solutions towards zero net electricity generation and zero investment. We chose 10 000 USD /kW in order to be above the resulting investment costs.

Impact of the Minimum Temperature Difference - Set of Pareto Optimal Solutions

Figure 4.23 confirms the overall impact of ΔT_{\min} on the set of Pareto optimal solutions. The trend of increasing cost with a decreasing minimum temperature difference is obvious. However, several clusters (or families) of solutions can be identified. Between two clusters the strict order by ΔT_{\min} is not always respected, which shows that other factors also have an influence (pressure etc.). The same is true for the generated electricity, as can be seen in figure 4.24. The generated electricity globally increases for the set of Pareto optimal solutions with decreasing minimum temperature difference.

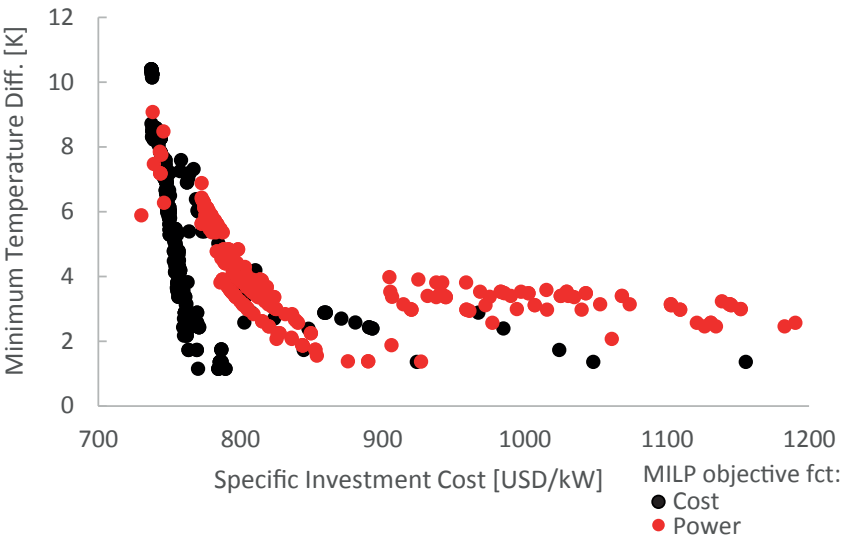


Figure 4.23: Impact of ΔT_{\min} on specific investment cost.

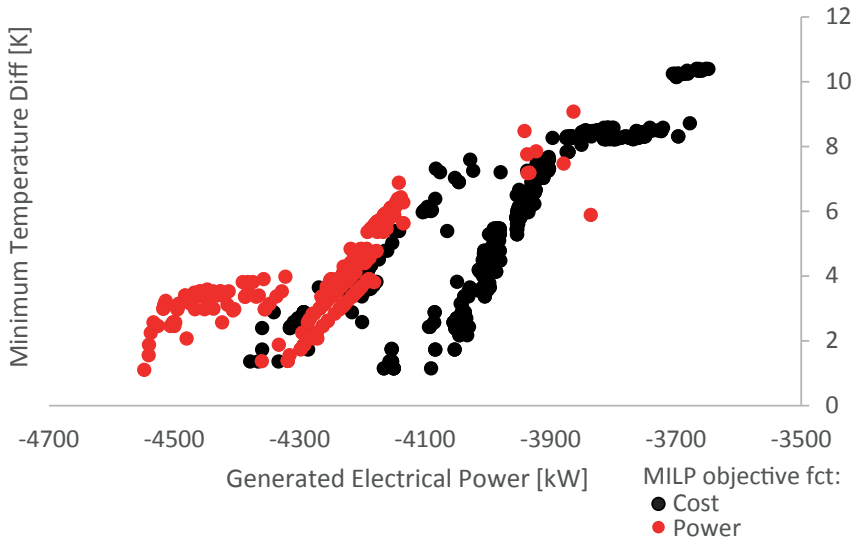


Figure 4.24: Impact of ΔT_{\min} on net electricity generation.

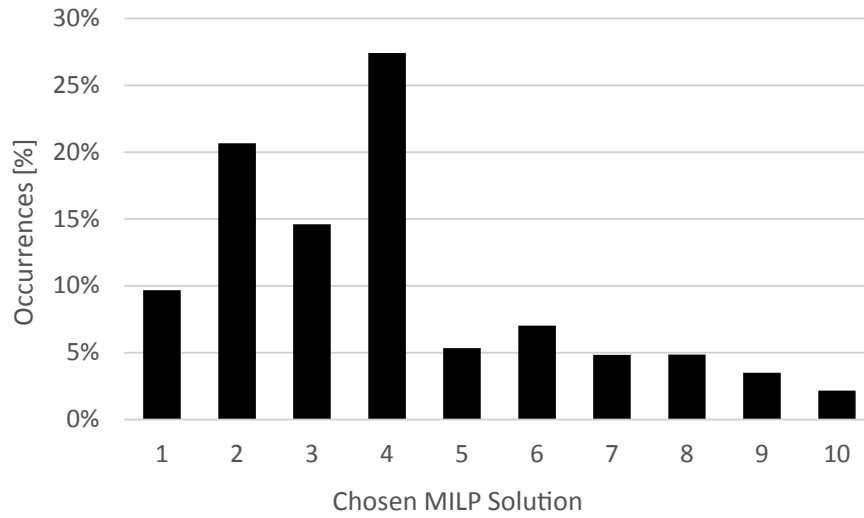


Figure 4.25: Histogram of the chosen MILP solution for an optimisation where one cycle is allowed and specific investment cost minimisation is the MILP objective function.

Discussion of the Solution Reliability Increase for Optimisations with One and Two ORCs

For the single ORC optimisation, with power maximisation as the objective function in the MILP, the solution of the post calculation is obviously the first result generated by the MILP. This is due to the fact that the only difference between the objective functions of the MILP (equation 4.37) and the multi objective optimisation (equation 4.46) are the friction and cooling losses. For the cost function however, the different objective functions can lead to different results. We introduced the solution reliability increase in section 4.4, to address this problem.

To measure the effectiveness of this novel methodology, the number of times each solution of the n -best has been found to be optimal is analysed. For the single ORC optimisation, with minimisation of the specific investment cost as the objective function in the MILP (equation 4.37) this is displayed in figure 4.25. Only solutions with a specific investment cost below 10 000 USD /kW have been considered. Out of the 23 215 generated solutions, 503 times the tenth solution was chosen, representing 2 %. In 90 % of all cases, the optimum would have been missed, had we not introduced the solution reliability increase.

For the optimisation allowing two cycles, the best solution of the MILP solver may not be the best solution in both cases, with cost minimisation and power maximisation. This happens, because the applied correction regarding the friction and cooling losses ($\dot{L}_{\text{turbogen}}$) depends on the number of chosen cycles. It is thus necessary to validate a choice of n . First we chose $n = 10$ for the n -best solutions, that was introduced to increase the reliability. Again, we include in this analysis only generated cycles with a specific investment cost of less than 10 000 USD /kW (which does not exclude any Pareto optimal solutions). In figure 4.26 we see the resulting histogram of solutions chosen by the post computation, for the case of using

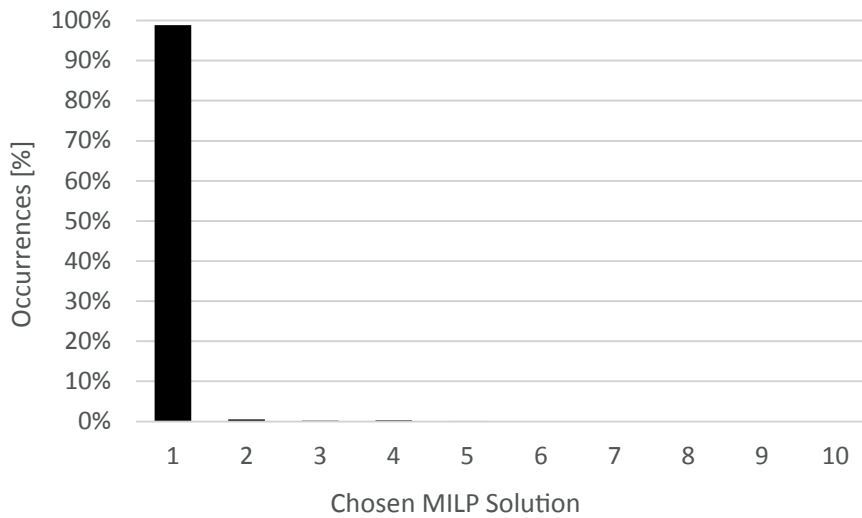


Figure 4.26: Histogram of the chosen MILP solution for an optimisation where two cycles are allowed and power maximisation is the MILP objective function.

the maximisation of the power output as an objective in the MILP. The tenth best solution was chosen only four times in the 29385 generations. The optimum would have been missed in less than 1 % of all cases, had we not introduced the method to increase the reliability. As discussed in section 4.4 the cases in which the optimal solution is not found with only one-best result from the MILP can have different origins, if cost minimisation is chosen as a MILP objective: the linearisation of the cost function, the friction and cooling losses and the overestimation of the heat exchanger surface in the cost functions of the MILP. This is reflected in the histogram (figure 4.27), where we can see that the optimal solution would have been missed in 86 % of all 28 165 cases. The tenth solution, and thus the constraint, was activated in 2686 configurations, representing almost 10 %.

It could be speculated that in some of the 2 % for the single ORC and 10 % for the double ORC cost optimisation, a higher number for n would have led to a better solution. The frequency of activation of the tenth best solution stays low enough to validate the choice of $n = 10$ for the single cycle and should be increased for the double cycle. Thus the double cycle optimisation with cost minimisation as MILP objective function has been executed again with $n = 15$. Figure 4.28 shows the corresponding histogram. It can be seen, that in only 4 % of all generations the 15th best solution was chosen. This corresponds to 4318 cases out of the total 23770 generations. We estimate this to be low enough. Figure 4.29 shows that it also led to a slight improvement of the set of Pareto optimal solutions. The choice of $n = 15$ could thus be validated for the double cycle optimisation with cost minimisation as MILP objective function. It should be noted, that in 82 % of all generations the optimal solution would not have been found without the solution reliability increase.

Overall, we can say that the introduction of the solution reliability increase by evaluating the n -best solutions as the number of solutions considered is adequate for the integration of ORCs.

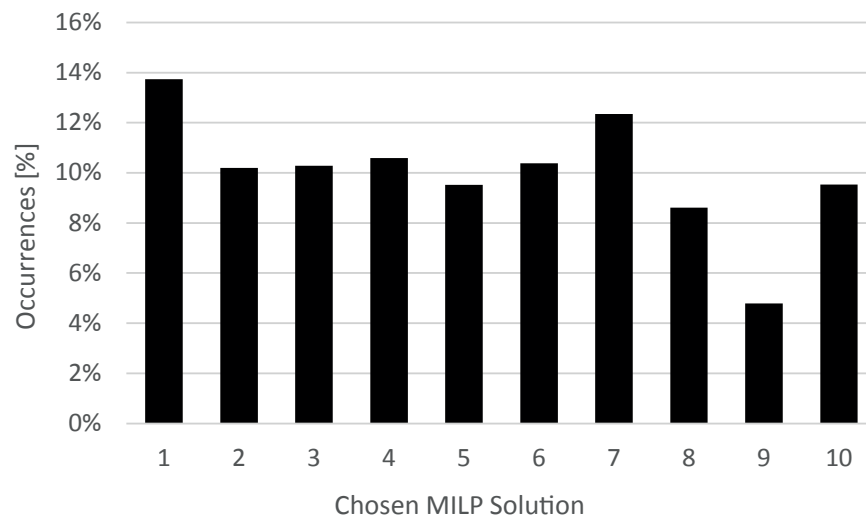


Figure 4.27: Histogram of the chosen MILP solution for an optimisation where two cycles are allowed and cost minimisation is the MILP objective function.

The 90 % of evaluations with the single ORC and minimisation cost as an objective, in which not the first solution was the optimal one, show the importance of the methodology. For the double ORC cost optimisation, the optimal solution would also have been missed frequently (82 %), which shows how important this development is when combining a multi objective non linear master optimisation with a linear single objective slave optimisation.

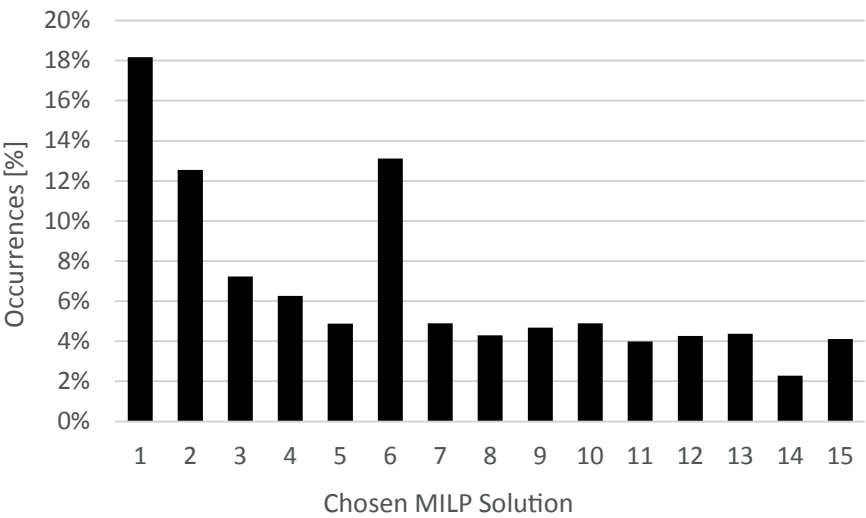


Figure 4.28: Histogram of the chosen MILP solution out of the 15-best for an optimisation where two cycles are allowed and cost minimisation is the MILP objective function.

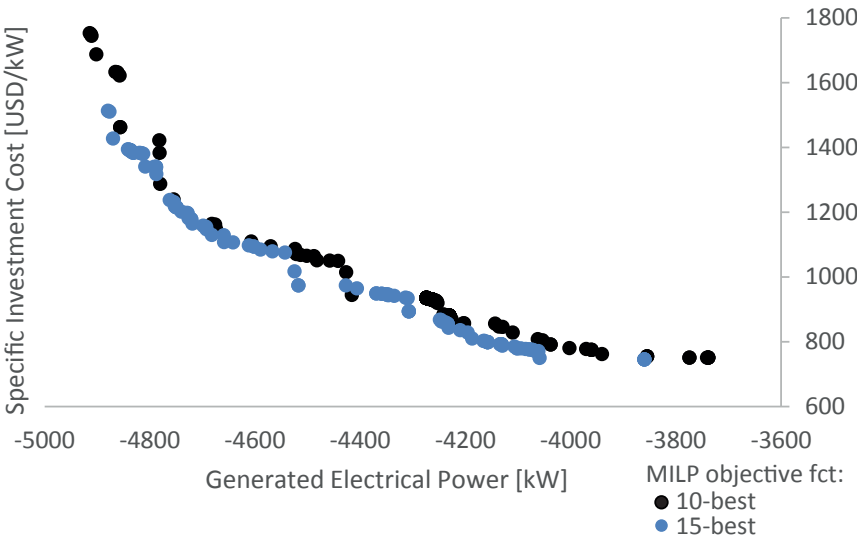


Figure 4.29: Pareto front of the integration of ORCs into a waste heat source from the cement process, allowing maximum two cycles with both MILP objective function for 10-best and 15-best.

Examples of Cycles Integrated with the Heat Source from Cement Industry

The example of a single ORC with the highest power generation could reach 4483 kW of electricity generation which corresponds to an exergy efficiency of 70 % with a specific investment cost of 1068 USD /kW. The cycle is shown in figure 4.30. The working fluid in this configuration is Propylcyclohexane. The minimum temperature difference for this cycle is 3.4 K. The specific investment costs are distributed as follows: heat exchangers 50 %, turbine 47 % and pump 3 %.

The specific investment cost could be as low as 737 USD /kW for an ORC which produces 3648 kW and has an exergy efficiency of 57 %. This is achieved with a cycle using Dodecane as a working fluid. The minimum temperature difference for this cycle is 10.4 K. The specific investment costs are distributed as follows: heat exchangers 33 %, turbine 64 % and pump 3 %. The cycle is shown in figure 4.31.

For the integration allowing up to two ORCs, the solution which has the lowest specific investment cost is a single cycle using again Propylcyclohexane as working fluid. The specific investment cost are 744 USD /kW and the net generated electricity is 3382 kW, it is thus slightly worse than the cost optimum for the single cycle optimisation. The minimum temperature difference for this cycle is 5.3 K. The specific investment costs are distributed as follows: heat exchangers 45 %, turbine 51 % and pump 3 %.

The cycle configuration allowing the highest electricity generation is composed of two cycles, one with Dodecane and another with Toluene as working fluids. It is shown in figure 4.32 and generates up to 5044 kW of electricity which corresponds to an exergy efficiency of 78 %. The minimum temperature difference for this cycle is 1.2 K. The specific investment cost are 2405 USD /kW and are distributed as follows: heat exchangers 72 %, turbine 27 % and pump 1 %.

From these examples, it can be seen that the net electricity generation compared to the proposed commercial ORC can be increased by almost 77 % for a single cycle at comparable specific investment costs. For the integration of two ORCs, the generation can be increased by 108 %, however the specific investment cost would be about twice as high.

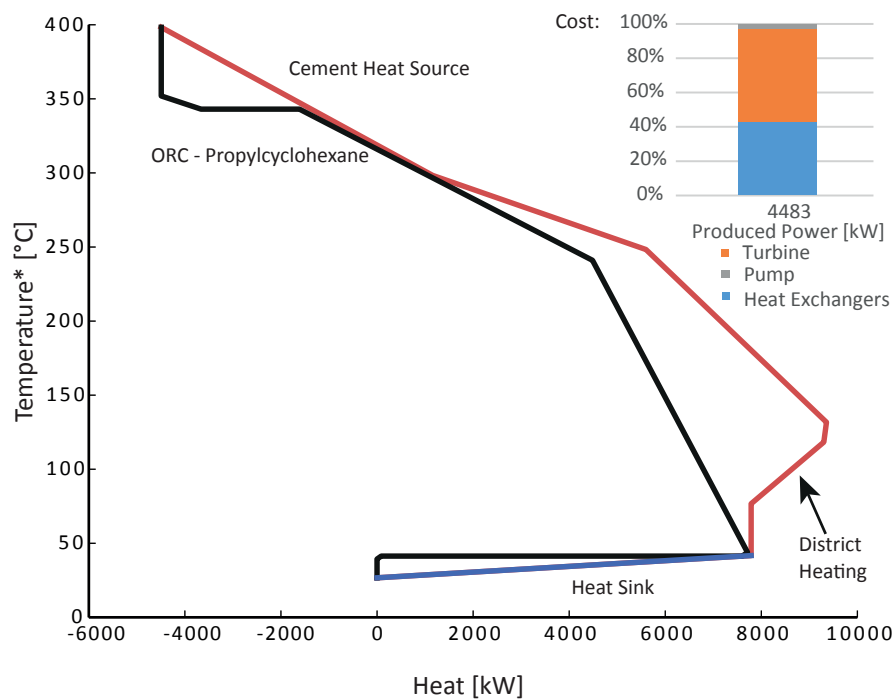


Figure 4.30: Integrated grand composite curve and cost distribution of Propylcyclohexane ORC with cement heat source.

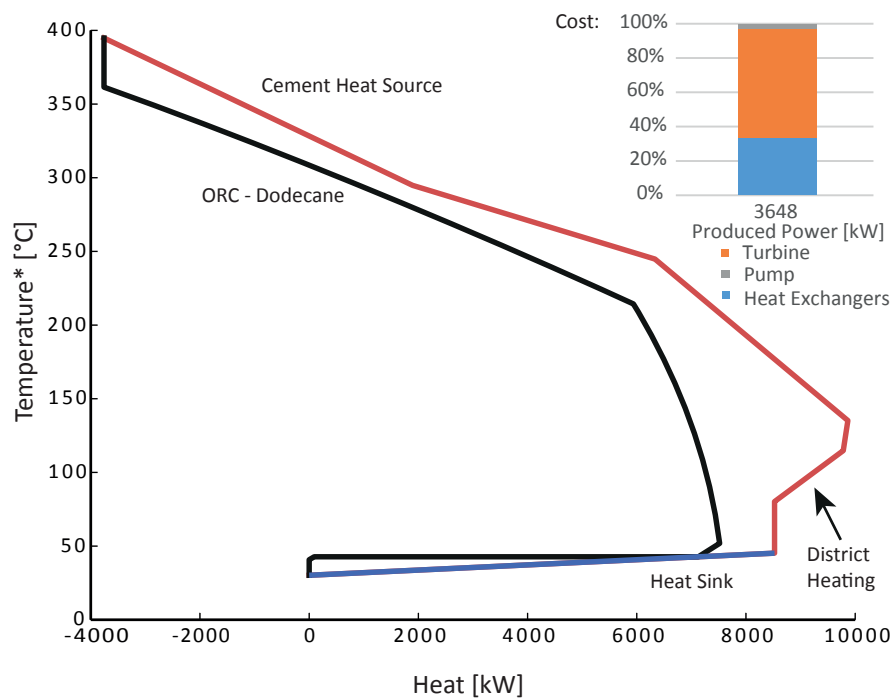


Figure 4.31: Integrated grand composite curve and cost distribution of Dodecane ORC with cement heat source.

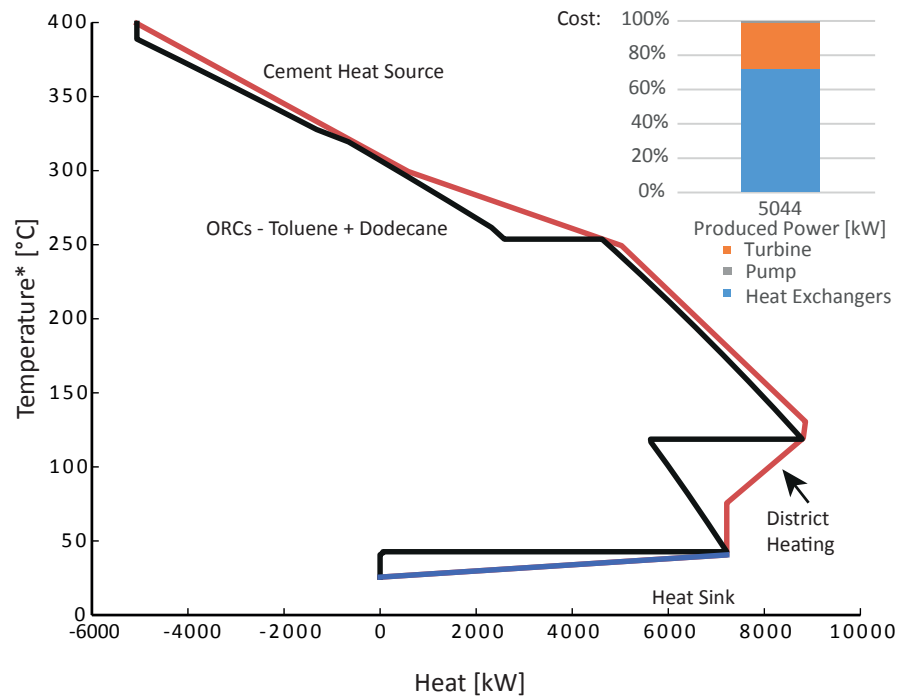


Figure 4.32: Integrated grand composite curve and cost distribution of two ORCs with Dodecane and Toluene with cement heat source.

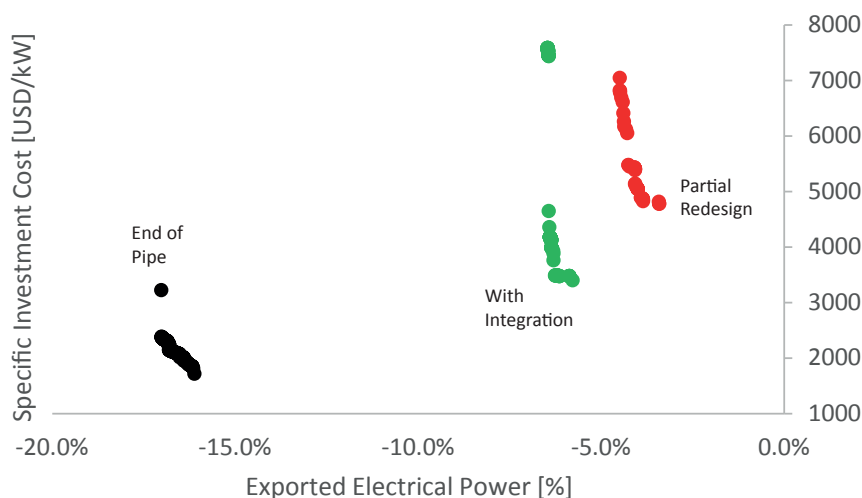


Figure 4.33: Pareto front of the integration of ORCs into the soluble instant coffee process, for the three studies (end of pipe, integration and partial redesign).

4.6.3 Integration of ORCs into the Soluble Instant Coffee Process

In figure 4.33, the Pareto fronts of single ORCs integrated into the soluble coffee process are shown. The three Pareto fronts correspond to the three different analyses of the plant and its waste heat potential. It shows the impact on the available waste heat, corresponding to the three analyses that have been explained in chapter 2, the waste heat that is available at the end of pipe of the process, the waste heat available after internal heat recovery and that after a partial redesign of the process. The generated electricity is relative to the heat that was released by the process in the end of pipe analysis. As a heat sink, a local surface water stream is assumed with a temperature of 8 °C and a cooling water release at 14 °C. This impacts the available exergy and up to 17 kW of electricity for every 100 kW of heat can be generated in the case of the end of pipe analysis, which corresponds to an exergy efficiency of 63 %. For the case of partial redesign, a maximum exergy efficiency of 49 % can be reached. In the case of the process with internal heat recovery, the shape of the composite curve makes the access to parts of the exergy difficult (figure 2.5), thus the exergy efficiency reaches a maximum of 41 %. As discussed in chapter 2, the specific investment cost, resulting from the low amount of exergy and the low temperature make an investment in an ORC unattractive for the analysis including a partial redesign of the process. They are over 4500 USD /kW.

4.7 Conclusion

We present a novel methodology that is adequate for the identification of suitable working fluids and cycle configurations for electricity production. The methodology is implemented in a software tool, which allows the identification of optimal ORC for any given heat source and heat sink. The tool is designed to use a multi objective optimisation as a master problem and the integration of the cycle(s) with the process, as well as the choice of the working fluid(s)

in an MILP solver as a slave problem. This ensures that all possible fluids are tested and the best choice for the set of decision variables is made. It reduces the problem greatly since the fluid selection is not a decision variable. The multi objective optimisation finds a set of Pareto optimal solutions regarding two objective functions: the minimisation of the specific investment cost and the maximisation of the generated electricity. Using the cost aspect is a way to account for differences in heat transfer and the electricity production at the same time.

A novel approach regarding the combination of the non-linear multi objective optimisation with a single objective MILP optimisation is introduced. The choice of only one objective in the MILP problem and the necessary linearisation of not linear objective functions, leads to solutions which are optimal regarding the MILP problem, but non-optimal regarding the multi objective optimisation. We have addressed this in two manners. First, the multi objective optimisation is run once for each objective of the MILP problem, leading to the development of two separate areas of the Pareto curve. And second, by recovering n -best solutions from the MILP instead of one. These solutions are then evaluated in a post calculation and the best of the set is transferred to the multi objective optimiser. For the optimisation using power maximisation as an objective function in the MILP, a value of $n = 10$ showed to be largely sufficient. Also for the optimisation with cost minimisation as an objective function and a single cycle, $n = 10$ results in precise solutions. However, for the MILP optimisation allowing up to two cycles and minimising the cost, a value of $n = 15$ should be used. The analysis also showed that in up to 90 % of all ORC evaluations, the first MILP solution was not the best one regarding the non-linear objective functions. This reveals the importance of this novel approach.

The generated costs, estimated by the tool have been compared with values from literature, it was found that it overestimates cost for very small installations (generating less than 10 kW) and that the cost for large installations are optimistic in comparison to the cost of a commercially available ORC; however they are in the same order of magnitude.

The tool was efficient in finding the optimal integration of an ORC into a heat source for which an offer of a commercially available ORC is available. It showed that an electricity generation of up to 77 % more compared to the commercially available ORC would be possible with a single cycle.

An estimation of the cost per produced kWh of electricity can be found in appendix C.

5 Conclusion

In an effort to limit the impact of industrial energy consumption on climate, fuel savings should be carried out through implementation of energy efficiency measures, where possible. Energy saving potentials should always be addressed before installing a waste heat valorisation system, such as an Organic Rankine Cycle (ORC). The motivation and topic of this thesis has therefore been defined as:

Developing a methodology that allows identifying maximum electricity production with the help of Organic Rankine Cycles from the waste heat of an industrial process, at the lowest specific cost, without jeopardising the increase of the process's thermal efficiency.

In light of the given problem definition we will present the main conclusions of this work. Building on this, we will define possible future research goals.

5.1 Results

Chapter 1 - Defining Waste Heat

No satisfying definition of waste heat, allowing to identify its unavoidable amount and the potential to recover work has been found in the literature. We have addressed this by combining the techniques of process integration, Pinch analysis and exergy analysis to define the energy and exergy potential of waste heat. This way, it is possible to simultaneously identify the saving potentials within the industrial process under consideration and the potential for waste heat recovery systems. An additional finding of this development is that in some cases, available exergy can only be accessed by changing the overall energy balance of the process.

Chapter 2 - Waste Heat Recovery: Studies and Examples

Different examples from industry have been studied regarding the evolution of their waste heat potentials with respect to an increase of the degree of integration of the industrial process. The waste heat decreases with increasing efficiency of the process. It is interesting to note that, the amount of waste heat as well as the temperature levels decrease, as a result the available exergy from waste heat recovery is reduced. Another, interesting finding in this context, resulting from a theoretical analysis of a representative cement production process, is that the extreme case of a partial redesign and a maximal integration would lead to almost no waste heat above ambient temperature. However, the process shows a large exergy pocket, which could be accessed by introducing a low temperature heat source.

By installing two low temperature Organic Rankine Cycle demonstrators, practical experience was gained and analysed. This analysis was conducted with the goal of obtaining practical knowledge, guiding the design of a realistic tool for the identification of optimal ORCs. The results show that a design with a direct heat exchange between source and working fluid led to less difficulties, due to reduced complexity, as compared to heat recovery with an intermediate water loop. Other key learnings from the demonstrators were that stainless steel should be used to avoid corrosion in the heat exchangers and the installation of a cooling system sized according to the size of the ORC is beneficial to avoid high pumping power.

Chapter 3 - Waste Heat Valorisation System Characterisation

With the goal of identifying parameters, which can be used to calibrate the mathematical models for identification of optimal ORCs for waste heat valorisation, the measurement data of the two ORC demonstrators were analysed. However, difficulties with the measurements led to highly incoherent data. Therefore, we introduced the technique of data reconciliation and used it to analyse the data collected during the measurement period. We developed a novel methodology of using parameters, identified in one time period (t), as virtual measurements in the next time period ($t + 1$). This methodology is suitable for increasing the a posteriori precision of the reconciled values in a steady state system and could therefore find application in sensible processes, such as the production of pharmaceuticals. Since the ORC demonstrators were mostly transient in their behaviour, we could not take full advantage of this enhanced reconciliation. However, the measurements were reconciled with “classical” data reconciliation. The analysis showed that the isentropic efficiency of the ORC turbine has an almost constant value around 85 % over a wide range of part load use. We also identified friction and cooling losses of the turbine as well as the overall heat transfer coefficients of the direct heat source to working fluid heat exchanger. An exergy analysis of the demonstrators revealed that exergy destruction in the heat transfer was very high, thus showing the need for good integration of an ORC with heat source and heat sink. Furthermore, the heat sink should be chosen at the lowest possible temperature to avoid exergy destruction.

Chapter 4 - Suitable Cycle Identification

Using the findings from chapters 2 and 3, a novel methodology and software tool was developed, capable of optimally integrating an Organic Rankine Cycle with any given heat source and heat sink. The study of literature on ORCs shows clearly that there is no single optimal solution of working fluid or cycle configuration to match the wide range of heat sources and sinks which are present in industry. Solutions must be tailor made for a given application. The methodology and tool that we developed addresses this by optimising simultaneously the cycle configuration, working parameters (such as pressure levels and temperatures) and the choice of the optimal working fluid. The result of an optimisation with the tool is a set of Pareto optimal solutions regarding two objective functions: (1) the maximisation of the electrical power, generated by the ORC and (2) the minimisation of the specific investment cost.

The tool is organised in a master multi objective optimisation and slave (single objective) mixed integer linear programming (MILP) optimisation. Thermodynamic and economic models are used in order to determine the characteristics of the generated solutions. A large database of working fluids is tested within the MILP problem (instead of the master optimisation), which allows to quickly find an optimal solution and to reduce the number of integer variables of the master optimisation. The used set of four decision variables for a single cycle and three more for every additional cycle was shown to be effective for finding adapted cycle configurations.

Combining a single objective MILP solver with a non-linear multi objective optimisation has been revealed to be problematic in two aspects: first, the choice of the objective function in the MILP optimisation influences the overall convergence of the Pareto optimal solutions; second, non-linearities and discontinuities in the objective functions (or their components) of the multi objective optimisation can be higher than the difference between two solutions in the linearised objective function of the MILP problem. We address the first issue by running the optimisation once for every objective function of the multi objective optimisation, with a corresponding objective function in the MILP problem. The second problem has been addressed by a novel approach of generating n -best solutions in the MILP solver, rather than only the optimal. These are re-evaluated after the MILP in a post calculation, which oftentimes changes their order. The constraint of $n = 10$ has been tested and found to be sufficient for single cycles, since in the optimisation showing the highest amount of non-linearities, the constraint has been activated in only 3 % of the generated solutions. It should be increased for cost optimisation with more than one cycle. For these cases, a value of $n = 15$ has been tested and validated. Without this method, the optimal solution would not have been found in up to 90 % of all cases, if cost minimisation is chosen as the MILP objective function.

Comparing the cost of the generated solutions originating from our methodology with values from literature and a commercially available system, the estimations are in the correct order of magnitude. In our tool, the cost of three types of equipment are estimated and used to

determine the specific investment cost. However, for very small units ($< 10\text{ kW}$), the costs are overestimated. This is on one hand due to the used cost functions, on the other hand due to the considered constant value for friction and cooling losses of the turbine and generator. For large installations we found cost to be rather optimistic, but within the order of magnitude of a commercially available ORC.

For ORCs above 10 kW , the share of the different equipments, regarding investment costs, was found to be in the range of 33 % to 72 % for the heat exchangers, 23 % to 58 % for the turbine and 1 % to 14 % for the pump. The heat exchangers have thus a lower share than the 90 % stated in some publications.

Main Contributions

In summary, a number of contributions were made in this work.

- We developed a novel definition of waste heat allowing to identify saving potential and available exergy potential of an industrial process.
- we developed a software tool which is able and suitable to integrate Organic Rankine Cycles into any waste heat source in an optimised manner,
 - considering different cycle configurations,
 - considering a large database of working fluids,
 - calibrated with practical experiences from two ORC demonstrators and several studies,
 - calibrated with reconciled unit parameters of the ORC demonstrators,
 - validated by application to two sources and analysis of different aspects.
- we identified the problems of combining a multi objective master optimisation and a single objective MILP slave optimisation and addressed them by
 - solving the MILP problem once for each objective of the master problem,
 - introducing a novel methodology of using n -best solutions of the MILP problem and re-evaluating them with the non-linear objective functions of the master problem.
- we developed a novel methodology for enhanced data reconciliation capable of increasing the a posteriori accuracy of the reconciled values of a steady state set of measurements.

5.2 Perspectives

Waste Cold

An interesting field to further explore is the quantification and use of cold as an exergy source or heat sink of heat at temperatures below the ambient. If heat sinks, under ambient temperature, exist in a process, they could be used to increase the efficiency of an ORC. However, a more common case remains the need for cooling within a process. Since combustibles are often relatively cheap compared to electricity, the proper reuse of cold within the process should be studied carefully. Additionally, the use of residual heat in order to run cooling technologies, in the form of tri-thermal systems, such as a mechanically coupled ORC and heat pump combinations or thermally driven heat pumps (such as absorption or adsorption heat pumps), could be economically interesting.

Enhanced Data Reconciliation

It would be interesting to mathematically prove or numerically demonstrate the equality of equation 3.2 and equation 3.5 for t towards infinity:

Quod esset demonstrandum:

$$\lim_{t \rightarrow \infty} \min_{y_t, x_t, y_{\pi, t}} \sum_i \frac{(y_{i,t} - \hat{y}_{i,t, \text{en}})^2}{\sigma_{i,t}^2} = \min_{y_t, x_t, \pi} \sum_t \sum_i \frac{(y_{i,t} - \hat{y}_{i,t, \text{trad}})^2}{\sigma_i^2} \quad (5.1)$$

Where the index en stands for enhanced reconciliation and trad for the traditional reconciliation. For the numerical demonstration, a long set of stationary data would be ideal. This would allow to complete the development given in chapter 2.

A clear comparison with the *Kalman filter* should be done. Enhanced Data Reconciliation has many similarities with the Kalman filter and an analytical comparison could be used to point out the similarities.

Cycle Identification

Mixtures: The next step in further developing the proposed tool, would be to add a module able to calculate mixtures of pure fluids from the REFPROP database, additionally to the predefined ones. This would allow to design custom mixtures using the most adapted slope for heat recovery from a given source and the analysis of Kalina cycles. This way the mixture composition could be introduced as decision variables in the multi objective optimisation.

Several possible ways are imaginable in order to achieve this. The way most coherent with the existing tool would be to add a single variable describing the mixing ratio between two fluids. With this mixing ratio variable, binary mixtures of pairs of all fluids could be introduced

Chapter 5. Conclusion

and tested in the thermodynamic and economic models and put to test in the MILP solver at the same time as all other cycles. This would be elegant, since only one additional decision variable would be needed and a large number of cycles could be added. The disadvantage could be the time to solve the MILP problem, which would increase due to the higher number of integer variables (number of cycles) in the MILP problem. Another way would be to assign a number to each fluid or fluid couples and introduce these as decision variables as well as the variable for the mixing ratio. The advantage would be the decreased solving time of the MILP solver. However, the solution of the multi objective optimisation could show difficulties, since the choice of fluids by the multi objective optimiser works best if a logical link between the different values of a variable exists. The introduction of mixtures, apart from being a programming task, is mainly a thermodynamic challenge. The mixtures predefined in the database are described by empirically defined mixing rules. For non predefined mixtures, REFPROP estimates these mixing rules, potentially introducing inaccuracies in the same order of magnitude as the difference between generated solutions.

Cost Function Refinement: As we have shown above, the cost functions for only three types of equipment lead to a correct order of magnitude for the total module cost estimate. However, it is possible to refine this estimate. The heat exchangers could be conceptually separated into different types using the respective surfaces, for example a plate heat exchanger for the condensation, instead of assuming the same type everywhere. Additionally, a decision variable for the minimum temperature difference in each heat exchanger could be introduced. A better cost model for the finned tube heat exchanger could be developed and a clear cost function for the generator could be introduced and the turbine cost function adapted. An additional point is the influence of volume on the equipment cost, which is especially relevant for working fluids at low pressures. An analysis of the influence on the cost could help refine the methodology.

Turbine and Generator Losses Function: Arguably, $\dot{L}_{\text{turbogen}}$ is a function related to the installed capacity rather than a constant value. It would be interesting to investigate such a function, which will probably depend on the surface of the machine, since cooling and friction losses depend on the surface of the turbine and generator. The surface is in return a function of the volume, which depends on the installed capacity. However, thorough analyses need to be conducted in order to obtain realistic results.

Uncertainties

Uncertainties could be considered at several levels of the tool, to make a better choice for a cycle.

Fuel Cost: With an uncertain development of costs for combustibles, it would be interesting to analyse how different price developments could influence the economics of an investment into energy efficiency measures within an industrial process. This influences the amount of available waste heat and thus the recovery of heat for electricity generation.

Electricity Price: The electricity price development massively influences the payback of an investment into waste heat recovery. If the price rises, the profitability will get better over time, but the last years have shown that electricity prices for industry did not develop in this direction.

Yearly operating time: The operating time of an industrial process depends on several factors, for example the maintenance intervals etc, but it mostly depends on the demand for the produced good(s). The development of the demand can fluctuate and thus the operating time could vary, thus influencing the produced amount of electricity by an ORC using waste heat.

Part Load Use

Related to the production (and thus the operating time) and to the type of process, an ORC could be used in part load. For some processes, the recoverable heat load is known in advance and the behaviour of an ORC in part load operation could be simulated. On the side of the ORC, the isentropic efficiency changes in part load operation, even though the LOVE project has shown that the changes are relatively small for a large range of operation modes. Other effects of a part load use concern the heat transfers, for example. The surface of the heat exchangers is designed for nominal load and oversized for part load, thus making smaller temperature gradients in the heat exchangers possible. If the part load hours are unknown, an uncertainty analysis could be carried out. All these factors influence the payback of an investment and a further development of the tool in this regard would be interesting.

A Working Fluids

The list of working fluids is given in tables A.1 to A.7, where T_C is the critical temperature, p_C the critical pressure and T_B the normal boiling temperature. The data for these tables were taken from: Lemmon et al. (2010); Calm (2008); Calm and Hourahan (2007); United Nations Environmental Programm (2014); U.S. Environmental Protection Agency (2014c); European Parliament and Council of the European Union (2014); Forster et al. (2013); U.S. Environmental Protection Agency (2014b); United Nations Framework Convention on Climate Change (2014); Facão and Oliveira (2009); U.S. Environmental Protection Agency (2010); Tejon Carbajal (2009); U.S. Environmental Protection Agency (2014a) and Bundesamt für Umwelt (2014). The fluids which are already under control due to the Montreal Protocol (United Nations Environmental Programm, 2014) are listed in bold. Also in bold and with an asterisk (*) are substances which are excluded due to their special character (highly toxic, radioactive or for thermodynamic reasons (critical temperature below $-100\text{ }^{\circ}\text{C}$)). In table A.6 and A.7 all the mixtures are shown, again the bold ones are those already under control of the Montreal Protocol and thus excluded from the possible choices. R508A and B, R510A and R416A were also excluded due to convergence problems of REFPROP. It must also be noted that following decisions made after the Kyoto Protoco (United Nations Framework Convention on Climate Change, 1997) and in an effort to reduce the climate gas emissions throughout the EU and Switzerland, many other fluids will be unavailable or their acquisition or use will be possible only under certain conditions. These vary in the different legal frameworks (Bundesamt für Umwelt, 2014; European Parliament and Council of the European Union, 2014) and over time. We will try to address that by limiting the choice to working fluids with a GWP smaller than 3000.

Table A.1: Pure Fluids from REFPROP Data Base Part I.

	T_c in °C	p_c in MPa	T_b in °C	GWP (100)	ODP	Atm. Lifetime
Acetone	235.0	4.7	56.1	0.5		
Ammonia	132.3	11.3	-33.3	0.9	0.0	0.0
Argon*	-122.5	4.9	-185.8	0.0	0.0	0.0
Benzene	288.9	4.9	80.1			
Butane	152.0	3.8	-0.5	20.0	0.0	0.0
Butene	146.1	4.0	-6.3			
Carbonyl Sulfide*	105.6	6.4	-50.2			
Cis-Butene	162.6	4.2	3.7			
CO*	-140.3	3.5	-191.5			
CO2	31.0	7.4	-78.5	1.0	0.0	50.0
Cyclohexane	280.5	4.1	80.7			
Cyclopentane	238.5	4.5	49.3	3.0		
Cyclopropane	125.2	5.6	-31.5		0.0	0.4
Decamethylcyclopentasiloxane (D5)	346.0	1.2	210.9			
Decamethyltetrasiloxane (MDM2)	326.3	1.2	194.4			
Decane	344.6	2.1	174.1			
Deuterium*						
Dimethyl Carbonate	284.2	4.8	90.0			
Dimethylether (DME)	127.2	5.3	-24.8	1.0	0.0	0.0
Dodecamethylcyclohexasiloxane (D6)	372.6	1.0	245.0			
Dodecamethylpentasiloxane (MD3M)	355.2	0.9	229.9			

Table A.2: Pure Fluids from REPPROP Data Base Part II.

	T_C in °C	p_C in MPa	T_B in °C	GWP (100)	ODP	Atm. Lifetime
Dodecane	385.0	1.8	216.2			
Ethane	32.2	4.9	-88.6	20.0	0.0	0.2
Ethanol	240.8	6.2	78.2			
Ethylene	9.2	5.0	-103.8		0.0	0.0
Fluorine*	-128.7	5.2	-188.1			
H2S*	100.0	9.0	-60.3			
Heavy Water*						
Helium*	-268.0	0.2	-268.9		0.0	
Heptane	267.0	2.7	98.4	3.0	0.0	
Hexamethyldisiloxane (MM)	245.6	1.9	100.3			
Hexane	234.7	3.0	68.7	3.0	0.0	
Hydrogen*	-240.0	1.3	-252.9		0.0	
Isobutan	134.7	3.6	-11.7	20.0	0.0	0.0
Isobutene	144.9	4.0	-7.0			
Isohexane	224.6	3.0	60.2			
Isopentane	187.2	3.4	27.8	20.0	0.0	0.0
Krypton	-63.7	5.5	-153.4		0.0	
Methane	-82.6	4.6	-161.5	25.0	0.0	12.0
Methanol	239.5	8.1	64.5			
Methyl Palmitate	481.9	1.4	329.2			
Methyl Stearate	501.9	1.2	356.4			
Methylcyclohexane	299.1	3.5	100.9			
Mlinolea	525.9	1.3	355.7			

Table A.3: Pure Fluids from REFPROP Data Base Part III.

	T_C in °C	p_C in MPa	T_B in °C	GWP (100)	ODP	Atm. Lifetime
Mlinolen	498.9	1.4	356.0			
Moleate	508.9	1.3	354.0			
N2O	36.4	7.3	-88.5	300.0		
Neon*	-228.7	2.7	246.1			
Neopentane	160.6	3.2	9.5			
Nitrogen*	-147.0	3.4	-195.8			
Nitrogen trifluoride	-39.2	4.5	-129.0	10970.0		740.0
Nonane	321.4	2.3	150.8			
Octamethylcyclotetrasiloxane (D4)	313.4	1.3	175.4			
Octamethyltrisiloxane (MDM)	290.9	1.4	152.5			
Octane	296.2	2.5	125.6			
Oxygen*	-118.6	5.0	-183.0			
Parahydrogen*	-240.2	1.3	-252.9			
Pentane	196.6	3.4	36.1	20.0	0.0	0.0
Perfluorobutane	113.2	2.3	-2.1	2600.0		8710.0
Perfluoropentane	147.4	2.1	29.8	4100.0		9010.0
Propane	96.7	4.3	-42.1	20.0	0.0	0.0
Propylcyclohexane	357.7	2.9	156.8			
Propylen	92.4	4.7	-47.7	20.0	0.0	0.0
Propyne	129.2	5.6	-25.2			
R11	198.0	4.4	23.7	4750.0	1.0	45.0
R113	214.1	3.4	47.6	6130.0	1.0	85.0

Table A.4: Pure Fluids from REFPROP Data Base Part IV.

	T_C in °C	p_C in MPa	T_B in °C	GWP (100)	ODP	Atm. Lifetime
R114	145.7	3.3	3.6	10040.0	1.0	300.0
R115	80.0	3.1	-38.9	7370.0	0.4	1700.0
R116	19.9	3.1	-78.1	10000.0	0.0	12200.0
R12	112.0	4.1	-29.8	10890.0	1.0	100.0
R123	183.7	3.7	27.8	77.0	0.0	1.3
R1234yf	94.7	3.4	-29.5	4.0		
R1234ze	109.4	3.6	-19.0	6.0		
R124	122.3	3.6	-12.0	609.0	0.0	5.8
R125	66.0	3.6	-48.1	3500.0	0.0	29.0
R13	28.9	3.9	-81.5	14420.0	1.0	640.0
R134a	101.1	4.1	-26.1	1430.0	0.0	14.0
R14	-45.6	3.8	-128.0	7390.0	0.0	50000.0
R141b	204.4	4.2	32.0	725.0	0.1	9.3
R142b	137.1	4.1	-9.1	2310.0	0.1	17.9
R143a	72.7	3.8	-47.2	4470.0	0.0	52.0
R152a	113.3	4.5	-24.0	124.0	0.0	1.4
R161	102.2	5.1	-37.6	12.0	0.0	0.2
R21	178.3	5.2	8.9	1.7	0.0	151.0
R218	71.9	2.6	-36.8	8830.0	0.0	2600.0

Table A.5: Pure Fluids from REEPROP Data Base Part V.

	T_C in °C	p_C in MPa	T_B in °C	GWP (100)	ODP	Atm. Lifetime
R22	96.1	5.0	-40.8	1810.0	0.1	12.0
R227ea	102.8	3.0	-16.4	3220.0	0.0	42.0
R23	26.1	4.8	-82.0	14760.0	0.0	270.0
R236ea	139.3	3.5	6.2	1350.0		10.7
R236fa	124.9	3.2	-1.4	9810.0	0.0	240.0
R245ca	174.4	3.9	25.1	693.0	0.0	6.2
R245fa	154.0	3.7	15.1	1030.0	0.0	7.6
R32	78.1	5.8	-51.7	675.0	0.0	4.9
R365mfc	186.9	3.3	40.2	782.0		8.6
R41	44.1	5.9	-78.3	92.0	0.0	2.4
RC318	115.2	2.8	-6.0	10250.0	0.0	3200.0
SF6 (Sulfur Hexafluoride)	45.6	3.8	-68.3	397.0		2.0
SO2	157.5	7.9	-10.0	300.0	0.0	
Tetradecamethylhexasiloxane (MD4M)	380.1	0.9	260.8			
Toluene	318.6	4.1	110.6			
Trans-Butene	155.5	4.0	0.9			
Trifluoroiodomethane	123.3	4.0	-21.9	1.0	0.0	0.0
Water	373.9	22.1	100.0	0.9	0.0	
Xenon	16.6	5.8	-108.1			

Table A.6: Mixtures from REFPROP Data Base Part I.

	Components	GWP (100)	ODP
Air*	N2, O2, Argon		
Amarillo*	Natural Gas		
Ekofisk*	Natural Gas		
Gulf Coast Gas*	Natural Gas		
High Co2 And Nitrogen Gas*	Natural Gas		
High Nitrogen Gas*	Natural Gas		
R401a	R22, R152a, R125	1200.0	0.0
R401b	R22, R152a, R124	1300.0	0.0
R401c	R22, R152a, R124	930.0	0.0
R402a	R125, Propane, R22	2800.0	0.0
R402b	R125, Propane, R22	2400.0	0.0
R403a	Propane, R22, R218	3100.0	0.0
R403b	Propane, R22, R218	4500.0	0.0
R404a	R125, R134a, R143a	3900.0	0.0
R405a	R22, R152a, R142b, RC318	5300.0	0.0
R406a	R22, Isobutane, R142b	1900.0	0.1
R407a	R32, R125, R134a	2100.0	0.0
R407b	R32, R125, R134a	2800.0	0.0
R407c	R32, R125, R134a	1800.0	0.0
R407d	R32, R125, R134a	1600.0	0.0
R407e	R32, R125, R134a	1600.0	0.0
R408a	R125, R143a, R22	3200.0	0.0
R409a	R22, R125, R142b	1600.0	0.0
R409b	R22, R124, R142b	1600.0	0.0
R410a	R32, R125	2100.0	0.0
R410b	R32, R125	2200.0	0.0
R411a	Propylen, R22, R152a	1600.0	0.0
R411b	Propylen, R22, R152a	1700.0	0.0
R412a	R22, R218, R142b	2300.0	0.1
R413a	R218, R134a, Isobutane	2100.0	0.0
R414a	R22, R124, Isobutane, R142b	1500.0	0.0
R414b	R22, R124, Isobutane, R142b	1400.0	0.0
R415a	R22, R152a	1500.0	0.0
R415b	R22, R152a	550.0	0.0
R416a	R134a, R124, Butane	1100.0	0.0
R417a	R125, R134a, Butane	2300.0	0.0

Appendix A. Working Fluids

Table A.7: Mixtures from REFPROP Data Base Part II.

	Components	GWP (100)	ODP
R418a	Propane, R22, R152a	1700.0	0.0
R419a	R125, R134a, DME	3000.0	0.0
R420a	R134a, R142b	1500.0	0.0
R421a	R125, R134a	2600.0	0.0
R421b	R125, R134a	3200.0	0.0
R422a	R125, R134a, Isobutane	3100.0	0.0
R422b	R125, R134a, Isobutane	2500.0	0.0
R422c	R125, R134a, Isobutane	3100.0	0.0
R422d	R125, R134a, Isobutane	2700.0	0.0
R423a	R134a, R227ea	2300.0	0.0
R424a	R125, R134a, Isobutane, Butane, Isopentane	2400.0	0.0
R425a	R32, R134a, R227ea	1500.0	0.0
R426a	R125, R134a, Butane, Isopentane	1500.0	0.0
R427a	R32, R125, R134a, R143a	2100.0	0.0
R428a	R125, R143a, Propane, Isobutane	3600.0	0.0
R429a	R152a, DME, Isobutane	13.9	0.0
R430a	R152a, Isobutane	95.0	0.0
R431a	R152a, Propane	38.3	0.0
R432a	Propylen, DME	1.6	0.0
R433a	Propylen, Propane	0.0	
R434a	R125, R134a, R143a, Isobutane	3245.0	0.0
R435a	R152a, DME	25.6	0.0
R436a	Propane, Isobutane	0.0	
R436b	Propane, Isobutane	0.0	
R437a	R125, R134a, Butane, Pentane	1805.0	
R438a	R32, R125, R134a, Butane, Isopentane	2265.0	0.0
R500	R12, R152a	8100.0	0.7
R501	R12, R22	4100.0	0.3
R502	R22, R115	4700.0	0.3
R503	R13, R23	15000.0	0.6
R504	R32, R115	4100.0	0.2
R507a	R125, R143a	4000.0	0.0
R508a	R23, R116	13000.0	0.0
R508b	R23, R116	13000.0	0.0
R509a	R22, R218	5700.0	0.0
R510a	DME, Isobutane		

B Streams of Cement Model

Below a table showing the heating and cooling requirements in our model for the representative cement production process. All values are for a clinker production mass flow rate of $27.9009 \frac{\text{kg}}{\text{s}}$.

Unit	Name	T_{in} °C	T_{out} °C	$\Delta T_{\text{min}}/2$ K	Load kW
Raw Mill	in	25.150	55.927	10.000	1254.830
Raw Mill	a	55.927	85.256	10.000	1254.830
Raw Mill	b	85.256	100.144	10.000	1254.830
Raw Mill	c	100.144	100.144	10.000	1254.830
Raw Mill	d	100.144	104.000	10.000	1254.830
Raw Mill	qla	25.150	104.000	10.000	113.216
Raw Mill	gas_sp	389.994	104.000	10.000	2477.260
Raw Mill	dust	389.994	104.000	10.000	2652.400
Suspension Pre-Heaters	cy8g	560.150	390.150	61.108	9017.620
Suspension Pre-Heaters	cy2g	700.150	560.150	61.591	7806.610
Suspension Pre-Heaters	cy3g	860.150	700.150	37.075	9297.370
Suspension Pre-Heaters	cy4g	880.150	860.150	5.000	1200.402
Suspension Pre-Heaters_p	cy1s	50.150	267.934	61.108	9017.620
Suspension Pre-Heaters_p	cy2s	267.934	436.968	61.591	7806.610
Suspension Pre-Heaters_p	cy3s	436.968	626.000	37.075	9297.370
Suspension Pre-Heaters_p	cy4s	850.150	850.151	5.000	1200.402
Calcination	hg_b	850.150	890.150	15.000	540.508
Calcination	comb	1100.150	1100.149	15.000	45208.200
Calcination	hg_a	1100.150	890.150	15.000	11358.100
Calcination_p	hs_a	626.000	850.150	15.000	11513.700
Calcination_p	ca_zone	850.150	850.151	15.000	39975.300
Calcination_p	hs_b	850.150	860.150	15.000	348.131
Kiln	comb_Kiln	2000.000	1999.999	100.000	605.630

Appendix B. Streams of Cement Model

Kiln	b_a	2000.000	1821.650	100.000	3124.290
Kiln	b_b	1821.650	1718.510	100.000	1953.840
Kiln	b_c	1718.510	1531.470	100.000	3881.810
Kiln	b_d	1531.470	1504.330	100.000	338.210
Kiln	b_e	1504.330	1222.430	100.000	5864.050
Kiln	b_f	1222.430	1177.160	100.000	894.941
Kiln	b_g	1177.160	1050.000	100.000	2709.880
Kiln	PrimaryFuel	25.150	60.150	50.000	25.882
Kiln	PrimaryAir	25.150	40.150	20.000	61.982
Kiln_p	c1_reac	850.150	850.151	100.000	1211.920
Kiln_p	c1_heat	850.150	900.000	100.000	1651.320
Kiln_p	c2_reac	900.000	900.001	100.000	595.844
Kiln_p	c2_heat	900.000	910.000	100.000	323.840
Kiln_p	c3_reac	910.000	910.001	100.000	2401.180
Kiln_p	c3_heat	910.000	1027.000	100.000	3609.030
Kiln_p	c4_reac	1027.000	1026.999	100.000	5525.060
Kiln_p	c4_heat	1027.000	1227.000	100.000	5948.130
Kiln_p	c5_reac	1227.000	1227.001	100.000	920.566
Kiln_p	c5_heat	1227.000	1327.000	100.000	2961.240
Kiln_p	c6_reac	1327.000	1327.001	100.000	445.109
Kiln_p	c6_heat	1327.000	1377.000	100.000	1508.730
Kiln_p	c7_reac	1377.000	1377.001	100.000	842.819
Kiln_p	c7_heat	1377.000	1450.150	100.000	2281.470
Kiln_p	c8_reac	1450.150	1450.151	100.000	605.630
Kiln_p	CO2_4	1227.000	1027.000	100.000	84.867
Kiln_p	CO2_3	1027.000	910.000	100.000	146.164
Kiln_p	CO2_2	910.000	900.000	100.000	24.742
Kiln_p	CO2_1	900.000	850.150	100.000	153.366
Kiln_p	CO2_0	850.150	850.000	100.000	0.612
Grate Clinker Cooler	st_air	25.150	1000.150	92.000	37.000
Grate Clinker Cooler	m_air_a	25.150	225.150	92.000	37.000
Grate Clinker Cooler	e_air_a	25.150	400.150	92.000	37.000
Grate Clinker Cooler_p	cl1	1450.150	650.000	92.000	37.000
Grate Clinker Cooler_p	cl2	650.000	250.000	92.000	37.000
Grate Clinker Cooler_p	cl3	250.000	100.150	92.000	37.000
Losses	gas_sp_l	389.994	104.000	10.000	1597.050
Losses	ql_fm	104.000	50.150	10.000	2115.110
Losses	cy1_l	560.150	390.150	61.108	1467.980
Losses	cy2_l	700.150	560.150	61.591	1166.510
Losses	cy3_l	860.150	700.150	37.075	1267.830
Losses	cy4_l	880.150	860.150	5.000	133.378
Losses	oscl	860.150	850.150	15.000	348.131

Losses	gasesandcd	890.150	880.150	15.000	668.473
Losses	l_comb_Kiln	2000.000	1999.999	100.000	566.006
Losses	l_b_a	2000.000	1821.650	100.000	953.274
Losses	l_b_b	1821.650	1718.510	100.000	387.267
Losses	l_b_c	1718.510	1531.470	100.000	327.688
Losses	l_b_d	1531.470	1504.330	100.000	268.108
Losses	l_b_e	1504.330	1222.430	100.000	357.478
Losses	l_b_f	1222.430	1177.160	100.000	89.369
Losses	l_b_g	1177.160	1050.000	100.000	29.790
Losses	ql_c_l	1450.150	650.000	92.000	37.000
Losses	ql_b_l	650.000	250.000	92.000	37.000
Losses	ql_a_l	250.000	100.150	92.000	37.000
Losses	qlo_l	1000.150	1000.149	92.000	37.000
Losses	dust_cool	104.000	45.150	20.000	9.494
Vented	cl4	225.150	35.150	0.100	1597.670
Vented	cl5	400.150	35.150	0.100	3125.710
Vented	gde	103.607	35.150	0.100	1300.410
Vented	utile	150.150	35.150	0.100	3613.170
Vented	ctwatercool	389.993	150.150	0.100	8202.130
Vented	hot_air_cmill	115.150	35.150	0.100	1287.460

C Economic Estimation of Electricity Generation Cost

To give an order of magnitude of the cost per unit of electricity produced C_{gen} , we will make a simple estimation. Starting from the specific investment cost $C_{\text{TM,spec}}$ [USD /kW_{el}] and assuming 2 % of these specific investment cost as operating cost per year, the cost of a kWh of electricity is estimated. The influencing factors are the yearly operating time t_{op} [h/year] and the payback or depreciation period t_{pb} [year]. Equation C.1 shows how C_{gen} [USD /kWh] is calculated:

$$C_{\text{gen}} = \frac{C_{\text{TM,spec}} + 0.02 \cdot C_{\text{TM,spec}} \cdot t_{\text{pb}}}{t_{\text{op}} \cdot 1 \text{ kWh /h} \cdot t_{\text{pb}}} \quad (\text{C.1})$$

This estimation supposes a constant value of money over time. We see that the payback periods of below 5 years, which are common in industry, need low investment cost and high yearly operating time, in order to be a grid parity (tables C.1 to C.3). However, if the cost are calculated over a lifetime of ten or 15 years as a utility company might do it, even with fewer yearly operating hours and higher investment cost. This shows that partnerships between industry and utility companies might be the way to proceed, to make investments into ORCs using waste heat viable.

Appendix C. Economic Estimation of Electricity Generation Cost

Table C.1: Cost per kWh of electricity C_{gen} in USD /kWh, for $t_{\text{pb}} = 5$ years, as a function of t_{op} and $C_{\text{TM,spec}}$.

$t_{\text{op}}:$	2000	3000	4000	5000	6000	7000	8000
	h/year	h/year	h/year	h/year	h/year	h/year	h/year
$C_{\text{TM,spec}}:$							
500 USD/kW	0.06	0.04	0.03	0.02	0.02	0.02	0.01
1000 USD/kW	0.11	0.07	0.06	0.04	0.04	0.03	0.03
1500 USD/kW	0.17	0.11	0.08	0.07	0.06	0.05	0.04
2000 USD/kW	0.22	0.15	0.11	0.09	0.07	0.06	0.06
2500 USD/kW	0.28	0.18	0.14	0.11	0.09	0.08	0.07
3000 USD/kW	0.33	0.22	0.17	0.13	0.11	0.09	0.08
3500 USD/kW	0.39	0.26	0.19	0.15	0.13	0.11	0.10
4000 USD/kW	0.44	0.29	0.22	0.18	0.15	0.13	0.11
4500 USD/kW	0.50	0.33	0.25	0.20	0.17	0.14	0.12
5000 USD/kW	0.55	0.37	0.28	0.22	0.18	0.16	0.14

Table C.2: Cost per kWh of electricity C_{gen} in USD /kWh, for $t_{\text{pb}} = 10$ years, as a function of t_{op} and $C_{\text{TM,spec}}$.

$t_{\text{op}}:$	2000	3000	4000	5000	6000	7000	8000
	h/year	h/year	h/year	h/year	h/year	h/year	h/year
$C_{\text{TM,spec}}:$							
500 USD/kW	0.03	0.02	0.015	0.012	0.01	0.0085714	0.0075
1000 USD/kW	0.06	0.04	0.03	0.024	0.02	0.0171429	0.015
1500 USD/kW	0.09	0.06	0.045	0.036	0.03	0.0257143	0.0225
2000 USD/kW	0.12	0.08	0.06	0.048	0.04	0.0342857	0.03
2500 USD/kW	0.15	0.1	0.075	0.06	0.05	0.0428571	0.0375
3000 USD/kW	0.18	0.12	0.09	0.072	0.06	0.0514286	0.045
3500 USD/kW	0.21	0.14	0.105	0.084	0.07	0.06	0.0525
4000 USD/kW	0.24	0.16	0.12	0.096	0.08	0.0685714	0.06
4500 USD/kW	0.27	0.18	0.135	0.108	0.09	0.0771429	0.0675
5000 USD/kW	0.3	0.2	0.15	0.12	0.1	0.0857143	0.075

Table C.3: Cost per kWh of electricity C_{gen} in USD /kWh, for $t_{\text{pb}} = 15$ years, as a function of t_{op} and $C_{\text{TM,spec}}$.

$t_{\text{op}}:$	2000	3000	4000	5000	6000	7000	8000
	h/year	h/year	h/year	h/year	h/year	h/year	h/year
$C_{\text{TM,spec}}:$							
500 USD/kW	0.02	0.01	0.01	0.01	0.01	0.01	0.01
1000 USD/kW	0.04	0.03	0.02	0.02	0.01	0.01	0.01
1500 USD/kW	0.07	0.04	0.03	0.03	0.02	0.02	0.02
2000 USD/kW	0.09	0.06	0.04	0.03	0.03	0.02	0.02
2500 USD/kW	0.11	0.07	0.05	0.04	0.04	0.03	0.03
3000 USD/kW	0.13	0.09	0.07	0.05	0.04	0.04	0.03
3500 USD/kW	0.15	0.10	0.08	0.06	0.05	0.04	0.04
4000 USD/kW	0.17	0.12	0.09	0.07	0.06	0.05	0.04
4500 USD/kW	0.20	0.13	0.10	0.08	0.07	0.06	0.05
5000 USD/kW	0.22	0.14	0.11	0.09	0.07	0.06	0.05

Bibliography

- Adams, B. M., Hart, W. E., Eldred, M. S., Dunlavy, D. M., Hough, P. D., Giunta, A. A., Griffin, J. D., Martinez-Canales, M. L., Watson, J.-P., Kolda, T. G., and others (2006). *DAKOTA, a Multilevel Parallel Object-oriented Framework for Design Optimization, Parameter Estimation, Uncertainty Quantification, and Sensitivity Analysis: Version 4.0 Users's Manual*. United States. Department of Energy.
- Aljundi, I. H. (2011). Effect of dry hydrocarbons and critical point temperature on the efficiencies of organic rankine cycle. *Renewable Energy*, 36(4):1196–1202.
- Ammar, Y., Joyce, S., Norman, R., Wang, Y., and Roskilly, A. P. (2012). Low grade thermal energy sources and uses from the process industry in the UK. *Applied Energy*, 89(1):3–20.
- Angelino, G. and Colonna di Paliano, P. (1998). Multicomponent working fluids for organic rankine cycles (ORCs). *Energy*, 23(6):449–463.
- Aspelund, A., Berstad, D. O., and Gundersen, T. (2007). An extended pinch analysis and design procedure utilizing pressure based exergy for subambient cooling. *Applied Thermal Engineering*, 27(16):2633–2649.
- Badr, O., O'Callaghan, P. W., and Probert, S. D. (1990). Rankine-cycle systems for harnessing power from low-grade energy sources. *Applied Energy*, 36(4):263–292.
- Becker, H., Vuillermoz, A., and Maréchal, F. (2012). Heat pump integration in a cheese factory. *Applied Thermal Engineering*, 43:118–127.
- Belsim (2011). *VALI 4: User Guide*. Rue Georges Berotte 29A, B-4470 Saint-Georges-sur-Meuse, Belgium.
- Benali, T., Tondeur, D., and Jaubert, J. N. (2012). An improved crude oil atmospheric distillation process for energy integration: Part i: Energy and exergy analyses of the process when a flash is installed in the preheating train. *Applied Thermal Engineering*, 32:125–131.
- Bendig, M., Maréchal, F., and Favrat, D. (2012). Defining the potential of usable waste heat in industrial processes with the help of pinch and exergy analysis. *Chemical Engineering Transactions*, 29:103–108.

Bibliography

- Bendig, M., Maréchal, F., and Favrat, D. (2013). Defining “waste heat” for industrial processes. *Applied Thermal Engineering*, 61(1):134–142.
- Bendig, M., Mian, A., and Maréchal, F. (2014a). Pinch-analysis and integration of the cement process, considering the integration of orcs. *Proceedings of the 27 th international conference on Efficiency, Cost, Optimization, Simulation and environmental impact of energy systems*.
- Bendig, M., Roessler, G., and Maréchal, F. (2014b). Enhanced data reconciliation. *Proceedings of the 27 th international conference on Efficiency, Cost, Optimization, Simulation and environmental impact of energy systems*.
- Bolliger, R. (2010). *Méthodologie de la synthèse des systèmes énergétiques industriels*. PhD thesis, EPFL, Lausanne, Switzerland.
- Bolliger, R., Palazzi, F., and Maréchal, F. (2007). Heat exchanger network (HEN) costs and performances estimation for multi-period operation. *Computer Aided Chemical Engineering*, 24.
- Borel, L. and Favrat, D. (2010). *Thermodynamics and Energy Systems Analysis: From Energy to Exergy*. EPFL Press.
- Borsukiewicz-Gozdur, A. and Nowak, W. (2007). Comparative analysis of natural and synthetic refrigerants in application to low temperature clausius–rankine cycle. *Energy*, 32(4):344–352.
- Brown, D., Maréchal, F., and Paris, J. (2005). A dual representation for targeting process retrofit, application to a pulp and paper process. *Applied Thermal Engineering*, 25(7):1067–1082.
- Bundesamt für Umwelt (2014). Kältemittel - rechtliche Grundlagen.
- Calm, J. and Hourahan, G. (2007). Refrigerant data update. *HPAC Heating, Piping, AirConditioning Engineering*, 79(1):50–52+63–64.
- Calm, J. M. (2008). The next generation of refrigerants – historical review, considerations, and outlook. *International Journal of Refrigeration*, 31(7):1123–1133.
- CENTRE, J. R. and Bureau, E. I. (2013). *Best Available Techniques (BAT) Reference Document for the Production of Cement, Lime and Magnesium Oxide*.
- Chammas, R. E. and Clodic, D. (2005). Combined cycle for hybrid vehicles. SAE Technical Paper 2005-01-1171, SAE International, Warrendale, PA.
- Chemical Engineering (2013). Chemical engineering. 10. 2013.
- Chen, H., Goswami, D. Y., Rahman, M. M., and Stefanakos, E. K. (2011). A supercritical rankine cycle using zeotropic mixture working fluids for the conversion of low-grade heat into power. *Energy*, 36(1):549–555.

- Chen, Y., Lundqvist, P., Johansson, A., and Platell, P. (2006). A comparative study of the carbon dioxide transcritical power cycle compared with an organic rankine cycle with r123 as working fluid in waste heat recovery. *Applied Thermal Engineering*, 26(17–18):2142–2147.
- Crowe, C. M. (1996). Data reconciliation — progress and challenges. *Journal of Process Control*, 6(2–3):89–98.
- Cziesla, F., Tsatsaronis, G., and Gao, Z. (2006). Avoidable thermodynamic inefficiencies and costs in an externally fired combined cycle power plant. *Energy*, 31(10–11):1472–1489.
- Dai, Y., Wang, J., and Gao, L. (2009). Parametric optimization and comparative study of organic rankine cycle (ORC) for low grade waste heat recovery. *Energy Conversion and Management*, 50(3):576–582.
- Desai, N. B. and Bandyopadhyay, S. (2009). Process integration of organic rankine cycle. *Energy*, 34(10):1674–1686.
- DiPippo, R. (2004). Second law assessment of binary plants generating power from low-temperature geothermal fluids. *Geothermics*, 33(5):565–586.
- Drescher, U. and Brüggemann, D. (2007). Fluid selection for the organic rankine cycle (ORC) in biomass power and heat plants. *Applied Thermal Engineering*, 27(1):223–228.
- Eddy, J. and Lewis, K. (2001). Effective generation of pareto sets using genetic programming. In *Proceedings of ASME Design Engineering Technical Conference*.
- Energetics and US DOE (2004). *Energy Use Loss and Opportunities Analysis: U.S. Manufacturing & Mining*. USA.
- Engin, T. and Ari, V. (2005). Energy auditing and recovery for dry type cement rotary kiln systems—a case study. *Energy Conversion and Management*, 46(4):551–562.
- European Energy Agency (2014). www.eea.europa.eu/data-and-maps/figures/co2-emissions-per-kwh-of-co2-kwh-iea-figure-3. Copenhagen, Denmark.
- European Parliament and Council of the European Union (2014). REGULATION (EU) no 517/2014 OF THE EUROPEAN PARLIAMENT AND OF THE COUNCIL of 16 april 2014 on fluorinated greenhouse gases and repealing regulation (EC) no 842/2006.
- European Union (2014). Eurostat - data explorer - electricity prices - appsso.eurostat.ec.europa.eu.
- Facão, J. and Oliveira, A. C. (2009). Analysis of energetic, design and operational criteria when choosing an adequate working fluid for small ORC systems. *ASME 2009 International Mechanical Engineering Congress & Exposition*, pages 13–19.
- Facão, J., Palmero-Marrero, A., and Oliveira, A. C. (2008). Analysis of a solar assisted micro-cogeneration ORC system. *International Journal of Low-Carbon Technologies*, 3(4):254–264.

Bibliography

- Forster, P., Ramaswamy, V., Artaxo, P., Bernsten, T., Betts, R., Fahey, D., Haywood, J., Lean, J., Lowe, D., Myhre, G., Nganga, J., Prinn, R., Raga, G., Schulz, M., and Van Dorland, R. (2013). *Changes in Atmospheric Constituents and in Radiative Forcing. In: Climate Change 2007: The Physical Science Basis. Contribution of Working Group I to the Fourth Assessment Report of the Intergovernmental Panel on Climate Change [Solomon, S., D. Qin, M. Manning, Z. Chen, M. Marquis, K.B. Averyt, M. Tignor and H.L. Miller (eds.)]*. Cambridge University Press, Cambridge, United Kingdom and New York, NY, USA.
- Fourer, R., Gay, D. M., and Kernighan, B. W. (1990). A modeling language for mathematical programming. *Management Science*, 36(5):519–554.
- Gassner, M. (2010). *Process Design Methodology for Thermochemical Production of Fuels from Biomass*. PhD thesis, EPFL, Lausanne, Switzerland.
- Gerber, L. (2012). *Integration of Life Cycle Assessment in the conceptual design of renewable energy conversion systems*. PhD thesis, EPFL, Lausanne, Switzerland.
- Gerber, L. and Maréchal, F. (2012). Defining optimal configurations of geothermal systems using process design and process integration techniques. *Applied Thermal Engineering*, 43:29–41.
- Goldstick, R. J. and Thumann, A. (1986). *Principles of Waste Heat Recovery*. Fairmont Press.
- Gu, W., Weng, Y., Wang, Y., and Zheng, B. (2009). Theoretical and experimental investigation of an organic rankine cycle for a waste heat recovery system. *Proceedings of the Institution of Mechanical Engineers, Part A: Journal of Power and Energy*, 223(5):523–533.
- Guthrie, K. (1969a). Capital cost estimating. *Chemical Engineering*, 76, no. 3:114.
- Guthrie, K. M. (1969b). Data and techniques for preliminary capital cost estimating. *Chemical Engineering*, pages pp.114–142.
- Guthrie, K. M. (1974). *Process Plant Estimating, Evaluation and Control*. Solana Beach, CA, USA.
- Hackl, R., Andersson, E., and Harvey, S. (2011). Targeting for energy efficiency and improved energy collaboration between different companies using total site analysis (TSA). *Energy*, 36(8):4609–4615.
- Hackl, R., Harvey, S., and Andersson, E. (2010). Total site analysis (TSA) stenuungsund.
- Heberle, F. and Brüggemann, D. (2010). Exergy based fluid selection for a geothermal organic rankine cycle for combined heat and power generation. *Applied Thermal Engineering*, 30(11–12):1326–1332.
- Heberle, F., Preißinger, M., and Brüggemann, D. (2012). Zeotropic mixtures as working fluids in organic rankine cycles for low-enthalpy geothermal resources. *Renewable Energy*, 37(1):364–370.

- Herzog, U., Lamare, T., Tognoni, A., Piazzesi, G., and Ksayer, E. B. (2014). Demonstration of low temperature ($< 120\text{ }^{\circ}\text{C}$) waste heat recovery for electricity generation by means of organic rankine cycle. *Proceedings of the 27 th international conference on Efficiency, Cost, Optimization, Simulation and environmental impact of energy systems*.
- Hewlett, P. (2004). *Lea's Chemistry of Cement and Concrete*. Butterworth-Heinemann.
- Heyen, G., Maréchal, E., and Kalitventzeff, B. (1996). Sensitivity calculations and variance analysis in plant measurement reconciliation. *Computers & Chemical Engineering*, 20, Supplement 1:S539–S544.
- Hnat, J. G. and Coles, W. F. (1985). Feasability assessment of cogeneration from a regenerative glass furnace. *IEEE Transactions on Industry Applications*, IA-21(4):1064–1069.
- Holmgren, K. (2006). Role of a district-heating network as a user of waste-heat supply from various sources – the case of göteborg. *Applied Energy*, 83(12):1351–1367.
- Hsu, S. T., Lin, F. Y., and Chiou, J. S. (2003). Heat-transfer aspects of stirling power generation using incinerator waste energy. *Renewable Energy*, 28(1):59–69.
- Hung, T.-C. (2001). Waste heat recovery of organic rankine cycle using dry fluids. *Energy Conversion and Management*, 42(5):539–553.
- IBM (2009). *IBM ILOG CPLEX V12.1 - User's Manual for CPLEX*.
- Illy, A. and Viani, R. (2005). *Espresso Coffee: The Science of Quality*. Academic Press.
- Imran, M., Park, B. S., Kim, H. J., Lee, D. H., Usman, M., and Heo, M. (2014). Thermo-economic optimization of regenerative organic rankine cycle for waste heat recovery applications. *Energy Conversion and Management*, 87:107–118.
- Incropera, F. P., DeWitt, D. P., Bergman, T. L., and Lavine, A. S. (2006). *Fundamentals of Heat and Mass Transfer*. John Wiley & Sons, Hoboken, NJ, auflage: 6. auflage edition.
- International Energy Agency (2007). *Tracking Industrial Energy Efficiency and CO₂ Emissions*. Paris, France.
- International Energy Agency (2009a). Cement technology roadmap 2009. Paris.
- International Energy Agency (2009b). *World Energy Outlook 2009*. vol. 2009oecd/IEA edition.
- International Energy Agency (2011). *Co-Generation and Renewables: Solutions for a low-carbon energy future*. Paris, France.
- International Energy Agency (2013). *Energy Efficiency Market Report 2013*. Paris, France.
- International Energy Agency (2014a). *Capturing the Multiple Benefits of Energy Efficiency*. Paris, France.

Bibliography

- International Energy Agency (2014b). *CO2 Emissions From Fuel Combustion Highlights 2014*. Paris, France.
- International Energy Agency (2014c). Energy efficiency - policies and measures databases.
- International Energy Agency (2014d). *Energy Efficiency Market Report 2014*. Paris, France.
- International Energy Agency (2014e). *Key World Energy Statistics 2014*. Paris, France.
- Jorge Facão, A. C. O. (2009). Analysis of energetic, design and operational criteria when choosing an adequate working fluid for small ORC systems. *ASME 2009 International Mechanical Engineering Congress & Exposition*, pages 13–19.
- Karellas, S., Leontaritis, A. D., Panousis, G., Bellos, E., and Kakaras, E. (2013). Energetic and exergetic analysis of waste heat recovery systems in the cement industry. *Energy*, 58:147–156.
- Kemp, I. C. (2011). *Pinch Analysis and Process Integration: A User Guide on Process Integration for the Efficient Use of Energy*. Butterworth-Heinemann.
- Klemeš, J. J. and Varbanov, P. S. (2012). Heat integration including heat exchangers, combined heat and power, heat pumps, separation processes and process control. *Applied Thermal Engineering*, 43:1–6.
- Klimes, J. (2013). *Handbook of Process Integration (PI): Minimisation of Energy and Water Use, Waste and Emissions*. Woodhead Publishing Limited.
- Kongtragool, B. and Wongwises, S. (2003). A review of solar-powered stirling engines and low temperature differential stirling engines. *Renewable and Sustainable Energy Reviews*, 7(2):131–154.
- Kretsovalis, A. and Mah, R. S. H. (1987). Effect of redundancy on estimation accuracy in process data reconciliation. *Chemical Engineering Science*, 42(9):2115–2121.
- Kuehn, D. and Davidson, H. (1976). Computer control II. mathematics of control. *Chemical Engineering Science*, (31):1199–1205.
- Lazzaretto, A., Toffolo, A., Manente, G., Rossi, N., and Paci, M. (2011). Cost evaluation of organic rankine cycles for low temperature geothermal sources. *Proceedings of the 24th International Conference on Efficiency, Cost, Optimization, Simulation and Environmental Impact of Energy Systems*, pages 3854–3868.
- Legendre, A.-M. (1805). *Nouvelles méthodes pour la détermination des orbites des comètes*. F. Didot.
- Legmann, H. (2002). Recovery of industrial heat in the cement industry by means of the ORC process. In *Cement Industry Technical Conference, 2002. IEEE-IAS/PCA 44th*, pages 29–35.
- Lemmon, E., Huber, M., and McLinden, M. (2010). NIST standard Reference Database 23: Reference fluid thermodynamic and transport properties - REFPROP. 9.0.

- Lemort, V., Cuevas, C., Teodorese, I., and Lebrun, J. (2007). Contribution à l'étude des cycles de rankine de récupération de chaleur.
- Leyland, G. B. (2002). *Multi-objective optimisation applied to industrial energy problems*. PhD thesis, EPFL, Lausanne, Switzerland.
- Linnhoff, B. and Dhole, V. R. (1992). Shaftwork targets for low-temperature process design. *Chemical Engineering Science*, 47(8):2081–2091.
- Linnhoff, B. and Flower, J. R. (1982). *A User Guide on Process Integration for the Efficient Use of Energy*. The Institution of Chemical Engineers, Rugby, UK.
- Linnhoff, B. and Hindmarsh, E. (1983). The pinch design method for heat exchanger networks. *Chemical Engineering Science*, 38(5):745–763.
- Liu, B.-T., Chien, K.-H., and Wang, C.-C. (2004). Effect of working fluids on organic rankine cycle for waste heat recovery. *Energy*, 29(8):1207–1217.
- Maalouf, Bou Lawz, E., and Clodic, D. (2012a). *Direct boiler (flue gas to fluid) design, construction and characterization - Deliverable 2.3 Report*. LOVE-Deliverables - FP7. ARMINES, Paris, France.
- Maalouf, S., Ksayer, E. B., and Clodic, D. (2012b). ORC finned - tube evaporator design and system performance optimization. *International Refrigeration and Air Conditioning Conference*.
- Madhawa Hettiarachchi, H. D., Golubovic, M., Worek, W. M., and Ikegami, Y. (2007). Optimum design criteria for an organic rankine cycle using low-temperature geothermal heat sources. *Energy*, 32(9):1698–1706.
- Mago, P. J., Chamra, L. M., Srinivasan, K., and Somayaji, C. (2008). An examination of regenerative organic rankine cycles using dry fluids. *Applied Thermal Engineering*, 28(8–9):998–1007.
- Maizza, V. and Maizza, A. (2001). Unconventional working fluids in organic rankine-cycles for waste energy recovery systems. *Applied Thermal Engineering*, 21(3):381–390.
- Maraver, D., Uche, J., and Royo, J. (2012). Assessment of high temperature organic rankine cycle engine for polygeneration with MED desalination: A preliminary approach. *Energy Conversion and Management*, 53(1):108–117.
- Maréchal, F. (2010). Pinch analysis. In *UNESCO Encyclopedia of Life Support Systems*, volume 1 of *Exergy, Energy System Analysis and Optimization*, page Chapter 3.19.1.7. EOLSS Publishers Co Ltd., Oxford, UK, UNESCO edition.
- Maréchal, F. and Favrat, D. (2005). Combined exergy and pinch analysis for optimal energy conversion technologies integration. *ECOS 2005, 18th International Conference on Efficiency, Cost, Optimization, Simulation and Environmental Impact of Energy Systems*, 1:177–184.

Bibliography

- Maréchal, F. and Kalitventzeff, B. (1997). Identification of the optimal pressure levels in steam networks using integrated combined heat and power method. *Chemical Engineering Science*, 52(17):2977–2989.
- Maréchal, F. and Kalitventzeff, B. (1998). Energy integration of industrial sites: tools, methodology and application. *Applied Thermal Engineering*, 18(11):921–933.
- Marechal, F. and Kalitventzeff, B. (2006). Utilities integration (energy, water). In *Computer Aided Process and Product Engineering*, volume 1, pages 327–381. WILEY-VCH Verlag GmbH & Co. KGaA, Weinheim, I. Puigjaner, G. Hayen edition.
- Marmolejo-Correa, D. and Gundersen, T. (2012). A comparison of exergy efficiency definitions with focus on low temperature processes. *Energy*, 44(1):477–489.
- MathWorks (2012). *MATLAB 2012b*. Natick, Massachusetts, USA.
- Mian, A. (2012). *Energetic Analysis of the Cement Production Process*. Università di Padova.
- Mian, A., Bendig, M., Piazzesi, G., Manente, G., Lazzaretto, A., and Maréchal, F. (2013). Energy integration in the cement industry. In Andrzej Kraslawski and Ilkka Turunen, editor, *Computer Aided Chemical Engineering*, volume Volume 32 of *23rd European Symposium on Computer Aided Process Engineering*, pages 349–354. Elsevier.
- Mikielewicz, D. and Mikielewicz, J. (2010). A thermodynamic criterion for selection of working fluid for subcritical and supercritical domestic micro CHP. *Applied Thermal Engineering*, 30(16):2357–2362.
- Minet, F., Heyen, G., Kalitventzeff, B., Di Puma, J., and Malmendier, M. (2001). Dynamic data reconciliation of regenerative heat exchangers coupled to a blast furnace. In Rafiqul Gani and Sten Bay Jørgensen, editor, *Computer Aided Chemical Engineering*, volume Volume 9 of *European Symposium on Computer Aided Process Engineering - 11 34th European Symposium of the Working Party on Computer Aided Process Engineering*, pages 1053–1058. Elsevier.
- Morandin, M., Hackl, R., and Harvey, S. (2014). Economic feasibility of district heating delivery from industrial excess heat: A case study of a Swedish petrochemical cluster. *Energy*, 65:209–220.
- Muller, D. C. A., Marechal, F. M. A., Wolewinski, T., and Roux, P. J. (2007). An energy management method for the food industry. *Applied Thermal Engineering*, 27(16):2677–2686.
- Navarrete, P. F. and Cole, W. (2001). *Planning, Estimating, and Control of Chemical Construction Projects*. Marcel Dekker Inc, New York, Auflage: rev and expanded edition.
- Papadopoulos, A. I., Stijepovic, M., and Linke, P. (2010). On the systematic design and selection of optimal working fluids for organic rankine cycles. *Applied Thermal Engineering*, 30(6–7):760–769.

- Peray, K. E. (1979). *Cement manufacturer's handbook*. Chemical Pub. Co.
- Peray, K. E. (1986). *The Rotary Cement Kiln*. CHEMICAL Publishing Company Incorporated (NY).
- Perry, R. H. and Green, D. W. (1997). *Perry's Chemical Engineers' Handbook*. McGraw-Hill Professional, New York, auflage: 7 edition.
- Perry, S., Klemeš, J., and Bulatov, I. (2008). Integrating waste and renewable energy to reduce the carbon footprint of locally integrated energy sectors. *Energy*, 33(10):1489–1497.
- Peters, M. S. and Timmerhaus, K. D. (1991). *Plant design and economics for chemical engineers*. McGraw-Hill, New York.
- Pouransari, N., Tanguy, D., Bocquenet, G., and Maréchal, F. (2014). Role of total site integration in energy-target modification of distillation columns. *Applied Thermal Engineering*.
- Quoilin, S., Declaye, S., Tchanche, B. F., and Lemort, V. (2011). Thermo-economic optimization of waste heat recovery organic rankine cycles. *Applied Thermal Engineering*, 31(14–15):2885–2893.
- Quoilin, S. and Lemort, V. (2009). Technological and economical survey of organic rankine cycle systems.
- Rayegan, R. and Tao, Y. X. (2011). A procedure to select working fluids for solar organic rankine cycles (ORCs). *Renewable Energy*, 36(2):659–670.
- Reilly, P. and Carpani, R. (1963). Application of statistical theory of adjustment to material balances. *Canadian chemical engineering conference*, (13th, Montreal, Canada).
- Romagnoli, J. A., Romagnoli, J. A., and Sanchez, M. C. (1999). *Data Processing and Reconciliation for Chemical Process Operations*. Academic Press Inc, San Diego.
- Rowe, D. M. (1995). *CRC Handbook of Thermoelectrics*. CRC Press.
- Roy, J. P., Mishra, M. K., and Misra, A. (2010). Parametric optimization and performance analysis of a waste heat recovery system using organic rankine cycle. *Energy*, 35(12):5049–5062.
- Saleh, B., Koglbauer, G., Wendland, M., and Fischer, J. (2007). Working fluids for low-temperature organic rankine cycles. *Energy*, 32(7):1210–1221.
- Satterthwaite, K. (2013). Petroleum coke economics in cement kilns to 2016. Roskill Information Services Ltd., London.
- Schuster, A., Karellas, S., and Aumann, R. (2010). Efficiency optimization potential in super-critical organic rankine cycles. *Energy*, 35(2):1033–1039.

Bibliography

- Schuster, A., Karellas, S., Kakaras, E., and Spliethoff, H. (2009). Energetic and economic investigation of organic rankine cycle applications. *Applied Thermal Engineering*, 29(8-9):1809–1817.
- Shengjun, Z., Huaixin, W., and Tao, G. (2011). Performance comparison and parametric optimization of subcritical organic rankine cycle (ORC) and transcritical power cycle system for low-temperature geothermal power generation. *Applied Energy*, 88(8):2740–2754.
- Smith, R., Jobson, M., and Chen, L. (2010). Recent development in the retrofit of heat exchanger networks. *Applied Thermal Engineering*, 30(16):2281–2289.
- Sorin, M. and Rheault, F. (2007). Thermodynamically guided intensification of separation processes. *Applied Thermal Engineering*, 27(7):1191–1197.
- Sprung, S. (2000). Cement. In *Ullmann's Encyclopedia of Industrial Chemistry*. Wiley-VCH Verlag GmbH & Co. KGaA.
- Stigler, S. M. (1990). *The History of Statistics: The Measurement of Uncertainty Before 1900*. Harvard Univ Pr, Cambridge, Mass., auflage: revised. edition.
- Stijepovic, M. Z. and Linke, P. (2011). Optimal waste heat recovery and reuse in industrial zones. *Energy*, 36(7):4019–4031.
- Sun, J. and Li, W. (2011). Operation optimization of an organic rankine cycle (ORC) heat recovery power plant. *Applied Thermal Engineering*, 31(11–12):2032–2041.
- Szargut, J. (1979). INTERNATIONAL PROGRESS IN SECOND LAW ANALYSIS. *Energy*, 5(8-9):709–718.
- Tchanche, B. F., Papadakis, G., Lambrinos, G., and Frangoudakis, A. (2009). Fluid selection for a low-temperature solar organic rankine cycle. *Applied Thermal Engineering*, 29(11–12):2468–2476.
- Tejon Carbajal, P. (2009). Natural refrigerants: The solutions.
- Townsend, D. W. and Linnhoff, B. (1983). Heat and power networks in process design. part i: Criteria for placement of heat engines and heat pumps in process networks. *AIChE Journal*, 29(5):742–748.
- Turton, R. (2012). *Analysis, synthesis, and design of chemical processes*. Pearson, Upper Saddle River, N.J.
- Uehara, H. and Ikegami, Y. (1990). Optimization of a closed-cycle OTEC system. *Journal of Solar Energy Engineering, Transactions of the ASME*, 112(4):247–256.
- Ullrich, C., Heyen, G., and Gerkens, C. (2009). Variance of estimates in dynamic data reconciliation. In Jacek Jeżowski and Jan Thullie, editor, *Computer Aided Chemical Engineering*, volume Volume 26 of *19th European Symposium on Computer Aided Process Engineering*, pages 357–362. Elsevier.

- Ulrich, G. D. (1984). *A guide to chemical engineering process design and economics*. Wiley.
- United Nations Environmental Programm (2014). Ozone secretariat - montreal-protocol.org.
- United Nations Framework Convention on Climate Change (1997). Kyoto protocol.
- United Nations Framework Convention on Climate Change (2014). Global warming potentials - unfccc.int.
- U.S. Environmental Protection Agency (2010). Transitioning to low-GWP alternatives in domestic refrigeration - EPA-430-f-10-042.
- U.S. Environmental Protection Agency (2014a). Global warming potentials and ozone depletion potentials of some ozone-depleting substances and alternatives listed by the SNAP program.
- U.S. Environmental Protection Agency (2014b). Global warming potentials of ODS substitutes | ozone layer protection | US EPA.
- U.S. Environmental Protection Agency (2014c). Regulatory programs | ozone layer protection | US EPA. Information on EPA regulatory programs to protect stratospheric ozone.
- Vaja, I. and Gambarotta, A. (2010). Internal combustion engine (ICE) bottoming with organic rankine cycles (ORCs). *Energy*, 35(2):1084–1093.
- Van Rossum, G. (2007). Python programming language. In *USENIX Annual Technical Conference*.
- Vatavuk, W. M. (2002). Updating the plant cost index. *Chemical Engineering*, (1. 2002):62–70.
- Verein Deutscher Ingenieure (VDI) and GVC (2006). *VDI-Wärmeatlas*. Springer, 10 edition.
- Vining, C. B. (2009). An inconvenient truth about thermoelectrics. *Nature Materials*, 8(2):83–85.
- Wang, J., Yan, Z., Wang, M., Ma, S., and Dai, Y. (2013). Thermodynamic analysis and optimization of an (organic rankine cycle) ORC using low grade heat source. *Energy*, 49:356–365.
- Wang, Y., Smith, R., and Kim, J.-K. (2012a). Heat exchanger network retrofit optimization involving heat transfer enhancement. *Applied Thermal Engineering*, 43:7–13.
- Wang, Z. Q., Zhou, N. J., Guo, J., and Wang, X. Y. (2012b). Fluid selection and parametric optimization of organic rankine cycle using low temperature waste heat. *Energy*, 40(1):107–115.
- Worrell, E., Price, L., Martin, N., Hendriks, C., and Meida, L. O. (2001). Carbon dioxide emissions from the global cement industry. *Annual Review of Energy and the Environment*, 26(1):303–329.

Bibliography

Yeretzian, C., Jordan, A., Badoud, R., and Lindinger, W. (2002). From the green bean to the cup of coffee: investigating coffee roasting by on-line monitoring of volatiles. *European Food Research and Technology*, 214(2):92–104.

Curriculum vitae

Personal details

Name	Matthias Bendig
Date of birth	14.08.1983
Citizenship	German
Contact	matthias.bendig@gmail.com

University Education

2010	–	2015	Ecole Polytechnique Fédérale de Lausanne (EPFL), Switzerland, <i>PhD, Industrial Process & Energy Systems Engineering.</i>
2004	–	2010	University of Stuttgart, Germany, <i>Diplomingenieur, Umweltschutztechnik.</i>
2007	–	2008	Université de Corse Pascal Paoli, France, <i>Systèmes Energétiques et Energies Renouvelables & Ingénierie Écologique.</i>
2007	–	2008	Université des Antilles et de la Guyane, France, <i>Ressources en Milieu Intertropical - Valorisation Energétique & Valorisation Chimique & Biotrop.</i>

Experience

05/2010	–	10/2010	Centre for Solar Energy and Hydrogen Research Baden-Württemberg (ZSW), Germany, <i>Diplomarbeit (Masterthesis) - Experimental optimisation of a methanation reactor for Bio-SNG synthesis from Biosyngas.</i>
11/2009	–	10/2010	Fichtner Consulting Engineers, Energy Economics Division, Germany, <i>Internship.</i>
09/2008	–	10/2009	University of Stuttgart, Germany, <i>Research Assistant - Solar Heated Absorption Cooling Cycle.</i>
01/2005	–	08/2007	University of Stuttgart, Germany, <i>Student Assistant in the international MSc programme WASTE.</i>